REPORT DOCUMENTATION PAGE		Form Approved OMB No. 0704-0188

1. AGENCY USE ONLY *(Leave blank)*	2. REPORT DATE August 31, 1997	3. REPORT TYPE AND DATES COVERED Final Technical Report 1 Mar 94 to 28 Feb 97 .

4. TITLE AND SUBTITLE	5. FUNDING NUMBERS
RESEARCH IN STRUCTURAL DYNAMICS	F49620-94-1-0127

6. AUTHOR(S)

Prof. D. Hodges

Prof. V. Berdichevsky

7. PERFORMING ORGANIZATION NAME(S) AND ADDRESS(ES)	8. PERFORMING ORGANIZATION REPORT NUMBER
School of Aerospace Engineering Georgia Institute of Technology Atlanta, GA 30332	

9. SPONSORING/MONITORING AGENCY NAME(S) AND ADDRESS(ES)	10. SPONSORING/MONITORING AGENCY REPORT NUMBER
AFOSR/NA 110 Duncan Ave, Suite B 115 Bolling AFB, DC 20332-8050	

11. SUPPLEMENTARY NOTES

12a. DISTRIBUTION AVAILABILITY STATEMENT	12b. DISTRIBUTION CODE
Approved for public release; distribution unlimited.	

13. ABSTRACT *(Maximum 200 words)*

This report addresses truncation in structural dynamics, energy thresholds in nonlinear vibration, dynamic potential of vibrating systems, and high-temperature diffusional creep. Study of the dynamics of elastic structures is usually based on structural models with a few degrees of freedom. In this connection it is important to understand how these degrees of freedom should be chosen and how the neglected degrees of freedom affect the accuracy of the model. It is shown that there is an energy threshold beyond which the laws of statistical mechanics become valid, requiring the consideration of all degrees of freedom. For excitation which is moderate (but below this threshold) methods are presented which show how to capture the leading degrees of freedom and how to take into account the neglected modes. The value of the energy threshold is driven by the specifics of models used so that small changes in the model can strongly increase the value of the threshold. The dynamic potential makes use of an analogy between thermodynamical energy and structural vibration. The existence of the dynamical potential reduces the number of experimentally determined functions to one. It is shown, and confirmed experimentally, how this leads to simple relations between excitations and responses of nonlinear vibrating systems. Finally, a nonlinear theory of diffusional plasticity is presented.

14. SUBJECT TERMS	15. NUMBER OF PAGES
	16. PRICE CODE

17. SECURITY CLASSIFICATION OF REPORT	18. SECURITY CLASSIFICATION OF THIS PAGE	19. SECURITY CLASSIFICATION OF ABSTRACT	20. LIMITATION OF ABSTRACT
UNCLASSIFIED	UNCLASSIFIED	UNCLASSIFIED	UL

DTIC QUALITY INSPECTED 3

RESEARCH IN STRUCTURAL

DYNAMICS

FINAL REPORT

Contract #F49620-94-1-0127

PI: Prof. D. Hodges
School of Aerospace Engineering
Georgia Institute of Technology
Atlanta GA 30332

Subcontract PI: Prof. V. Berdichevsky
Mechanical Engineering Department
Wayne State University
Detroit MI 48202

Duration period: March 1, 1994 - August 31, 1997

Objectives:

The study was conducted in the following areas:

- A. Truncation
- B. Statistical properties of high-energy vibrations
- C. Dynamical potential
- D. Diffusional creep at high temperatures

Objectives of topic A : to develop methods of truncation of continuum equations in structural dynamics which capture the major features of vibrations

Objectives of topic B : to study the properties of the energy threshold in high-energy vibrations

Objectives of topic C : to study dynamical potential of vibrating systems theoretically and experimentally

Objectives of topic D : to develop theory of diffusional creep at high temperatures

Accomplishments:

<u>Topic A</u> : Study of dynamics of elastic structures is usually based on modeling the structure by a finite-dimensional system with a few degrees of freedom. In this connection it is important to understand (1) in which way these degrees of freedom should be chosen, (2) how many degrees of freedom should be kept, and (3) how do the neglected degrees of freedom affect the kept ones. These issues have been addressed in the research. It turns out that the answers to the posed questions depend significantly on the level of excitation: there is an energy threshold such that if energy exceeds this threshold the laws of statistical mechanics become valid and none of the degrees of freedom can be neglected. We study the case of moderate energy of excitation which is lower than the energy threshold but is still high enough to activate nonlinear interactions. For the case of string vibrations, a simple methods has been developed which allows one to capture the leading degrees of freedom and take into account the influence of neglected modes on the leading ones. The reasoning is quite general, and the answers are given in the form which admits application to many elastic structures.

<u>Topic B</u> : It was known for about 25 years that there exists an energy threshold for vibrations of elastic structures such that, for energy vibrations exceeding the energy threshold, vibrations are practically chaotic. We established also that the laws of statistical

mechanics are valid for vibrations with such high energy. In the previous studies, the value of energy threshold was found to be relatively small. We found that this is caused by the specifics of the models used, and small "physical disturbances" of the models (we add wave dispersion) yields much higher values of the energy threshold.

Topic C : If parameters of excitation applied to an elastic structure are tuned, the system undergoes the changes which in many cases are reminiscent of phase transitions in classical thermodynamics. The question arises: is there an analogy of thermodynamical energy for structural vibrations? The positive answer for systems with small dissipation has been given by the PI (1993). The properties of the corresponding "thermodynamical function", dynamical potential, have been studies theoretically and experimentally in this project. The very fact that the dynamical potential exists seems as important as the existence of energy for elastic bodies. It has immediate applications: usually, one is interested in establishing the relations between excitations and responses of vibrating systems; the existence of dynamical potential reduced the number of experimentally determined functions to one. The theory of dynamical potential is applicable only to devices with high efficiency (small dissipation). An experimental setup has been developed to determine the dynamical potential of a nonlinear oscillator. The experiments confirmed the theoretical predictions.

Topic D : One of the promising directions in material sciences is the development of materials with grain size on the order of nanometers. In such materials, the major mechanism of plastic deformation is the vacancy diffusion. This mechanism is also a leading one for usual polycrystals at high temperatures and low stresses. Diffusional plasticity theory differs significantly from dislocational plasticity theory because vacancy diffusion is a scalar phenomenon. Development of the theory of diffusional plasticity has been conducted in collaboration with Dr. R. Bagley (UTSA) and Dr. P. Hazzledine (Wright-Patterson Lab). Nonlinear theory of diffusional plasticity has been proposed. A linear version of this theory has been applied to the prediction of macroscopic and microscopic behavior of polycrystal bodies with periodic microstructure. Constitutive equations have been obtained in an explicit form. The cell problem for microfields was formulated for secondary creep, and the corresponding variational principle was established. Dependence

of macroparameters on microcharacteristics has been found. It was shown that primary creep is governed by nonlocal equations. Numerical simulations were conducted for honeycomb structures.

<u>Byproducts</u> : An understanding of statistical mechanics of continua achieved helped to develop statistical mechanics of point vortices (V. Berdichevsky, Statistical Mechanics of Point Vortices, Physical Review E, v.51, pp. 4432-4452, 1995) and obtain for the first time the velocity profiles of turbulent flows without the use of phenomenological constants (V. Berdichevsky, A. Fridlyand, V. Sutyrin, Prediction of Turbulent Velocity Profiles in Couette and Poiseuille Flows from First Principles, Physical Review Letters, v.76, no. 21, pp. 3967-3970, 1996).

Personnel Supported:
PI: Prof. V. Berdichevsky (1 summer month)
Post Doc: Dr. V. Sutyrin (part-time)
Graduate Students: E. Mueller, P. Matusov (part-time)
Consulting: Dr. B. Shoykhet

Publications:
1. V. Berdichevsky, Thermodynamics of Chaos and Order, Longman, 1997 (to appear)
2. Berdichevsky, V., Kim, W.W., Ozbek, A., Dynamical Potential for Nonlinear Vibrations of Cantilevered Beam, J. Sound and Vibrations, v. 179, 151-164, 1995
3. Berdichevsky, V., Possible Scenarios of Nonlinear Vibrations of High Energies, Proc. ASME Conference of Acoustics and Vibrations, v. 3B, 877-879, ASME, NY, 1995
4. Berdichevsky, V., Shoykhet, B., Homogenization problem for Bulk Diffusional Creep, Proc. of Conference on Continuum Models and Discrete Systems, Varna, 1995, pp. 100-111, World Scientific, 1996
5. V. Berdichevsky, P. Hazzledine, B. Shoykhet, Micromechanics of Diffusional Creep, Int. J. Engineering Science, 1997 (to appear)
6. V. Berdichevsky, Thermodynamics and Parametric Response of Slightly Dissipative Systems, J. Appl. Mech. 1996 (submitted)
7. V. Berdichevsky, P. Matusov, Truncation in Elastodynamics: Influence of Neglected Degrees of Freedom on the Leading Ones, J. Appl. Mech., 1996 (submitted)
8. P. Matusov, Experimental Determination of Dynamical Potential for Nonlinear Oscillator, J. Appl. Mech., 1997 (submitted)

A review of topics A and B is given in Chapters 3 and 4 of the monograph [1] (Attachment 1).

The original results on these topics are presented in papers [7] (Attachment 2) and [3] (Attachment 3).

Papers [2] (Attachment 4) and [6] (Attachment 5) are concerned with theoretical and computational aspects of the theory of dynamical potential while the experimental results are presented in paper [8] (Attachment 6). Theory of diffusional creep is studied in [4] (Attachment 7) and [5] (Attachment 8).

Interactions:
a. Meetings.
V. Berdichevsky, P. Hazzledine, B. Shoykhet, Micromechanics of Diffusional Creep, ASME Mechanics and Materials Conference, UCLA, June 1995

V. Berdichevsky, Possible Scenarios of Nonlinear Vibrations at High Energies, ASME Conference on Acoustics and Vibrations, Boston, September 1995

V. Berdichevsky, B. Shoykhet, Homogenization Problem for Bulk Diffusional Creep, Conference on Continuum Models and Discrete Systems, Varna, June 1995

V. Berdichevsky, Diffusional Creep, Seminar Presentation at Mechanics Lab at the University of Paris, France, June 1995

Workshop on Mathematical Methods in Material Sciences, University of Minnesota, September 1995 (participation)

Annual Meeting of Division of Fluid Dynamics, American Physical Society, CA, November 1995 (participation)

Workshop on Ultra-High Reynolds Number Flows, Brookhaven National Lab, June 1996 (participation)

V. Berdichevsky, Research in Structural Dynamics, AFOSR Structural Mechanics Workshop, VA, June 1996

Statistical Mechanics Conference, Rutgers University, December 1996 (participation)

Statistical Mechanics Conference, Rutgers University, May 1997 (participation)

V. Berdichevsky, On statistical mechanics of ideal fluid, Workshop on Arnold's stability and Arnold's Festival, Toronto, June 1997

b. Collaboration.
The study of topic D was conducted in close collaboration with R. Bagley and P. Hazzledine from Wright-Patterson Lab and Dr. B. Shoykhet (Reliance Electric).

New Discoveries:
Two findings seem possible to qualify as discoveries:
1. A method of truncation of continuum equations which takes into account the influence of the neglected modes.
2. A method of fast calculations of mode interactions based on the identity found in [1].

List of Attachments:
1. Chapters 3 and 4 of the monograph [1]
2. Paper [7]
3. Paper [3]
4. Paper [2]
5. Paper [6]
6. Paper [8]
7. Paper [4]
8. Paper [5]

Chapter 3

Free Vibrations of a System of Oscillators

Usually, mechanical and physical low-dimensional Hamiltonian systems are not ergodic. Nevertheless, they can be approximately ergodic if the parameters are in a certain range. In this chapter, systems of nonlinear oscillators are considered. They demonstrate ergodic properties if energy exceeds some threshold value. This behavior is, perhaps, generic for all elastic vibrational systems.

3.1 Henón-Heiles oscillators

The Henón-Heiles oscillators. One of the first examples of chaotic motion of a low-dimensional system was discovered by M. Henón and C. Heiles in 1964 [90]. They considered a system of two oscillators. The first oscillator is simply a harmonic oscillator with the Hamilton function

$$H_1 = (p_1{}^2 + q_1{}^2)/2$$

The second oscillator is a nonlinear oscillator with the following properties: it has a stable equilibrium point at $q_2 = 0$, the frequency of linear vibrations in the vicinity of this equilibrium point is equal to the frequency of the first oscillator, and if q_2 exceeds some value, the oscillator tends to escape the origin. The potential energy $U_2(q_2)$ is chosen as

$$U_2(q_2) = \frac{1}{2}q_2^2 - \frac{1}{3}q_2^3$$

Of course, this is an approximation of a situation where the second oscillator has two stable equilibrium positions and one studies vibrations in the vicinity of one of them.

The oscillators interact. The interaction energy is asymmetric and is

$$H_{12} = q_1{}^2 q_2,$$

so the total Hamilton function is

$$H = \frac{1}{2}(p_1^2 + p_2^2) + U(q_1, q_2),$$

$$U(q_1, q_2) = \frac{1}{2}q_1^2 + U_2(q_2) + q_1^2 q_2 \tag{3.1}$$

The dynamical equations are

$$\dot{q}_1 = p_1, \quad \dot{q}_2 = p_2, \quad \dot{p}_1 = -(q_1 + 2q_1 q_2), \quad \dot{p}_2 = -(q_2 - q_2^2 + q_1^2) \tag{3.2}$$
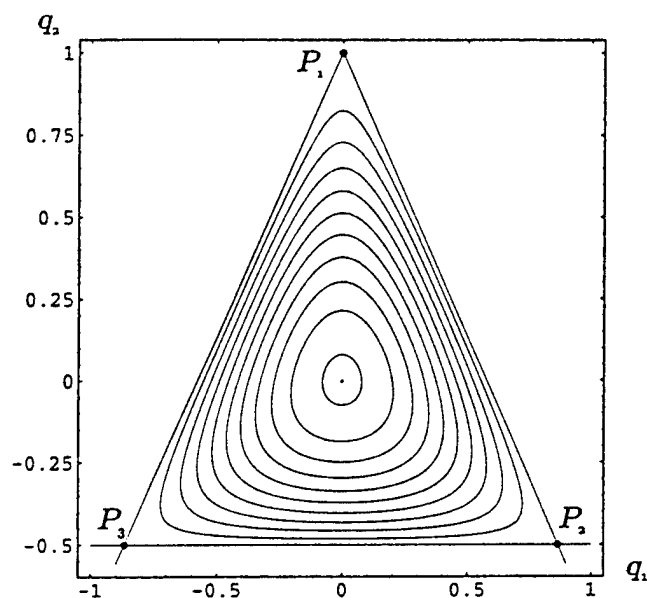
Fig. 3.1: Contour plot of the potential energy of the Henón-Heiles oscillators

This system has one stable equilibrium point at the origin, $q_1 = q_2 = 0$, and three unstable equilibrium points: $P_1(q_1 = 0, q_2 = 1)$, $P_2(\sqrt{3}/2, -1/2)$, $P_3(-\sqrt{3}/2, -1/2)$. They are shown in the contour plot of potential energy $U(q_1, q_2)$ (Fig. 3.1). The separatrics connecting the unstable points are straight lines. These separatrics correspond to an energy level $U = 1/6$. All contour lines with energy levels less than $1/6$ are inside the triangle $P_1P_2P_3$.

Poincare sections. The dynamics of oscillators can be described in a very informative way by means of Poincare sections. Consider a trajectory $p_1(t), q_1(t), p_2(t), q_2(t)$ of equations (3.2). Since energy is the integral of motion, the trajectory is, in fact, given by three functions, and the fourth one is determined by the energy equation

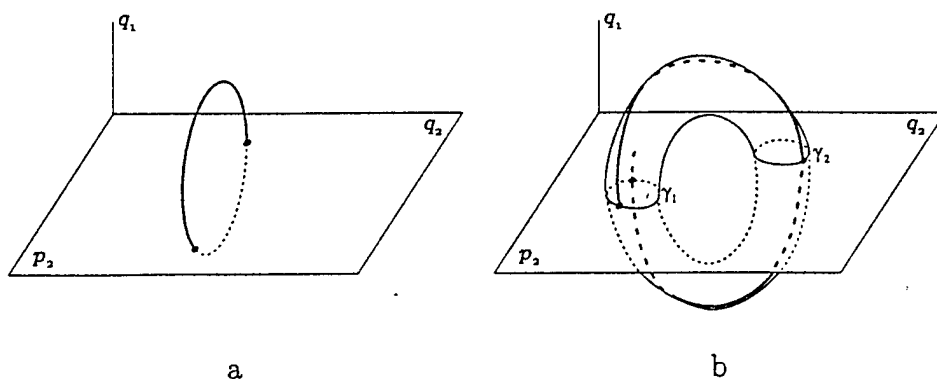$$H(p_1, q_1, p_2, q_2) = E = \text{const} \tag{3.3}$$

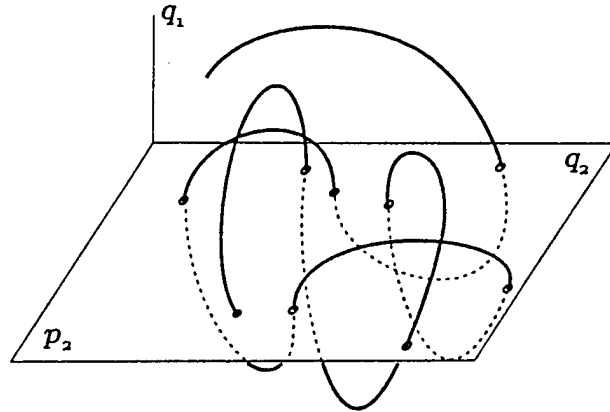Fig. 3.2: Image on a Poincare section of a periodic trajectory (a) and invariant torus (b)

Fig. 3.3: Chaotic trajectory and its image on a Poincare section

For definiteness, let the energy equation be used to find $p_1(t)$. Then, the trajectory of the system is a curve in three-dimensional space of the variables q_1, p_2 and q_2. Consider cross-sections of the trajectory with the plane $q_1 = 0$. This is a set of points which is called a Poincare section. If the trajectory is periodic, the Poincare section consists of a finite number of points.

Two points on a Poincare section correspond to the trajectory shown in Fig. 3.2a. If the trajectory lies on a torus in (q_1, p_2, q_2)-space, then the successive cross-sections of the trajectory and the plane $q_1 = 0$ belong to the curves γ_1 and γ_2, shown in Fig. 3.2b. In a typical situation, a torus is a member of family of embedded tori, and one sees two families of embedded curves in the Poincare section. If the successive cross-sections of the trajectory and the plane do not form a certain pattern, the trajectory is thought to be chaotic (Fig. 3.3).

Qualitative picture of vibration. The behavior of Henón-Heiles oscillators depends on the energy level of the initial disturbance. If the energy is small enough, the interaction is not profound and the oscillators vibrate independently. In (q_1, p_2, q_2)-space there is a family of embedded tori. Cross-sections of these tori with the plane $q_2 = 0$ are shown in Fig. 3.3a for $E = 10^{-3}$. The cross-sections are obtained by numerical integration of dynamical equations for various initial data. For $E = 10^{-2}$, a new family of tori appears, as is seen from Fig. 3.4b. For $E = 0.125$ one observes a chaotic sea with islands of ordered motion (Fig. 3.4c). The islands are images of tori similar to the one shown in Fig. 3.2b. Although the "chaotic component" of motion is well presented, the the motion is far from being ergodic: the chaotic trajectory does not cover the whole energy surface. Note that the scales are chosen different in Fig. 3.4a,b,c because the maximum magnitudes of vibrations are different for various values of energy; they are on the order of $\sqrt{E}$.

The chaotic sea expands if the energy is increased. For $E = 1/6$, the chaotic sea occupies almost the whole energy surface (Fig. 3.4d) except for four thin islands. There might also be some small islands which are not visible at this resolution. Since the total volume of the islands of ordered motion is small, one can expect that the motion of the Henón-Heiles oscillators is approximately ergodic, and all the relations of statistical mechanics and thermodynamics apply. In this section the results of
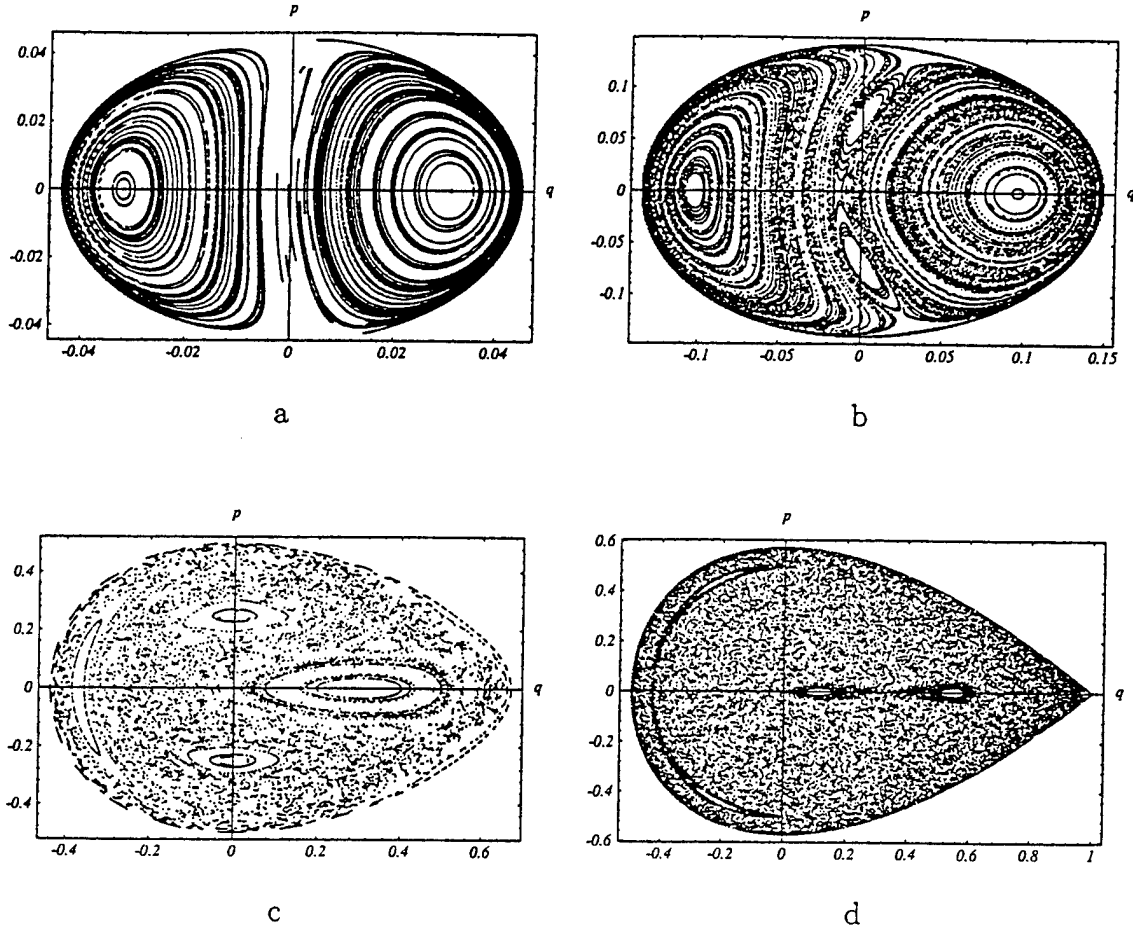
Fig. 3.4: Poincare sections of Henon-Heiles oscillators for the values of energy $E = 10^{-3}$ (a), $E = 10^{-2}$ (b), $E = 0.125$ (c), $E = 1/6$ (d)

numerical experiments which show that this is really the case are presented and discussed.

Phase volume. The key quantity in the "thermodynamics" of Henón-Heiles oscillators is the volume of phase space, $\Gamma(E)$, bounded by the energy surface $H(p_1, p_2, q_1, q_2) = E$. This volume can be expressed in terms of the area, $A(e)$, of the region in the (q_1, q_2)-plane, bounded by the curve $U(q_1, q_2) = e$. Indeed, one can write

$$\Gamma(E) = \int_{H(p_1, p_2, q_1, q_2) \leq E} dp_1 dp_2 dq_1 dq_2 =$$

$$= \int \left[\int_{p_1^2 + p_2^2/2 \leq E - U(q_1, q_2)} dp_1 dp_2 \right] dq_1 dq_2 =$$
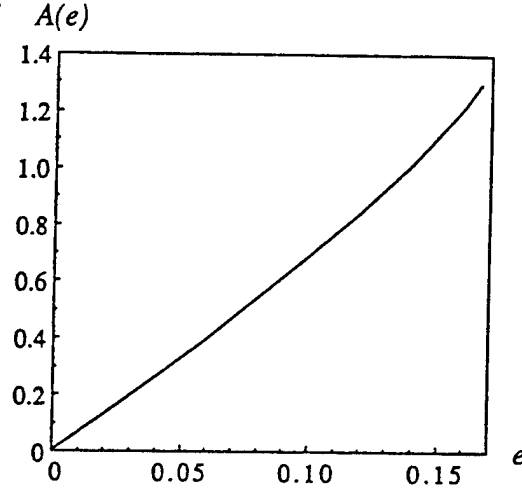
$$= 2\pi \int [E - U(q_1, q_2)] dq_1 dq_2$$

Fig. 3.5: Dependence of area, $A(e)$, bounded by the contours in Fig. 3.1, on the energy level

This last integral is taken over the region where the integrand is positive. It can also be written as

$$\Gamma(E) = 2\pi \int_0^E (E - e) dA(e)$$

Integrating by parts, we obtain

$$\Gamma(E) = 2\pi \int_0^E A(e) de \qquad (3.4)$$

Hence,

$$\frac{d\Gamma}{dE} = 2\pi A(E) \qquad (3.5)$$

From (1.61) and (1.50), we obtain the following expressions for entropy and temperature of the Henón-Heiles oscillators

$$S(E) = \ln \int_0^E A(e) de + \text{const},$$

$$T(E) = \frac{1}{A(E)} \int_0^E A(e) de \qquad (3.6)$$

The area $A(e)$ can be calculated using the expression

$$A(e) = \int_{\frac{1}{2}y^2 + U_2(x) + y^2 x \le e} dx\, dy = 2 \int_{e - U_2(x) \ge 0} \left[\frac{2 \left[e - U_2(x) \right]}{1 + 2x} \right]^{1/2} dx \qquad (3.7)$$

The integral in (3.7) could be reduced to a standard elliptic integral. However, numerical integration is just as efficient. The dependence of A on e is shown in Fig. 3.5.

Probability density function. Besides temperature, we shall study probability density functions of the coordinates and momentum of each oscillator and denote them

by $f_1(p, q)$ and $f_2(p, q)$, respectively. Consider first the probability density function of the second oscillator, $f_2(p, q)$. This probability density function is equal to zero outside the region of possible values of p_2, q_2, i.e. the set of all points in the (p_2, q_2)-plane which could be visited by trajectories of the system. Denote this region by R_2. If the oscillators move ergodically, R_2 is a set of such points (p_2, q_2) that for some values of (p_1, q_1), the equality $H(p_1, p_2, q_1, q_2) = E$ is satisfied. In order to describe R_2 explicitly, it is convenient to introduce the function

$$h_2(p_2, q_2) = \min_{p_1, q_1} H(p_1, p_2, q_1, q_2) \tag{3.8}$$

The region R_2 is determined by the inequality

$$h_2(p_2, q_2) \leq E \tag{3.9}$$

The value of the function $h_2(p_2, q_2)$ is obviously equal to the energy of the second oscillator,

$$h_2(p_2, q_2) = \tfrac{1}{2}{p_2}^2 + U_2(q_2),$$

and the region of admissible values of p_2, q_2 coincides with the interior of the energy surface of the second oscillator in its free vibrations.

Following the general scheme, in order to find f_2 one has to calculate the entropy of the system with the kinematic constraints $p_2 = p$, $q_2 = q$. Trajectories $p_1(t)$ and $q_1(t)$ of the constrained system lie on the curve

$$\tfrac{1}{2}({p_1}^2 + {q_1}^2) + {q_1}^2 q = E - \tfrac{1}{2}p^2 - U_2(q) \tag{3.10}$$

Curve (3.10) is an ellipse with half-axes

$$a = \sqrt{2\left[E - \frac{1}{2}p^2 - U_2(q)\right]} \quad \text{and} \quad b = \sqrt{2\left[E - \frac{1}{2}p^2 - U_2(q)\right]} \frac{1}{\sqrt{1 + 2q}}$$

The area bounded by this ellipse is

$$\Gamma_2(E, p, q) = 2\pi \left[E - \frac{1}{2}p^2 - U_2(q)\right] \Big/ \sqrt{1 + 2q}$$

Hence, the entropy of the constrained system is

$$S_2(E, q_2, p_2) = \ln \frac{E - \frac{1}{2}p_2^2 - U_2(q_2)}{\sqrt{1 + 2q_2}} + \text{const} \tag{3.11}$$

From the generalized Einstein relation (2.3) and the expression for entropy (3.11) and phase volume (3.5), we find the probability density function of the coordinates and momentum of the second oscillator:

$$f_2(E, p, q) = \frac{1}{\partial \Gamma / \partial E} \frac{\partial}{\partial E} e^{S_2(E, p, q)} = \frac{1}{A(E)\sqrt{1 + 2q}} \tag{3.12}$$

Note a remarkable peculiarity of this function: it does not depend on momentum.
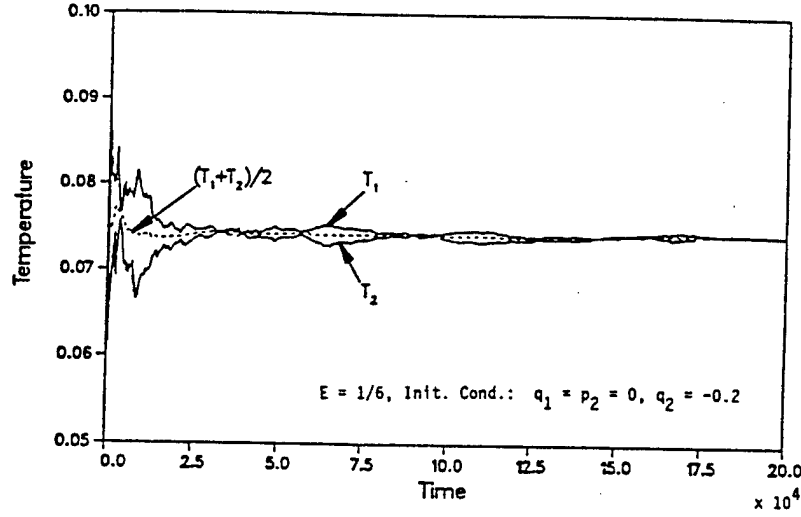
Fig. 3.6: Convergence of the temperature of the oscillators to a common value for a trajectory in a chaotic sea

Similarly, one can find the probability density function of the first oscillator. The domain of this function is

$$h_1(p_1, q_1) \leq E,$$

where

$$h_1(p_1, q_1) = \min_{p_2, q_2} H(p_1, p_2, q_1, q_2) = \frac{1}{2}p_1^2 + q_1^2 - \frac{2}{3}(\frac{1}{4} + q_1^2)^{3/2} + \frac{1}{12} \qquad (3.13)$$

The trajectories of the constrained system with the prescribed values of $p_1 = p$ and $q_1 = q$ lie on a curve in the (p_2, q_2)-plane:

$$\frac{1}{2}p_2^2 + \frac{1}{2}q_2^2 - \frac{1}{3}q_2^3 + q^2 q_2 = E - \frac{1}{2}(p^2 + q^2)$$

It bounds the region with area

$$\Gamma_1(E, p, q) = 2 \int p_2 dq_2 =$$

$$= 2\sqrt{2} \int_a^b \left[\left[E - \frac{1}{2}(p^2 + q^2) \right] - \frac{1}{2}q_2^2 + \frac{1}{3}q_2^3 - q^2 q_2 \right]^{1/2} dq_2 \qquad (3.14)$$

where a and b are the two smallest zeros of the integrand. Thus,

$$f_1(p, q) = \frac{1}{2\pi A(E)} \frac{\partial \Gamma_1}{\partial E}$$

Since the integrand is zero at the bounds, the differentiation with respect to the energy can be interchanged with integration. Hence,

$$f_1(p, q) = \frac{1}{2\pi A(E)} \sqrt{2} \int_a^b \left[E - \frac{1}{2}(p^2 + q^2) - \frac{1}{2}x^2 + \frac{1}{3}x^3 - q^2 x \right]^{-1/2} dx \qquad (3.15)$$
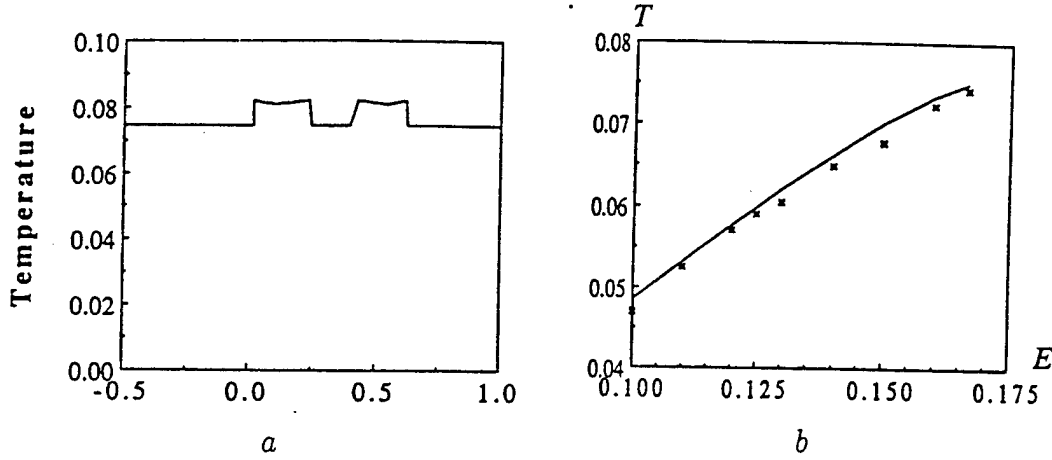
Fig. 3.7: a) Temperature distribution along the line $p_2 = 0$ for energy level $E = 1/6$. Islands of ordered motion are "hotter" than the chaotic sea b) Dependence of the temperature of chaotic trajectories on energy; the solid line corresponds to ergodic theory (formula (3.6)), crosses show numerical results

This integral can be found for each p, q by numerical integration. Now we proceed to the comparison of these relations with numerical results.

Temperature. The first important question is: how strongly do the islands of ordered motion affect the equipartition law? It is natural to calculate the "temperatures" of the oscillators,

$$T_1 = \frac{1}{\theta} \int_0^\theta p_1^2 dt, \quad T_2 = \frac{1}{\theta} \int_0^\theta p_2^2 dt \qquad (3.16)$$

for various energy levels and various starting points. Figure 3.6 shows the dependence of T_1 and T_2 on the averaging time θ for a chaotic trajectory at the maximum energy level, $E = 1/6$. It can be seen clearly that T_1 and T_2 converge to a common value $T = (T_1 + T_2)/2 \cong 0.07433$. The error $|T_1 - T_2|/T$ is less than 0.1%. A number of calculations performed for chaotic trajectories on this energy level yield the same result. This supports the validity of the equipartition law for the highest energy level.

Temperatures of trajectories of ordered motion show the same behavior; however the rate of convergence is much faster. One might assume that it occurs because of the smaller dimensionality of a torus compared with that of an energy surface.

On the islands crossing the q_2-axis, the temperatures T_1 and T_2 converge quite quickly towards $T = 0.0819$. On the left islands, the temperatures T_1 and T_2 clearly stabilize but they apparently do not converge towards the same value. However, the difference between T_1 and T_2 is rather small ($\Delta T = 0.0007$ or about 1% of the average temperature).

Figure 3.7a shows a profile of the mean temperature T along the q_2 axis ($p_2 = 0$) for the maximum energy, $E = 1/6$. It can be seen that the temperature on the islands of ordered motion is slightly higher than the temperature of the chaotic sea.
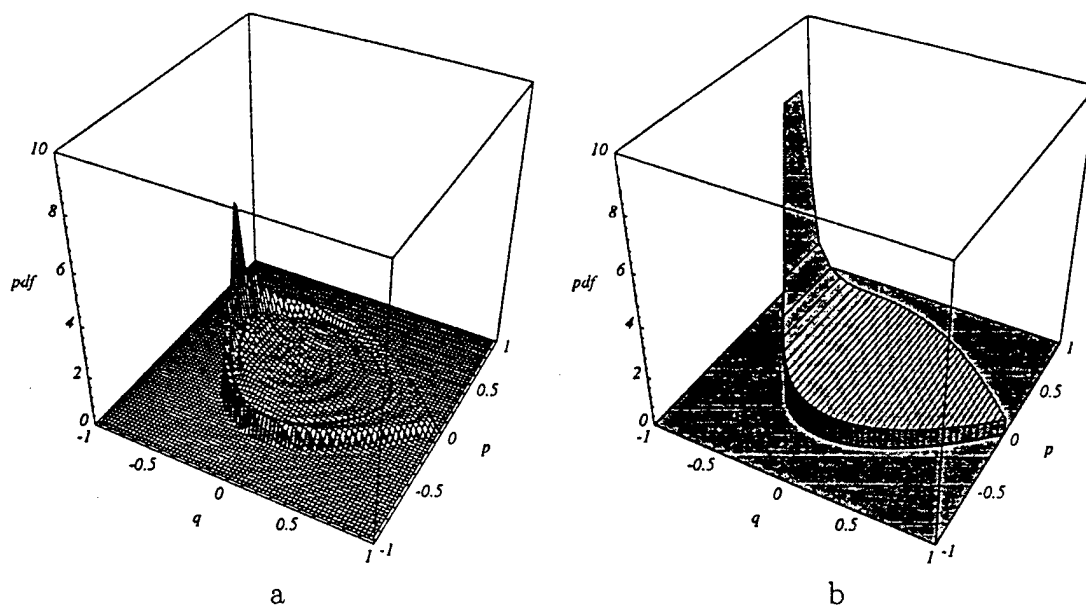
a   b

Fig. 3.8: Probability density functions of the second oscillator: a) numerical calculation; b) ergodic theory, formula (3.12)

Similar numerical experiments for lower energy levels show the same type of behavior as observed for the maximum energy. Figure 3.7b shows the mean temperature T of chaotic trajectories as well as the ergodic temperature T, calculated according to (3.6), versus energy E.

A surprising result of numerical simulations is that the equipartition law is approximately valid even for moderate and low energy levels for both chaotic and ordered trajectories, although in these cases the fraction of the phase space that is occupied by islands of ordered motion is quite large and the assumption of ergodicity is strongly violated. It is natural to assume that this is caused by coincidence of the linear frequencies of the two oscillators and the special form of the energy of interaction which results in resonance. In order to eliminate resonance effects, a modification of the Henón-Heiles system,

$$H = \frac{1}{2}p_1^2 + \frac{1}{2}\alpha p_2^2 + \frac{1}{2}q_1^2 + U_2(q_2) + q_1^2 q_2$$

was tested for different values of the distortion parameters α (such as $\alpha = 1.5$ or $\alpha = 2.5$). It turns out that for chaotic trajectories the equipartition law is valid with approximately the same accuracy as for Henón-Heiles oscillators if the size of the region of ordered motion is small compared to the size of the region of chaotic motion. The temperatures of trajectories on islands of ordered motion can differ essentially, no matter how big these islands are. That justifies the assumption that the validity of the equipartition law in the case of moderate energy vibrations of the Henón-Heiles oscillators is due to their resonant frequencies.
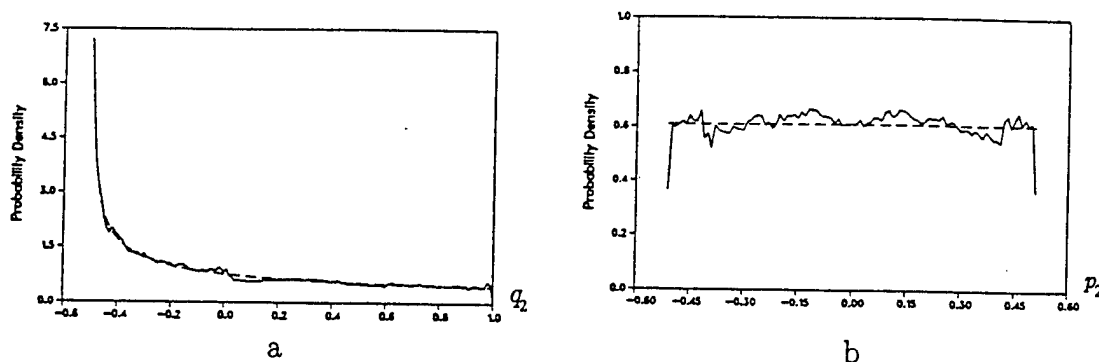
Fig. 3.9: Two-dimensional slices of the probability density function of the second oscillator for maximum energy, $E = 1/6$, a) along the line $p_2 = 0$, b) along the line $q_2 = -0.3$. Solid and dashed lines correspond to numerical simulation and ergodic theory, respectively.

Numerical simulations of probability density functions. A numerical probability density function was obtained by a simple bin-counting experiment, during which the trajectory of the system is calculated for a very long time interval. The probability of the event that the trajectory of the system is within a region A of its phase space is determined by the number of times the trajectory was observed to be within A divided by the total number of observations. Figure 3.8b shows the probability density function f_2 according to (3.12) for $E = 1/6$, while Fig. 3.8a depicts its numerically obtained counterpart. In order to compare the "ergodic prediction" (formula (3.12)) and numerical results, two-dimensional slices of the probability density functions for specific q or p are shown in Figs. 3.9a, 3.9b, 3.10a and 3.10b. Figure 3.9a shows the ergodic and numerical probability density functions of positions of the second oscillator at $p_2 = 0$ for the maximum energy level. The values of the real curve are captured very nicely by the ergodic theory; maximal error is below 3%. The small fluctuation should presumably level out for longer calculation times. However, there are some dents, like the one between $q_2 = 0$ and $q_2 = 0.2$ that are caused by islands of ordered motion (compare to Fig. 3.4d). Fig. 3.9b shows the probability density function of the momentum of the second oscillator for $q_2 = -0.3$. According to ergodic theory, the probability density function f_2 of the momentum is constant (see Fig. 3.8). The real probability density function obeys this property well at all points except at the two dents. Apparently, they are caused by two islands of ordered motion which are crossed by the line $q_2 = -0.3$ on Fig. 3.4d. Similar results for the probability density function of the first oscillator are shown in Figs. 3.10a and 3.10b.

For lower energies, these deviations from ergodic theory are larger. The probability density functions are shown in Figs. 3.11a and 3.11b for moderate energy, $E = 1/8$.

It is interesting that with respect to the real one, the ergodic curve is located in such a way as to provide similar momentum characteristics. In particular, the differences in the calculation of temperature do not exceed 3%.
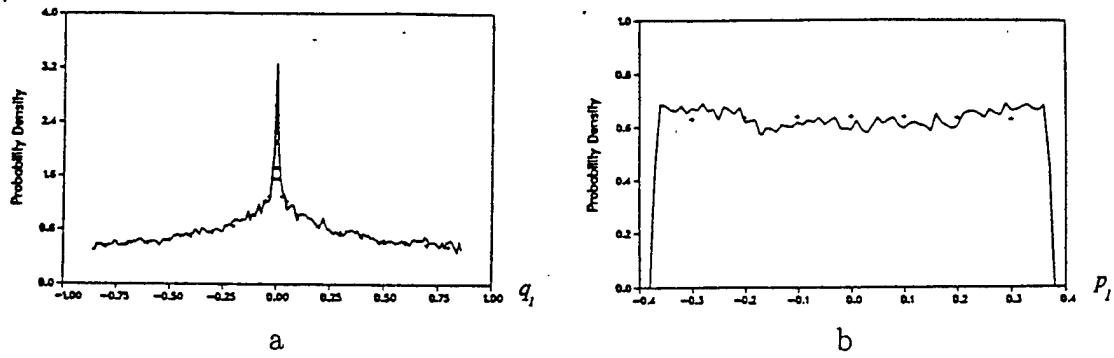
Fig. 3.10: Two-dimensional slices of the probability density function of the first oscillator for maximum energy level, $E = 1/6$: a) along the line $p_1 = 0$, b) along the line $q_1 = -0.5$. The solid line corresponds to numerical simulations, crosses to ergodic theory

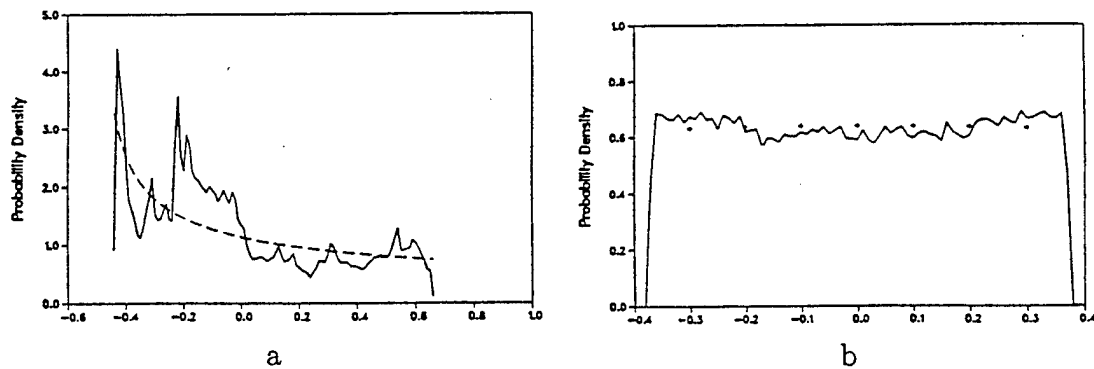Fig. 3.11: Probability density function of the second oscillator for moderate energy, $E = 0.125$: a) slice along the line $p_2 = 0$, b) slice along the line $q_2 = -0.5$. The solid line represents numerical simulations, the dashed line and crosses correspond to ergodic theory

3.2   Fermi-Pasta-Ulam problem

A few decades ago it was a common belief that systems with many degrees of freedom move chaotically. There was much indirect evidence, like Brownian motion of small heavy particles in fluids, but direct experiments were difficult. This is why, when a new powerful computer appeared at Los Alamos Lab in 1952 and challenging problems were solicited from physicists to show the abilities of the new machine, Fermi, Pasta and Ulam suggested studying numerically the dynamics of a multidimensional nonlinear system, and checking the validity of the equipartition law. The mechanical system chosen was a chain of mass particles connected by nonlinear springs (Fig. 3.12a). Computer simulations were run for 64 particles with two end particles clamped. It was expected that the system would evolve to equilibrium, and that the particle temperatures, $T_i = \langle \dot{q}_i^2/m \rangle$ (q_i is the coordinate of the ith particle), would become equal. Surprisingly, this was not observed. On the contrary, the system showed an ordered recurrent motion. This "paradox" is usually referred to as the FPU (Fermi-Pasta-Ulam) problem.

An understanding of the FPU problem was achieved by KAM (Kolmogorov-Arnold-Moser) theory. KAM theory studies the dynamics of slightly disturbed integrable Hamiltonian systems. Integrable systems are systems which can be transformed to a system of noninteracting oscillators by some change of generalized coordinates. That determines the geometrical structure of the phase flow for integrable systems. In the case of one oscillator, the trajectories are some closed curves in phase space. For a system of two oscillators, each trajectory γ_1 of the first oscillator and each trajectory γ_2 of the second oscillator form a curve on a two-dimensional torus in four-dimensional (p_1, q_1, p_2, q_2)-phase space. Choosing various initial data for γ_1, γ_2, one gets different curves on the torus. There is only one trajectory passing through a given point of the torus. The torus is determined by the curves γ_1 and γ_2, i.e. by two parameters, say, the initial values of the energies of each oscillator. Thus, there is a two-parameter family of tori. The tori are called invariant tori because each trajectory starting on some torus stays on this torus forever. The two-parameter family of two-dimensional invariant tori covers the whole four-dimensional phase space.

For a system of n oscillators, the invariant tori are n-dimensional. Each torus is determined by n parameters, the initial values of the energies of each oscillator. The n-parameter family of n-dimensional invariant tori covers $2n$-dimensional phase space.

KAM theory studies Hamiltonian systems with the Hamilton function

$$H = H_0(p, q) + \varepsilon H_1(p, q) \tag{3.17}$$

where $H_0(p, q)$ is the Hamilton function of an integrable system, εH_1 is a disturbing Hamilton function, and ε is small. Can the Hamiltonian system (3.17) be ergodic? KAM theory gives a negative answer. It turns out that the majority of invariant tori survive a small disturbance, they are just slightly deformed. Some of the invariant tori are destroyed by the disturbance and transformed into a chaotic sea. The volume of the chaotic sea (and destroyed tori) tends to zero for $\varepsilon \to 0$. The disturbed system

For definiteness, we focus on the chains with two fixed ends,

$$q_0 = 0, \quad q_{n+1} = 0 \tag{3.19}$$

So, the system has n degrees of freedom, $q_1,...,q_n$. The summation in (3.18) is carried over i from 1 to n, and conditions (3.19) are used to determine the energy of the end springs. The dynamical equations are

$$\dot{p}_i = \frac{1}{\Delta}\left[\Phi'\left(\frac{q_{i+1}-q_i}{\Delta}\right) - \Phi'\left(\frac{q_i-q_{i-1}}{\Delta}\right)\right], \quad \dot{q}_i = \frac{p_i}{m} \tag{3.20}$$

In linear theory, $\Phi = \frac{1}{2}C\gamma^2$, where C=constant. Fermi, Pasta and Ulam considered models where

$$\Phi = C\left(\frac{1}{2}\gamma^2 + \frac{\alpha}{3}\gamma^3 + \frac{\beta}{4}\gamma^4\right) \tag{3.21}$$

In the current literature, the cases $\alpha = 0$ and $\beta = 0$ are called the β-FPU model and the α-FPU model, respectively. In most cases we deal with the β-FPU model.

Strings. One of the ways in which chains can appear is a finite-dimensional truncation of one-dimensional continua. To be specific consider plane nonlinear vibrations of an elastic string of length l with the ends pinned (Fig. 3.12b). Let $w(t,x)$ be the lateral displacement of the string.

For moderate amplitudes, the kinetic and potential energies of the spring are

$$K = \int_0^l \frac{1}{2}\rho A w_t^2 dx \tag{3.22}$$

$$U = \int_0^l AE_Y\left[\frac{1}{2}\left(\overset{\circ}{\gamma} + \frac{1}{2}w_x^2\right)^2 + \frac{1}{2}h^2 w_{xx}^2\right]dx \tag{3.23}$$

Here ρ, A, $\overset{\circ}{\gamma}$ and E_Y are the mass density, cross-sectional area, initial longitudinal strain and Young's modulus, respectively; derivatives with respect to x and t are denoted by the corresponding indices. The string is supposed to be stretched, so $\overset{\circ}{\gamma} > 0$. The constant h is determined by the diameter and the shape of the cross-section and is proportional to $\sqrt{A}$. For a circular cross-section of diameter d and isotropic material, $h = d/4$. The two terms of (3.23) are the extension and the bending energies.

It is convenient to introduce dimensionless variables

$$y = \frac{x}{l}, \quad u = \frac{w}{l\sqrt{2\overset{\circ}{\gamma}}}, \quad \tau = \sqrt{\frac{E_Y\overset{\circ}{\gamma}}{\rho l^2}}\, t \tag{3.24}$$

With these variables, the dimensionless Lagrange functional becomes

$$L \equiv \frac{K-U}{2E_Y Al\overset{\circ}{\gamma}^2} = \int_0^1 \left(\frac{1}{2}u_\tau^2 - \frac{1}{2}u_y^2 - \frac{1}{4}u_y^4 - \frac{1}{2}\sigma u_{yy}^2\right)dy \tag{3.25}$$

The parameter $\sigma = h^2/\overset{\circ}{\gamma}l^2$ determines the dimensionless bending rigidity of the spring; it is small for a thin string with high initial tension and increases if the initial tension is released.

The string dynamics is governed by the equation

$$u_{\tau\tau} = \left(u_y + u_y^2 - \sigma u_{yyy}\right)_y \tag{3.26}$$

and the boundary conditions

$$u(\tau, 0) = u(\tau, 1) = 0 \,; \quad \sigma u_{yy}(\tau, 0) = \sigma u_{yy}(\tau, 1) = 0 \tag{3.27}$$

If $\sigma = 0$, the equations are considerably simplified:

$$u_{\tau\tau} = \left(u_y + u_y^3\right)_y \tag{3.28}$$

$$u(\tau, 0) = u(\tau, 1) = 0 \tag{3.29}$$

The corresponding Lagrange functional is

$$L = \int\limits_0^1 \left(\frac{1}{2}u_\tau^2 - \frac{1}{2}u_y^2 - \frac{1}{4}u_y^4\right) dy \tag{3.30}$$

To perform numerical simulations of string dynamics, one needs to develop a finite-dimensional truncation of the continuum model. There are many ways to do that. One way, the finite-difference truncation, yields the β-FPU model. In this case, the segment $[0, 1]$ is divided into equal pieces of length Δ, and the values q_i of the function u at the points $i\Delta$ are considered as independent degrees of freedom. The derivative u_y is approximated by $(q_{i+1} - q_i)/\Delta$ on the segment $[(i + 1)\Delta, i\Delta]$, while the integral

$$\int\limits_{i\Delta}^{(i+1)\Delta} u_\tau^2 dy$$

is approximated by $\dot{q}_{i+1}^2\Delta$. Then, the Lagrange functional (3.30) is transformed into the approximate Lagrange function

$$L = \sum_{i=1}^{N} \left(\frac{1}{2}\dot{q}_i^2 - \frac{1}{2}\left(\frac{q_{i+1} - q_i}{\Delta}\right)^2 - \frac{1}{4}\left(\frac{q_{i+1} - q_i}{\Delta}\right)^4\right)\Delta \tag{3.31}$$

The corresponding Hamilton function,

$$H = \sum_{i=1}^{N} \left(\frac{1}{2\Delta}p_i^2 + \frac{1}{2}\left(\frac{q_{i+1} - q_i}{\Delta}\right)^2 \Delta + \frac{1}{4}\left(\frac{q_{i+1} - q_i}{\Delta}\right)^4 \Delta\right) \tag{3.32}$$

is the Hamilton function of the β-FPU model with $\beta = 1$, and $C = m = \Delta$.

Rubber rods. Chains also appear as finite-difference truncations of other continuum models, in particular, nonlinear longitudinal vibrations of elastic isotropic rods.

In this case, the motion is characterized by one function, $u(t, x)$, the longitudinal displacement of the material point x. The Lagrange functional is

$$\int_0^l A\left(\frac{1}{2}\rho u_t^2 - U(u_x)\right)dx$$

where ρ and A are the mass density and cross-sectional area in the unloaded state, $u_x \equiv \partial u/\partial x$ is the strain, and U is the volume density of elastic energy. To have a pronounced nonlinearity, the strain u_x should be on the order of unity. There are materials (rubber and some polymers) which remain elastic at such high strains. For such a material at moderate strains

$$U = \frac{1}{2}E_Y\left(u_x^2 + \frac{1}{3}\alpha u_x^3 + \frac{1}{4}\beta u_x^4\right) \tag{3.33}$$

is an acceptable approximation. The finite-difference truncation of (3.33) yields the FPU chain model. For strains close to -1, approximation (3.33) fails because U has a singularity at strain value $u_x = -1$. This value corresponds to the collapse of the material segment to a point. The simplest model that takes into account the singularity at $u_x = -1$ is a Neo-Hookian material, which has the energy density

$$U = \frac{\mu}{2}u_x^2\frac{3 + u_x}{1 + u_x} \tag{3.34}$$

Here μ is the shear modulus for small strains. Model (3.34) describes the elastic properties of rubber-like materials quite well. Numerical simulations performed for the finite-difference truncation of model (3.34) show that it behaves qualitatively similarly to the β-FPU model, and we focus here only on the β-FPU model.

String vibrations in mode coordinates. Consider now the modes of continuum string vibrations. The linear eigenmodes of string vibrations are

$$u_k(y) = \sin \pi k y$$

Any function $u(\tau, y)$ can be presented as a Fourier series of eigen-modes,

$$u(\tau, y) = \sum_{k=1}^{\infty} a_k(\tau) \sin \pi k y \tag{3.35}$$

The functions $a_k(\tau)$ are the mode coordinates. To obtain dynamical equations for $a_k(\tau)$ one has to express the Lagrange functional in terms of a_k. Substituting (3.35) into (3.25), we have

$$2L = \sum_{k=1}^{\infty}\left[\frac{1}{2}\dot{a}_k^2 - \frac{1}{2}\left(1 + \sigma(\pi k)^2\right)(\pi k)^2 a_k^2\right] - \frac{\pi^4}{2}\sum_{k,l,m,n=1}^{\infty} klmn A_{klmn}a_k a_l a_m a_n \tag{3.36}$$

Here we use the following notation:

$$A_{klmn} = \int_0^1 \cos \pi k x \cos \pi l x \cos \pi m x \cos \pi n x \, dx =$$

$$= \frac{1}{8}[\delta(k + l - m - n) + \delta(k - l + m + n) +$$
$$+ \delta(k + l + m - n) + \delta(k + l - m + n) +$$
$$+ \delta(k - l + m - n) + \delta(k - l - m + n) +$$
$$+ \delta(k - l - m - n)] \tag{3.37}$$

The dot denotes derivative with respect to dimensionless time τ.

The Lagrange functional, and, henceforth, the equations, can be simplified by the change of unknown functions, $a_k \to b_k$:

$$b_k = \pi k a_k \tag{3.38}$$

In terms of b_k, the Lagrange functional is

$$L = K - U, \tag{3.39}$$

$$2K = \sum_{k=1}^{\infty} \frac{1}{2\pi^2 k^2} \dot{b}_k^2, \ 2U = \sum_{k=1}^{\infty} \frac{1}{2} \left(1 + \sigma\pi^2 k^2\right) b_k^2 - \frac{1}{2} \sum_{k,l,m,n=1}^{\infty} A_{klmn} b_k b_l b_m b_n$$

The corresponding equations of motion are

$$\frac{1}{(\pi k)^2} \ddot{b}_k = - \left(1 + \sigma(\pi k)^2\right) b_k^2 - 2 \sum_{k,l,m,n=1}^{\infty} A_{klmn} b_l b_m b_n \tag{3.40}$$

The coefficients A_{ijkl} characterize nonlinear interactions between modes. They are all on the order of unity. Note an important property of A_{ijkl} which follows from (3.37): if i is even and j, k, l are odd, then, since $\pm j, \pm k, \pm l$ are also odd, $A_{ijkl} = 0$. Similarly, $A_{ijkl} = 0$ if i is odd, and j, k, l are even. This means that even modes themselves cannot excite odd modes and vice versa. Even modes act on odd modes only if the latter have already been excited (b_i is not zero for at least one odd mode). The same is true for the influence of odd modes on the even ones. This suggest that there are invariant subspaces on the energy surface. They are formed by trajectories which start from even initial data and odd initial data. The existence of multidimensional invariant sets does not contradict ergodicity, but might increase the time needed to approach equipartition.

Thermodynamical and continuum limits. The laws of statistical mechanics are often derived in the so-called thermodynamical limit. This means that the number of particles and energy per unit volume are kept constant while the size of the system, the total energy and the the total number of particles, N, tend to infinity. In our case, this corresponds to a fixed particle distance Δ, and fixed energy per unit length, while the length of the chain, $l = N\Delta$, and the total energy, E, tend to infinity.

One might consider another limit, a continuum limit, where the length l and total energy E, are fixed, while the total number of particles, N, tends to infinity. In this case, the distance between neighboring particles, $\Delta = l/N$, tends to zero. In general, these two limits are different. However, the chain dynamics possesses the following remarkable property: the thermodynamical limit can be obtained from the continuum limit by scaling. Indeed, consider a finite-dimensional truncation of the

string dynamics (3.31). Let us make a change of variables $q_i \rightarrow u_i$, $q_i = u_i \Delta$, and simultaneously scale the time, $t \rightarrow \hat{\tau}$, $t = \hat{\tau} N$. Then the Lagrange function becomes

$$L = \frac{1}{N} \hat{L}, \tag{3.41}$$

$$\hat{L} = \sum_i \left[\frac{1}{2} \left(\frac{du_i}{d\hat{\tau}} \right)^2 - \frac{1}{2} (u_{i+1} - u)^2 - \frac{1}{4} (u_{i+1} - u)^4 \right] \tag{3.42}$$

The Lagrange function $\hat{L}$ corresponds to the dynamics of N particles with the spacing equal to 1. If $N \rightarrow \infty$, the length of the chain goes to infinity. Keeping the ratio of total energy to N constant corresponds, as follows from (3.41), to the continuum limit in q-variables. For definiteness, in discussing the case of large N we always deal with the continuum limit. The energy in the continuum limit corresponds to the "energy per particle" in the thermodynamical limit.

Note one more useful scaling. For the β-FPU model in u-variables,

$$\hat{L} = \sum_i \left[\frac{1}{2} \left(\frac{du_i}{d\hat{\tau}} \right)^2 - \frac{1}{2} (u_{i+1} - u)^2 - \frac{1}{4} \beta (u_{i+1} - u)^4 \right]$$

The change of variables $u_i \rightarrow \hat{u}_i$,

$$u_i = \frac{\hat{u}_i}{\sqrt{\beta}}$$

transforms the Lagrange function to

$$\hat{L} = \frac{1}{\beta} L_1, \quad L_1 = \sum_i \left[\frac{1}{2} \left(\frac{d\hat{u}_i}{d\hat{\tau}} \right)^2 - \frac{1}{2} (\hat{u}_{i+1} - \hat{u})^2 - \frac{1}{4} (\hat{u}_{i+1} - \hat{u})^4 \right],$$

where L_1 is the Lagrange function of the β-FPU model with $\beta = 1$ Hence, without loss of generality, one can set $\beta = 1$.

3.4   Energy threshold

Now we proceed to the discussion of experimental evidence for ergodicity of motion of chains and strings. The behavior of chains and finite-dimensional truncations of string dynamics are similar, therefore we focus mostly on string vibrations in mode coordinates. The simplest probe for ergodicity is equipartition of energy. One has to measure the temperatures of each mode,

$$T_k = \frac{1}{\theta} \int_0^\theta \frac{1}{2\pi^2 k^2} \dot{b}_k^2 dt \tag{3.43}$$

and determine whether they are equal. The time of observation should be long enough to warrant the convergence of the right-hand side of (3.43) to a limit value.
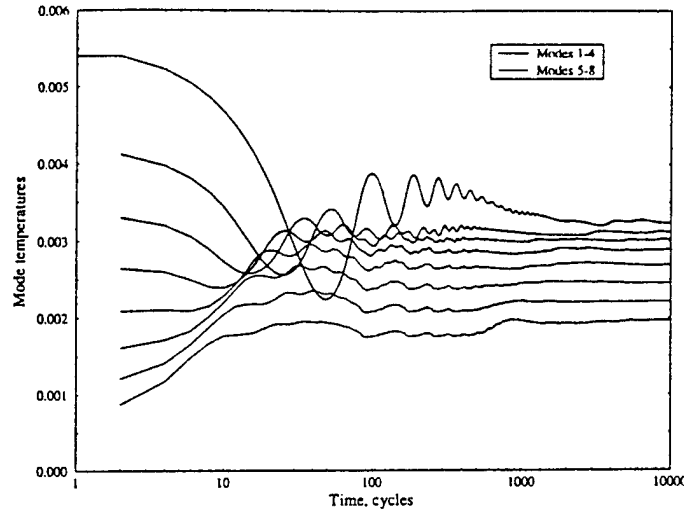
Fig. 3.13: Typical evolution of mode temperatures in time for moderate energies $E = 0.02$ in an 8-mode system.

A typical dependence of temperatures on the time of observation is shown in Fig. 3.13 for an 8-mode system. Time is measured in "cycles", the period of the slowest mode, which is 2 (in terms of dimensionless time τ). Initially, all modes were excited in such a way that amplitudes and velocities were decaying with the mode number. The total energy of initial excitation is 0.02. It seems that after about 5000 cycles all temperatures approach their limit values. These values differ. Other runs for the same value of initial energy show similar behavior. This suggests that the system is not ergodic for $E = 0.02$.

For higher values of energy, $E = 0.095$, temperatures show a clear tendency to converge to a single value (Fig. 3.14). After 1000 cycles, the difference in temperatures is on the order of 10%; after 10000 cycles it does not exceed 2%.

Do we really observe the absence of equipartition for $E = 0.02$? Could it be that temperatures eventually converge to a common value after a longer time of observation? It is not clear at present, and computer experiments can hardly answer these questions. All the conclusions we are going to make are based on the assumption that the results of the observations made for the time of about $10^4 - 10^5$ periods of the slowest mode stay the same for an infinite time of observation.

To quantify the degree of equipartition, one can use the following characteristic:

$$C^* = \frac{\left[\sum_{i=1}^{N} T_i\right]^2}{\sum_{i=1}^{N} T_i^2} \tag{3.44}$$

It has a simple meaning. If only one mode is excited, say $T_1 \neq 0$, $T_2 = \ldots = T_N = 0$, then $C^* = 1$. If all modes are excited and equipartition holds, then $T_1 = T_2 = \ldots = T_N$, and $C^* = N$. Thus, C^* characterizes the number of degrees of freedom involved in the motion. The maximum value of C^* is equal to N. This value is reached if and only if equipartition holds. Hence, C^* is a measure of equipartition as well. To compare the motion of different systems, it is convenient to normalize C^* and consider
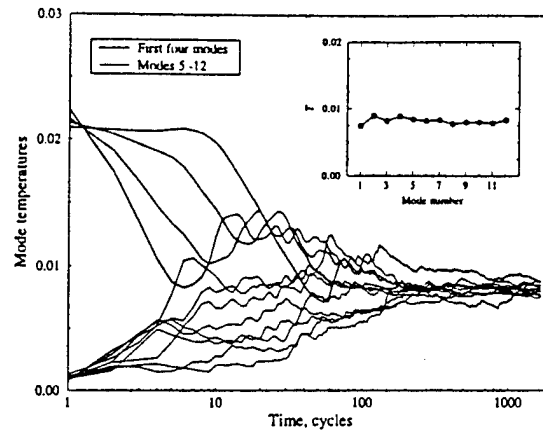
Fig. 3.14: Typical evolution of mode temperatures in time for a high energy of excitation, $E = 0.095$ in a 12-mode system. The insert shows the temperature distribution over the modes

the number $C = C^*/N$, which represents the relative amount of effectively excited degrees of freedom. The dependence of C on time shows the process of involving in the motion the additional degrees of freedom. If equipartition holds, $C = 1$.

A typical dependence of C on time is shown in Fig. 3.15. In this figure, the results are presented for four runs with duration of 1,500 periods of the slowest mode (or cycles); initially, the potential energy was evenly distributed among the first four modes, while all velocities were zero; the total number of modes is 12. The values of the energy are 0.002, 0.01, 0.05 and 0.095.

Figure 3.15 shows that the system provided with higher energy reaches equipartition very fast, within a few hundred cycles. The less energy is supplied to the system initially, the longer it takes to reach equipartition. When the energy is small, equipartition does not seem to be reached. The insert in the figure shows the temperature spectra at the end of the runs. In the case of $E = 0.002$, the temperatures of the first and second modes are by more than an order of magnitude higher than those of modes 7-12, showing no equipartition. The next figure (3.16) suggests that transition to equipartition is, to some extent, a threshold-like phenomenon. In this figure, values of C are plotted for the 12-mode system after 1000 cycles. Each point corresponds to some initial data. It shows that for $E \leq 0.05$, all values of C are possible for each value of energy. However, for $E \geq 0.05$, $C \approx 1$ for all runs made.

The value of energy $E_c = 0.05$ is the critical value of energy at which the transition to equipartition occurs. Of course, in reality, the qualitative change of the character of motion occurs in some range of values of energy, and the particular value $E_c = 0.05$ is a rough location of this range.

Above the energy threshold, the trajectories exponentially diverge and numerical errors grow exponentially. The numerical trajectory can go far away from the true trajectory with the same initial conditions. A discrepancy appears between the numerical results and the real dynamics of the system. It is natural to expect, however, that, although the trajectories of the "numerical dynamical system" may be far from the trajectories of the original dynamical system, the statistical characteristics are
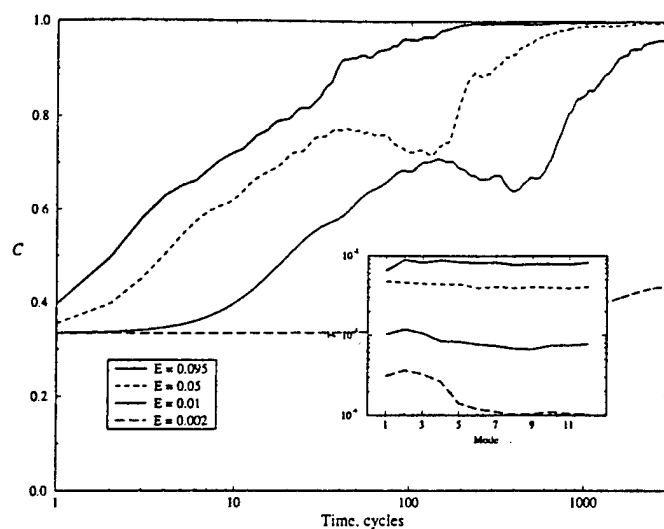
Fig. 3.15: Typical dependence of the number of effectively excited degrees of freedom on time for four levels of energy. The insert shows the temperature distribution over the modes for these values of energy
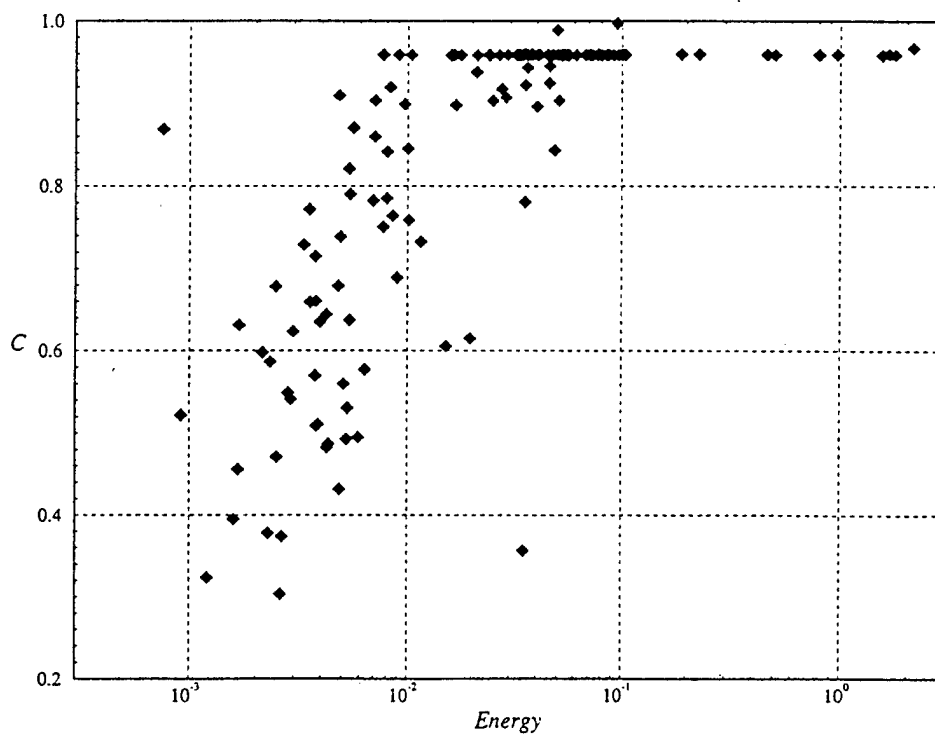

Fig. 3.16: Determination of the energy threshold. Each point corresponds to some choice of initial conditions. For energies exceeding 0.05, equipartition is practically exact
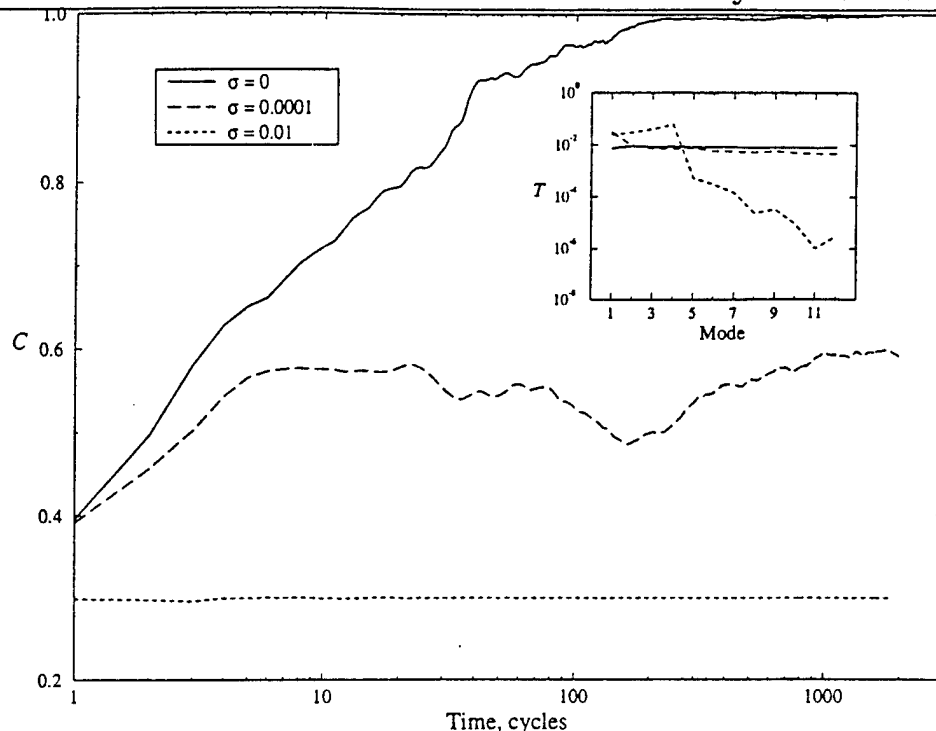
Fig. 3.17: Dependence of effective numbers of exited degrees of freedom on σ. The insert shows final temperature distribution

predicted correctly, and the above-mentioned numerical results can be applied to the original dynamical system. It was proved ([4], [37]) that a numerical (or noisy) trajectory will stay close to some true trajectory (with, maybe, different initial data) for all time if the system is uniformly hyperbolic. Similar results were obtained for some nonuniformly hyperbolic systems in [89].

Probes of equipartition are the roughest tests for ergodicity. It is much more convincing of a test to compare probability density functions predicted by ergodic theory with numerical results. These comparisons have been conducted in [148] and support the expected ergodic character of motion above the energy threshold.

3.5   Role of mode resonances

The value of the energy threshold depends on the number of degrees of freedom and the characteristics of bending rigidity, σ. It turns out that the dependence on bending rigidity is quite strong. This can be explained by the ease of energy transfer between modes for $\sigma = 0$ due to commensuration of natural linear frequencies. Indeed, let the first mode be excited initially. The first mode has frequency $\overset{o}{\omega}_1 = \pi$. The coefficient $A_{3111} \neq 0$. Therefore, the spectrum of the elastic interaction force $A_{3111}b_1^3$ contains the frequency $3\overset{o}{\omega}_1 = 3\pi$ which is the linear eigenfrequency of the third mode. Hence, vibrations of the third mode are resonant and are easily developed. Considering the fifth mode we note that the coefficient A_{5311} is no equal to zero. The spectrum of the interaction force, $A_{5311}b_3b_1^2$, acting on the fifth mode contains the frequency 5π,

which is its eigenfrequency. Thus, the fifth mode also goes into a resonance regime. In the same way, other interaction forces have in their spectra resonant frequencies, and energy easily flows from one mode to another. If $\sigma \neq 0$, the natural frequencies are detuned and energy transfer is impeded.

This hypothetical picture of string vibrations is supported by numerical simulations. Figure 3.17 shows the dependence of C on time for a 12-mode system for the following values of σ $0, 10^{-4}$ and 10^{-2}, and the same value of energy of initial excitation. The insert shows the terminal temperature spectra. For $\sigma = 0$, energy is equipartitioned among all modes. Detuning of linear oscillators by adding small $\sigma = 10^{-4}$, perhaps, increases the energy threshold, and vibrations become nonergodic. For $\sigma = 10^{-2}$, further growth of the energy threshold occurs, and the number of initially excited degrees of freedom does not change.

3.6   Massless approximation

Experiments show that, usually, only a few degrees of freedom are effectively excited in vibrating elastic structures which possess, in principle, infinitely many of them. In part, this may be caused by friction. For example, the viscous friction force acting on the kth mode is proportional to μk^2, where μ is the friction coefficient. Thus, there is some number k_0 of modes with non-negligible amplitudes, while all modes with higher numbers are damped. The number of undamped modes, k_0, depends on μ and grows if $\mu \rightarrow 0$. There is also another reason for low dimensionality which is not related to dissipation. Consider expression (3.39) for the Lagrange function. The coefficients of the interaction energy, A_{ijkl}, are on the order of unity. The rigidities $1 + \sigma \pi^2 k^2$ are on the order of unity for $\sigma = 0$, and grow as k^2 for $\sigma \neq 0$. "Masses" of modes, the coefficients in the expression for kinetic energy decay as k^{-2}. If $\dot{b}_k$ is on the order of b_k, then kinetic energy of kth mode can be neglected in comparison with elastic energy of this mode for large k, and the problem of the determination of b_k becomes a static problem. In this case, all degrees of freedom can be separated into two categories: leading degrees of freedom with low k, $k \leq k_0$, and driven degrees of freedom with large k, $k > k_0$. Driven degrees of freedom follow the leading ones. The dependence of driven degrees of freedom on the leading ones is determined from the static equations

$$\frac{\partial U}{\partial b_k} = 0, \quad k > k_0 \tag{3.45}$$

Low-dimensional dynamics is governed by Hamiltonian equations with the effective Lagrange function

$$L_{eff} = K - U_{eff}, \quad 2K_{eff} = \sum_{k=1}^{k_0} \frac{1}{2\pi^2 k^2} \dot{b}_k^2, \quad 2U_{eff}(b_1, ... b_{k_0}) = \min_{b_{k_0+1}, b_{k_0+2}, ...} U \tag{3.46}$$

The number of leading modes, k_0, is determined by a desirable accuracy.

There is an obstacle for this mechanism of low-dimensionality to work. If higher modes are in resonance with low modes then the kinetic energy of high modes is of the same order as the elastic energy and cannot be neglected. If resonances are
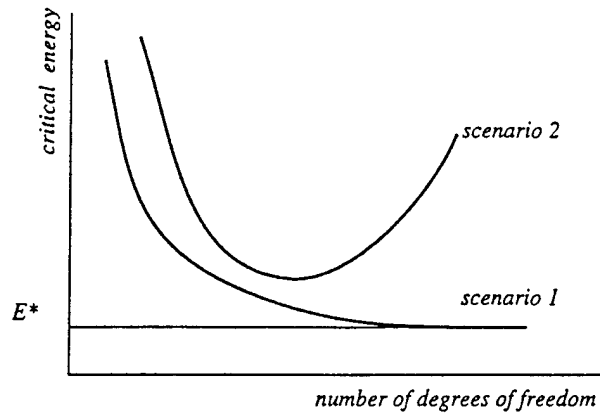
Fig. 3.18: Two scenarios for the dependence of the critical energy on the number of degrees of freedom

absent and excitation energy is below the energy threshold, the vibrations are really low-dimensional. The reader is referred to [21] for further details.

3.7 Possible scenarios of nonlinear vibrations

To discuss the behavior of the elastic continuum, one may consider the limit $N \to \infty$ for a finite-dimensional truncation (for example, a mode truncation) of continuum equations. The character of vibrations depends crucially on the dependence of energy threshold E_c on N for large N. Numerical simulations conducted as $N \leq 128$ indicate that E_c decreases when N grows. In the range $10 \leq N \leq 130$, the critical energy behaves approximately as $1/N$. It is not known what happens for larger N. Logically, there are four possible situations: if $N \to \infty$, then either $E_c \to 0$ or $E_c \to E^* = $ const or $E_c \to \infty$ or the limit of E_c does not exist. The first case, where the critical energy E_c goes to zero for $N \to \infty$, is probably not realized because one would observe chaotic continuum motion for any, even a very small, energy of excitation. This would contradict the infinite-dimensional version of KAM theory, which is likely to be valid for elastic continua. Two other cases, where E_c tends to some finite limit E^* and $E_c \to \infty$ for $N \to \infty$, are schematically shown in Fig. 3.18. They correspond to two qualitatively different behaviors of continua which we refer to as scenario 1 and scenario 2.

Scenario 1 (*Self-dissipation*). This is the case of the existence of the finite limit for critical energy. The major features of the dynamics of continua in this case seem to be the following. If the energy of initial excitation E is less than E^*, then nothing special occurs. The bulk of studies of linear and nonlinear elastic vibrations pertains to this case. However, if the energy of excitation exceeds E^*, then the continuum shows a very peculiar behavior. For definiteness, let only a few modes be excited initially. In the course of the motion, energy is redistributed over all modes in a such a way as to reach equipartition. Since an infinite number of modes is involved in the motion, the energy of each mode is equal to zero at the final stage. So, one would observe a process with an increasing number of excited modes, in which the energy of each
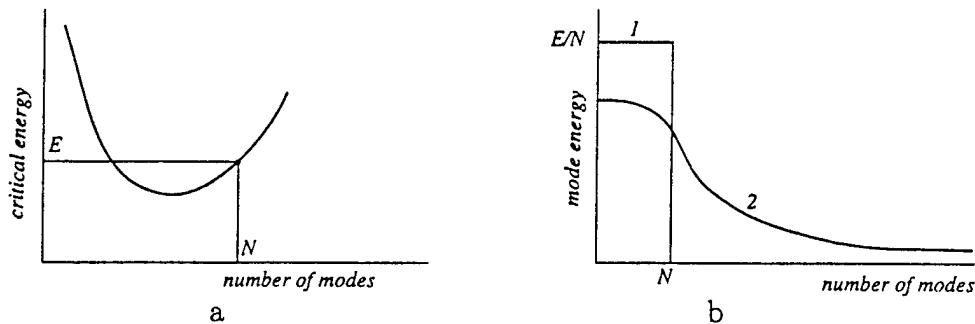
Fig. 3.19: Truncation of the continuum for scenario 2: (a) choice of initial energy, (b) energy spectrum for continuum vibrations (2) and truncation (1)

mode eventually tends to zero, while the total energy is conserved. Since the energy of each particular mode tends to zero, the displacement goes to zero. Derivatives of displacements remain finite due to conservation of energy. Therefore, displacements are getting more and more nonsmooth. One might call this case "self-dissipation" due to the decay of displacements in time. Remember that the system does not have a "built-in" dissipation.

Scenario 2 (*Universal Spectrum*). In this case, the energy threshold tends to infinity for $N \to \infty$. Therefore, the laws of statistical mechanics are not valid for any, even a very high, energy of excitation. However, one can speculate on a possibility of other "universal laws." Let the initial energy be E, and let this value correspond to the number N on the graph the "critical energy vs. number of degrees of freedom" (Fig. 3.19a). Consider an excitation of the continuum where only the first N modes are excited initially. For N-degrees-of-freedom truncation of the continuum, the motion would be approximately ergodic while the energy would be equally distributed over modes (Fig. 3.19b, line 1).

In the continuum, other modes take energy from the first N modes. Therefore, for a continuum the energy spectrum should have the form of line 2 in Fig. 3.19b. Note that the energy transfer from low to high modes may be a fast precess as the development of shock waves during a finite time indicates.

It is natural to assume that the spectrum 2 is universal in the following sense: it is the same for any choice of initial excitation of the first N modes possessing the same energy E. It is interesting that the spectrum 2 in Fig. 3.19b looks qualitatively the same as Planck's spectrum for quantum oscillators: high-frequency oscillations are frozen.

None of the numerical experiments for chains show the growth of critical energy for large N and the feasibility of scenario 2. This relates, probably, to the fact that only chains with the nearest neighbor interaction have been considered so far. These chains do not have any characteristic dimension (in the limit $N \to \infty$), while the minimum point on the plot in Fig. 3.18 is determined by some characteristic length. Continua with higher space derivatives may provide the necessary additional parameter with a dimension of length.

3.8   Miscellaneous

In this section the facts which were useful in numerical experiments for chains and strings are summarized.

Normal modes of chains. Let the energy of the chain vibrations be small. Then, the nonlinear terms are negligible, $\Phi(\gamma) = \frac{1}{2} C\gamma^2$, and the equations of motion (3.20) become

$$m\ddot{q}_s = \frac{C}{\Delta^2}(q_{s+1} - 2q_s + q_{s-1}) \tag{3.47}$$

Here $s = 1,...,n$ and $q_0 = q_{n+1} = 0$. If $q(t,x)$ is a smooth function and $q(t, s\Delta) \equiv q_s(t)$, $m = \rho\Delta$, $C = c^2\Delta$, then, for $\Delta \to 0$, equation (3.47) transforms to the wave equation

$$\rho\frac{\partial^2 q(t,x)}{\partial t^2} = c^2\frac{\partial^2 q(t,x)}{\partial x^2}$$

as it should.

Our next goal is to find a coordinate transformation such that the chain becomes a system of noninteracting oscillators. It is convenient to extend the chain and introduce q_s with negative s, setting $q_{-1} = -q_1,...,q_{-n} = -q_n$, $q_{-n-1} = -q_{n+1}$. Then, the dynamics of the original chain is equivalent to the dynamics of a chain of $N = 2n + 2$ particles with fixed ends and antisymmetric motion in space, $q_s = -q_{-s}$.

Consider traveling wave solutions of equations (3.47)

$$q_s = e^{i(s\lambda - \omega t)} \tag{3.48}$$

where s and ω are some parameters. Substituting (3.48) into (3.47), we see that (3.48) is a solution of the dynamical equations if and only if λ and ω are linked by the dispersion relation

$$m\omega^2 = \frac{2C}{\Delta^2}(1 - \cos\lambda) \tag{3.49}$$

If $\Delta \to 0$ and $\lambda = k\Delta$, $m = \rho\Delta$, $C = c\Delta$, the dispersion relation for chains transforms into the dispersion relation for the wave equation,

$$\rho\omega^2 = c^2 k^2$$

For each couple (ω, λ) which satisfies the dispersion relation (3.49), the couple $(\omega, -\lambda)$ also satisfies the dispersion relation. Thus, the functions

$$e^{i(s\lambda - \omega t)} - e^{i(-s\lambda - \omega t)} = 2ie^{-i\omega t}\sin s\lambda \tag{3.50}$$

are the solutions of the dynamical equations.

Consider the solutions of the form (3.50) which obey boundary conditions $q_0 = 0$, $q_{n+1} = 0$. Since $\sin(n+1)\lambda = 0$, there are n admissible λ,

$$\lambda_1 = \frac{\pi}{n+1}, \quad \lambda_2 = \frac{2\pi}{n+1}, \quad ..., \quad \lambda_n = \frac{n\pi}{n+1}$$

and the corresponding n modes of vibration,

$$\varphi_1(s) = \sin\frac{\pi s}{n+1}, \quad \varphi_2(s) = \sin\frac{2\pi s}{n+1}, \quad ..., \varphi_n(s) = \sin\frac{n\pi s}{n+1} \tag{3.51}$$

The remarkable feature of the functions $\varphi_1(s)$, ..., $\varphi_n(s)$ is that any vibration of the chain, i.e. the set $q_1(t),...,q_n(t)$, can be presented as a linear combination of mode vibrations,

$$q_s(t) = \sum_{k=1}^{n} \hat{q}_k(t)\varphi_k(s) \tag{3.52}$$

and there is a one-to-one correspondence $q_s \Leftrightarrow \hat{q}_k$. Moreover, in mode coordinates $\hat{q}_k$ the chain splits into a system of noninteracting oscillators. The frequencies of the oscillators are determined by the dispersion relation (3.49),

$$m\omega_k^2 = \frac{2C}{\Delta^2}\left(1 - \cos\lambda_k\right) = \frac{2C}{\Delta^2}\left(1 - \cos\frac{\pi k}{n+1}\right) = \frac{4C}{\Delta^2}\sin^2\frac{\pi k}{2(n+1)} \tag{3.53}$$

Derivation of these properties is based on the discrete Fourier transform, the essential facts about which are reviewed in the next subsection.

Discrete Fourier transform. Consider N complex numbers $\hat{q}_0, ..., \hat{q}_{N-1}$ and sums

$$q_k = \sum_{m=0}^{N-1} \hat{q}_m e^{2\pi i m k/N}, \quad k = 1, ..., N \tag{3.54}$$

Let us multiply (3.54) by $e^{-2\pi i s k/N}$ and take the sum over k. We get

$$\sum_{k=1}^{N} q_k e^{-2\pi i s k/N} = \sum_{m=0}^{N-1} \hat{q}_m \sum_{k=1}^{N} e^{2\pi i (m-s)k/N} \tag{3.55}$$

The sum on the right hand side of (3.55) can be simplified by the means of the following identity: for integer r, $0 \le r \le N - 1$,

$$\sum_{k=1}^{N} e^{2\pi i r k/N} = N\delta(r) \tag{3.56}$$

where $\delta(r) = 0$ if $r \ne 0$ and $\delta(0) = 1$. Indeed, $e^{2\pi i r/N} + e^{2\cdot 2\pi i r/N} + ... + e^{N\cdot 2\pi i r/N} = \alpha + \alpha^2 + ... + \alpha^N$ where $\alpha = e^{2\pi i r/N}$. Since

$$1 + \alpha + \alpha^2 + ... + \alpha^{N-1} = \frac{1 - \alpha^N}{1 - \alpha} \tag{3.57}$$

and $\alpha^N = e^{2\pi i r} = 1$, the sum (3.57) is equal to zero for any $\alpha \ne 1$, i.e. for any $r \ne 0$. For $r = 0$, $\alpha = 1$, the sum is equal to N. So, (3.56) is true.

The proof shows that identity (3.56) holds for any number r if the function $\delta(r)$ is replaced by a periodic function $\delta_N(r)$, with the period N: $\delta_N(r) = 0$ if $r \ne \pm Nk$, k is any integer, $\delta_N(r) = 1$ if $r = \pm Nk$,

$$\sum_{k=1}^{N} e^{2\pi i r k/N} = N\delta_N(r) \tag{3.58}$$

Return now to (3.55). The last sum in (3.55) can be calculated using identity (3.56). Since $m < N$ and $s < N$, $|m - s| < N$, and the sum is equal to $N\delta(m - s)$. Thus,

$$\hat{q}_m = \frac{1}{N}\sum_{k=1}^{N} q_k e^{-2\pi i s k/N} \tag{3.59}$$

The transform of $\hat{q}_m$ to q_k in (3.54) is called a discrete Fourier transform. Formula (3.59) shows that the discrete Fourier transform is reversible.

The discrete Fourier transform has two properties which make it useful for our purposes:

$$\sum_{k=1}^{N} q_k q_k^* = N \sum_{m=0}^{N-1} \hat{q}_m \hat{q}_m^*$$ (3.60)

and

$$\sum_{k=1}^{N} (q_k - q_{k-1})(q^*_k - q^*_{k-1}) = 4N \sum_{m=0}^{N-1} \sin^2 \frac{\pi m}{N} \hat{q}_m \hat{q}_m^*$$ (3.61)

Here a star denotes the complex conjugate. Formulas (3.60) and (3.61) can be checked by direct inspection,

$$\sum_{k=1}^{N} q_k q^*_k = \sum_{k=1}^{N} \sum_{m=0}^{N-1} \hat{q}_m e^{2\pi imk/N} \sum_{s=0}^{N-1} \hat{q}_s^* e^{-2\pi isk/N} = \sum_{m=0}^{N-1} \sum_{s=0}^{N-1} \hat{q}_m \hat{q}_s^* \sum_{k=1}^{N} e^{2\pi i(m-s)k/N} =$$

$$= \sum_{m=0}^{N-1} \sum_{s=0}^{N-1} \hat{q}_m \hat{q}_s^* N\delta(m-s) = N \sum_{m=0}^{N-1} \hat{q}_m \hat{q}_m^*$$ (3.62)

and

$$\sum_{k=1}^{N} (q_k - q_{k-1})(q^*_k - q^*_{k-1}) =$$

$$\sum_{k=1}^{N} \sum_{m=0}^{N-1} \hat{q}_m (e^{2\pi imk/N} - e^{2\pi im(k-1)/N}) \sum_{s=0}^{N-1} \hat{q}_s^* (e^{-2\pi isk/N} - e^{-2\pi is(k-1)/N}) =$$

$$= \sum_{m=0}^{N-1} \sum_{s=0}^{N-1} \hat{q}_m (1 - e^{-2\pi im/N}) \hat{q}_s^* (1 - e^{2\pi is/N}) \sum_{k=1}^{N} e^{2\pi i(m-s)k/N} =$$

$$= \sum_{m=0}^{N-1} \sum_{s=0}^{N-1} \hat{q}_m e^{-\pi im/N} (e^{\pi imN} - e^{-\pi im/N}) \hat{q}_s^* e^{\pi is/N} (e^{-\pi is/N} - e^{\pi is/N}) N\delta(m-s) =$$

$$= 4N \sum_{m=0}^{N-1} \sin^2 \frac{\pi m}{N} \hat{q}_m \hat{q}_m^*$$ (3.63)

Note that (3.54) and (3.59) stay valid if shifts in the numbering of q_k and $\hat{q}_m$ are made: k may take values $1+l_1, ..., N+l_1$ while m may have values $l_2, l_2+1, ..., N+l_2-1$ for any integers l_1, l_2. Equations (3.60) and (3.61) also admit such shift as one can check writing the chain of equalities (3.62) and (3.63).

Applying the discrete Fourier transform to chain vibrations, we choose k and m taking values $-n, -n+1, ..., n, n+1$, and $N = 2(n+1)$. We have

$$q_k = \sum_{m=-n}^{n+1} \hat{q}_m e^{2\pi imk/N}, \quad \hat{q}_m = \frac{1}{N} \sum_{k=-n}^{n+1} q_k e^{-2\pi imk/N}$$ (3.64)

Actually, the summation in (3.64) should be conducted up to n: by the condition $q_{n+1} = 0$, while $\hat{q}_{n+1} = 0$ due to the antisymmetry of q_k $q_{-k} = -q_k$:

$$\hat{q}_{n+1} = \frac{1}{N} \sum_{k=-n}^{n} q_k e^{-2\pi i(n+1)k/N} = \frac{1}{N} \sum_{k=-n}^{n} q_k e^{-\pi ik} =$$

$$= \frac{1}{N} \sum_{k=1}^{n} q_k (e^{-\pi i k} - e^{\pi i k}) = -\frac{2i}{N} \sum_{k=-n}^{n} q_k \sin \pi k = 0$$

It follows from (3.64) that $\hat{q}_m$ are pure imaginary and antisymmetric due to the antisymmetry of q_k:

$$\hat{q}^{*}_m = -\hat{q}_m, \quad \hat{q}_m = -\hat{q}_{-m} \tag{3.65}$$

If one sets $\hat{q}_m = -\frac{1}{2} i \tilde{q}_m$, the Fourier transform (3.64) can be written in real variables as

$$q_k = \sum_{m=1}^{n} \tilde{q}_m \sin \frac{\pi m k}{n+1}, \quad k = 1, ..., n$$

$$\tilde{q} = \frac{4}{N} \sum_{m=1}^{n} q_k \sin \frac{\pi m k}{n+1}, \quad m = 1, ..., n \tag{3.66}$$

However, it is usually more convenient to work with the complex form (3.64).

The identities (3.60) and(3.61) take the form

$$\sum_{k=1}^{n} q_k^2 = N \sum_{s=1}^{n} |\hat{q}_s|^2, \quad \sum_{k=1}^{n+1} (q_k - q_{k-1})^2 = 4N \sum_{m=1}^{n} \sin^2 \frac{\pi m}{N} |\hat{q}_m|^2 \tag{3.67}$$

Normal modes of chains (continued). Comparing (3.66) with (3.51) and (3.52), we see that in the problem under consideration, the discrete Fourier transform is identical to the transformation to mode coordinates. Let us derive the energy expression in mode coordinates. Since in translational coordinates q_k

$$K = \frac{1}{2} \sum_{k=1}^{n} m \dot{q}_k^2, \quad U = \frac{1}{2} \sum_{k=1}^{n} C \left(\frac{q_k - q_{k-1}}{\Delta} \right)^2,$$

using the properties (3.67) of the discrete Fourier transform, in mode coordinates we obtain

$$K = \frac{N}{2} m \sum_{s=1}^{n} \left| \frac{d\hat{q}_s}{dt} \right|^2 = \frac{mN}{8} \sum_{s=1}^{n} \left| \frac{d\tilde{q}_s}{dt} \right|^2, \quad U = \frac{C}{8\Delta^2} 4N \sum_{s=1}^{n} \sin^2 \frac{\pi s}{2(n+1)} \tilde{q}_s^2 \tag{3.68}$$

So, in mode coordinates the chain is a set of noninteracting oscillators with natural frequencies

$$\omega_s = \sqrt{\frac{C}{m\Delta^2}} \, 2 \sin \frac{\pi s}{2(n+1)} \tag{3.69}$$

as claimed.

Interaction energy in terms of translational coordinates. We constructed two finite-dimensional truncations for string dynamics: truncation (3.31) in terms of translational coordinates, q_i, and truncation (3.39) in terms of mode coordinates. Each one has certain advantages. In translational coordinates, interactions are local: each particle is affected only by its nearest neighbors. This makes numerical simulations very effective: one needs to perform $O(N^2)$ numerical operations per time step. In mode coordinates, modes do not interact at all in a linear regime, but for high energy of excitation each mode affects the motion of almost all others. An unpleasant

consequence is that the number of numerical operations per time step is on the order of $O(N^4)$. On the other hand, there is a considerable pay off in the use of mode coordinates: the mechanisms of vibrations are seen more clearly. The increase of the number of numerical operations is compensated to some extent by a decrease in the number of modes to be considered. To have the same accuracy of the approximation of the continuum motion, one needs 10-20 nodes per the shortest wave length which causes the number of degrees of freedom in translational coordinates to be increased accordingly. Note also that incorporation of bending rigidity is much simpler in mode coordinates.

Fortunately, for string vibrations it is possible to develop a form of dynamical equations which combines the advantages of both truncations. This form is based on the following identity.

Let q_k and $\hat{q}_m$ be related by the Fourier transformation (3.64). Note that q_k are periodic with period N due to (3.64). In particular,

$$q_{n+1} = q_{-n-1} \quad \text{and} \quad q_{n+2} = q_{-n} \tag{3.70}$$

Consider the sum

$$\sum_{k=-n}^{n+1} (q_{k+1} - q_k)^2 (q^*_{k+1} - q^*_k)^2 \tag{3.71}$$

in the general setting when q_k may be complex and not necessarily antisymmetric ($q_k \neq -q_{-k}$). In the calculation of the end terms of the sum, the periodicity condition (3.70) is imposed. The following identity holds for this sum:

$$\sum_{k=-n}^{n+1} (q_{k+1} - q_k)^2 (q^*_{k+1} - q^*_k)^2 =$$

$$8N \sum_{m,r,s,t=-n}^{n+1} \delta(m+r-t-s) \sin\frac{\pi m}{N} \sin\frac{\pi r}{N} \sin\frac{\pi s}{N} \sin\frac{\pi t}{N} \hat{q}_m \hat{q}_r \hat{q}_s \hat{q}_t \tag{3.72}$$

Before proving this identity, let us discuss its consequences. Let q_k be real and antisymmetric, and $q_{n+1} = 0$, while $\hat{q}_k^*$ is purely imaginary and antisymmetric, and $\hat{q}_{n+1} = 0$. We introduce real variables

$$b_m = 2i\hat{q}_m \sin\frac{\pi m}{N} \tag{3.73}$$

Then, identity (3.72) becomes

$$2\sum_{k=0}^{n} (q_{k+1} - q_k)^4 = N \sum_{m,r,s,t=-n}^{n} \delta(m+r-s-t) b_m b_r b_s b_t \tag{3.74}$$

The variables b_m are symmetric: $b_{-m} = b_m$. Thus, (3.74) is transformed into

$$2\sum_{k=0}^{n} (q_k - q_{k-1})^4 = 16N \sum_{m,r,s,t=1}^{n} A_{mrst} b_m b_r b_s b_t$$

where A_{mrst} are the coefficients (3.37). Finally,

$$\Phi = \frac{1}{4} \sum_{m,r,s,t=1}^{n} A_{mrst} b_m b_r b_s b_t = \frac{1}{32N} \sum_{k=0}^{n} (q_{k+1} - q_k)^4 \qquad (3.75)$$

Here, q_k related to b_m by

$$q_k = \sum_{m=-n}^{n} \hat{q}_m e^{2\pi imk/N} = \sum_{m=1}^{n} \hat{q}_m \left(e^{2\pi imk/N} - e^{-2\pi imk/N} \right) =$$

$$= \sum_{m=1}^{n} 2i \sin \frac{2\pi mk}{N} \hat{q}_m = \sum_{m=1}^{n} \frac{\sin \frac{2\pi mk}{N}}{\sin \frac{\pi m}{N}} b_m \qquad (3.76)$$

We see that the mode interaction (3.75) can be made local in translational coordinates q_k if the latter are introduced by means of (3.76). This suggests the following procedure for calculating the interaction force, $\partial\Phi/\partial b_m$. Since

$$\frac{\partial\Phi}{\partial b_m} = \frac{1}{8N} \sum_{k=0}^{n} (q_{k+1} - q_k)^2 \frac{\partial(q_{k+1} - q_k)}{\partial b_m} =$$

$$= \frac{1}{8N} \sum_{k=0}^{n} (q_{k+1} - q_k)^3 \frac{\sin \frac{2\pi m(k+1)}{N} - \sin \frac{2\pi mk}{N}}{\sin \frac{\pi m}{N}} =$$

$$= \frac{1}{4N} \sum_{k=0}^{n} (q_{k+1} - q_k)^3 \cos \frac{\pi m(2k+1)}{N} \qquad (3.77)$$

one has, for given b_m, to find $q_{k+1} - q_k$ from (3.76). This reduces the problem to the discrete cos-Fourier transform of b_m. Indeed,

$$q_{k+1} - q_k = \sum_{m=-n}^{n} \hat{q}_m \left(e^{2\pi im(k+1)/N} - e^{2\pi imk/N} \right) =$$

$$= \sum_{m=-n}^{n} \hat{q}_m e^{2\pi imk/N} e^{\pi im/N} \left(e^{\pi im/N} - e^{-\pi im/N} \right) =$$

$$= \sum_{m=-n}^{n} 2i\hat{q}_m \sin \frac{\pi m}{N} e^{\pi im \frac{2k+1}{N}} \qquad (3.78)$$

Thus,

$$q_{k+1} - q_k = 2 \sum_{m=1}^{n} b_m \cos \pi m \frac{2k+1}{N}$$

If N is a power of 2, one can use the fast Fourier transform to find $q_{k+1} - q_k$. It requires $O(N \log N)$ numerical operations. Then another $O(N \log N)$ operations are required to perform the calculations in (3.77) since this is also a discrete cos-Fourier transform of $(q_{k+1} - q_k)^3$.

Identity (3.72) can be proved by plugging (3.78) into (3.71):

$$\sum_{k=-n}^{n+1} (q_{k+1} - q_k)^2 ({q^*}_{k+1} - {q^*}_k)^2 =$$

$$\sum_{k=-n}^{n} \sum_{m,r,s,t=-m}^{n+1} 2i\hat{q}_m \sin \frac{\pi m}{N} \, 2i\hat{q}_r \sin \frac{\pi r}{N} \, 2i\hat{q}_s \sin \frac{\pi s}{N}$$

$$2i\hat{q}_t \sin \frac{\pi t}{N} \, e^{2\pi i(m+r-s-t)k/N} \, e^{\pi i(m+r-s-t)/N} \tag{3.79}$$

Since

$$e^{\pi i(m+r-s-t)/N} \sum_{k=-n}^{n+1} e^{2\pi i(m+r-s-t)k/N} = N\delta(m+r-s-t) \tag{3.80}$$

(3.79) transforms into (3.72) (the last factor in (3.79) can be set equal to unity due to (3.80)).

Chapter 4

Slightly Damped Systems

Classical equilibrium thermodynamics and statistical mechanics were derived in chapters 1 and 2 for Hamiltonian ergodic dynamical systems. The next question is: what kind of thermodynamics takes place if the underlying microdynamics is neither Hamiltonian nor ergodic? It is very unlikely that something general can be said about these cases. However, it is likely that some features of classical thermodynamics are inherited by "slightly non-Hamiltonian" systems from Hamiltonian systems. An important class of slightly non-Hamiltonian systems is systems with small dissipation. In this chapter, "thermodynamics" of such systems is considered. It turns out that the major feature of classical equilibrium thermodynamics, the existence of thermodynamic potentials, is characteristic also for thermodynamics of slightly dissipative systems. "Macrobehavior" of slightly dissipative systems is governed by constitutive equations which are potential. The potential is the Lagrange function averaged over the attractor. In the first section, the main features of what we call equilibrium thermodynamics are summarized.

4.1   What is equilibrium thermodynamics?

Equilibrium thermodynamics of a system studies the response of this system to a slow change of external parameters. Schematically, one can speak of a black box with some input, external parameters $y_1, ... y_n$, and some output, the characteristics of the response $F_1, ... F_n$, which are also called thermodynamical forces. Without loss of generality, the number of output parameters can be taken equal to the number of input parameters. The internal dynamics of the black box is governed by some dynamical system. The input parameters have to change slowly on the characteristic scale of the internal dynamics.

The behavior of the black box is characterized by the dependence of the output, F_i, on the input, y_i,

$$F_1 = F_1(y_1, ... y_n), \ ... \ , F_n = F_n(y_1, ... y_n) \tag{4.1}$$

Equations (4.1) are called constitutive equations. They determine the "macrobehavior" of the black box.

The central assertions of equilibrium thermodynamics can be stated in the following way:

1. For some choice of thermodynamical forces, the constitutive equations are potential. More precisely, there exists energy, E, a function of $y_1, ..., y_n$, and some parameter, entropy, such that

$$F_i = \frac{\partial E(S, y_1, ..., y_n)}{\partial y_i} \tag{4.2}$$

2. Entropy, S, is the only characteristic of the internal state of the black box which penetrates in "slow" macrodynamics. Entropy is not changed in the course of a slow change of y. The initial value of entropy depends on the internal state of the black box at the beginning of the process. One may say that the macrodynamics of the black box remembers the initial data of the microdynamics only by means of entropy.

3. There is a characteristic of the black box, temperature,

$$T = \frac{\partial E}{\partial S} \tag{4.3}$$

which possesses the following property: two bodies in contact have equal temperatures after some transitional period.

All three statements can be derived from the assumption that the internal dynamics of the black box is Hamiltonian and ergodic. [1] Thermodynamic forces are averaged over the fast motion derivatives $\partial H / \partial y$. The question under consideration is: what is different if the internal dynamics is not Hamiltonian? Here, we consider two examples: elastic vibrations damped by small dissipation and fluid motion at high Reynolds numbers. We show that the major feature of equilibrium thermodynamics of ergodic Hamiltonian systems, the potentiality of constitutive equations, is characteristic for these dissipative systems as well.[2] Entropy disappears from constitutive relations because dissipative systems do not remember initial conditions (there is another possible view on entropy of dissipative systems which is discussed in section 4.4).

In order to have steady vibrations which seem analogous to thermodynamical equilibrium states some exciting force should be applied to the system; otherwise, the system returns to the rest position. We proceed with the discussion of dynamical effects caused by the external periodic force and small dissipation for the case of Duffing's oscillator.

4.2   Duffing's oscillator: geometry of phase space

Consider an oscillator with one degree of freedom, x, and potential energy $\Phi = \frac{1}{2}kx^2 + \frac{1}{4}lx^4$. The motion of the oscillator is governed by the equation

$$m\ddot{x} + \varkappa\dot{x} + kx + lx^3 = F(t) \tag{4.4}$$

Here $F(t)$ is an external force which is assumed to be periodic, and $\varkappa$ is the friction coefficient. This equation was first studied by Duffing at the beginning of this century and was named after him. It has received a lot of attention in the last few decades

---

[1]Statements 1 and 2 were derived in chapter 1. The third statement can be obtained if one assumes that a) "to put two systems in contact" means to form a new Hamiltonian system with Hamilton function $H = H_1 + H_2 + H_{12}$ where H_1 and H_2 are the Hamilton functions of the two systems and H_{12} is the interaction energy, b) $H_{12} << H_1$ and $H_{12} << H_2$ and c) the new system is ergodic.

[2]For fluid motion this statement is conditioned by vanishing the term (4.50) in the limit of zero viscosity.
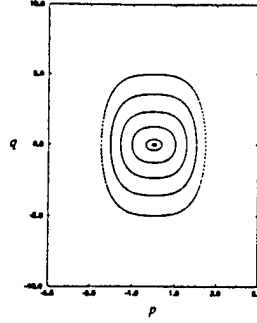
Fig. 4.1: Curves of constant energy in (p, q)-phase space for a free Duffing oscillator $(\alpha = \beta = 1)$

as it presents one of the simplest nonlinear systems which demonstrates extremely complex behavior.

To acquire a better understanding of the dynamics of Duffing's oscillator with small dissipation, it is very useful to investigate first the geometry of trajectories for zero dissipation which will be done in this section.

First, let us transform Duffing's equation to a nondimensional form,

$$\frac{d^2q}{d\tau^2} + \mu \frac{dq}{d\tau} + \alpha q + \beta q^3 = f(\tau) \tag{4.5}$$

where $f(\tau)$ is a periodic function with period 1, and

$$q = \frac{x}{x_0}, \quad \alpha = \frac{k\left(\frac{2\pi}{\omega}\right)^2}{m}, \quad \beta = \frac{l x_0^3}{m\lambda}, \quad f = \frac{F}{m\lambda},$$

$$\lambda = x_0 \left(\frac{\omega}{2\pi}\right)^2, \quad \tau = \frac{\omega}{2\pi} t, \quad \mu = \frac{2\pi \varkappa}{m\omega};$$

x_0 and ω are some characteristic length and the frequency of the external force, respectively.

Let us start from the case of zero external force. In this case, we have an autonomous nonharmonic oscillator with the Hamilton function

$$H = \frac{p^2}{2} + \alpha \frac{q^2}{2} + \beta \frac{q^4}{4}, \quad p = \dot{q} \tag{4.6}$$

We assume that $\alpha > 0$ and $\beta > 0$. The trajectories of this oscillator are closed curves $H(p, q) = E = $ const. They are shown in Fig. 4.1 for $\alpha = \beta = 1$. Since we are going to investigate the nonautonomous case, it is convenient to view the trajectories in three-dimensional (p, q, τ)-phase space.

In (p, q, τ)-phase space, all trajectories lie on surfaces of cylinders, the bases of which are the closed curves of Fig. 4.1. The structure of the phase space is the same as in integrable Hamiltonian systems; the inessential difference is that we now have a family of embedded cylinders instead of invariant tori. It turns out that KAM theory is applicable to this case, and the addition of a small periodic force
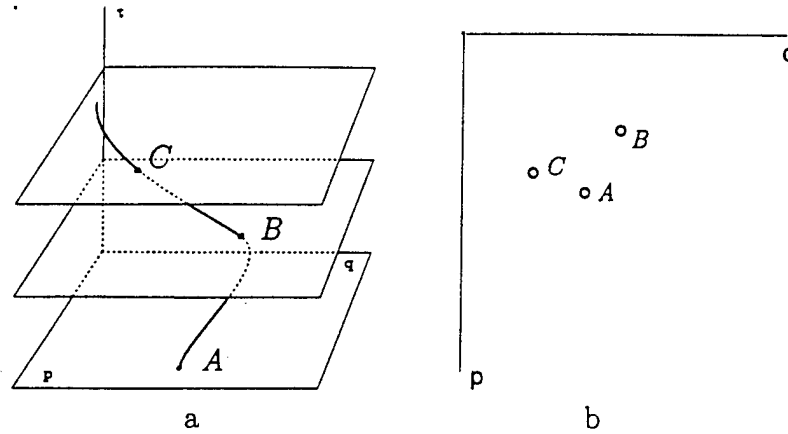
Fig. 4.2: The Poincare section of a trajectory in (p, q, τ)-phase space is a projection of points $A, B, C, \ldots$ on (p, q)-plane

can be considered as a small perturbation of the integrable system. The periodic force disturbs periodically the majority of cylinders, while the rest of the cylinders are destroyed and replaced by chaotic trajectories.

A good method to visualize the trajectories is to utilize Poincare sections, which should be adjusted to the periodic character of the exciting force: Poincare sections show successive positions of phase points for times $\tau = 0, 1, 2, \ldots$ (see Fig. 4.2). (Remember that unity is the period of the exciting force.)

For periodic trajectory with period one, the Poincare section consists of one point. The Poincare section contains two points for the periodic trajectory with the period 2, etc. The absence of a certain pattern is a characteristic feature of a chaotic trajectory.

Consider the harmonic excitation

$$f(\tau) = a + b \sin 2\pi\tau \qquad (4.7)$$

A typical Poincare section for a relatively small excitation ($a = 0$, $b = 2$) is presented in Fig. 4.3. Figure 4.3 shows the following. If a trajectory starts at some point A, the next positions would be $A_1, A_2, \ldots$. After a long time, the positions densely cover a closed curve, a. It is clear that this Poincare map represents a trajectory which goes along a cylinder, and a is the cross-section of the cylinder and the plane $\tau = 0$. Since the cylinder is periodic in τ, the cross-sections of the cylinder with the planes $\tau = 1, 2, \ldots$ form the same curve, a. Starting from other initial points one obtains other closed curves. So, there exists a family of periodic cylindrical surfaces. If the radius of the cross-section decreases, the cylindrical surfaces become slender, and eventually collapse to a curve in (p, q, τ)-phase space. This curve is periodic in τ with period 1. It is represented by the point O in Fig. 4.3.

The functions $p(\tau)$ and $q(\tau)$ are some periodic functions,

$$p(\tau) + iq(\tau) = \sum_k A_k e^{2\pi i k \tau} \qquad (4.8)$$

In principle, all harmonics are presented in the sum (4.8). In this sense, one speaks of superharmonic resonance: all frequencies, which are multiple frequencies of the external force, are excited.
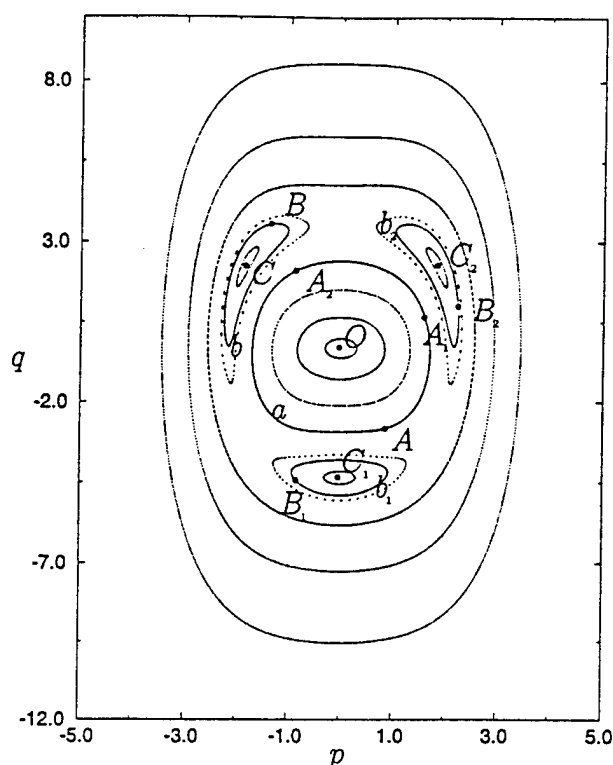
Fig. 4.3: Poincare section for Duffing's oscillator for small amplitude of excitation $(a = 0, b = 2)$

Figure 4.3 reveals a remarkable phenomenon – the appearance of subharmonic resonance, which is the motion with frequency less than the frequency of the external force, and, correspondingly, the period of response is larger than the period of the exciting force. This motion is represented by three "islands" in Fig. 4.3. If the initial position is chosen at point B, then, after time $\tau = 1$, the next position, B_1 is on the other "island". After time $\tau = 2$, the trajectory is at the point B_2, on the third island. After time $\tau = 3$, the trajectory returns to the first island. After a while, the points densely cover the curves b, b_1 and b_2. It is clear that these curves are the cross-sections of a cylindrical surface in (p, q, τ)-phase space with planes $\tau = 0, \tau = 1$ and $\tau = 2$. The cylindrical surface is periodic with period 3.

The three-dimensional picture of two cylindrical surfaces with periods 1 and 3 is shown in Fig. 4.4. The darker tube corresponds to vibrations with period 1, while the lighter tube represents the vibrations with period 3. Cylinders with period 3 also form a family of nested surfaces. If the diameters of cross-sections are decreased, the cylinders collapse to a curve with the period 3. It is represented by three points C, C_1 and C_2 which are the centers of the three islands. So, the subharmonic resonance observed is the motion which contains harmonics with frequency equal to 1/3 of the frequency of the external force (and all its multiple frequencies as well).

KAM theory predicts the existence of destroyed cylinders for arbitrarily small values of the force amplitude, b, but for b which are very small it is not easy to find destroyed cylinders by computer simulations – they occupy too small a part of phase
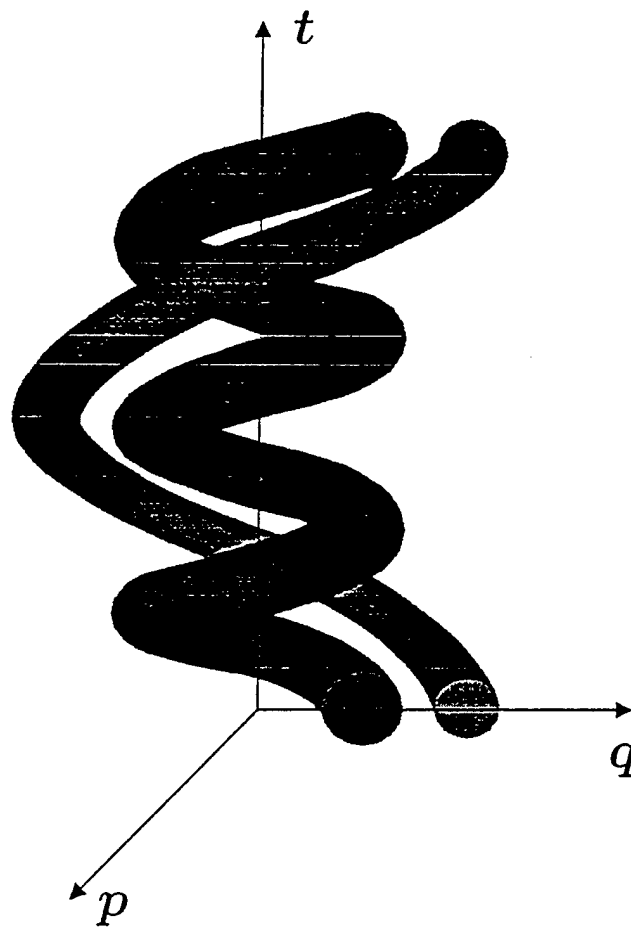
Fig. 4.4: Two tubes in phase space corresponding to vibrations with the period of the exciting force (darker one) and tripled period of the exciting force (subharmonic resonance).

space and, in addition, can be hidden by computational errors.

If b is large enough, a chaotic sea emerging from the destroyed cylinders can easily be seen (Fig. 4.5). An interesting pecularity of this picture is the appearance of additional islands: subharmonic resonances with the periods 2 and 5. The families of cylinders are numbered in Fig. 4.5 by their periods. A family of cylinders with period 5 is embedded in the family of cylinders with period 1. The period 1 family is surrounded by the family with period 3. On the periphery of this figure, there are two families with period 2.

Increasing the amplitude of the excitation leads to more and more complex pictures of motion. The Poincare section is shown in Fig. 4.6 for $a = 0$, $b = 12$, where subharmonic vibrations with periods varying from 1 to 40 can be seen; the corresponding islands are marked by their periods, and different families of the same period are marked by letters.

The complexity of the geometry of phase space is a generic feature of nonlinear vibrations. As another example, the Poincare section of a cantilevered beam exited by a periodic force at the unclamped edge[1] is shown in Fig. 4.7. The reader is invited to give a mechanical interpretation of this picture.

The dynamics of Duffing's oscillator is certainly nonergodic – there are many islands of ordered motion. The picture of vibrations looks so complicated that no simple thermodynamical relations can be expected to describe them. Help comes from a source which has been ignored so far – dissipation. It turns out that dissipation significantly simplifies the complex pictures considered and makes "thermodynamical questions" sensible.

Dissipation causes all complex "microstructure" of the phase space to disappear: all trajectories fall on a number of attractors. For moderate a and b, the trajectories leave the invariant cylinders and approach the central trajectories of the corresponding islands, which become limit cycles. Some islands can be completely destroyed by dissipation. The number of limit cycles depends on the value of the friction μ, and parameters a, b, α and β. If the friction μ is small enough, a number of limit cycles survive. For the large enough value of μ there is only one limit cycle. In general, tubes with smaller periods do survive for larger values of dissipation, and the ones with large periods disappear even with small dissipation.

For larger amplitudes a and b, a strange attractor might appear. A natural conjecture is that a strange attractor emerges at a place previously occupied by a chaotic sea of a Hamiltonian system. This conjecture is supported by the Poincare sections in Fig. 4.8a and Fig. 4.8b. Figure 4.8a shows the Poincare section of a Hamiltonian system for $a = 0$, $b = 2975$, $\mu = 0$. Figures 4.8b, Fig. 4.8c and Fig. 4.8d are the Poincare sections for $\mu = 0.1$ and $\mu = 1.0$. The same initial data were chosen for all four cases. It is seen from Fig. 4.8a and b that the chaotic sea of Hamiltonian system really transforms into some chaotic attractor while two islands collapse to a

---

[1]The Lagrange function in this example is [19]

$$L = \frac{1}{2}\left(1 + cq^2\right)\dot{q}^2 - \frac{1}{2}aq^2 - \frac{1}{2}bq^4 + Aq + Bq\sin\nu t,$$

the value of parameters are $a = 10, b = 0, c = 1, A = 0, B = 10, \nu = 2\pi$.
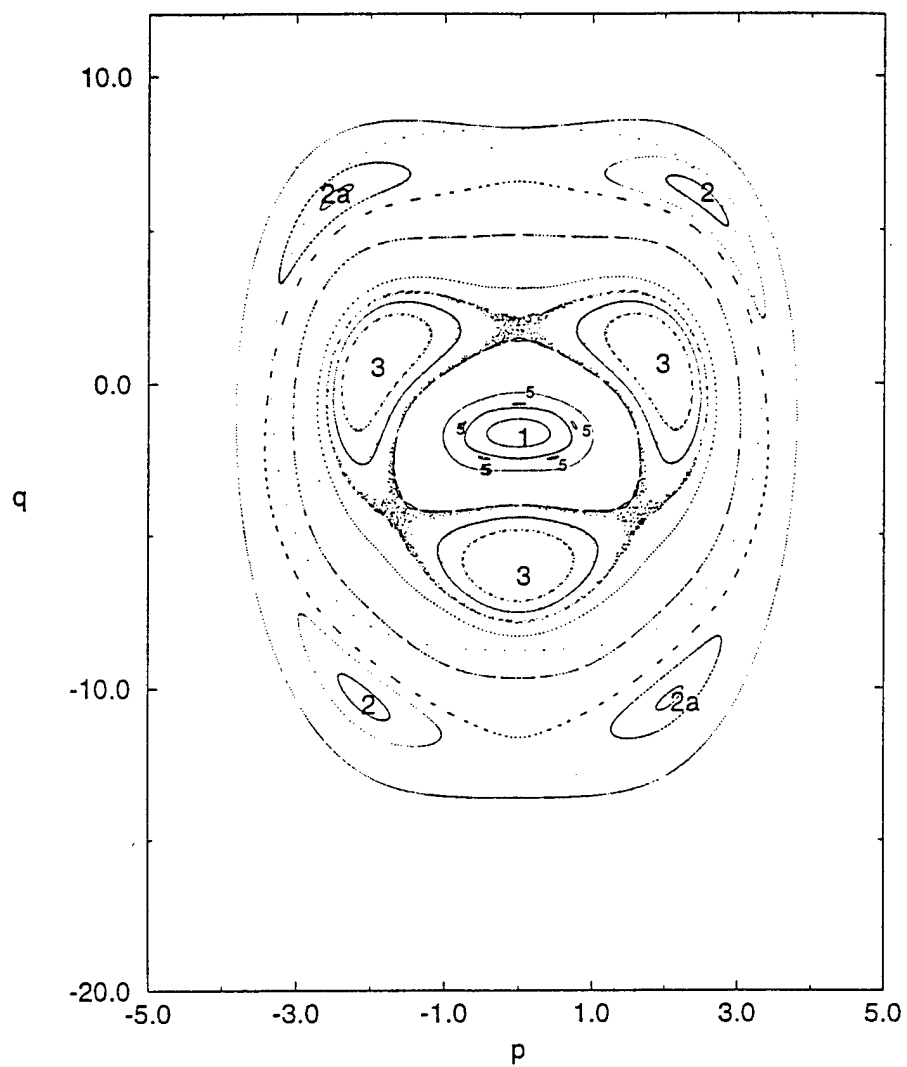
Fig. 4.5: Poincare section for moderate excitation ($a = 0, b = 10$). Subharmonic resonances with the periods 2, 3 and 5 are seen.
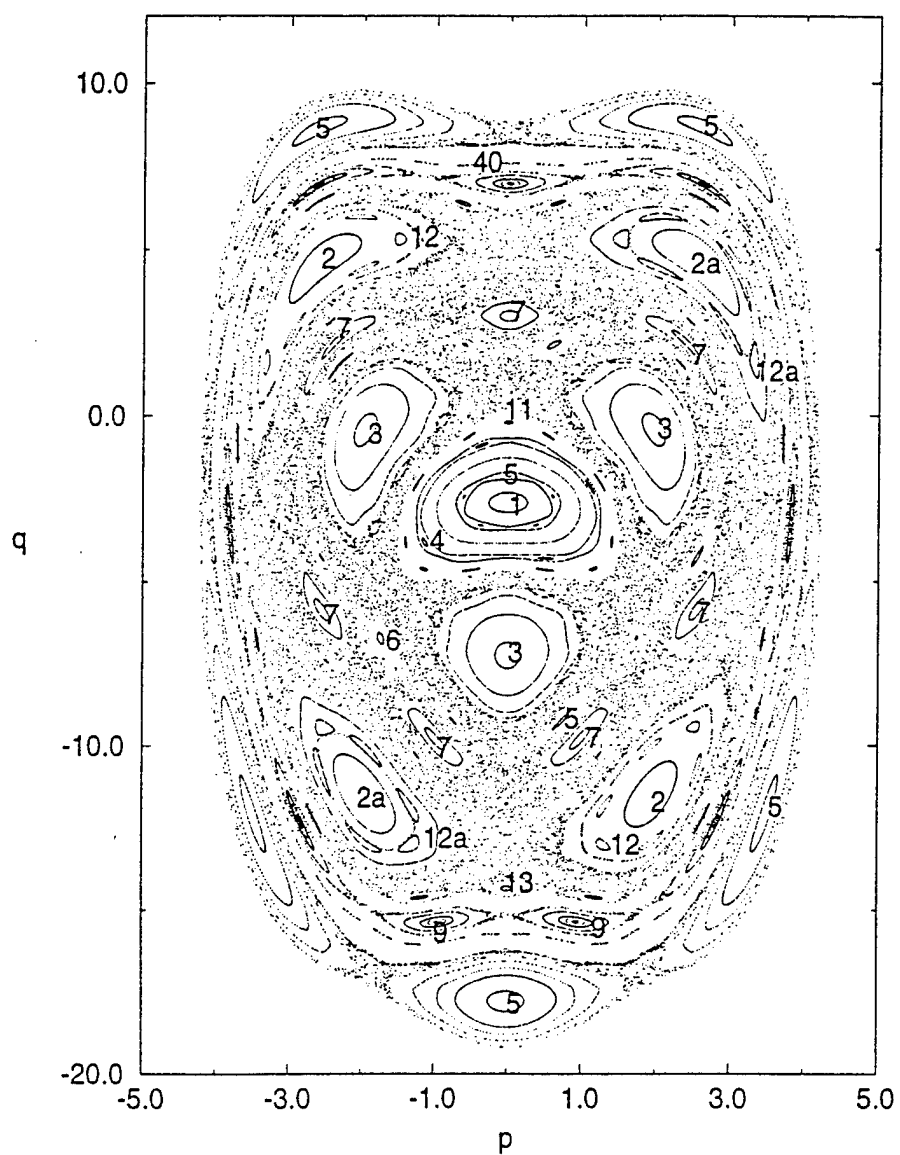
Fig. 4.6: Poincare section for large excitation ($a = 0, b = 16, \mu = 0$)
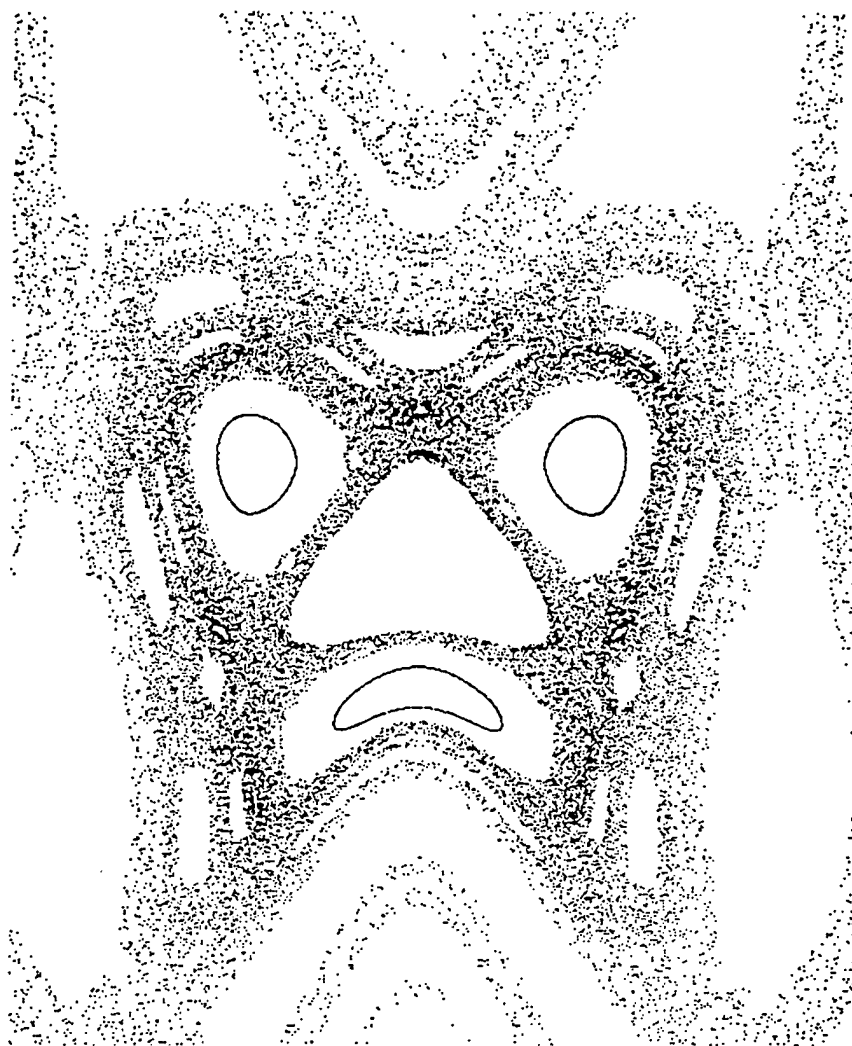
Fig. 4.7: Poincare section for vibrations of a cantilevered beam exited by periodic force at the unclamped end
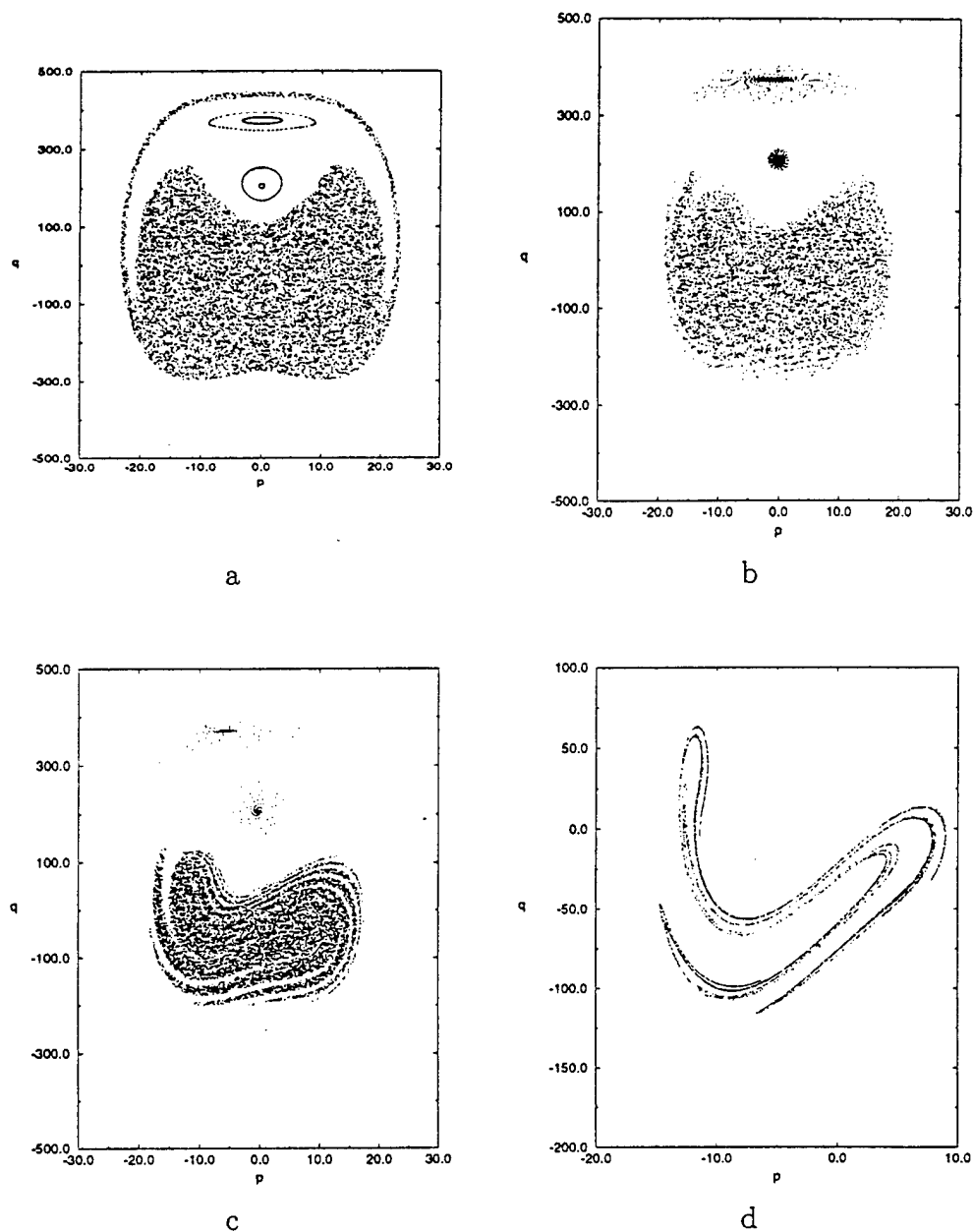
Fig. 4.8: Poincare section of a) undamped, harmonically exited Duffing oscillator $(a = 0, b = 2975, \mu = 0)$, b) slightly damped Duffing oscillator $(a = 0, b = 2975, \mu = 10^{-2})$, c) Duffing oscillator with moderate damping $(a = 0, b = 2975, \mu = 0.05)$ and d) Duffing oscillator with large damping $(a = 0, b = 2975, \mu = 1.0)$

limit cycle. Chaotic attractor seems close to the chaotic see for small friction though "the handle" in Fig. 4.8a is lost. For large value of μ the limit cycle dies, and only the strange attractor exists. We return to the discussion of Fig. 4.8 in section 4.5

4.3   Thermodynamics of limit cycles

Now we are going to show that slow change of parameters of limit cycles yields potential constitutive equations.

Consider a mechanical system with one degree of freedom and the Hamilton function which depends on time explicitly; this dependence is caused by external periodic forces. The period of the external force is $2\pi/\omega$. After scaling time to make the period equal to 2π,

$$L = \omega p \frac{dq}{d\tau} - H(p, q, \tau, y) \tag{4.9}$$

Here y are the slowly changing parameters, and H is periodic in $\tau = \omega t$ with period 2π. The dynamical equations are

$$\omega \frac{dp}{d\tau} = -\frac{\partial H}{\partial q} - \mu \frac{\partial H}{\partial p}, \quad \omega \frac{dq}{d\tau} = \frac{\partial H}{\partial p} \tag{4.10}$$

The friction coefficient μ is small.

For Duffing's oscillator excited by an external force $F(\tau)$,

$$H = \frac{p^2}{2m} + k\frac{q^2}{2} + l\frac{q^4}{4} - F(\tau)q \tag{4.11}$$

In applications, the most interesting slow parameters are the characteristics of the external force. For example, the coefficients of the Fourier series for $F(\tau)$

$$F(\tau) = \sum a_k \cos k\tau + b_k \sin k\tau \tag{4.12}$$

can be the slowly changing parameters.

Consider a limit cycle of equations (4.10). The period of the limit cycle, θ, may be equal to the period of the exciting force, 2π, or may have larger values 4π, 6π, ... The limit cycle is a periodic curve in (p, q, τ)-phase space. This curve depends on the values of the parameters y. The parametric equations of the limit cycle are

$$p = p(\tau, y), \quad q = q(\tau, y) \tag{4.13}$$

Let us average the Lagrange function of the oscillator over the limit cycle,

$$\bar{L} \equiv \langle L \rangle \equiv \frac{1}{\theta} \int\limits_0^\theta \left(\omega p(\tau, y) \frac{dq(\tau, y)}{d\tau} - H(p(\tau, y), q(\tau, y), y) \right) d\tau \tag{4.14}$$

The average Lagrange function, $\bar{L}$, is a function of the slowly changing parameters, y.

Let us find the derivatives $\bar{L}$ with respect to y. We have

$$\frac{\partial \bar{L}}{\partial y} = \frac{1}{\theta} \int\limits_0^\theta (\omega \frac{\partial p}{\partial y} \frac{\partial q}{\partial \tau} + \omega p \frac{\partial^2 q}{\partial \tau \partial y} - \frac{\partial H}{\partial p} \frac{\partial p}{\partial y} - \frac{\partial H}{\partial q} \frac{\partial q}{\partial y} - \frac{\partial H}{\partial y}) d\tau \qquad (4.15)$$

Integrating the second term of the integrand by parts and taking into account the fact that contributions at $\tau = 0, \theta$ cancel out due to periodicity of p and q, we rewrite (4.15) as

$$\frac{\partial \bar{L}}{\partial y} = \frac{1}{\theta} \int\limits_0^\theta \left[\frac{\partial p}{\partial y} \left(\omega \frac{\partial q}{\partial \tau} - \frac{\partial H}{\partial p} \right) - \frac{\partial q}{\partial y} \left(\omega \frac{\partial p}{\partial \tau} + \frac{\partial H}{\partial q} \right) - \frac{\partial H}{\partial y} \right] d\tau \qquad (4.16)$$

The last expression can be simplified using (4.10). We obtain

$$\frac{\partial \bar{L}}{\partial y} = - \left\langle \frac{\partial H}{\partial y} \right\rangle + \mu \left\langle \omega \frac{\partial q}{\partial \tau} \frac{\partial q}{\partial y} \right\rangle \qquad (4.17)$$

If the derivatives of $\partial q/\partial \tau$ and $\partial q/\partial y$ remain bounded for $\mu \to 0$, then the last term of (4.17) vanishes in the limit of small dissipation, and we get

$$\frac{\partial \bar{L}}{\partial y} = - \left\langle \frac{\partial H}{\partial y} \right\rangle \qquad (4.18)$$

Recalling that y is actually a set of parameters, $y_1, ..., y_m$, and defining the "thermodynamic forces", F_i, by the relations

$$F_i = - \left\langle \frac{\partial H}{\partial y_i} \right\rangle , \qquad (4.19)$$

we obtain the constitutive equations,

$$F_i = \frac{\partial \bar{L}(y)}{\partial y_i} \qquad (4.20)$$

Introduction of "thermodynamic forces" by (4.19) is analogous to that in classical thermodynamics. The thermodynamic forces (4.19) usually have an obvious physical interpretation. For example, if the slow parameters are the Fourier coefficients a_k, b_k of the series (4.12), then

$$- \left\langle \frac{\partial H}{\partial a_k} \right\rangle = \langle q \cos k\tau \rangle , \quad - \left\langle \frac{\partial H}{\partial b_k} \right\rangle = \langle q \sin k\tau \rangle \qquad (4.21)$$

The quantities (4.21) are the Fourier coefficients of the response. We denote them by $\bar{q}_k$ and $\hat{q}_k$, correspondingly. The constitutive equations (4.20) mean that there is a function, $\bar{L}$, of the Fourier coefficients of the exciting force, a_k, b_k, such that

$$\bar{q}_k = \frac{\partial \bar{L}(a, b)}{\partial a_k}, \quad \hat{q}_k = \frac{\partial \bar{L}(a, b)}{\partial b_k} \qquad (4.22)$$

So, the Fourier coefficients of the response are potential functions of the Fourier coefficients of the exciting force.

The function $\bar{L}$ can be considered as a function of all a_k and b_k, $k = 1, 2, \ldots$. If this function is known, then, for a particular excitation, say,

$$F(\tau) = a_0 + b_1 \sin \tau \tag{4.23}$$

the response characteristics are determined by the equations

$$\bar{q}_0 = \left.\frac{\partial \bar{L}}{\partial a_0}\right|_{\substack{a_1=a_2=\ldots=0 \\ b_2=b_3=\ldots=0}}, \quad \bar{q}_1 = \left.\frac{\partial \bar{L}}{\partial a_1}\right|_{\substack{a_1=a_2=\ldots=0 \\ b_2=b_3=\ldots=0}}, \ldots$$

$$\hat{q}_1 = \left.\frac{\partial \bar{L}}{\partial b_1}\right|_{\substack{a_1=a_2=\ldots=0 \\ b_2=b_3=\ldots=0}}, \quad \hat{q}_2 = \left.\frac{\partial \bar{L}}{\partial b_2}\right|_{\substack{a_1=a_2=\ldots=0 \\ b_2=b_3=\ldots=0}}, \ldots \tag{4.24}$$

If one is interested only in the "reciprocal" characteristics of the response, $\bar{q} = \langle q \rangle$ and $\hat{q} = \langle q \sin \tau \rangle$, then the function P can be introduced by the variational problem

$$P(a_0, b_1) = \mathop{Extr}_{\substack{a_1, a_2, \ldots \\ b_2, b_3, \ldots}} \bar{L}(a_0, a_1, a_2, \ldots ; b_1, b_2, \ldots) \tag{4.25}$$

Here $\mathop{Extr}\limits_{a,b}$ stands for the calculation of the stationary point with respect to a, b.

The constitutive relations for $\bar{q}$ and $\hat{q}$ can be written in terms of the functions P as

$$\bar{q} = \frac{\partial P(a_0, b_1)}{\partial a_0}, \quad \hat{q} = \frac{\partial P(a_0, b_1)}{\partial b_1} \tag{4.26}$$

For nonlinear vibrations, the functions $\bar{L}$ and P can be found, probably, only from real or numerical experiments. The range of viscosity in which potentiality holds with acceptable accuracy can also be determined only experimentally. For the Duffing oscillator (4.5) with $\alpha = \beta = 1$ and periodic excitation $F = a + b \sin \tau$, the function P has been found [22] for the limit cycle corresponding to the central island in Fig. 4.5:

$$P(a_0, b_1) = \alpha_0 + \alpha_1 a + \alpha_2 a^2 + \alpha_3 b^2 + \alpha_4 a^2 b \tag{4.27}$$

Here $\alpha_0 = -0.1584$, $\alpha_1 = 0.3835$, $\alpha_2 = 0.1787$, $\alpha_3 = -0.0065$, $\alpha_4 = -0.0003$. The constitutive equations are

$$\bar{q} = \frac{\partial P}{\partial a} = \alpha_1 + 2\alpha_2 a + 2\alpha_4 ab, \quad \hat{q} = \frac{\partial P}{\partial b} = \alpha_3 + \alpha_4 a^2 \tag{4.28}$$

The errors in the constitutive equations (4.28) are less than 0.1% for small friction, $\mu < 0.1$. Errors reach 8% for high friction, $\mu = 10$.

We call the function P the dynamical potential of an attractor.

The constitutive equation (4.22) can be inverted, and the excitation characteristics, a_k and b_k, can be expressed in terms of the response characteristics, $\bar{q}_k$ and $\hat{q}_k$. In order to do that, consider the average value of $H_0(p, q) - p\dot{q}$ over the limit cycle,

where H_0 is the Hamilton function of free vibrations (the total Hamilton function, H, is equal to $H_0(p, q) - F(\tau)q$). Setting

$$\bar{L}^* = \langle H_0 - p\dot{q} \rangle \, ,$$

we have

$$\bar{L}^* = \langle F(\tau)q \rangle - \langle p\dot{q} - H \rangle = \langle F(\tau)q \rangle - \bar{L} = \sum a_k \bar{q}_k + b_k \hat{q}_k - \bar{L} \qquad (4.29)$$

If $\bar{L}$ is considered to be a function of a_k and b_k, then $\bar{L}^*$ is Legendre's transform of $\bar{L}$, the function of $\bar{q}_k$ and $\hat{q}_k$, and the following relations hold:

$$a_k = \frac{\partial \bar{L}^*}{\partial \bar{q}_k}, \quad b_k = \frac{\partial \bar{L}^*}{\partial \hat{q}_k} \qquad (4.30)$$

This statement can be put into the form of a variational principle: the response of the system is a stationary point of the function

$$\bar{L}^*(\bar{q}_k, \hat{q}_k) - \sum (a_k \bar{q}_k + b_k \hat{q}_k) \qquad (4.31)$$

The function $\bar{L}^*(\bar{q}_k, \hat{q}_k)$ contains all the necessary information on the response. In principle, it is determined by the following variational problem: find a stationary point of the action functional of free vibrations

$$I(p, q) = \frac{1}{\theta} \int_0^\theta \left(\omega p \frac{\partial q}{\partial \tau} - H_0(p, q) \right) d\tau \qquad (4.32)$$

on the set of all functions $p(\tau)$ and $q(\tau)$ with period θ, which obey the constraints

$$\langle q \cos k\tau \rangle = \bar{q}_k, \quad \langle q \sin k\tau \rangle = \hat{q}_k \qquad (4.33)$$

The stationary value of the functional I is a function of $\bar{q}_k$, $\hat{q}_k$. It is equal to $-\bar{L}^*$.

If the external force is presented not in terms of Fourier series but in a series of some set of functions, $\psi_k(\tau)$,

$$F = \sum a_k \psi_k(\tau)$$

the previous relations stay valid if $\bar{q}_k$ are determined by

$$\bar{q}_k = \langle q \, \psi_k \rangle$$

If the oscillator has a number of limit cycles, each limit cycle is characterized by some potential. A change of parameters causes the limit cycles to deform, disappear, bifurcate, etc. The dynamical potential should play in these transformations a role which is similar to internal energy in the theory of phase transformations.

4.4   On thermodynamical entropy of limit cycles

The constitutive equations for limit cycles (4.20), in contrast to the constitutive equation of classical thermodynamics, do not contain entropy. This seems quite natural because in the constitutive equations of classical thermodynamics entropy represents memory of initial data, while no memory of initial data exists for dissipative systems. Although, beyond doubt, there are no characteristics of limit cycles which possess all the properties of the entropy of classical equilibrium thermodynamics, there are characteristics which have some features of entropy. In this section, we show that for an oscillator excited by a periodic force, the relation between logarithm of the frequency of the external force and temperature of vibrations is similar to that between entropy and temperature in classical thermodynamics, and, in this respect, the logarithm of frequency is analogous to entropy.

To establish this fact, we differentiate (4.14) with respect to ω. The dependence of the functions $p(\tau)$ and $q(\tau)$ on ω, which is not mentioned explicitly in (4.14), stems from the fact that the dynamical equations (4.10) contains ω as a parameter. The total contribution of the derivatives of $\partial p/\partial \omega$ and $\partial q/\partial \omega$ is zero in the same way that the contribution of $\partial p/\partial y$ and $\partial q/\partial y$ is zero in (4.15). Thus,

$$\frac{\partial \bar{L}}{\partial \omega} = \left\langle p\frac{dq}{d\tau} \right\rangle \tag{4.34}$$

According to the dynamical equations (4.10), the right-hand side of (4.34) can be written as $\omega^{-1}\langle p\partial H/\partial p\rangle$. We can define the temperature of vibrations in the same way as in the nondissipative case, as

$$T = \left\langle p\frac{\partial H}{\partial p} \right\rangle$$

Hence,

$$\frac{\partial \bar{L}}{\partial \omega} = \frac{1}{\omega}T$$

So, in addition to the previous constitutive equations (4.20), we get the constitutive equation

$$\frac{\partial \bar{L}}{\partial \ln \omega/\omega_0} = T \tag{4.35}$$

where ω_0 is some characteristic frequency, for example, the frequency of linear vibrations.

In the case of linear vibrations, the validity of the constitutive equations can be checked by inspection. Indeed, let $H_0 = p^2/2m + kq^2/2$ and $F = a\sin\omega t$. We have to check the relations

$$\bar{q} \equiv \langle q\sin\omega t\rangle = \frac{\partial \bar{L}}{\partial a}, \quad T \equiv \langle m\dot{q}^2\rangle = \frac{\partial \bar{L}}{\partial \ln \omega/\omega_0} \tag{4.36}$$

The limit cycle of the linear oscillator with the friction coefficient $\varkappa$ is

$$q(\tau, a, \omega) = \alpha\sin\tau + \beta\cos\tau$$

where the constants α, β are

$$\alpha = a\frac{(k - ma^2)}{\Delta}, \quad \beta = \frac{\varkappa \omega a}{\Delta}, \quad \Delta \equiv (k - m\omega^2)^2 + \varkappa \omega^2$$

Therefore,

$$\left\langle \dot{q}^2 \right\rangle = \frac{a^2 \omega^2}{2\Delta}, \quad \left\langle q^2 \right\rangle = \frac{1}{2\Delta}, \quad T = m\left\langle \dot{q}^2 \right\rangle = \frac{ma^2\omega^2}{2\Delta} \tag{4.37}$$

and

$$\bar{L} = \frac{a^2(k - m\omega^2)}{4\Delta} \tag{4.38}$$

For $\varkappa \to 0$

$$\bar{L} = \frac{a^2}{4(k - m\omega^2)}, \quad \bar{q} = \frac{a}{2(k - m\omega^2)}, \quad T = \frac{ma^2\omega^2}{2(k - m\omega^2)^2} \tag{4.39}$$

and the constitutive equations (4.36) follow from (4.39).

For linear friction-free vibrations the dynamical potential has a singularity when the frequency of excitation approaches the eigenfrequency of the oscillator, $\omega_0 = \sqrt{k/m}$.

In the vicinity of resonance, one might expect violation of the constitutive equations because, in principle, the neglected terms $\varkappa \left\langle \dot{q}\partial q/\partial a \right\rangle$ and $\varkappa \left\langle \dot{q}\partial q/\partial \omega \right\rangle$ might be finite even if the friction tends to zero since q and $\dot{q}$ go to infinity. Inspection shows that the first relation (4.36) turns out to be true even for finite $\varkappa$, while the second one is no longer valid. It follows from (4.37) and (4.38) that for $\varkappa \neq 0$

$$\omega\frac{\partial \bar{L}}{\partial \omega} = T\left[1 - \frac{\varkappa^2(\omega^2 + k/m)}{(k - m\omega^2) + \varkappa^2\omega^2}\right]$$

Thus, the second constitutive relation (4.36) is true for small $\varkappa$ away from resonance, and its error is on the order of $\varkappa^2$. In the vicinity of resonance the value $\omega\partial\bar{L}/\partial\omega$ is not equal to T. For $\omega_0 = \omega$ we have $\omega\partial\bar{L}/\partial\omega = -T$. Note that the cause which keeps the oscillator from exploding at the resonance is the friction force. One might expect that in the case of nonlinear resonance, when the oscillator does not blow up due to an elastic Hamiltonian force, the second relation (4.36) may still be valid in the vicinity of resonance.

It is natural to consider the variable $\bar{q}$ as a variable characterizing the "internal state" of the oscillator. Then, the variable a is the corresponding "thermodynamical force". In classical thermodynamics, the constitutive equations of a system with an internal variable $\bar{q}$ are

$$a = \frac{\partial E(\bar{q}, S)}{\partial \bar{q}}, \quad T = \frac{\partial E(\bar{q}, S)}{\partial S} \tag{4.40}$$

To put equation (4.36) in this form, we introduce Legendre's transform of the function $L(a, \omega)$ with respect to the variable a:

$$P = a\bar{q} - \bar{L}$$

Then,

$$\frac{\partial P}{\partial \bar{q}} = a, \quad \frac{\partial P}{\partial \omega} = -\frac{\partial \bar{L}}{\partial \omega}$$

and (4.40) holds for the oscillator if entropy is determined by the relation

$$S = \ln \frac{\omega_0}{\omega} \tag{4.41}$$

while P plays the role of energy.

4.5   Is there thermodynamics of strange attractors?

The limit cycle is an example of an attractor, a set in phase space which "attracts" the trajectories. If the force is small, then there is one attractor – the limit cycle. For a larger force, an additional limit cycle might appear. Depending on the initial conditions, the trajectory approaches one or another limit cycle. The region in (p, q, τ)-phase space for every point of which the trajectory goes to the same limit cycle is called a basin of the attractor.

The appearance of two limit cycles is accompanied by an interesting phenomenon: vibrations become in some sense unpredictable. The matter is that the boundary between the two basins is extremely intricate, and a small physically unobservable change of initial data may turn the trajectory from one attractor to another.

Note that each limit cycle is a solution of the dynamical equations: if the initial data are chosen exactly on the limit cycle, the phase trajectory coincides with the limit cycle.

Further increase of the magnitude of the external force leads to the appearance of additional attractors with very complex geometrical structure, due to which they acquired the name of "strange attractors". In contrast to a limit cycle, for which Poincare's map consists of a single point for a cycle of period 1 or of m points for a cycle of a period m, the Poincare section for a strange attractor is a set of points with a complex geometry. A numerical approximation of this set by a trajectory of Duffing's equation is shown in Fig. 4.8b. Strange attractors also consist of trajectories of dynamical equations. In (p, q, τ)-phase space they form a set which looks like spaghetti. Each trajectory of Duffing's oscillator approaches some trajectory on the attractor.

To have sensible "thermodynamics" we need the time average over a trajectory not to depend on the initial data. This requires the average value of any smooth function over each trajectory of the attractor to be the same. It is natural to call such attractors ergodic attractors. The first problem we face in considering the "thermodynamics" of the strange attractor of Duffing's oscillator is that it is not known whether or not this attractor is ergodic. There are some numerical observations undermining its ergodicity [22]. Calculation of the average value of q as a function of θ,

$$\frac{1}{\theta} \int_0^\theta q(t) dt$$

shows that the average value keeps vibrating even for very large θ, on the order of $\tau = 10^6$. A possible reason is that the attractor consists of a number of simply connected interwoven attracting sets, and the trajectory keeps moving from one set to another.

Another difficulty is the contribution of dissipation. Limit cycles are some disturbed trajectories of a Hamiltonian system. The disturbance vanishes if the friction coefficient goes to zero. An attempt to observe similar behavior for attractors has been undertaken in [22]. For the value of force parameters at which the strange attractor exists ($a = 0.05$, $b = 2975$), the Poincare sections for a Hamiltonian system were obtained (the friction μ was set equal to zero). This map is shown in Fig. 4.8a. The well-developed chaotic sea can be seen. For small dissipation, two attractors were observed: a large chaotic sea and the limit cycle (Fig. 4.8b).

Depending on the initial conditions, the trajectory approaches either the chaotic set or the limit cycle. It was expected that the strange attractor should appear within the chaotic sea if $\mu \neq 0$, while the family of tubes collapses to a limit cycle. Calculations during the first 50,000 cycles confirmed this hypothesis. However, longer runs ($\theta \approx 100,000$) revealed that each trajectory leaves the chaotic sea and goes to the limit cycle. There might be two reasons for such behavior. First, the strange attractor does exist but its distance from the basin boundary is small and the trajectory jumps from the basin of the strange attractor to the basin of the limit cycle due to numerical errors. Second, the strange attractor does not exist for very small μ. The chaotic set is a set of "transitional chaos". After passing through this set, the trajectory falls into the limit cycle. It is not clear at the moment which reason is the real one.

For larger friction, the strange attractor certainly does exist. The corresponding Poincare's map is shown in Fig. 4.8c. It is interesting to observe the transformation of the chaotic sea in Fig. 4.8a through the chaotic set in Fig. 4.8b and the strange attractor in Fig. 4.8c to the familiar worm-type structure of Fig. 4.8d.

If strange attractors do not exist for $\mu \to 0$ and appear only for finite μ, then the existence of thermodynamical potentials seems questionable in the exact mathematical sense. Approximately, the potentiality of the constitutive relations may, nevertheless, hold for finite μ with good accuracy, as we have seen for limit cycles of Duffing's oscillator.

4.6 On thermodynamics of attractors: general case of a closed system

The derivation of the potentiality law can be generalized to an arbitrary closed system. We assume that the kinematics of the system is characterized by variables $u(t)$ where u is either a finite-dimensional vector or a finite-dimensional vector field. The governing equations are

$$\frac{\delta L}{\delta u} + f(u, u_t) = 0 \tag{4.42}$$

where L is the Lagrange function, $\delta L/\delta u$ is its variational derivative and f is the friction force. The external force which causes the motion of the system is supposed to

be potential, and the potential of external force is included in the Lagrange function. It is assumed that trajectories in phase space tend to an attractor, and for $f \to 0$ the attractor converges to a set consisting of the trajectories of the limit system

$$\frac{\delta L}{\delta u} = 0$$

The attractor is supposed to be ergodic in the following sense: average values of any functional $\phi(u, u_t)$ over a trajectory of the attractor do not depend on the trajectory. This assumption makes the average value of any functional independent of initial data.

Let L be a function of the parameters $y = (y_1, ..., y_k)$. The average value of any function becomes a function of the parameters y. Denote the average value of L by P,

$$P(y) = \langle L \rangle$$

Determining the derivatives of P with respect to y, we get

$$\frac{\partial P}{\partial y_i} = \lim_{\theta \to \infty} \frac{1}{\theta} \left[\int_0^\theta \left(\frac{\delta L}{\delta u}, \frac{\partial u}{\partial y_i} \right) dt + \int_0^\theta \frac{\partial L}{\partial y_i} dt + \left(\frac{\delta L}{\delta u_t} \frac{\partial u}{\partial y_i} \right)\Big|_0^\theta \right]$$

We assume that $\delta L/\delta u_t$ and $\delta u/\delta y_i$ are bounded for all t. Then, the last term vanishes for $\theta \to \infty$. The first terms approaches zero when friction goes to zero. Therefore,

$$\frac{\partial P}{\partial y_i} = \left\langle \frac{\partial L}{\partial y_i} \right\rangle \tag{4.43}$$

The averaged derivatives $\partial L/\partial y$ form "generalized forces" which are reciprocal to the parameters y_i. If y_i are considered to be the input parameters of the system, $\langle \partial L/\partial y \rangle$ are the corresponding output parameters, and equations (4.43) are the constitutive equations.

4.7   On thermodynamics of closed fluid flows

An interesting particular case is that of a fluid flow in a container. Let us first state the corresponding variational principle. Consider a container (a finite region V in 3-D space) occupied by an ideal fluid. Let ξ^a ($a = 1, 2, 3$) be the Lagrangian coordinates of the fluid particles. The Lagrangian coordinates take values in some region V_0 in the 3-D space of Lagrangian coordinates. Denote by x^i the Cartesian coordinates of an observer's frame in the actual 3-D space. The trajectory of a particle ξ^a is

$$x^i = x^i (\xi^a, t) \tag{4.44}$$

"To know the fluid motion" means "to know the functions $x^i(\xi^a, t)$".

The Jacobian $\Delta = \det \|\partial x^i/\partial \xi^a\|$ characterizes the change of volume in the transition from Lagrangian coordinates to Eulerian coordinates. The density ρ is determined by the law of conservation of mass,

$$\rho = \frac{\rho_0 (\xi^a) \Delta_0 (\xi^a)}{\Delta} \tag{4.45}$$

where ρ_0 and Δ_0 are the values of the density and Δ at the initial time instant t_0. Note that Δ can be either greater or less than zero; the determinant Δ_0 has the same sign as Δ, thus density is necessarily positive.

We consider the motion which is not detached from or does not penetrate the walls: each particle, which is on the wall at the initial moment, stays on the wall in the course of the motion. In terms of the functions $x^i(t, \xi^a)$ that means

$$x^i(t, \xi^a) \in \partial V \quad \text{if} \quad \xi^a \in \partial V_0 \tag{4.46}$$

where ∂V and ∂V_0 are the boundaries of V and V_0, respectively. Note that the boundary ∂V may consist of a number of pieces, some of which move. The moving part of ∂V is denoted by $\Sigma(t)$. For example, $\Sigma(t)$ might be the surface of rotor blades.

Let the initial and final positions of the particles be given,

$$x^i(t_0, \xi^a) = x_0^i(\xi^a), \quad x^i(t_1, \xi^a) = x_1^i(\xi^a) \tag{4.47}$$

Then, the adiabatic motion of the ideal compressible fluid is a stationary point of the functional

$$I\left[x^i(\xi^a, t)\right] = \int\limits_{t_0}^{t_1} \int\limits_{V_o} \rho \left(\frac{1}{2} \frac{\partial x^i(t, \xi^a)}{\partial t} \frac{\partial x_i(t, \xi^a)}{\partial t} - U(\rho) \right) \Delta d^3\xi dt \tag{4.48}$$

on the set of the functions $x^i(t, \xi^a)$ which obey the constraints (4.46) and (4.47). Summation over repeated indices is implied.

Stationary points of the functional (4.48) satisfy the equations of motion of an ideal fluid in Lagrangian coordinates

$$\rho \frac{\partial^2 x^i(\xi^a, t)}{\partial t^2} = -\frac{\partial p}{\partial x_i} \tag{4.49}$$

Here p is the notation for function $\rho^2 \partial U / \partial \rho$.

Now, let the viscosity of the fluid be not equal to zero. Fluid dynamics is governed be the Navier-Stokes equations which have the form (4.42) with friction force $\mu \Delta v_i$ (μ-viscosity). Assuming that the problem contains slow parameters y and differentiating (4.48) with respect to y, we obtain under the same assumption as in section 4.6, the constitutive equation (4.43). The assumptions made are the boundedness of the derivatives $\partial L / \partial u_t$ and $\partial u / \partial y$, and vanishing of the term $< (\partial L / \partial u_t, \partial u / \partial y) >$ when the viscosity tends to zero. In the case of fluid flow, $\partial L / \partial u_t$ has a physical interpretation of fluid velocity and, thus, is bounded. The derivative $\partial u / \partial y$ for fluid flow is $\partial x(t, \xi, y) / \partial y$. Its boundedness (after an appropriate time scaling, if necessary) seems intuitively correct. The major concern is the term $< (\delta L / \delta u, \partial u / \partial y) >$ which, for viscous fluids, is

$$\lim_{\theta \to \infty} \frac{1}{\theta} \int\limits_0^\theta \int\limits_V -\mu \Delta v_i \frac{\partial x_i(t, \xi, y)}{\partial y} d^3x \, dt \tag{4.50}$$

This term is reminiscent of the average dissipation of the flow,

$$\lim_{\theta \to \infty} \frac{1}{\theta} \int\limits_0^\theta \int\limits_V \mu \frac{\partial v_i}{\partial x_j} \left(\frac{\partial v_i}{\partial x_j} + \frac{\partial v_j}{\partial x_i} \right) d^3x \, dt \qquad (4.51)$$

Kolmogorov conjectured that the integral (4.51) remains finite when $\mu \to 0$ because the gradient of the velocity grows. The total orders of derivatives of $x(t, \xi, y)$ in (4.50) and (4.51) are the same (remember that $v^i = \partial x^i / \partial t$). Nevertheless, it is perhaps possible that the integral (4.50) tends to zero if $\mu \to 0$ because the derivative with respect to parameters may reduce the smoothness of $x(t, \xi, y)$ less than the derivatives with respect to space coordinates and time. If this is the case, the parametric response of turbulent flow is controlled by one function, the dynamical potential.

4.8   On thermodynamics of open fluid flows

Thermodynamics of open flows differ drastically from thermodynamics of closed flows. The matter is that the system does not consist of the same set of particles: new particles permanently come into play. In order to understand the situation, we must first extend the Hamilton variational principle, which was originally formulated for closed systems, to open ones. We will do that for fluid flows; the extension to other open systems is similar.

It is convenient to consider open flows in terms of Eulerian coordinates. We start from consideration of the Hamilton variational principle for closed systems in Eulerian coordinates.

Variational principle in Eulerian coordinates. To obtain the variational principle in Eulerian coordinates, one needs to choose some functions of x^i and t as required functions instead of functions of Lagrangian coordinates $x^i(\xi^a, t)$. A natural candidate for the basic required kinematical characteristics are inverse functions of $x^i(\xi^a, t)$:

$$\xi^a = \xi^a \left(x^i, t \right) \qquad (4.52)$$

The velocity $v^i \left(\xi^a, t \right) = \partial x^i \left(\xi^a, t \right) / \partial t$ becomes a function of the Eulerian coordinate x^i if ξ^a is expressed in terms of x^i and t by the means of (4.52). To obtain an explicit expression for the velocity in terms of the derivatives of the functions $\xi^a(t, x)$, we set the condition that the Lagrangian coordinates do not change along the trajectories of the particles,

$$\frac{\partial \xi^a \left(x^i, t \right)}{\partial t} + v^i \frac{\partial \xi^a}{\partial x^i} = 0 \qquad (4.53)$$

Equation (4.53) can be considered as a system of three linear algebraical equations with respect to three unknown quantities v^i. The determinant of this system,

$$\det \left\| \frac{\partial \xi^a}{\partial x^i} \right\| = \frac{1}{\Delta} \qquad (4.54)$$

is not equal to zero, therefore

$$v^i = -x_a^i \xi_t^a \qquad (4.55)$$

where $\xi^a_t = \partial\xi^a/\partial t$, and x^i_a are the components of the matrix which is the inverse of the matrix $\|\xi^a_i\|$ with $\xi^a_i = \partial\xi^a/\partial x^i$. The functional (4.48) can be considered as a functional on the set of functions $\xi^a(x^i, t)$

$$I\left\{\xi^a\left(x^i, t\right)\right\} = \int\limits_{t_0}^{t_1}\int\limits_V \rho\left(\tfrac{1}{2}v_i v^i - U(\rho)\right)d^3xdt = \int\limits_{t_0}^{t_1}\int\limits_V \rho\left\{\tfrac{1}{2}x^i_a x_{ib}\frac{\partial\xi^a}{\partial t}\frac{\partial\xi^b}{\partial t} - U(\rho)\right\}d^3xdt$$

(4.56)

where ρ is given by (4.45), while Δ is determined by (4.54).

The set of admissible functions $\xi^a(x^i, t)$ is determined by the constraints

$$\xi^a\left(x^i, t\right) \in \partial V_0 \quad \text{if} \quad x^i \in \partial V$$

(4.57)

$$\xi^a\left(x^i, t\right) = \xi^a_o\left(x^i\right), \quad \xi^a\left(x^i, t_1\right) = \xi^a_1\left(x^i\right)$$

(4.58)

Constraints (4.57) and (4.58) are inversions of (4.46) and (4.47), respectively.

The variational principle in Eulerian coordinates states that the real motion of an ideal fluid is a stationary point of the functional (4.56) on the set of functions $\xi^a(x^i, t)$, determined by the constraints (4.57) and (4.58). Varying the functional (4.56) with respect to the admissible functions $\xi^a(x^i, t)$, one gets the equations of motion of an ideal fluid. For the reader's convenience, we present here a derivation of this fact; the derivation follows [24].

Consider first a functional of the general form

$$I = \int\limits_{t_0}^{t_1}\int\limits_{V(t)} \Lambda\left(\xi^a, \xi^a_i, \xi^a_t, x^i\right) d^3xdt$$

Then,

$$\delta I = \int\limits_{t_0}^{t_1} dt\left[\int\limits_{V(t)} \frac{\delta\Lambda}{\delta\xi^a}\partial\xi^a d^3x + \int\limits_{\partial V(t)} \partial\xi^a\left(\frac{\partial\Lambda}{\partial\xi^a_i}n_i - \frac{\partial\Lambda}{\partial\xi^a_t}c\right)d^2x\right] +$$

$$+ \left[\int\limits_{V(t)} \frac{\partial\Lambda}{\partial\xi^a_t}\partial\xi^a d^3x\right]_{t_0}^{t_1}$$

(4.59)

where $\delta\Lambda/\delta\xi^a$ is the variational derivative,

$$\frac{\delta\Lambda}{\delta\xi^a} = \frac{\partial\Lambda}{\partial\xi^a} - \frac{\partial}{\partial x_i}\frac{\partial\Lambda}{\partial\xi^a_i} - \frac{\partial}{\partial t}\frac{\partial\Lambda}{\partial\xi^a_t},$$

(4.60)

n_i are the components of the unit outward normal vector at ∂V, and c is the velocity of the surface ∂V along the normal to this surface.

Let us show that the equation $\delta\Lambda/\delta\xi^a = 0$ can be transformed into the usual form of equations of an ideal fluid,

$$\frac{\partial\rho v_i}{\partial t} + \frac{\partial}{\partial x^j}\left(\rho v_i v^j + p\delta^j_i\right) + \rho\frac{\partial\Phi(x)}{\partial x^i} = 0, \quad p = \rho^2\frac{\partial U(\rho)}{\partial\rho}$$

(4.61)

if

$$\Lambda = \rho \left(\frac{v^2}{2} - U(\rho, \xi^a) - \Phi(x) \right) \tag{4.62}$$

$\Phi(x)$ is the potential of the body forces, and the density and velocity are expressed in terms of ξ^a, ξ_i^a and ξ_t^a by (4.45), (4.54) and (4.55). To transform (4.60) into (4.61), we need the identity

$$\xi_i^a \frac{\delta\Lambda}{\delta\xi^a} = -\partial_i\Lambda - \frac{\partial}{\partial x^k}\left(\xi_i^a \frac{\partial\Lambda}{\partial\xi_k^a} - \Lambda\delta_i^k\right) - \frac{\partial}{\partial t}\left(\xi_i^a \frac{\partial\Lambda}{\partial\xi_t^a}\right) \tag{4.63}$$

and the relations

$$\xi_i^a \frac{\partial\Lambda}{\partial\xi_j^a} - \Lambda\delta_i^j = -\rho v_i v^j - \rho^2 \frac{\partial U}{\partial\rho}\delta_i^j, \quad \frac{\partial\Lambda}{\partial\xi_t^a}\xi_i^a = -\rho v_i, \quad \partial_i\Lambda = -\rho\frac{\partial\Phi}{\partial x_i} \tag{4.64}$$

Identity (4.63) is obtained by multiplying (4.60) by ξ_i^a, summing over a and differentiating by parts,

$$\xi_i^a \frac{\delta\Lambda}{\delta\xi^a} = \xi_i^a \frac{\partial\Lambda}{\partial\xi^a} - \frac{\partial}{\partial x^k}\left(\xi_i^a \frac{\partial\Lambda}{\partial\xi_k^a}\right) - \frac{\partial}{\partial t}\left(\xi_i^a \frac{\partial\Lambda}{\partial\xi_t^a}\right) + \frac{\partial\Lambda}{\partial\xi_k^a}\frac{\partial\xi_k^a}{\partial x^i} + \frac{\partial\Lambda}{\partial\xi_t^a}\frac{\partial\xi_t^a}{\partial x^i}$$

$$= -\partial_i\Lambda - \frac{\partial}{\partial x^k}\left(\xi_i^a \frac{\partial\Lambda}{\partial\xi_k^a} - \Lambda\delta_i^k\right) - \frac{\partial}{\partial t}\left(\xi_i^a \frac{\partial\Lambda}{\partial\xi_t^a}\right)$$

Here $\partial_i\Lambda$ is the partial derivative of Λ with respect to x_i for fixed ξ^a, ξ_i^a, ξ_t^a. To derive (4.64), we need the relations

$$\frac{\partial x_b^i}{\partial\xi_k^a} = -x_a^i x_b^k, \quad \xi_i^a \frac{\partial\rho}{\partial\xi_j^a} = \rho\delta_i^j, \quad \xi_i^a \frac{\partial v^j}{\partial\xi_k^a} = v^k\delta_i^j, \quad \xi_i^a \frac{\partial v^j}{\partial\xi_t^a} = -\delta_i^j \tag{4.65}$$

The first formula, (4.65) is obtained by differentiating the equality $x_b^i\xi_j^b = \delta_j^i$ with respect to ξ_k^a,

$$\frac{\partial x_b^i}{\partial\xi_k^a}\xi_j^b + x_b^i\delta_a^b\delta_j^k = 0$$

and contracting with x_a^j. The second formula (4.65) follows from the relation $\frac{\partial\Delta^{-1}}{\partial\xi_i^a} = \Delta^{-1}x_a^i$. Indeed,

$$\frac{\partial\rho}{\partial\xi_i^a} = \frac{\partial}{\partial\xi_i^a}\rho_o\Delta_o\Delta^{-1} = \rho x_a^i$$

The last two relations (4.65) can be derived from the first one and (4.55)

$$\frac{\partial v^i}{\partial\xi_k^a} = -\frac{\partial}{\partial\xi_k^a}x_b^i\xi_t^b = x_a^i x_b^k\xi_t^b = -x_a^i v^k, \quad \frac{\partial v^i}{\partial\xi_t^a} = -x_a^i$$

Equation (4.61) follows from (4.60) and (4.64).

If the positions of the particles are prescribed at $t = t_0, t_1$, then $\partial\xi^a = 0$ at $t = t_0, t_1$ and the last term in (4.59) vanishes. If the particles do not penetrate through or
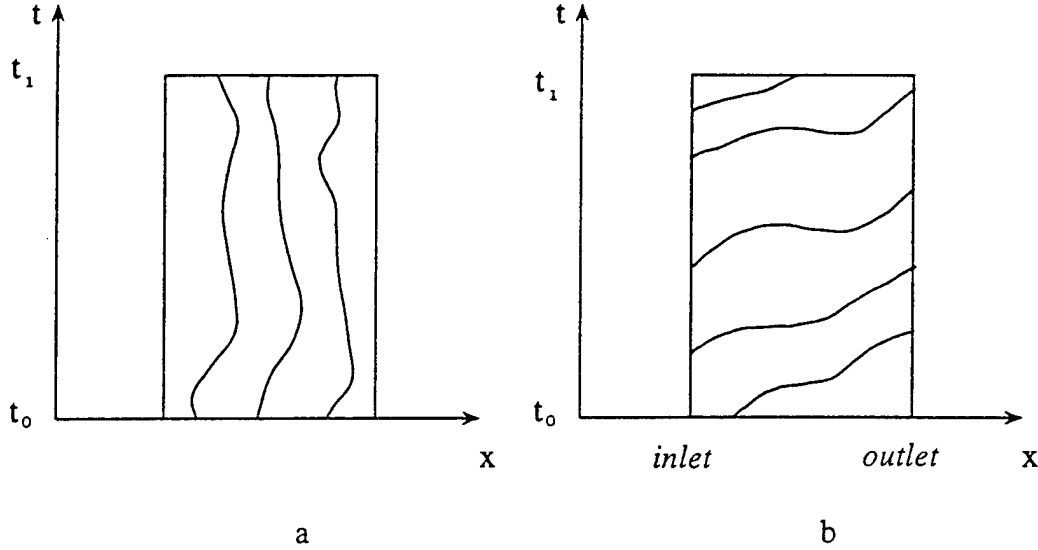
Fig. 4.9: Geometry if the particle trajectory in space-time for closed (a) and open (b) flows

detach from the boundary, $c = v_i n_i$, and the second term in (4.59) vanishes as well. Thus, the condition $\delta I = 0$ results in the equations of motion of an ideal fluid.

Note for further reference that in accordance with (4.64), the variation of the action functional becomes

$$\delta I = \int\limits_{t_0}^{t_1} dt \left\{ \int\limits_{\partial V(t)} \partial \xi^a x_a^i \left[\left(-\rho v_i v^j + (\Lambda - p) \delta_i^j \right) n_j + \rho v_i c \right] d^2 x \right\} - \left[\int\limits_{V(t)} \partial \xi^a x_a^i \rho v_i d^3 x \right]_{t_0}^{t_1}$$

$$(4.66)$$

Variational principle for open flows. To obtain an extension of the formulated variational principle to open flows, consider motion in four-dimensional space-time. A symbolic picture of motion in a closed container is shown in Figure 4.9a. Each trajectory connects the initial and final positions of the fluid particles, which are considered to be given. A typical open flow is shown in Fig. 4.9b. Each trajectory also connects the initial and final positions, but now some of the initial positions are at the inlet of the flow, while part of the final positions are at the outlet of the flow. In closed flows, the most natural choice of Lagrangian coordinates is an identification of Lagrangian coordinates with Eulerian ones at the initial time, $\xi^1 (x^i, t_0) = x^1, \xi^2 (x^i, t_0) = x^2, \xi^3 (x^i, t_0) = x^3$. In open flows, it is easy to identify one of the Lagrangian coordinates with the moment of the appearance of the particle, while two others can be coordinates of the point at the inlet, where the particle appears for the first time.

Consider now the initial and the final positions of the fluid particles at the inlet and outlet as given. The stationary points of the action functional are sought on the set of functions $\xi^a (x^i, t)$, which satisfy constraints (4.57), (4.58) along with the

following conditions at the inlet and the outlet:

$$\xi^a\left(x^i, t\right) = \xi^a_{in}\left(x^i, t\right) \quad \text{at the inlet}$$

$$\xi^a\left(x^i, t\right) = \xi^a_{out}\left(x^i, t\right) \quad \text{at the outlet}$$

(ξ^a_{in} and ξ^a_{out} are some prescribed functions). Then, the second term in (4.59) vanishes even if there is a flow through ∂V. Thus, the action functional has a stationary point at the real motion of an ideal fluid.

Parametric response of open flows. Consider the flow of an ideal compressible fluid through a region V. To include into consideration the case of compressor flow, we assume that there are some moving rigid bodies (e.g. rotor blades) inside the region V. The surface of the moving bodies is denoted by $\Sigma(t)$. In addition, there might be vortex sheets: the moving surfaces $S(t)$ on which the tangent components of the velocity have a jump while the normal components are continuous.

The inlet and outlet are flat surfaces. Denote the Cartesian coordinates of the inlet by $x^\alpha(\alpha = 1, 2)$. The coordinate x^3 is directed along the normal to the inlet and the outlet. Particles entering the flow field are marked by Lagrangian coordinates $\xi^\alpha, \xi^3 \equiv \xi$. We choose ξ^α to be equal to the coordinates x^α of the point of the inlet where the particle appears for the first time, while ξ is identified with the time when the particle enters the flow.

The derivatives $\partial \xi^\alpha / \partial x^i$ and $\partial \xi / \partial x^i$ can be expressed in terms of velocity at the inlet as

$$\xi^\alpha_\beta = \delta^\alpha_\beta, \quad \xi^\alpha_3 = -\frac{v^\alpha}{v}, \quad \xi^3_\alpha = 0, \quad \xi^3_3 = -\frac{1}{v} \tag{4.67}$$

where v^α and $v \equiv v_3$ are the transversal and the axial components of velocity at the inlet.

To derive (4.67), we note that according to the way ξ^α and ξ were introduced, at the inlet

$$\frac{\partial \xi^\alpha}{\partial x^\beta} = \delta^\alpha_\beta, \quad \frac{\partial \xi^\alpha}{\partial t} = 0, \quad \frac{\partial \xi}{\partial x^\alpha} = 0, \quad \frac{\partial \xi}{\partial t} = 1 \tag{4.68}$$

Using equations (4.53) at the inlet,

$$v^\beta \frac{\partial \xi^\alpha}{\partial x^\beta} + v \frac{\partial \xi^\alpha}{\partial x^3} = 0, \quad 1 + v \frac{\partial \xi}{\partial x^3} = 0$$

and (4.68), we arrive at (4.67).

At the inlet, the matrix $\|x^i_a\|$ has components

$$x^\alpha_\mu = \delta^\alpha_\mu, \quad x^\alpha_3 = -v^\alpha, \quad x^3_\alpha = 0, \quad x^3_3 = -v$$

and the determinant $\Delta_o = -v$.

The natural control parameters of fluid flow are discharge Q, frequency of rotation of the moving body ν, and the parameters of the geometry λ. (We denote by λ the set of geometrical parameters $\lambda_1, ..., \lambda_s$.)

It is assumed that ξ^a are some functions of $x^\alpha, \tau = \nu t, \nu, Q, \lambda$, and have bounded derivatives with respect to these arguments.

According to the formulated variational principle, we define the dynamical potential P by the relation

$$P(Q, \nu, \lambda) = \left\langle \int\limits_{V} \rho \left(\frac{1}{2} v_i v^i - U(\rho) \right) d^3 x \right\rangle \tag{4.69}$$

Here and until the end of this section $\langle . \rangle$ means the average with respect to dimensionless time τ over the attractor.

Let us find the derivatives of P with respect to parameters Q, ν and λ. As for a nonlinear oscillator, one can use formula (4.59) to determine these derivatives. However, there are complications requiring some corrections of (4.59) for this purpose. First, the integrand in (4.69) depends explicitly on parameter Q. Dependence on Q appears by means of the determinant Δ_0 through the expression for the density $\rho = \rho_o \Delta_o / \det \| \partial \xi / \partial x \|$. Since $\Delta_0 = -v$, where v is the velocity at the inlet, a change of Q causes a change of Δ_0. One may assume that v is proportional to Q: $v = Qu$, where u is some function of x^α independent of Q. Second, the integrand in (4.69) depends also explicitly on ν. Dependence on ν is caused by the dependence of the velocity on ν for any given τ, $v^i = -x_a^i \xi_\tau^a \nu$ ($\xi_\tau^a \equiv \partial \xi^a / \partial \tau$). Third, the geometry of the region V is changed due to the variation of the parameters λ.

The contributions to (4.59) caused by the variations Q and ν are

$$\left\langle \int\limits_{V(t)} \left(\frac{\partial \Lambda}{\partial \rho} \frac{\rho_0}{|\xi_i^a|} \frac{\partial \Delta_0}{\partial Q} \delta Q + \frac{\partial \Lambda}{\partial v^i} \left(-x_a^i \xi_\tau^a \right) \delta \nu \right) d^3 x \right\rangle =$$

$$= \left\langle \int\limits_{V(t)} \left(\frac{\partial \Lambda}{\partial \rho} \rho \frac{\partial \ln \Delta_o}{\partial Q} \delta Q + \frac{\partial \Lambda}{\partial v^i} v^i \frac{\delta \nu}{\nu} \right) d^3 x \right\rangle =$$

$$= \frac{\delta Q}{Q} \left(P - \left\langle \int\limits_{V} p \, d^3 x \right\rangle \right) + \frac{\delta \nu}{\nu} \left\langle \int\limits_{V} \rho v_i v^i d^3 x \right\rangle \tag{4.70}$$

The change of position of piece B of boundary ∂V causes an additional term

$$\left\langle \int\limits_{B} \Lambda \delta n \, d^2 x \right\rangle \tag{4.71}$$

to appear where δn is the displacement of B along its normal. Collecting (4.59), (4.70) and (4.71) and taking into account (4.66), we obtain

$$\delta P = \frac{\delta Q}{Q} \left(P - \left\langle \int\limits_{V} p \, d^3 x \right\rangle \right) + \frac{\delta \nu}{\nu} \left\langle \int\limits_{V} \rho v_i v^i d^3 x \right\rangle +$$

$$\left\langle \int\limits_{\partial V} \partial \xi^a x_a^i \left[\left(-\rho v_i v^j + (\Lambda - p) \delta_i^j \right) n_j + \rho v_i c \right] d^2 x \right\rangle + \left\langle \int\limits_{B} \Lambda \delta n \, d^2 x \right\rangle \tag{4.72}$$

The last two terms may be written more elaborately. The boundary ∂V consists of inlet, outlet, moving surfaces $\Sigma(t)$ and $S(t)$, varied surface B and a remainder,

which is some immovable surface A. At A, $\delta n = 0$, $c = 0$, $v^i n_i = 0$. The vector $\partial \xi^a x_a^i$ is a tangent to A. Thus, the surface integral over A in (4.72) disappears.

At the inlet, $\xi^\alpha = x^\alpha$ and $\xi = t$ independently of the value of the parameters Q, ν and λ. Therefore, $\partial \xi^a = 0$. Since $\delta n = 0$ at the inlet as well, the surface integral over the inlet vanishes.

At the outlet, $c = 0$, $\delta n = 0$, and the integral over the outlet is

$$\left\langle \int_{outlet} \partial \xi^a x_a^i \left(-\rho v_i v^j - \rho \left(\frac{p}{\rho} + U - \frac{v^2}{2} \right) \delta_i^j \right) n_j d^2 x \right\rangle \tag{4.73}$$

The vector $\partial \xi^a x_a^i$ has a simple geometrical interpretation. Consider the position vector of the particle $\xi^a : x^i (\tau, \xi^a, \lambda)$. The identity

$$x^i (\tau, \xi^a (\tau, x, \lambda), \lambda) \equiv x^i \tag{4.74}$$

holds. Differentiating this identity with respect to λ, we get

$$\frac{\partial x^i}{\partial \xi^a} \frac{\partial \xi^a}{\partial \lambda} + \frac{\partial x^i}{\partial \lambda} = 0 \tag{4.75}$$

Hence, $\partial x^i = -\partial \xi^a x_a^i$ is the translation vector of the particles at the outlet caused by variation of the parameters.

It is convenient to write (4.73) in terms of enthalpy, $i = U + (p/\rho)$,

$$\left\langle \int_{outlet} \partial \xi^a x_a^k \rho \left(v_k v^j + \left(i - \frac{v^2}{2} \right) \delta_k^j \right) n_j d^2 x \right\rangle \tag{4.76}$$

At the surface, $\Sigma(t) v^j n_j = c$. If the set of parameters λ does not contain geometrical parameters of the surface $\Sigma(t)$, i.e. $\Sigma(t)$ moves in the same way for all values of λ, then $\delta n = 0$ at $\Sigma(t)$, while the vector $\partial x^i = -x_a^i \partial \xi^a$ is tangent to Σ. Therefore, the integral over Σ is equal to zero.

At the surface S, integration is conducted over both sides of S. Since on each side $v^i n_i = c$ and $\partial x^i n_i = \delta n$, the integral over S is equal to

$$\left\langle \int_{S(t)} \partial x^i n^i [p] d^2 x \right\rangle \tag{4.77}$$

where $[p]$ is the pressure drop across S. One may assume that pressure is continuous on vortex sheets. Then (4.77) vanishes.

At the surface B, $\partial x^i n_i = \delta n$ and $v^j n_j = c$. Therefore, the integral over B is

$$\left\langle \int_B \delta n p d^2 x \right\rangle$$

Denote by F a generalized force corresponding to a change of λ,

$$F = \left\langle \int_B \frac{\delta n}{\delta \lambda} p d^2 x \right\rangle$$

Note an important case: if λ is the radius of some pipe inside V, then F coincides with the integral of the average pressure over the pipe surface,

$$F = \int_B \langle p \rangle \, d^2 x$$

Finally, for δP, we have

$$\delta P = \frac{\delta Q}{Q} \left(P - \left\langle \int_V p d^3 x \right\rangle \right) + \frac{2\delta\nu}{\nu} \left(P + \left\langle \int_V \rho U d^3 x \right\rangle \right) +$$
$$- \left\langle \int_{outlet} \partial \xi^a x_a^i \rho \left(v_k v^j + \left(i - \frac{v^2}{2} \right) \delta_k^j \right) n_j d^2 x \right\rangle + \left\langle \int_{B+\Sigma} \delta n p d^2 x \right\rangle \qquad (4.78)$$

Consider the most practically interesting case, where the tangent velocity at the outlet is negligible compared to the axial velocity. Then, the third term becomes

$$- \left\langle \int_{outlet} \partial \xi^a x_a^i n_k \rho \left(\frac{1}{2} v_k v^k + i \right) d^2 x \right\rangle \qquad (4.79)$$

Assume that fluctuations of $\partial \xi^a x_a^i$ and dynamical enthalpy $v^2/2 + i$ are small compared to their average values. Accept also that the average value of the dynamical enthalpy is practically constant over the outlet. Then, the integral (4.79) is simplified to

$$- \tilde{I} \int_{outlet} \partial \langle \xi^a \rangle \, \langle x_a^i \rangle \, n_i d^2 x \qquad (4.80)$$

where $\tilde{I}$ is the average dynamical enthalpy,

$$\tilde{I} = \left\langle \rho \left(\frac{1}{2} v_k v^k + i \right) \right\rangle \qquad (4.81)$$

Further simplifications are possible if we assume that the average value $\langle \xi^\alpha \rangle$ does not depend on λ due to turbulent mixing: it seems reasonable to accept that any fixed point of the outlet can be reached from any point of the inlet with some probability and the probability distribution does not depend on values of λ. Then, the average value $\langle \xi^\alpha \rangle$ certainly does not depend on λ. The difference $t - \langle \xi \rangle$ is the average time which particles spend inside the device, and we denote it by $\Theta(\lambda)$. The factor $\langle x_3^i \rangle \, n_i$ can be transformed into $\langle \partial x^i / \partial \xi \rangle \, n_i = \partial \bar{x} / \partial \xi$, where $\bar{x} = \langle x^3 \rangle$. The function $\bar{x}(\xi, \lambda)$ determines the (average) position of a particle on the x^3-axis, which was at the inlet at instant ξ. Since fluctuations of $\xi(t, x, \lambda)$ are assumed to be small compared to $\langle \xi(t, x, \lambda) \rangle$, in the vicinity of the outlet $\langle \xi \rangle \approx t - \Theta(\lambda)$, and differentiation of $\bar{x}$ with respect to ξ is equivalent to differentiation with respect to time. Thus, $\partial \bar{x} / \partial \xi$ is equal to the average velocity at the outlet, v_{out}. Finally, (4.79) becomes

$$I \partial \Theta \qquad (4.82)$$

where $I = \tilde{I} S_{out} v_{out}$, and S_{out} is the cross-sectional area of the outlet.

Collecting (4.78)-(4.82), we arrive at the constitutive equations

$$\frac{\partial P}{\partial Q} = \frac{1}{Q}\left(P - \left\langle \int_V p\,d^3x\right\rangle\right) + I\frac{\partial \Theta}{\partial Q}$$

$$\frac{\partial P}{\partial \nu} = \frac{2}{\nu}\left(P + \left\langle \int_V \rho U\,d^3x\right\rangle\right) + I\frac{\partial \Theta}{\partial \nu} \qquad (4.83)$$

$$\frac{\partial P}{\partial \lambda_m} = F_m + I\frac{\partial \Theta}{\partial \lambda_m} \quad , \quad m = 1,...,s$$

If the integrals of p and U in (4.83) can be neglected (which seems possible for high values of the discharge Q), then we have three functions P, I and Θ which should be found from experiments in order to establish the constitutive relations.

Truncation in Elastodynamics: Influence of Driven Degrees of Freedom on the Leading Ones

V. Berdichevsky*and P. Matusov

Mechanical Engineering, Wayne State University, Detroit MI 48202.

email: vberd@me1.eng.wayne.edu, peter@peter.eng.wayne.edu

Abstract. The problem of truncation of continuum equations is discussed. It is shown that, under some conditions, the modes are splitted into two categories: leading modes and driven modes. Dynamics of driven modes is completely determined by dynamics of leading modes. There is also some backward interaction: the standard truncation ignoring the influence of the neglected modes on the kept ones may yield incorrect results. A simple rule for incorporation of the influence of the driven modes is proposed. The limitations for this rule are outlined. The general statements are supported by numerical simulations for string vibrations.

1 Introduction

Experiments show (see, for example, [1], [2]) that, usually, only a few degrees of freedom are effectively excited in vibrating elastic structures which possess, in principle, infinitely many of them. The purpose of this paper is to discuss this phenomenon, and develop a method of constructing adequate finite-dimensional models.

---

*Member of ASME

The truncation problem can be formulated as follows. Kinematics of any elastic continuum can be described by a countable set of generalized coordinates $q_1, \ldots, q_n, \ldots$. Vector with the components $(q_1, \ldots, q_n, \ldots)$ is denoted by q. Physical properties of the structure are given by the expressions for kinetic energy $K(q, \dot{q})$, elastic energy $U(q)$, and dissipative function $D(q, \dot{q})$. External forces are assumed to be potential, the potential is denoted by $\Phi(q, t)$. Lagrange's function of the system has the form

$$L(q, \dot{q}, t) = K(q, \dot{q}) - U(q) + \Phi(q, t). \tag{1.1}$$

We assume that K and D are positive quadratic forms with respect to $\dot{q}_i$:

$$K = \frac{1}{2} a_{ij}(q) \dot{q}_i \dot{q}_j, \tag{1.2}$$

$$D = \frac{1}{2} \mu_{ij}(q) \dot{q}_i \dot{q}_j. \tag{1.3}$$

Summation over repeated indices is implied. The governing dynamical equations are

$$\frac{d}{dt} \frac{\partial L}{\partial \dot{q}_i} - \frac{\partial L}{\partial q_i} + \frac{\partial D}{\partial q_i} = 0 \tag{1.4}$$

Friction coefficients μ_{ij} are supposed to be small; the only role of dissipation in our study is to lead phase trajectories to an attractor.

A distinctive feature of elastic structures in the framework of physically linear theory is that elastic energy is a quartic polynom of q:

$$U = \frac{1}{2} A_{ij} q_i q_j + \frac{1}{3} A_{ijk} q_i q_j q_k + \frac{1}{4} A_{ijkl} q_i q_j q_k q_l, \tag{1.5}$$

while "masses" a_{ij} are some constants.

The questions under consideration are: in which cases the infinite-dimensional dynamical system (1.1)-(1.5) can be approximated by a low-dimensional system? How to construct the low-dimensional system?

We single out a class of problems for which we show that the low-dimensional system has coordinates $q_1, \ldots, q_k$ and the effective elastic energy of the system can be taken as

$$\bar{U}(q_1, \ldots, q_k, t) = \min_{q_{k+1}, q_{k+2}, \ldots} (U(q) - \Phi(q, t)). \tag{1.6}$$

2

For the case of string vibrations, truncation (1.6) works with good accuracy while the standard truncation

$$\bar{U}_{st}(q_1, \ldots, q_k, t) = U(q) - \Phi(q, t)\Big|_{q_{k+1} = q_{k+2} = \ldots = 0} \qquad (1.7)$$

may yield incorrect results.

In terms of continua the truncation (1.6) means the following. Let $U(u)$ be the energy functional of elastic medium occupying the region V, u is displacement field in V. Denote by ϕ the eigenmodes of linear vibrations of this media normalized by the condition (ρ - mass density):

$$\int_V \rho \phi_i \phi_j d^3 x = \delta_{ij}. \qquad (1.8)$$

Let $\Phi(u, t)$ be the linear functional of the work done by external forces. Consider the variational problem

$$\bar{U} = \min_u \left[U(u) - \Phi(u, t) \right], \qquad (1.9)$$

where minimum is sought on the set of all admissible functions u obeying the constraints

$$\langle u\phi_1 \rangle = q_1, \ldots, \langle u\phi_k \rangle = q_k \qquad (1.10)$$

and t is a parameter. Minimum value in the variational problem (1.9) is a function of $q_1, \ldots q_k$ and t : $\bar{U} = \bar{U}(q_1, \ldots, q_k, t)$.

The Lagrange's function of the proposed truncation has the form:

$$\bar{L} = \frac{1}{2} \sum_{i=1}^{k} \dot{q}_i^2 - \bar{U}(q_1, \ldots, q_k, t). \qquad (1.11)$$

The way to choose the leading modes $\phi_1, \ldots, \phi_k$ and the number of modes k is discussed in Section 6.

The text is organized as follows. In the next Section we describe the idea underlying our approach. In Section 3 the basic equations for the example studied numerically, the string vibrations, are presented. In Sections 4 and 5 the counter examples for validity of the proposed truncation are presented; they outline the expected range of applicability of our approach. Then, in Section 6, we show that our truncation works better than the traditional one.

3

2 An observation

First, consider the truncation problem in the simplest case of linear vibrations when q are so small that the terms of the third and fourth order in (1.5) can be neglected. It is convenient to make a linear change of variables diagonalizing matrices a_{ij} and A_{ij}; matrix a_{ij} can be made unit under this transformation. The new variables are called mode coordinates and have the sense of the amplitudes of eigenmodes. We keep for the mode coordinates the same notation, q. In mode coordinates, Lagrange function takes the form

$$L = \sum_i \left(\frac{1}{2} \dot{q}_i^2 - \frac{1}{2} A_i q_i^2 + F_i(t) q_i \right). \tag{2.1}$$

The system forms a set of noninteracting oscillators with unit masses and rigidities A_i. Rigidity A_i is related to eigenfrequency of the ith mode $\overset{\circ}{\omega}_i$ by $A_i = \overset{\circ}{\omega}_i^2$. It is assumed, for simplicity, that all modes have different eigenfrequencies. The modes are numbered in the order of increased eigenfrequencies.

Truncation of an infinite-dimensional system makes sense if its motion is finite-dimensional. This means that the motion of the system can be recovered with an appropriate accuracy in terms of motion of some finite-dimensional system. At first glance, truncation of the linear system (2.1) is impossible because external forces may excite as many modes as one wishes. However, the situation is not so hopeless due to the following property of elastic structures: $\overset{\circ}{\omega}_i \to \infty$ if $i \to \infty$. To make use of this property let us change variables

$$q_i \to x_i : x_i = \overset{\circ}{\omega}_i q_i. \tag{2.2}$$

In the new variables Lagrange function takes the form

$$L = \sum_i \left(\frac{1}{2 \overset{\circ}{\omega}_i^2} \dot{x}_i^2 - \frac{1}{2} x_i^2 + \frac{F_i(t)}{\overset{\circ}{\omega}_i} x_i \right). \tag{2.3}$$

We see that "masses" $\overset{\circ}{\omega}_i^{-2}$ tend to zero for $i \to \infty$. Therefore, if the spectra of $F_i(t)$ are bounded and do not contain components with the eigenfrequencies $\overset{\circ}{\omega}_i$, inertia terms can be

4

neglected for large i, and we arrive at the static problem: to find x_i for large i one has to minimize the function

$$\min_{x_i} \sum_i \left(\tfrac{1}{2} x_i^2 - \frac{F_i(t) x_i}{\overset{\circ}{\omega}_i} \right).$$

In this formula time t plays the role of a parameter.

This simple observation forms the basis of our approach in nonlinear case. Let us denote by A_{ijk} and A_{ijkl} the ratios

$$A_{ijk} \doteq \frac{B_{ijk}}{\overset{\circ}{\omega}_i \overset{\circ}{\omega}_j \overset{\circ}{\omega}_k}, \qquad A_{ijkl} \doteq \frac{B_{ijk}}{\overset{\circ}{\omega}_i \overset{\circ}{\omega}_j \overset{\circ}{\omega}_k \overset{\circ}{\omega}_l}.$$

The equality sign $\doteq$ means that there is no summation over repeated indices.

The change of variables (2.2) yields the following expression for energy function $U - \Phi$:

$$U - \Phi = \tfrac{1}{2} x_i x_i + \tfrac{1}{3} A_{ijk} x_i x_j x_k + \tfrac{1}{4} A_{ijkl} x_i x_j x_k x_l - F_i(t) x_i / \overset{\circ}{\omega}_i .$$

Let A_{ijk} and A_{ijkl} be bounded for all i, j, k, l. Masses of modes in x_i-variables tend to zero for $i \to \infty$. It is natural to assume that for sufficiently large k, depended on the accepted accuracy, masses of all modes with $i \geq k$ can be set equal to zero. Then determination of all x_i with $i \geq k$ becomes a static problem: for given $x_1, \ldots, x_k$ and t find the minumum value of the function

$$\bar{U}(x_1, x_2, \ldots, x_k, t) = \min_{x_{k+1}, x_{k+2}, \ldots} (U - \Phi). \tag{2.4}$$

Then dynamics of the truncated system is governed by Lagrange's function

$$\bar{L} = \sum_i \frac{1}{2} \dot{x}_i^2 - \bar{U}(x_1, \ldots, x_k, t). \tag{2.5}$$

Returning back to the q-variables we obtain the formulas given in Introduction.

In reality, the situation is not so simple. There are some obstacles for our rule to be true. We discuss them in Sections 4 and 5 for the case of nonlinear string vibrations. In the next Section the equations of string dynamics are introduced.

5

3 Strings

Consider plane nonlinear vibrations of an elastic string of the length l with pinned ends (Fig.1). Let $w(t, x)$ be the lateral displacements of the string.

For moderate amplitudes, kinetic and potential energy are as follows:

$$K = \int\limits_0^l \frac{1}{2}\rho A w_t^2 dx, \tag{3.1}$$

$$U = \int\limits_0^l \left\{ A E_Y \left[\frac{1}{2}\left(\gamma + \frac{1}{2}w_x{}^2\right)^2 + \frac{1}{2}h^2 w_{xx}^2 \right] - F(x,t)w \right\} dx. \tag{3.2}$$

Here ρ, A, γ and E_Y are mass density, cross-section area, initial longitudinal strain and Young modulus, respectively; derivatives with respect to x and t are denoted by the corresponding indices. Constant h is determined by the diameter and shape of cross-section and proportional to $\sqrt{A}$. For circular cross-section of diameter d and isotropic material $h = d/4$. The first two terms in (3.2) are extension and bending energies, the last term is the potential of external force $F(x,t)$.

Let us introduce dimensionless variables

$$y = \frac{x}{l}, \quad u = \frac{w}{l\sqrt{2\gamma}}, \quad \tau = \sqrt{\frac{E_Y \gamma}{2\rho l^2}}t, \quad f = \frac{Fl\sqrt{2\gamma}}{A E_Y \gamma^2}. \tag{3.3}$$

In these variables the dimensionless Lagrangian takes the form:

$$L = \frac{K - U}{E_Y A l \gamma^2} = \int\limits_0^1 \left[\frac{1}{2}u_\tau^2 - \left(\frac{1}{2}u_y^2 + \frac{1}{4}u_y^4 + \frac{1}{2}\sigma u_{yy}^2 \right) + f(\tau, y)u \right] dy. \tag{3.4}$$

Parameter $\sigma = h^2/\gamma l^2$ is the dimensionless bending rigidity, it is small for thin strings with high initial tension and increases if initial tension is released. Nonzero bending rigidity provides the dispersion of linear waves.

String dynamics is described by the equation

$$u_{\tau\tau} = \left[u_y + u_y^3 - \sigma u_{yyy} \right]_y + f(\tau, y) + g(u, u_\tau), \tag{3.5}$$

6

where g is friction force. Physical nature and special form of friction force is inessential for what follows since damping is assumed to be small.

Consider a pinned string:

$$u(\tau,0) = u(\tau,1) = u_{yy}(\tau,0) = u_{yy}(\tau,1) = 0. \tag{3.6}$$

The linear eigenmodes of linear vibrations are:

$$u_k(y) = sin\pi ky.$$

Any function $u(\tau,y)$ can be presented in the form of Fourier series of eigenmodes

$$u(\tau,y) = \sum_{k=1}^{\infty} a_k(\tau) \sin \pi ky. \tag{3.7}$$

In modal approach the dynamics of strings is considered in terms of mode amplitudes $a_k(\tau)$. To obtain dynamical equations for $a_k(\tau)$ one has to express Lagrange's functional (3.4) in terms of mode amplitudes a_k. Substituting (3.7) into (3.4) we have:

$$2L = \sum_{k=1}^{\infty} \left\{ \frac{1}{2} \dot{a}_k{}^2 - \frac{1}{2}\left(1 + \sigma(\pi k)^2\right)(\pi k)^2 a_k^2 + f_k a_k \right\} - \frac{\pi^4}{2} \sum_{k,l,m,n=1}^{\infty} klmn A_{klmn} a_k a_l a_m a_n. \tag{3.8}$$

Here we use the notation:

$$
\begin{aligned}
f_k &= 2\int_0^1 f(\tau,y) sin\pi ky dy, \\
A_{klmn} &= \int_0^1 \cos\pi kx \cos\pi lx \cos\pi mx \cos\pi nx dx = \\
&= \frac{1}{8} \big[\quad \delta(k+l+m-n) + \delta(k+l-m+n) \\
&\quad + \ \delta(k+l-m-n) + \delta(k-l+m+n) \\
&\quad + \ \delta(k-l+m-n) + \delta(k-l-m+n) \\
&\quad + \ \delta(k-l-m-n) \big],
\end{aligned} \tag{3.9}
$$

where $\delta(k)$ means the function which is equal to zero for $k \neq 0$, and equal to unity for $k = 0$. Dot denotes derivative with respect to τ. Note that interaction between modes is very complex: each mode interacts with all other modes.

It is seen from (3.8) that Lagrange's functional, and, henceforth, the equations, can be simplified by the change of unknown functions $a_k \rightarrow b_k$:

$$b_k = \pi k a_k. \qquad (3.10)$$

In terms of b_k, Lagrange's functional takes the form

$$2L = \sum_{k=1}^{\infty} \left[\frac{1}{2(\pi k)^2} \dot{b}_k^2 - \frac{1}{2} \left(1 + \sigma(\pi k)^2\right) b_k^2 + \frac{f_k}{\pi k} b_k \right] - \frac{1}{2} \sum_{k,l,m,n=1}^{\infty} A_{klmn} b_k b_l b_m b_n. \qquad (3.11)$$

The corresponding equations of motion are

$$\frac{1}{(\pi k)^2} \ddot{b}_k = - \left(1 + \sigma(\pi k)^2\right) b_k - 2 \sum_{k,l,m,n=1}^{\infty} A_{klmn} b_l b_m b_n + \frac{f_k}{\pi k} - g_k. \qquad (3.12)$$

Coefficients A_{ijkl} characterize nonlinear interactions between modes. They all are of order unity. Note an important property of A_{ijkl} following from (3.9) : if i is even and j, k, l are odd, then, since $\pm j \pm k \pm l$ are also odd, $A_{ijkl} = 0$. Similarly, $A_{ijkl} = 0$ if i is odd and j, k, l are even. This means that even modes themselves cannot excite odd modes and vice versa. Even modes act on odd modes only if the latter have already been excited (q_i for at least one odd i are not zeros). The same is true for influence of odd modes on the even ones.

Let spectrum of external force is zero for frequencies greater than $\pi k_0 \sqrt{1 + \sigma(\pi k_0)^2}$, k_0 is some integer. In accordance with the recipe proposed, one has to put the left hand side of equations (3.12) equal to zero for all $k \geq k_0$. Then equations for b_k, $k \geq k_0$, become algebraical equations. This simplifies essentially the numerical procedure because the time step for integration (which should be a small fraction of the shortest timescale in the system) now can only be chosen small enough to resolve the vibrations with the frequency $\pi k_0 \sqrt{1 + \sigma(\pi k_0)^2}$, much larger than if we had to resolve vibrations with higher frequencies.

There are some obstacles for this recipe to be universal. One of them is equipartition of energy for high energy vibrations.

4 Obstacle One: Equipartition of Energy.

Free vibrations. For the first time equipartition of energy in string-like systems has been studied numerically by Fermi, Pasta, and Ulam in 1954 [3]. They considered a finite-difference truncation of equation (3.5) with $\sigma = 0, f = 0, g = 0$. Equations of their finite-difference approximation are equivalent to dynamical equations of a finite chain of mass particles connected by nonlinear springs. It was a common belief that nonlinear systems with very many degrees of freedom should move ergodically. One of the features of ergodic motion is equipartition of energy. In the case of a chain of mass particles equipartition of energy means that averaged kinetic energies of all particles are equal:

$$\left\langle m_1 \dot{q}_1^2 \right\rangle = \left\langle m_2 \dot{q}_2^2 \right\rangle = ... = \left\langle m_N \dot{q}_N^2 \right\rangle. \tag{4.1}$$

Here m_i and q_i are the mass and displacement of the ith particle, and $\langle \cdot \rangle$ means time average over trajectory: for any function $\phi(q, \dot{q})$

$$\langle \phi \rangle = \lim_{\theta \to \infty} \frac{1}{\theta} \int_0^\infty \phi\left(q(t), \dot{q}(t)\right) dt. \tag{4.2}$$

Average value in (4.1) does not depend on trajectory for ergodic systems. The common value (4.1) is called by definition absolute temperature.

Numerical simulations have been conducted by Fermi, Pasta, and Ulam for a chain of initially disturbed 64 particles. The expected equipartition of energy has not been observed. This "paradox" was named Fermi-Pasta-Ulam (FPU) problem. Explanation has been given by KAM theory [4]. For small values of initial energy the nonlinear system stays close to the linear system which is integrable and, therefore, is not ergodic. Further numerical studies supported this explanation. It was shown ([5] - [8]) that there is energy threshold exceeding of which yields equipartition. In their experiments Fermi, Pasta, and Ulam did not reach energy threshold. Note that the laws of equilibrium statistical mechanics, and, in particular, equipartition of energy, are based only on ergodicity of motion and stay valid for low-dimensional systems (see [9], [10]).

If equipartition of energy occurs none of the modes can be neglected. Thus, there is a necessary condition for applicability of our truncation: energy of vibration should not exceed energy threshold.

In order to determine the value of energy threshold we conducted a series of numerical simulations for the system with the number of modes $N = 8, 12$, and 16. In terms of finite-difference truncation it corresponds to a chain of approximately 80 to 160 particles if one put 10 particles per the shortest spatial wave period which is 1/16 - 1/8 in our case. The integration has been performed using Runge-Kutta scheme of the 7th order, with resolution of 70 to 200 points per period of the highest mode. The accuracy of integration has been verified by two methods: conservation of energy and reverse integration. The total energy was proven to conserve with 10^{-7} accuracy for the runs being as long as 10,000 periods of the lowest mode. Within a range of nondimensional energy values up to 1 (far above equipartition threshold) the integration was reversible within an interval of approximately 5,000 longest cycles[1].

To verify the tendency of the system to equipartition we create some initial perturbation and track the temporal behavior of the mode temperatures $T_k = \langle \dot{b}_k^2 / 2\pi^2 k^2 \rangle, k = 1, \ldots, N$.

A typical dependence of temperatures T_i on time is shown on Fig.2 for a moderate value of initial energy. It is seen that no equipartition is observed.

We found that for energy of initial disturbance exceeding some value $E^* = 5 * 10^{-2}$ the typical picture of dependence of modal temperatures on time is like shown in Fig.3. It is not clear whether the value $E^* = 5 * 10^{-2}$ is really a good approximation for threshold energy. First, E^* should be the energy threshold for most of initial data while we have checked this fact for several dozens of initial data. Second, the trajectories of the dynamical system (3.12) exponentially diverge if initial energy is of an order E^*, and it is not clear whether our numerical simulations reflect correctly the dynamics of original dynamical system.

---

[1] The transition time to equipartition is typically longer with only a few modes excited initially, but for initial values close to equipartition it is usually reached within a few thousand cycles.

The value of threshold energy $E^* = 5 * 10^{-2}$ is very close to the values obtained earlier in [11] (and, after appropriate scaling, [6] - [8]). In contrast to the previously conducted computations for chains, in our simulations the equipartition state has been reached in many cases with very low initial energy. The most probable cause is the absense of exact mode resonanses in chains (see below).

To estimate whether the oscillations in real strings can be close to equipartition, consider a 10m long steel string with Young modulus $E_Y \approx 2 * 10^{11}$Pa, cross-sectional area 0.1 cm^2, and pre-strain $\gamma = 10^{-3}$. Then energy of vibrations corresponding to non-dimensional equipartition energy $E^* = 0.05$ is about 2 Joules, characteristic strains are of order $3 * 10^{-4}$ while characteristic lateral displacements of order 0.5m, this value is large but not unattainable.

Fig.3 exhibits the behavior of the mode temperatures in course of free dynamics of a 12-mode system (3.12) without dispersion and dissipation. Initially the first four modes were excited with amplitude 0.2 and zero initial velocity (corresponding to nondimensional elastic energy of 0.095). The final temperature spectrum is almost homogeneous, thus very close to equipartition state.

To quantify the degree of equipartition reached the following characteristic can be employed:

$$C^* = \frac{\left[\sum_{i=1}^{N} T_i\right]^2}{\sum_{i=1}^{N} T_i^2}, \tag{4.3}$$

where T_i are the mode temperatures. The characteristics C^* has a simple meaning. If only one mode is excited, $C^* = 1$. If all modes are excited and equipartition holds, $T_1 = T_2 = \ldots = T_N$, and $C^* = N$. Thus, C^* measures how many degrees of freedom are involved in motion. Maximum value of C^* is equal to N. It is reached only if equipartition holds. Hence, C^* is also a measure of equipartition. To compare different motions, it is convenient to normalize C^* and consider the number $C = C^*/N$, which represents the relative amount of effectively excited degrees of freedom. Dependence of C on time shows how the new degrees of freedom are being involved in motion. The typical dependence is shown in Fig.4.

11

This Figure illustrates the results for four runs with duration 1,500-3,000 cycles; the system (3.12) has been excited with zero velocities and initial potential energy evenly distributed among the first four modes. The computaions are performed for initial energy 0.002, 0.01, 0.05 and 0.095.

At moderate energies of initial perturbation, the process of establishing of temperature equilibrium can take very long time. In such cases the temporal behvior of the value C can give a clue to future dynamics.

It can be clearly seen that the system provided with higher energy reaches equipartition very fast, just in a few hundred longest oscillation periods. The less energy is supplied to the system initially, the longer it takes to reach equipartition. When the energy is less than some certain value, equipartition seems never be reached. The insert in the Figure shows the temperature spectra at the end of the runs. In a case of $E = 0.002$ temperature of the first and second modes are by more than an order more than those of modes 7-12, showing no equipartition.

Figure 5 supports our conclusion that energy threshold value is 0.05. It is seen that for $E^* > 0.05$ practically all modes are equally excited for all tested initial conditions. For $E^* < 0.05$ there are initial conditions for which energy is not equipartitioned among modes.

Note that the equipartition of energy can be reached from some initial conditions at energies substantially smaller than E^*. This implies further limitation for the truncation proposed.

Other aspects of this topic can be found in [11], [12].

Forced vibrations. In the case of forced vibrations energy is no longer an integral of motion. The major characteristic of the level of nonlinearity becomes averaged energy.

We conducted numerical simulations for the case of a concentrated force $\mathcal{F}$ acting perpendicularly to the spring at a point very close to one end:

$$\mathcal{F}(\tau, y) = \mathcal{F}\delta(y - y_0)\cos\omega\tau, \qquad y_0 \ll 1.$$

12

The corresponding modal force magnitudes f_k are

$$f_k = 2\mathcal{F}\sin\pi k y_0 \cos\omega\tau \approx 2\mathcal{F}\pi k y_0 \cos\omega\tau.$$

The product $\mathcal{M} = \mathcal{F}y_0$ represents the moment acting on the string near its pinned end.

Figure 6 represents the temporal behavior of the system being excited with a moment $\mathcal{M} = 0.01, 0.035$, and 0.1 oscillating with a frequency $\omega = \pi$. The excitation frequency has been chosen equal to the eigenfrequency of the first mode to shorten the transient process. The average values of total energy near the end of each run were 4.6, 0.31, and 0.07, respectively.

5 Obstacle Two: Mode Resonanses.

In linear approximation modes do not interact. Each mode is excited directly by external force. Our truncation does certainly work if the spectra of external forces do not contain eigenfrequencies. Otherwise, inertia terms are of the same order as elastic forces and dynamics of high modes is far from being static. If energy of vibrations increases, nonlinear mode interactions are activated. The dynamical behavior of the structure becomes depending crucially on whether the eigenmodes are in resonance. Consider for example system (3.12) for $\sigma = 0, f_k = 0, g_k = 0$. Let the first mode is excited initially. The spectrum of the first mode contains the frequency $\overset{\circ}{\omega}_1 = \pi$. Coefficient $A_{3111} \neq 0$. Therefore the spectrum of elastic interaction force $A_{3111}x_1^3$ contains the frequency $3\overset{\circ}{\omega}_1 = 3\pi$ which is the linear eigenfrequency of the third mode. Hence, vibrations of the third mode will be resonant and inertia term will be of the order of elastic force. Considering the fifth mode we note that the coefficient A_{5311} is non-zero. The spectrum of interaction force $A_{5311}x_3x_1^2$, acting on the fifth mode, contains the frequency 5π which is its eigenfrequency. Thus, the fifth mode also vibrates in a resonance regime. Continuing this consideration we see that all modes have in their spectra resonant frequencies, and inertia terms cannot be neglected. Fortunately, the considered

13

case is the worst one: if σ is not zero, the eingenfrequencies are, in general, detuned, and our truncation start working. Here are some numerical examples.

Figure 7 illustrates the free dynamics of a 12-mode system (3.12) with a very small dispersion coefficient $\sigma = 10^{-4}$, with initial conditions exactly the same as for a case shown in Fig.3. The energy of initial excitation $E = 0.104$, which is definitely above the energy threshold found in Section 4 for $\sigma = 0$.

We see a remarkable phenomenon: the temperature distribution in the system is far from equipartition - it eventually evolves to a steeply decaying spectrum shown in the insert, where temperature of the first mode is six times greater than that of the 12th mode. This shows that the resonances play a crucial role in the formation of ergodic behavior. The system with a very small detuning from resonances does not exhibit ergodic motion for the same level of energy.

To further explore the effect of detuning on equilibrium temperature spectrum, several runs have been performed for $\sigma = 0, \ldots, 0.01$. The dependencies of C on time for cases with $\sigma = 0, 10^{-4}$, and 10^{-2} are shown in Figure 8 together with terminal temperature spectra. In the last case the value of C is almost constant, showing very little energy transfer from initially excited four modes to upper ones.

Note that if one approximates the string of length unity by a chain of N particles ([5]-[7]), the following dependence of linear eigenfrequency of the kth mode on a mode number k appears ([13]):

$$\omega_k^2 - 2\sin^2 \tfrac{k}{2N} = 0.$$

Since this dependence is nonlinear, there is no exact resonances between modes, and redistribution of energy among modes occurs at higher energy levels. This explains the fact that equipartition threshold found for chains exceeds that for system of modes (3.12) with $\sigma = 0$.

14

6 A Justification of Truncation.

The above observations suggest that in a nonlinear system with many degrees of freedom truncation is possible if there are no exact internal resonances between the modes, and the vibration energy is less than energy threshold. If, in addition, energy is pumped into low modes, the higher modes become driven by lower ones, while kinetic energy of high modes is negligible, and the truncation proposed might work.

To check the accuracy of our truncation we consider the 12-modes vibration as "exact", and approximate it by 2-mode truncation, i.e. by putting masses of the 3rd to 12th modes equal to zero. Amplitudes of the 3rd to 12th mode vibrations are determined by static equations. The string is excited by a periodic moment acting near the pinned end, and damped by equal friction forces $g_k = const$. The standard 2-mode truncation corresponds to equating the amplitudes of higher modes to zero.

Figure 9 represents the distribution of elastic energy over the modes for forced vibrations of the exact 12-mode system, the standard 2-mode truncation and the proposed 2-mode truncation. Elastic energy of the kth mode is, by definition, $\langle \frac{1}{4}(1 + \sigma\pi^2 k^2)b_k^2\rangle$. It can be seen that the proposed truncation has remarkable accuracy, while the standard truncation substantially overestimates the values of energy of lower modes and gives no information about the motion of higher modes.

Fig.10 shows how increasing the number of the modes kept improves the standard truncation. Comparing Fig.9 and 10 we see that even 6-mode standard truncation does not work as good as 2-mode truncation proposed.

It is difficult to expect that any truncation can predict instant characteristics of vibrations. Integral characteristics, nevertheless, should be predicted, otherwise the truncation is useless. Among integral characteristics the most interesting are the energy spectra and distribution functions. Distribution function $f(a)$ of some function of time $\phi(t)$ determines the portion of observation time, $f(a)\Delta a$, during which function $\phi(t)$ takes the values in the interval $[a, a + \Delta a]$. Figure 11 illustrate the distribution functions for the 1st and 2nd mode

15

momenta, respectively. The distribution functions have been calculated after the transition period is over, and the system moves over the attractor in phase space.

Note that distribution function of the harmonics, $A cos t$, is $f(a) = 1/\sqrt{A^2 - a^2}$. It has singularities at the points $a = \pm A$ because the harmonics spend considerable time in the vicinity of its maximum and minimum. In numerical simulations, since the averaging is made over a finite time interval, singularities are transformed into sharp maxima. Multiple maxima observable in Fig.11 correspond to multiple harmonics of the excitation frequency. It can be seen that distribution functions of the proposed truncation match the exact ones with a good accuracy for the first mode and qualitatively correct for the second one. Although the distribution function differs more for the second mode, it predicts average values $\langle p^2 \rangle$ and $\langle p^4 \rangle$ with accuracy 0.12% and 0.44%, respectively.

7 Conclusion

We have shown that a possible mechanism of low dimensionality of elastic vibrations of continua is the fast decay of inertia with the number of modes. The neglection of inertia terms for higher modes yields a low-dimensional model with good predictive power. This "massless" approximation fails if energy of excitation is too high and/or there are resonant modes.

Acknowledgements

References

[1] Paidoussis, M.P., Cusumano, J.P., and Copeland, G.S., "Low-dimensional chaos in a

flexible tube conveying fluid," *Transactions of the ASME. Journal of Applied Mechanics*, Vol. 59, No. 1, March 1992, pp. 196 – 205.

[2] Cusumano, J.P., Sharkady, M.T., and Kimble, B.W., "Experimental measurements of dimensionality and spatial coherence in the dynamics of a flexible-beam impact oscillator.," *Philosophical Transactions of the Royal Society, Series A (Physical Sciences and Engineering)*, Vol. 347, No. 1683, May 1994, pp. 421 – 438.

[3] Fermi, E., Pasta, J., and Ulam, S., "Studies of nonlinear problems. 1. Technical Report LA-1940," Technical report, Los Alamos Scientific Laboratory, May 1955.

[4] Arnold, V.I., Kozlov, V.V., and Neishtadt, A.I., *Mathematical Aspects of Classical and Celestial Mechanics*, volume 3 of *Encyclopaedia of mathematical sciences,*, Springer-Verlag, Berlin; New York, 1988.

[5] Izrailev, F. M. and Chirikov, B. V., "Statistical properties of a nonlinear string," *Soviet Physics - Doklady*, Vol. 11(1), 1966, pp. 30 – 32, Translated from Doklady Akademii Nauk SSSR, vol.166, No.1.

[6] Boccieri, P., Scotti, A., Bearzi, B., and Loinger, A., "Anharmonic chain with Lennard-Jones interaction," *Physical Review A*, Vol. 2, No. 5, 1970, pp. 2013 – 2019.

[7] Galgani, L. and Scotti, A., "Recent progress in classical nonlinear dynamics," *Revista Del Nuovo Cimenta*, Vol. 2(2), 1972, pp. 189 – 209.

[8] Kantz, H., Livi, R., and Ruffo, S., "Equipartition thresholds in chains of anharmonic oscillators," *Journal of Statistical Physics*, Vol. 76, No. 1-2, July 1994, pp. 627 – 643.

[9] Berdichevsky, V., "A connection between thermodynamical entropy and probability," *Journal of Applied Mathemtics and Mechanics (PMM)*, Vol. 52(36), 1988, pp. 738 – 746.

17

[10] Berdichevsky, V. and Alberti, M. v, "Statistical mechanics of Henon-Heiles oscillator," *Physical Review A*, Vol. 44, No. 2, 1991, pp. 858 – 865.

[11] Mueller, E., "Statistical properties of high-energy rod vibrations," Master's thesis, School of Aerospace Engineering, Georgia Institute of Technology, Atlanta, Georgia, August 1994.

[12] Berdichevsky, V., "Possible scenarios of nonlinear vibrations at high energy," *Proceedings of 1995 ASME Conference on Acoustics and Vibrations, NY*, Vol. 3, p.B, 1995, pp. 877 – 879.

[13] Kunin, I.A., *"Elastic media with microstructure"*, Ed.3, vol.1,2, Springer-Verlag, Berlin, Heidelberg, 1982.

Figure Captions

Fig.1. Elastic string with pinned ends.

Fig.2. A typical dependence of modal temperatures on time in free dynamics for moderate energy excitation . Graph shows modal temperatures for 8-mode system without dispersion or dissipation ($\sigma = g = 0$). Time is measured in terms of cycle, the period of the lowest mode oscillations. Initially all the modes have been excited with amplitudes and velocities decaying with increasing of mode number, total initial energy is $E = 0.0214$.

Fig.3. Behavior of mode temperatures for free dynamics of 12-mode system (3.12) with $\sigma = 0$ and $g_k = 0$. The insert shows the temperature spectrum at the end of a 1,500-cycle-long run. Total energy of 0.095 has been initially evenly distributed among the first four modes.

Fig.4. Time variations of C in free dynamics of the system (3.12) with $\sigma = g = 0$ provided initially with energy 0.002, 0.01, 0.05, and 0.095. The insert shows the temperature spectrum at the end of 1,500-3,000-cycle long runs.

Fig.5. Values of C for a 12-mode system ($\sigma = g = 0$) obtained for different energies of initial perturbation at $\tau = 1000$ periods of the 1st mode (or sooner if $C = 1 - 1/(2N) = 0.958$ has been reached).

Fig.6. Forced dynamics of the string (3.12) excited with a periodic moment at one end $f_k = 2\pi k \mathcal{M} \sin \pi t$, $\mathcal{M} = 0.01, 0.035$, and 0.1. Dispersion and dissipation parameters are set equal to zero.

Fig.7. Behavior of mode temperatures for free dynamics of a 12-mode system (3.12) with $\sigma = 10^{-4}$ and $g_k = 0$. The insert shows the temperature spectrum at the end of a 2,000-cycle-long run.

Fig.8. Forced dynamics of the system (3.12) under the same excitation as shown in Fig.6, but with dispersion taken into account: $\sigma = 0, 10^{-4}$, and 10^{-2}.

Fig.9. Energy spectra for forced dynamics of a 12-mode system (3.12), standard and proposed 2-mode truncation with $\sigma = 0.01$, $g_k = 0.01$, and $f_k(\tau) = \pi k \sin \tau$.

Fig.10. Energy spectra for forced dynamics of a 12-mode system (3.12) and standard truncation with 2, 4, and 6 modes left with $\sigma = 0.01$, $g_k = 0.01$, and $f_k(\tau) = \pi k \sin \tau$.

Fig.11. Distribution functions for momentum of the 1st mode (left) and 2nd mode (right) for forced dynamics of a 12-mode system (3.12), and the proposed 2-mode truncation ($\sigma = 0.01$, $g_k = 0.01$, and $f_k(\tau) = \pi k \sin \tau$).
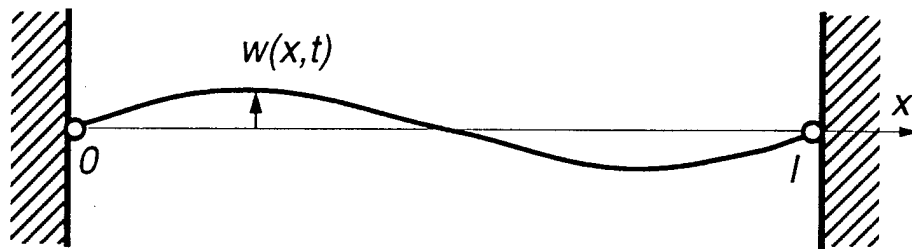
Figure 1:
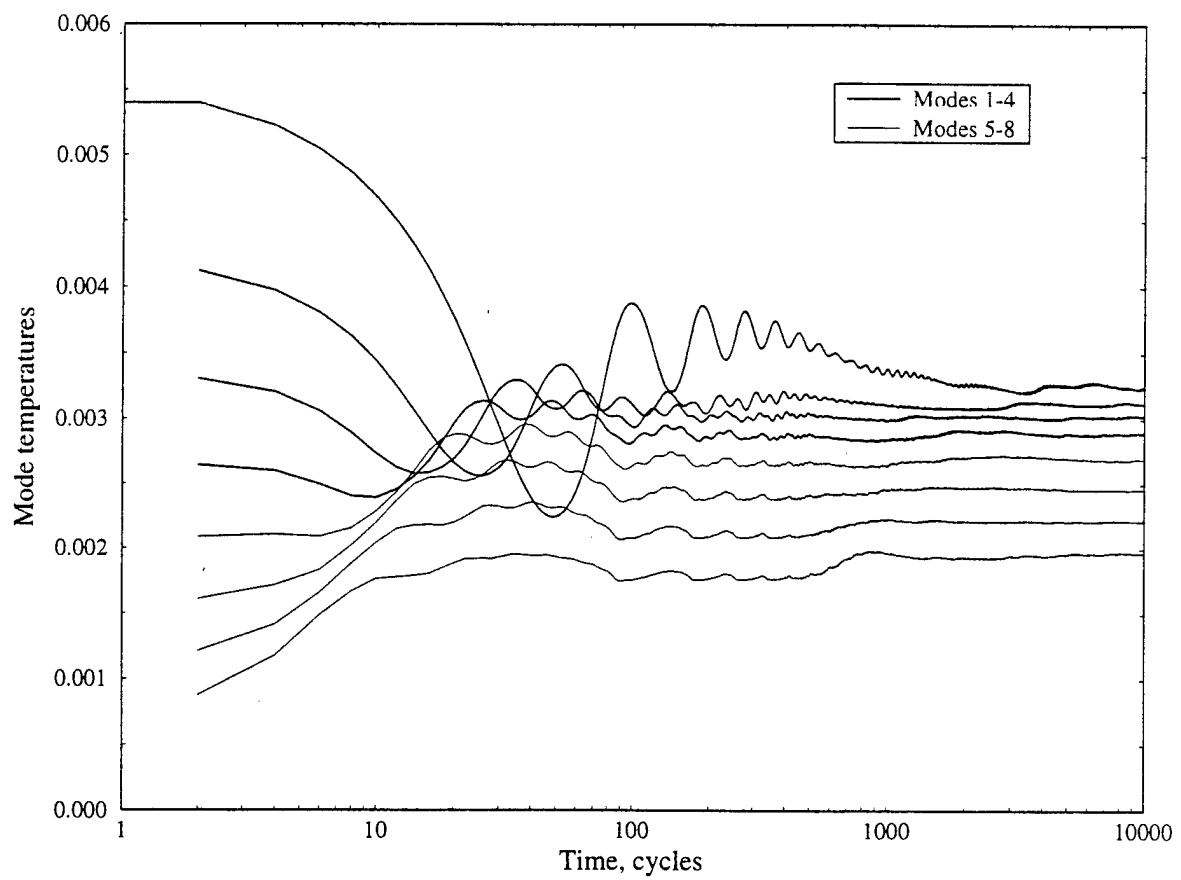
Figure 2:
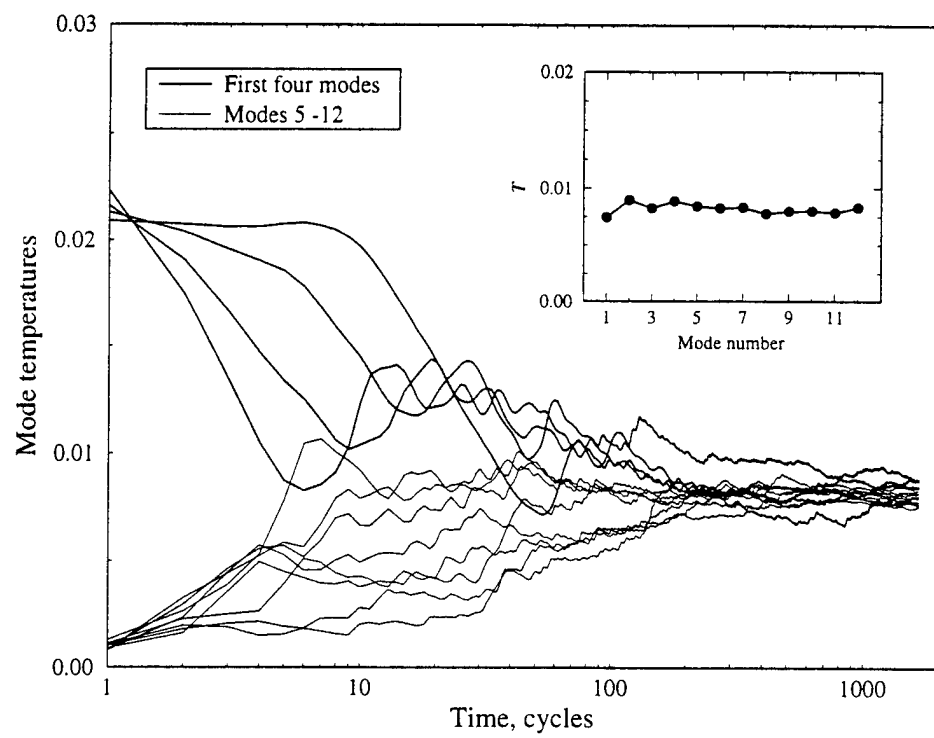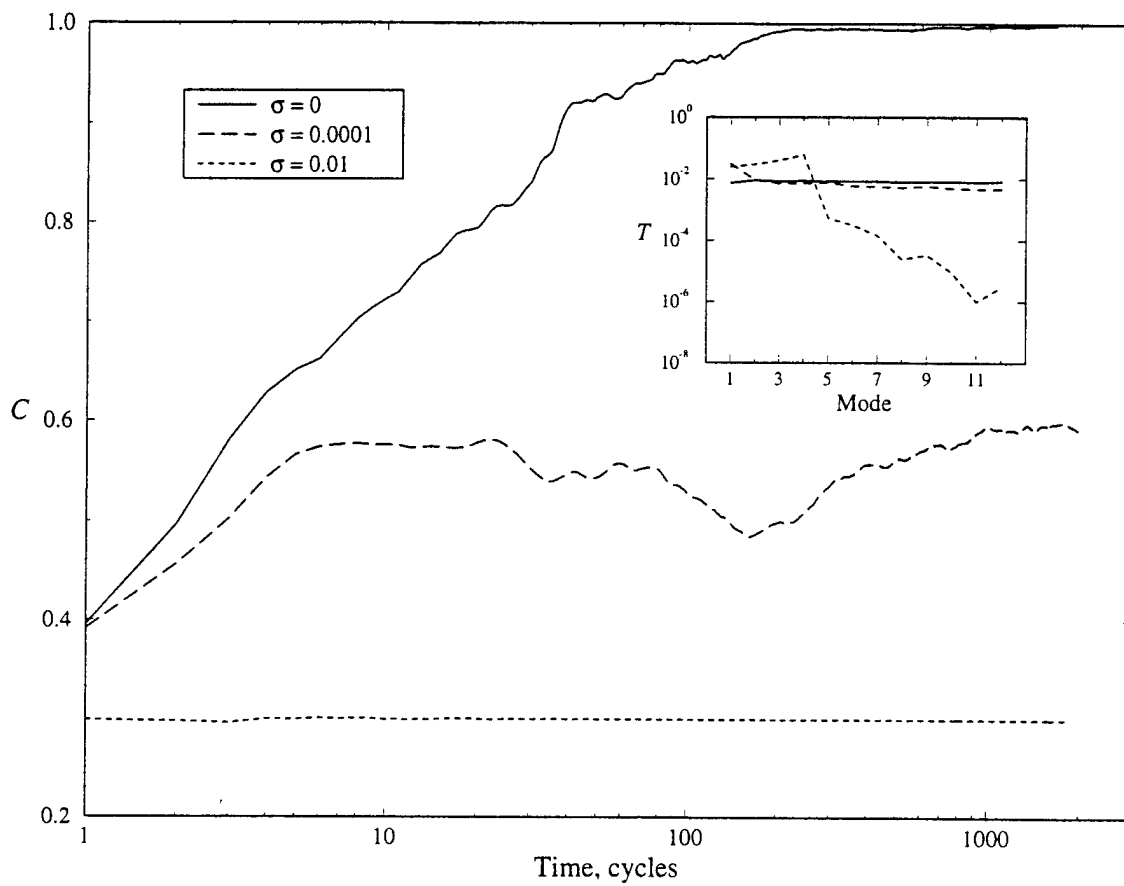
Figure 3:
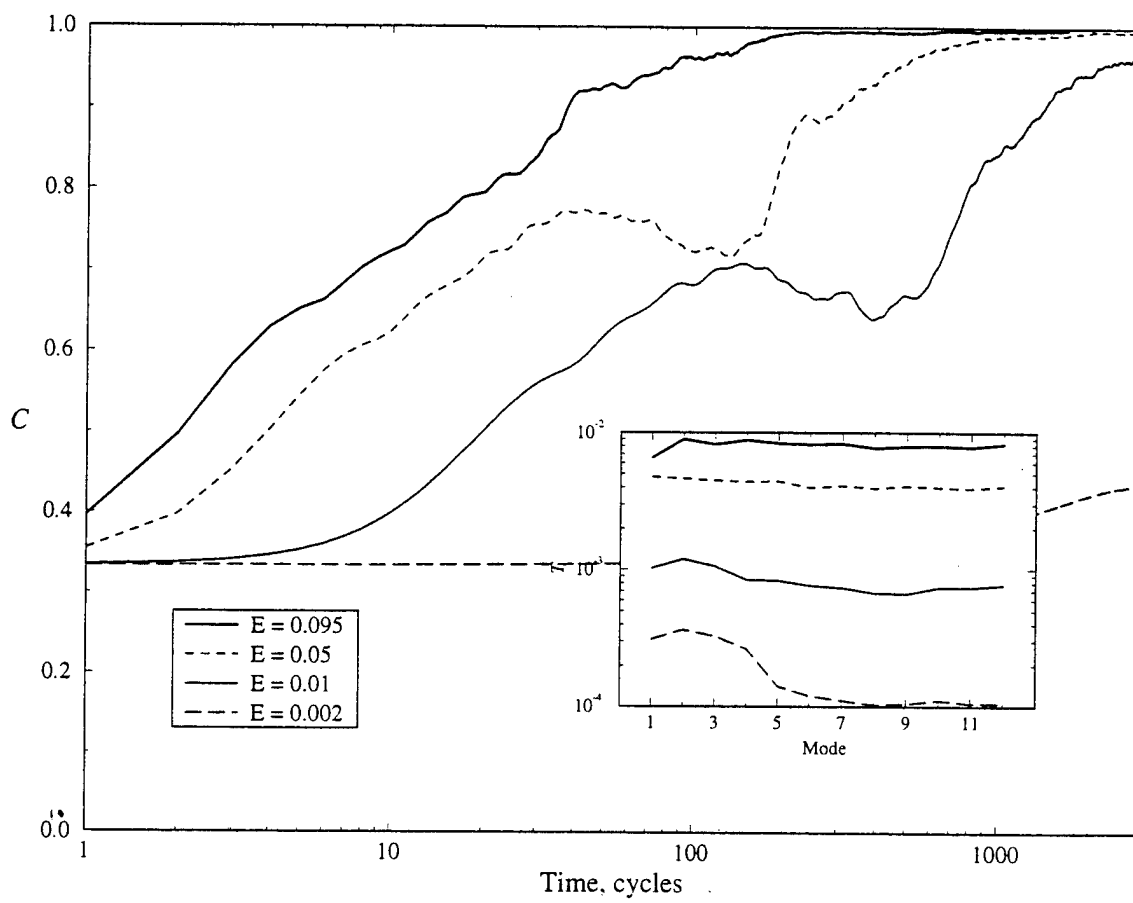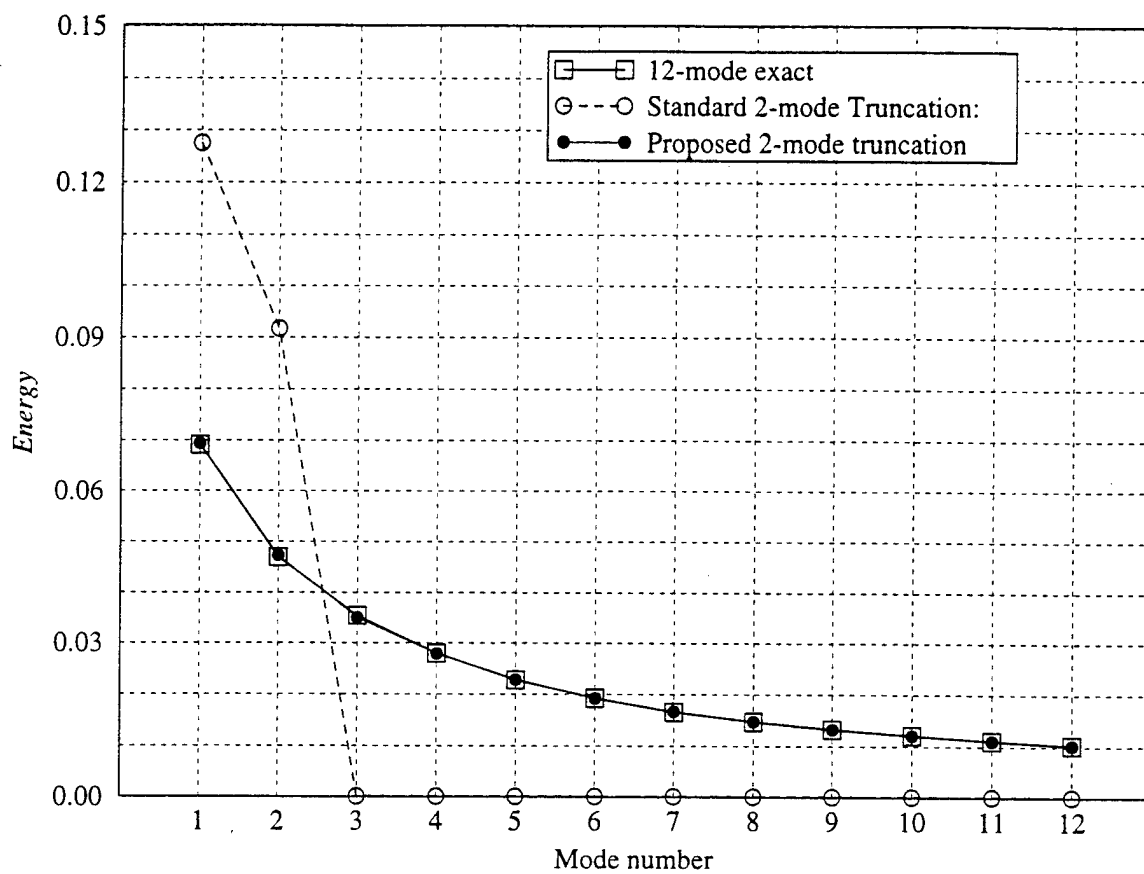
Figure 4:
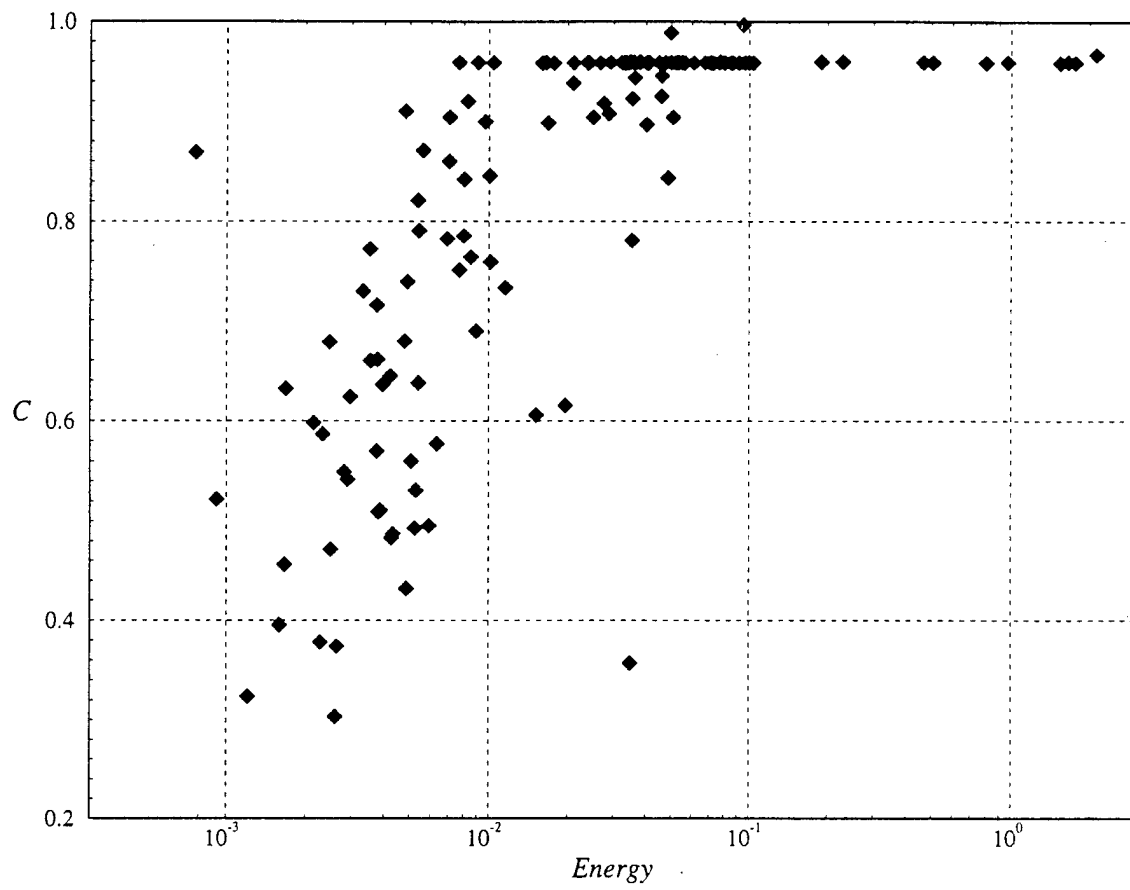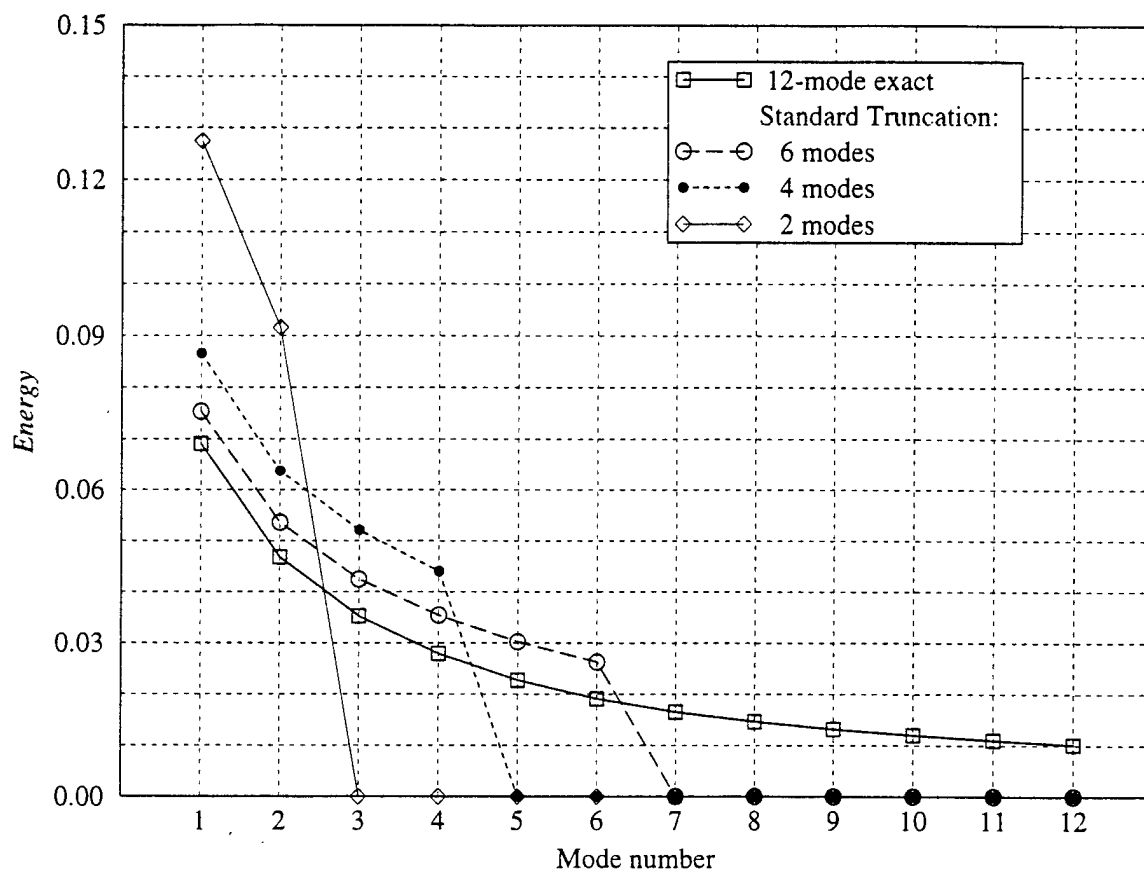
Figure 5:
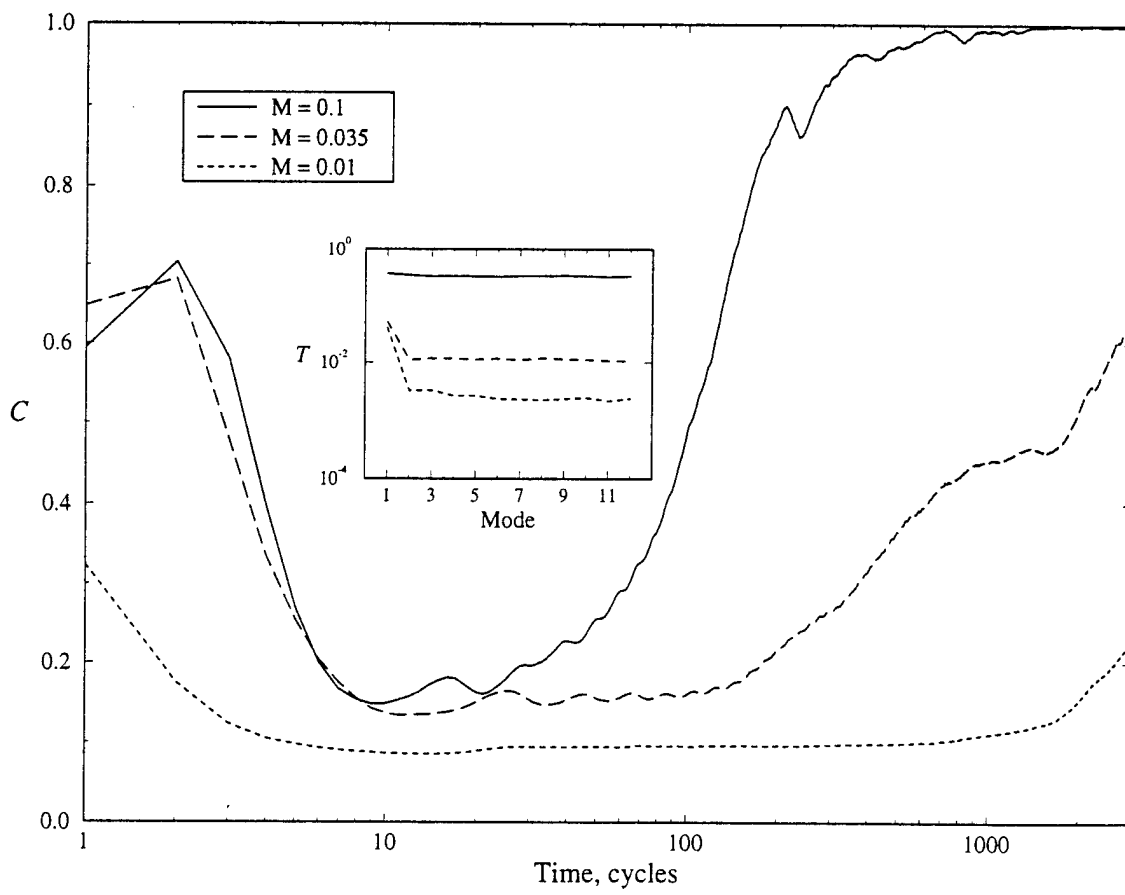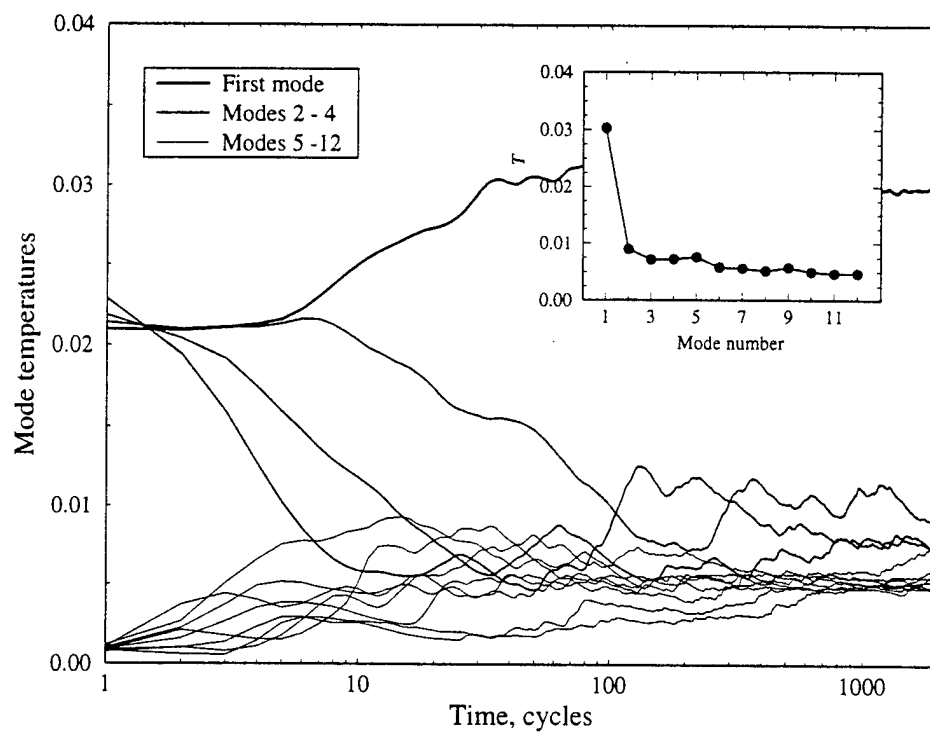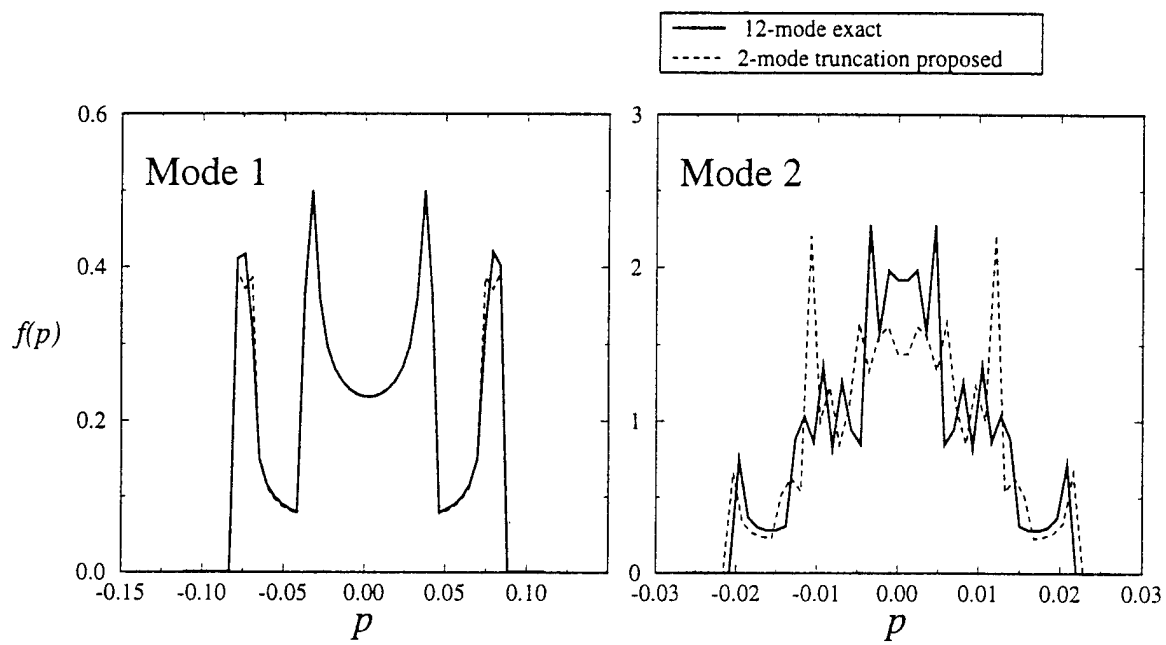
Figure 6:

Figure 7:

Figure 8:

Figure 9:

Figure 10:

Figure 11:

POSSIBLE SCENARIOS OF NONLINEAR VIBRATIONS AT HIGH ENERGIES

Victor L. Berdichevsky
Mechanical Engineering Department
Wayne State University
Detroit, Michigan

ABSTRACT The results of numerical simulations of nonlinear string dynamics are considered. Possible extrapolations of these results to nonlinear elastic continua leads to qualitatively different ways of dynamical behavior. They are described and discussed.

The effects of nonlinearity in vibrations of elastic systems are more or less understood if energy of vibrations is low enough to make the nonlinear terms just a correction of the linear ones. If energy of vibrations is high and nonlinearity plays a significant or leading role, there is an expectation that dynamics becomes so chaotic that the laws of statistical mechanics can be applied. The first attempt to check this expectation has been made by Fermi et al. (1955). They considered a chain of N mass particles connected by nonlinear springs. In accordance with statistical mechanics, equipartition of energy should be observed

$$\left\langle m\dot{u}_1^2 \right\rangle = \left\langle m\dot{u}_2^2 \right\rangle = ... = \left\langle m\dot{u}_N^2 \right\rangle \qquad (1)$$

where m is the particle mass, $\dot{u}_1^2, ..., \dot{u}_N^2$ are the particle velocities, and $< \; >$ denotes the time average along a trajectory: for any function $\rho\left(u_j, \dot{u}_j\right)$

$$\left\langle \rho(u_j, \dot{u}_j) \right\rangle = \lim_{\Theta \to \infty} \frac{1}{\Theta} \int_0^\Theta \rho(u_j(t), \dot{u}_j(t))\, dt \qquad (2)$$

For systems considered in statistical mechanics (ergodic systems) motion is chaotic and the average values do not depend on the initial data. The common value (1) is called, by definition, the absolute temperature T. Equipartition of energy is a necessary condition for the laws of statistical mechanics to be true (for details see, for example, Berdichevsky (1988), and Berdichevsky and von Alberti (1991)).

The system of 64 particles considered by Fermi, Pasta and Ulam showed a surprising result: equipartition does not hold while the system exhibits a recurrent motion. Further studies (Boccieri et al.(1970), Galgani and Scotti (1972), Chirikov et al.(1973), and Thirumalai and Mountain (1989)) explained that this result was caused by the small energy of initial excitation: for energies exceeding some critical value one does observe equipartition.

During last four years a detailed numerical study of chain dynamics has been conducted by my graduate students A. Ozbek, I. Shekhtman, V. Volovoi, E. Mueller. Summary of this study one can find in M.S. Thesis by E. Mueller (1994) and in (Berdichevsky (1993)). An important point of the study is that not only equipartition but also other laws of statistical mechanics are valid if energy of initial excitation exceeds some critical value E^c.

To discuss the behavior of elastic continuum, one might consider the limit $N \to \infty$ assuming that elastic continuum can be approximated by a chain of mass particles. At present, the reliable simulations have been conducted for $N \leq 128$. The qualitative graph of the dependence of critical energy E^c on N is shown in Fig. 1.
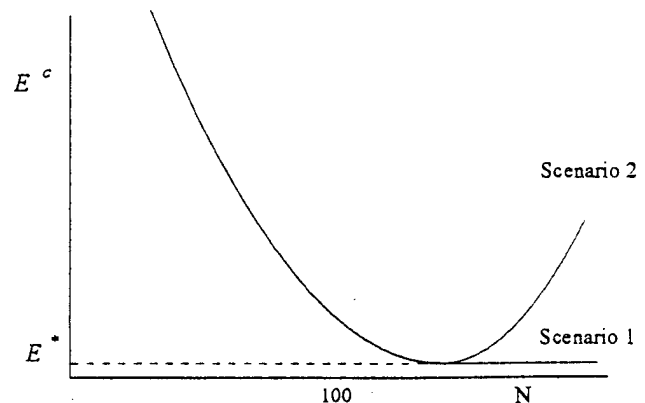

Fig. 1. Critical energy vs. number of particles

In the range $10 \leq N \leq 130$ critical energy behaves approximately as $1/N$.

Dynamics of continua depends crucially on the limit behavior of E^c for $N \rightarrow \infty$. Critical energy E^c cannot go to zero for $N \rightarrow \infty$ because in this case one would observe chaotic motion for any, even very small, energy of excitation. This contradicts to KAM theory, established for elastic continua by S. Kuksin (1989). Two other cases are possible: E^c tends to some finite limit E^* for $N \rightarrow \infty$ or $E^c \rightarrow \infty$ for $N \rightarrow \infty$. They correspond to two qualitatively different behaviors of continua which we refer to as scenario 1 and scenario 2.

Scenario 1 (*Selfdissipation*) This is the case of bounded critical energy. The major features of the dynamics of continua in this case are the following. If energy of initial excitation E is less than E^*, then one does not have something peculiar. However, if energy of excitation exceeds E^* then continuum shows a very unusual behavior. Let, for definitness, only a few modes are excited initially. In the course of motion energy is redistributed over all modes in a way to reach equipartition. Since an infinite number of modes is involved in the motion, energy of each mode is equal to zero at the final stage. So, one would observe a process with an increasing number of excited modes, in which energy of each mode eventually tends to zero while total energy is conserved. Since energy of each particular mode tends to zero, displacement go to zero. Derivatives of displacements stay finite due to conservation of energy. Therefore, displacements are getting more and more nonsmooth. One might call this case "selfdissipation" due to decay of displacements in time. Remind that the system considered does not have a "built-in" dissipation.

Scenario 2 (*Universal Spectrum*) In this case upper energy threshold tends to infinity for $N \rightarrow \infty$. Therefore, the laws of statistical mechanics are not valid for any, even very high, energy of excitation. However, a possibility of other "universal laws" appears. Let initial energy be E_0, and this value corresponds to the number $2N_0$ on the graph "critical energy vs. number of degrees of freedom" (Fig. 2).
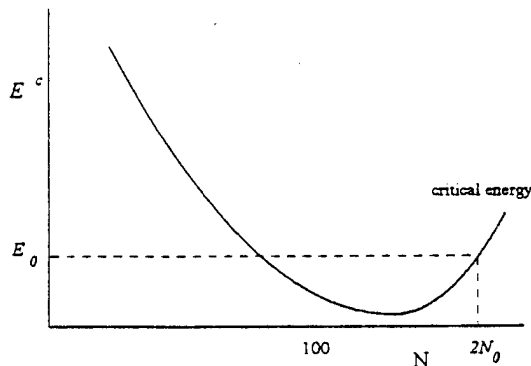
Fig. 2. Critical energy vs. number of degrees of freedom in Scenario 2.

Consider an excitation of the continuum when only the first N_0 modes are excited initially. For "$2N_0$ degrees of freedom"

truncation of the continuum the motion would be approximately ergodic while energy were equally distributed over modes (Fig. 3, line 1). In continuum, other modes take energy from the first N_0 modes. Therefore, for continuum the energy spectrum has the form of line 2 on Fig. 3. It is natural to assume that this spectrum is universal in the following sense: it is the same for any choice of initial excitation of the first N_0 modes possessing the same energy E_0.
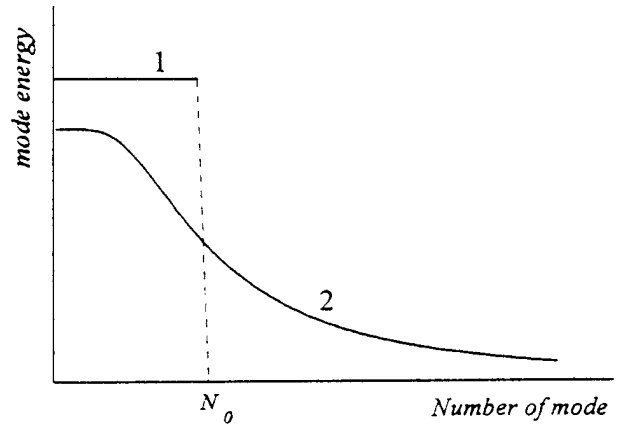
Fig. 3. Energy spectrum in Scenario 2.

None of the numerical experiments show the growth of critical energy for large N and a feasibility of the scenario 2. This relates, probably, to the fact that only particle chains with the nearest neighbor interaction have been considered so far. These chains do not have any characteristic dimension (in the limit $N \rightarrow \infty$), while the point of minimum on the plot in Fig. 2 is determined by some characteristic length. Perhaps, continua with the higher space derivatives provide the necessary additional parameter with the dimension of length..

Note that the results of the above mentioned numerical simulations can be used for speculations about continuum behavior with great precautions, because, if equipartition takes place, energy of short waves is comparable with energy of long waves, and modeling of continuum with a chain does not make sense. Strictly speaking, in numerical simulations for continua one has to determine critical energy as energy threshold for long wave excitations allowing the total number of modes be, say, 10 times larger than the number of long wave modes. To my knowledge, numerical simulations of such kind have not been conducted. However, it is difficult to expect that the behavior of critical energy for long wave excitation is different from the one shown in Fig. 1.

The above discussion shows that it is very interesting to study the dynamics of chains for large N. Unfortunately, $N \approx 1000$ is very close to the maximum capabilities of modern workstations because one has to conduct long term simulations with very small time step to resolve high frequency oscillations.

Conclusion.

It is suggested that there are two types of behavior of nonlinear elastic continua at high energies. For some continua (like strings) the regime of selfdissipation might be developed when displacements tends to zero while their derivatives stay

finite due to conservation of energy. For continua possessing a characteristic length parameter (like coupled torsional-lateral vibrations of elastic beams) another scenario is possible with the formation of an universal energy spectrum. Although the consideration in this paper concerns with the one-dimensional case, the situation seems generic, and the same type of behavior should be expected for two-dimensional and three-dimensional elastic continua.

Acknowledgment

References

Berdichevsky, V., 1988, "A Connection Between Thermodynamial Entropy and Probability", *Journal of Applied Mathematics and Mechanics* (PMM U.S.S.R.), vol. 52, No. 35, pp. 738-746.

Berdichevsky, V., and von Alberti, M., 1991, "Statistical Mechanics of Henon-Heliles Oscillators," *Physical Review A*, vol. 44, No. 2, pp. 858-865.

Berdichevsky, V., 1993, "Statistical Mechanics of Structural Vibrations," Symposium and Workshop on Nonlinear Dynamics, Cornell Univ.

Bocchiery, P., Scotti, A., Bearzi, B., and Loinger, A., 1970, "Anharmonic Chain with Lennard-Jones Interation," *Physical Review A*, v. 2, pp. 2013-2019.

Chirikov, B., Izrailev, F., and Tayursky, V., 1973, "Numerical Experiments on the Stochastic Behavior of Dynamical Systems with a few Degrees of Freedom," *Computer Physics Communications*, 5, pp. 11-16.

Galgani, I., and Scotti, A., 1972, "Recent Progress in Classical Nonlinear Dynamics," *Revisita del Nuovo Cimento*, v. 2, 189-209.

Fermi, E., Pasta, J., and Ulam, S., 1955, "Studies of Nonlinear Problems," Los Alamos Scientific Laboratory, Report LA-1540.

Kuksin, S.B., 1989, "An Averaging Theorem For Distributed Conservative Systems And Its Application to Von Karman's Equations", *Journal of Applied Mathematics and Mechanics* (PMM U.S.S.R.), v.53, no 2, pp.150-157.

E. Mueller, 1994, "Statistical Properties of Nonlinear Beam Dynamics," Master Thesis, School of Aerospace Engineering, Georgia Tech., Atlanta.

Thirumalai, D., and Mountain, R.D., 1989, "Probes of Equipartition in Nonlinear Hamiltonian Systems," *Journal of Statistical. Physics*, v. 57, pp. 789-801.

Attachment 4

DYNAMICAL POTENTIAL FOR NON-LINEAR VIBRATIONS OF CANTILEVERED BEAMS

V. L. Berdichevsky and W.-W. Kim

School of Aerospace Engineering, Georgia Institute of Technology, Atlanta, Georgia 30332-0150, U.S.A.

AND

A. Özbek

School of Civil Engineering, Georgia Institute of Technology, Atlanta, Georgia 30332-0150, U.S.A.

Recently it was shown that averaged characteristics of non-linear vibrations are potential functions of load parameters in the limit of small dissipation. The question of the range of dissipation for which potentiality takes place remained open. In this paper, we study this question for the case of non-linear vibrations of a cantilever beam excited harmonically at the unclamped end. We develop a non-linear one-degree-of-freedom beam model and show that the existence of a dynamical potential of beam vibrations can be guaranteed with acceptable accuracy even for sufficiently large dissipation.

1. INTRODUCTION

The dynamical behavior of non-linear structures is extremely complex [1-5]. For engineering applications, however, one usually needs some rough averaged characteristics of the responses. For example, consider a cantilever beam excited by a periodic force applied at the non-clamped end (Figure 1). The force $F(t)$ is assumed to be harmonic:

$$F(t) = A + B \sin \nu t. \tag{1}$$

The constant force A and the amplitude of excitation B are assumed to be large enough to create finite beam displacements. The vertical displacement of the right end, $q(t)$, might be a very complicated function of time, even if it is periodic. Some rough information about this displacement can be extracted from two characteristics:

$$\bar{q} = \langle q \rangle, \qquad \hat{q} = \langle q \sin \nu t \rangle$$

where $\langle \cdot \rangle$ denotes the time averaging operator along a trajectory: for any function $\phi(t)$, $\langle \phi \rangle$ indicates the limit

$$\langle \phi \rangle = \lim_{\theta \to \infty} \frac{1}{\theta} \int_0^\theta \phi(t) \, dt.$$

For linear vibrations, it is known [6, 7] that

$$q(t) = \bar{q} + r \sin (\nu t + \varphi),$$

where r is the amplitude of vibrations and φ is the phase angle. The phase angle φ is proportional to damping. For small damping, we may neglect φ and, since $\langle \sin^2 \nu t \rangle = 1/2$,
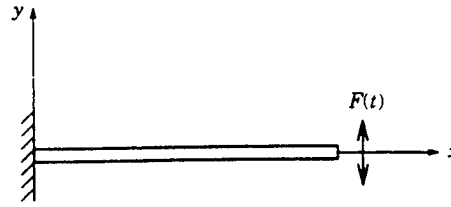
Figure 1. The co-ordinate system of a cantilever beam excited by a harmonic force.

$\hat{q} = r/2$. Therefore, for linear vibrations with small dissipation, $\bar{q}$ and $\hat{q}$ determine the tip displacement completely. For general non-linear vibrations, there are also many other characteristics. However, $\bar{q}$ and $\hat{q}$ are the most energetically important Fourier amplitudes because the average value of the potential energy due to the external force F can be expressed in terms of only $\bar{q}$ and $\hat{q}$:

$$\langle Fq \rangle = A\bar{q} + B\hat{q}. \tag{2}$$

The beam motion occurs along the attractor. Usually, attractors are limit cycles, but there are also chaotic attractors. In any case, $\bar{q}$ and $\hat{q}$ depend only on the attractor. Attractors are changed in the course of slow changes in the load parameters A and B. Therefore, quantities $\bar{q}$ and $\hat{q}$ are some functions of A and B:

$$\bar{q} = \bar{q}(A, B), \qquad \hat{q} = \hat{q}(A, B). \tag{3}$$

Equations (3) are constitutive equations of averaged beam dynamics.

As was established in reference [8], there exists a function, the dynamical potential $\mathscr{P}(A, B)$, such that the right sides of equation (3) are derivatives of this potential if damping is sufficiently small:

$$\bar{q} = \partial \mathscr{P}/\partial A, \qquad \hat{q} = \partial \mathscr{P}/\partial B. \tag{4}$$

For the sake of self containence, the derivation of equation (4) will be given in section 3.

The dynamical potential $\mathscr{P}$ completely determines the *macro-behavior* of the beam: one has to know only one function $\mathscr{P}$ to predict the response of the system for any given value of load parameters. The dynamical potential is equal to the averaged value of the Lagrangian over the attractor.

One can take into consideration any number of characteristics of the response. For example, if one is interested in knowing the quantity $\bar{q}_1 = \langle q \cos vt \rangle$, one needs to consider the more complicated excitation

$$F(t) = A + A_1 \cos vt + B \sin vt$$

and find the dynamical potential $\mathscr{P}_1$ as a function of three variables $\mathscr{P}_1 = \mathscr{P}_1(A, A_1, B)$. Then, $\bar{q}$, $\bar{q}_1$ and $\hat{q}$ are determined from the equations

$$\bar{q} = \partial \mathscr{P}_1(A, A_1, B)/\partial A, \qquad \bar{q}_1 = \partial \mathscr{P}_1(A, A_1, B)/\partial A_1, \qquad \hat{q} = \partial \mathscr{P}_1(A, A_1, B)/\partial B. \tag{5}$$

The dynamical potential $\mathscr{P}$ in equation (4) can be obtained from $\mathscr{P}_1$ by taking A_1 equal to zero:

$$\mathscr{P}(A, B) = \mathscr{P}_1(A, 0, B).$$

One might also consider the averaged characteristics of beam displacements somewhere along the beam. To calculate the corresponding dynamical potential, the dynamical problem should be studied, with the corresponding additional force as in the above

example: a force is added at the point at which the averaged displacement is to be calculated.

The potentiality of the above form of constitutive equations was established in the limit of zero dissipation or, in other words, for a sufficiently small friction coefficient. It remains unknown, however, how small is *sufficiently small*. The aim of this paper is to fill in this gap for non-linear beam vibrations.

To simplify our considerations, we model the beam vibrations by a system with one degree of freedom and conduct numerical simulations for this model. Classical beam theory is presented in section 2, the existence of dynamical potential is established in section 3, a one-degree-of-freedom beam model is developed in section 4 and the results of the numerical simulations are discussed in section 5.

2. LAGRANGIAN OF CLASSICAL BEAM THEORY

Let x and y be Cartesian co-ordinates in the plane of beam vibrations; the x-axis coincides with the undeformed centerline of the beam. Denote the x- and y-projections of the beam displacements by u_x and u_y; $u_x = u_x(t, x)$ and $u_y = u_y(t, x)$. We assume that there is no extention–twist, twist–bending or bending–bending coupling for vibrations in the x–y and x–z planes. Therefore, the lateral beam vibrations in the x–y plane can be considered separately from the other vibrations. The Lagrangian L of beam theory has the form [9]

$$L = K - U, \qquad K = \tfrac{1}{2}\rho S(u_{x,t}^2 + u_{y,t}^2), \qquad U = \tfrac{1}{2}(ES\gamma^2 + EI\Omega^2). \tag{6}$$

Here, K and U are the kinetic and internal energy, respectively, commas in indices denotes derivatives ($u_{x,t} \equiv \partial u_x/\partial t$, $u_{x,x} \equiv \partial u_x/\partial x$), ρ, S, E and I are the mass density, the cross-sectional area, Young's modulus and the inertia moment, and γ and Ω are measures of extension and bending:

$$\gamma = u_{x,x} + \tfrac{1}{2}(u_{x,x}^2 + u_{y,x}^2), \qquad \Omega = \tau_x\tau_{y,x} - \tau_y\tau_{x,x}. \tag{7, 8}$$

Here, τ_x and τ_y are x- and y-projections of the unit tangent vector to the deformed centerline:

$$\tau_x = \frac{1 + u_{x,x}}{\sqrt{1 + 2\gamma}}, \qquad \tau_y = \frac{u_{y,x}}{\sqrt{1 + 2\gamma}}. \tag{9}$$

The larger the lateral displacements, the smaller the contribution of extension γ should be. Therefore, for finite displacements Kirchhoff's theory of inextensional vibrations can be used. Since $\gamma = 0$, in Kirchhoff's theory, internal energy takes the simple form

$$U = \tfrac{1}{2}EI\Omega^2. \tag{10}$$

The expressions of bending measure Ω in terms of displacement is obtained by substituting equation (9), where one takes $\gamma = 0$, into equation (8):

$$\Omega = (1 + u_{x,x})u_{y,xx} - u_{y,x}u_{x,xx}. \tag{11}$$

where the displacements u_x and u_y are subjected to the inextensibility constraint

$$\gamma = u_{x,x} + \tfrac{1}{2}(u_{x,x}^2 + u_{y,x}^2) = 0 \tag{12}$$

and the kinematical boundary conditions are

$$u_x = 0, \quad u_y = 0, \quad u_{y,x} = 0 \qquad \text{at } x = 0. \tag{13}$$

The dynamical equation of beam theory follows from equating to zero the variation of action:

$$\int_{t_1}^{t_2} \int_0^l L \, dx \, dt = \int_{t_1}^{t_2} \int_0^l [\tfrac{1}{2}\rho S(u_{x,t}^2 + u_{y,t}^2) - \tfrac{1}{2}EI\Omega^2] \, dx \, dt. \tag{14}$$

Since the bending measure is a quadratic function of displacement derivatives, the Lagrangian is a quartic function of derivatives. However, it is possible to reformulate Kirchhoff's theory in such a way that the Lagrangian is a quadratic function of displacement derivatives, as it is in the linear theory. This modification was suggested in reference [9]. The modification is based on the identity

$$\Omega^2 = [(1 + u_{x,x})u_{y,xx} - u_{y,x}u_{x,xx}]^2 = u_{x,xx}^2 + u_{y,xx}^2, \tag{15}$$

which is valid for functions u_x and u_y obeying equation (12). To prove equation (15), let us differentiate equation (12) with respect to x. We have

$$(1 + u_{x,x})u_{x,xx} + u_{y,x}u_{y,xx} = 0. \tag{16}$$

Squaring equation (16), we obtain the relation

$$(1 + u_{x,x})^2 u_{x,xx}^2 + 2u_{y,x}(1 + u_{x,x})u_{x,xx}u_{y,xx} + u_{y,x}^2 u_{y,xx}^2 = 0. \tag{17}$$

Adding equation (17) to the left side of equation (15) and taking into account the relation

$$(1 + u_{x,x})^2 + u_{y,x}^2 = 1, \tag{18}$$

which comes from equation (12), we obtain the right side of equation (15).

Substituting expression (15) for Ω^2, one obtains the Lagrangian

$$L = \tfrac{1}{2}\rho S(u_{x,t}^2 + u_{y,t}^2) - \tfrac{1}{2}EI(u_{x,xx}^2 + u_{y,xx}^2). \tag{19}$$

The remarkable point is that the Lagrangian (19) is quadratic as in linear theory. Non-linearity comes into play only by means of the inextensibility constraint (12). The penalty for removing non-linear terms from the Lagrangian is an increase in the order of the derivatives. At a first glance, that leads to the possibility of satisfying two boundary conditions for both displacements u_x and u_y at each end. However, conditions which are additional to the classical ones are contained, in fact, in the inextensibility condition (12): $u_{x,x}$ can be calculated at both ends in terms of $u_{y,x}$. For example, for a cantilever beam, $u_{y,x} = 0$ at $x = 0$. Therefore, in accordance with the inextensibility condition (12),

$$u_{x,x} = 0 \qquad \text{at } x = 0. \tag{20}$$

The second root of equation (12), $u_{x,x} = -2$, is not considered here. We do not need a more detailed consideration of the boundary conditions because the beam motion will be presented by a simplified model of one degree of freedom.

3. EXISTENCE OF DYNAMICAL POTENTIAL

Let a cantilever beam be excited by a periodic force $F = A + B \sin \nu t$, which is applied for definiteness at the unclamped edge. The motion of the beam is governed by the equations

$$\frac{\delta L}{\delta u_x} \equiv -\frac{\partial}{\partial t}\frac{\partial L}{\partial u_{x,t}} - \frac{\partial}{\partial x}\frac{\partial L}{\partial u_{x,x}} + \frac{\partial^2}{\partial x^2}\frac{\partial L}{\partial u_{x,xx}} = \text{dissipative terms},$$

$$\frac{\delta L}{\delta u_y} \equiv -\frac{\partial}{\partial t}\frac{\partial L}{\partial u_{y,t}} - \frac{\partial}{\partial x}\frac{\partial L}{\partial u_{y,x}} + \frac{\partial^2}{\partial x^2}\frac{\partial L}{\partial u_{y,xx}} = \text{dissipative terms}. \tag{21}$$

Here, L is the Lagrangian, defined by equations (6)–(9). The specific form of the dissipative terms is not important. The boundary conditions are

$$u_x = u_y = u_{y,x} = 0 \quad \text{at } x = 0, \qquad \frac{\partial L}{\partial u_{x,x}} - \frac{\partial}{\partial x}\frac{\partial L}{\partial u_{x,xx}} = 0 \quad \text{at } x = l,$$

$$\frac{\partial L}{\partial u_{y,x}} - \frac{\partial}{\partial x}\frac{\partial L}{\partial u_{y,xx}} = A + B \sin \nu t \quad \text{at } x = l, \qquad \frac{\partial L}{\partial \Omega} = 0 \quad \text{at } x = l. \tag{22}$$

Motion occurs along an attractor. We assume that the attractor is a limit cycle with period θ, which is a multiple of the period of the exciting force $2\pi/\nu$: $\theta = 2\pi n/\nu$, where n is an integer. Displacements u_x and u_y are periodic functions of time with period θ. The limit cycle depends on parameters A and B. Therefore, we may write

$$u_x = \varphi(t, x, A, B), \qquad u_y = \psi(t, x, A, B). \tag{23}$$

Consider the quantity

$$\mathscr{P} = \left\langle \int_0^l L \, dx \right\rangle + \langle (A + B \sin \nu t)\psi(t, l, A, B)\rangle. \tag{24}$$

It is assume that functions (23) are substituted in the expression for L, equations (6)–(9), in order to perform the integration in equation (24).

The quantity $\mathscr{P}$ is a function of the parameters A and B. We are going to show that $\mathscr{P}$ is the dynamical potential of this problem, i.e., that in the limit of zero dissipation,

$$\langle \psi|_{x=l}\rangle = \partial \mathscr{P}/\partial A, \qquad \langle \psi|_{x=l} \sin \nu t\rangle = \partial \mathscr{P}/\partial B. \tag{25}$$

To prove equation (25), let us find derivatives of $\mathscr{P}$ with respect to A and B. For derivative $\partial \mathscr{P}/\partial A$, we have

$$\frac{\partial \mathscr{P}}{\partial A} = \left\langle \int_0^l \left[\frac{\partial L}{\partial u_{x,t}}\frac{\partial^2 \varphi}{\partial t \, \partial A} + \frac{\partial L}{\partial u_{y,t}}\frac{\partial^2 \psi}{\partial t \, \partial A} + \frac{\partial L}{\partial u_{x,x}}\frac{\partial^2 \varphi}{\partial x \, \partial A} + \frac{\partial L}{\partial u_{y,x}}\frac{\partial^2 \psi}{\partial x \, \partial A} \right.\right.$$
$$\left.\left. + \frac{\partial L}{\partial u_{x,xx}}\frac{\partial^3 \varphi}{\partial x^2 \, \partial A} + \frac{\partial L}{\partial u_{y,xx}}\frac{\partial^3 \psi}{\partial x^2 \, \partial A} \right] dx \right\rangle. \tag{26}$$

After integration by parts, expression (26) takes the form

$$\frac{\partial \mathscr{P}}{\partial A} = \left\langle \int_0^l \left(\frac{\partial L}{\partial u_x}\frac{\partial \psi}{\partial A} + \frac{\delta L}{\delta u_y}\frac{\partial \varphi}{\partial A} \right) dx \right\rangle + \left\langle \left(\frac{\partial L}{\partial u_{x,x}} - \frac{\partial}{\partial x}\frac{\partial^2 L}{\partial u_{x,xx}} \right)\frac{\partial \varphi}{\partial A}\bigg|_{x=l} \right\rangle$$
$$+ \left\langle \left(\frac{\partial L}{\partial u_{y,x}} - \frac{\partial}{\partial x}\frac{\partial L}{\partial u_{y,xx}} - A - B \sin \nu t \right)\frac{\partial \psi}{\partial A}\bigg|_{x=l} \right\rangle$$
$$+ \left\langle \left(\frac{\partial L}{\partial u_{x,xx}}\frac{\partial^2 \varphi}{\partial x \, \partial A} + \frac{\partial L}{\partial u_{y,xx}}\frac{\partial^2 \psi}{\partial x \, \partial A} \right)\bigg|_{x=l} \right\rangle$$
$$+ \frac{1}{\theta}\int_0^l \left[\frac{\partial L}{\partial u_{x,t}}\frac{\partial \varphi}{\partial A} + \frac{\partial L}{\partial u_{y,t}}\frac{\partial \psi}{\partial A} \right]_0^\theta dx + \langle \psi(t, l, A, B)\rangle. \tag{27}$$

The terms omitted in equation (27) are the zeros due to the boundary conditions at the clamped edge: $\varphi = \psi = \partial \psi/\partial x = 0$ at $x = 0$ (note that $\partial \varphi/\partial A = \partial \psi/\partial A = \partial^2 \psi/\partial x \, \partial A = 0$ at $x = 0$ due to these conditions).

The first term in the integral (27) is negligible in the limit of zero dissipation as a consequence of the equations of motion (21). The second and third terms in equations (27) are zero due to the boundary conditions (22). The fourth term is equal to zero because the integrand is proportional to $\partial L/\partial \Omega$, the bending moment at the unclamped edge which

is zero in accordance with equation (22). The fifth integral is equal to zero due to periodicity of motion. Therefore, equation (27) is reduced to the first relation (25). The second relation (25) is proved similarly. The proof in the case of the inextensible beam is also analogous.

Our goal is to investigate how large the contribution is of the neglected dissipative terms in equation (25). To this end, in the next section, we deveope a one-degree-of-freedom non-linear beam model and conduct numerical simulations in order to find the deviations from the potentiality of the constitutive relations.

4. ONE-DEGREE-OF-FREEDOM BEAM MODEL

We consider beam vibrations for which $u_{x,x}$ is small compared to unity. In this case, the inextensibility constraint (12) takes the form

$$u_{x,x} + \tfrac{1}{2}u_{y,x}^2 = 0. \tag{28}$$

Equation (28), along with the clamping condition, $u_x = 0$ at $x = 0$, allows to find u_x in terms of u_y:

$$u_x = -\tfrac{1}{2}\int_0^x u_{y,x}^2 \, \mathrm{d}x. \tag{29}$$

Note that the displacement $u_x(t, x)$ satisfies the boundary condition (20).

We assume the simplest approximation (one degree of freedom) of displacement $u_y(t, x)$:

$$u_y(t, x) = \phi(x)q(t). \tag{30}$$

Here $\phi = \mathrm{d}\phi/\mathrm{d}x = 0$ at $x = 0$, and $\phi = 1$ at $x = l$ where l is the beam length. Substituting equation (30) into equation (29), we obtain the approximate expression for u_x:

$$u_x = \psi(x)q^2, \qquad \psi(x) = -\tfrac{1}{2}\int_0^x \phi_{,x}^2 \, \mathrm{d}x. \tag{31}$$

Trial functions (30) and (31) lead to the expression for the Lagrangian of a one-degree-of-freedom beam model:

$$L = \tfrac{1}{2}\dot{q}^2(1 + cq^2) - \tfrac{1}{2}aq^2 - \tfrac{1}{2}bq^4, \tag{32}$$

where

$$a = \frac{EI \int_0^l \phi_{,xx}^2 \, \mathrm{d}x}{\rho S \int_0^l \phi^2 \, \mathrm{d}x}, \qquad b = \frac{EI \int_0^l \psi_{,xx}^2 \, \mathrm{d}x}{\rho S \int_0^l \phi^2 \, \mathrm{d}x}, \qquad c = 4\frac{\int_0^l \psi^2 \, \mathrm{d}x}{\int_0^l \phi^2 \, \mathrm{d}x}. \tag{33}$$

The final equation governing the non-linear vibrations of the one-degree-of-freedom cantilever beam is given by

$$(1 + cq^2)\ddot{q} + cq\dot{q}^2 + aq + 2bq^3 = A + B \sin \nu t - \mu\dot{q}. \tag{34}$$

Here we have added a small linear viscous damping term to the right side. This equation differs from the Duffing equation by two terms. $cq^2\ddot{q}$ and $cq\dot{q}^2$.

4. RESULTS OF NUMERICAL SIMULATIONS

Equation (34) was integrated using the sixth order Runge–Kutta method. In all simulations, coefficients a, b and c were set to unity (in accordance with equation (33), these coefficients are positive). Note that two of them can be always made equal to unity by suitable rescaling. In order to understand the behavior of the beam for the case of small

dissipation, it is very useful to consider first its motion for zero dissipation. We start from the case of free vibrations.

4.1. FREE VIBRATIONS ($A = B = 0, \mu = 0$)

Consider the trajectories of the beam tip in the phase space (t, p, q), $p = (1 + cq^2)\dot{q}$. The Hamiltonian of our model has the form

$$H(p, q) = \tfrac{1}{2}\frac{p^2}{(1 + cq^2)} + \tfrac{1}{2}aq^2 + \tfrac{1}{2}bq^4. \tag{35}$$

The trajectories are the curves defined by conservation of energy:

$$H(p, q) = E = \text{constant.} \tag{36}$$

Equation (36) means that every trajectory, started from some point on an energy surface $H(p, q) = \text{constant}$, belongs to this surface for all time. These trajectories are shown in Figure 2.

Let $\Gamma(E)$ be the volume of the phase space bounded by the energy surface $H(p, q) = E$,

$$\Gamma(E) = \int_{H(p, q) \leqslant E} dp\, dq. \tag{37}$$

For a periodic trajectory, the volume $\Gamma(E)$ during one period can be rewritten as

$$\Gamma(E) = 2 \int_{q_{min}}^{q_{max}} |p|\, dq, \tag{38}$$

where

$$p = \pm\sqrt{(1 + cq^2)(2E - aq^2 - bq^4)}, \tag{39}$$

$$q_{max} + \sqrt{[-a + \sqrt{a^2 + 8bE}]/2b}, \qquad q_{min} = -\sqrt{[-a + \sqrt{a^2 + 8bE}]/2b}. \tag{40}$$

The dependence of $\Gamma(E)$ on E is shown in Figure 3.

The period of vibration P can be expressed in terms of function $\Gamma(E)$ [1]:

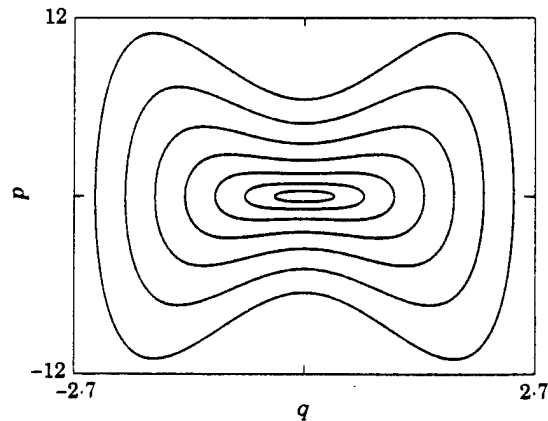$$P = \frac{d\Gamma}{dE} = 2 \int_{q_{min}}^{q_{max}} \sqrt{\frac{1 + cq^2}{2E - aq^2 - bq^4}}\, dq. \tag{41}$$

Figure 2. The energy surfaces $H(p, q) = \text{constant}$ in (p, q) phase space; $a = b = c = 1$, $A = B = 0$, $\mu = 0$.
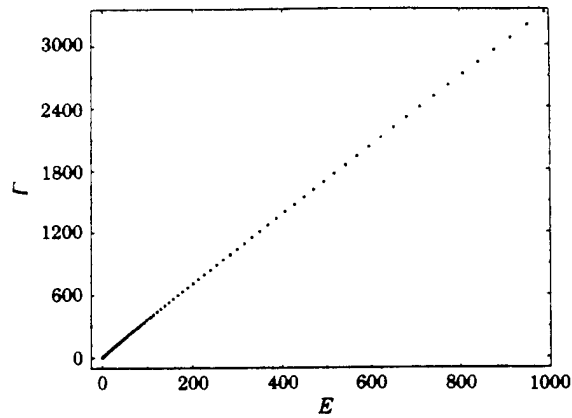
Figure 3. The dependence of the phase volume $\Gamma(E)$ on energy E; $a = b = c = 1$, $A = B = 0$, $\mu = 0$.

Limit values of the frequency of vibrations $\omega = 2\pi/P$ for $E \to 0$ and $E \to \infty$ can easily be found from equations (40) and (41):

$$\omega = 2\sqrt{b} \quad \text{as } E \to \infty, \qquad \omega = \sqrt{a} \quad \text{as } E \to 0.$$

We see that the frequency is in some finite range. In particular, for $a = b = 1$, the frequency has a value between $\omega = 1$ and $\omega = 2$. In contrast, the frequencies of many dynamical systems, such as the pendulum, tend to zero in the course of energy growth. The dependence of frequency ω on energy E is shown in Figure 4(a). This graph is useful in order to determine the most pronounced resonance which occurs if the frequency of the given harmonic force, v, coincides with the natural frequency ω.

4.2. EXCITED VIBRATIONS

Now, let the beam be excited. Let us set the frequency of excitation v equal to some natural frequency. If we take, for example, $v = \pi/2$, the corresponding value of energy of free vibration is $E \simeq 8.384$ for $a = b = 1$, as is seen from Figure 4(b). The trajectory which has that energy level should show chaotic behavior. The larger B (or A) is, the larger the chaotic region will be. In Figures 5(a)–(e) is shown the onset of the chaotic region in the course of the increase of B. Note that Figure 5(a) is a typical Poincaré map which shows successive positions of points for times $t = 0, \tau, 2\tau, \ldots$, where $\tau = 2\pi/v$ is the period of the exciting force.
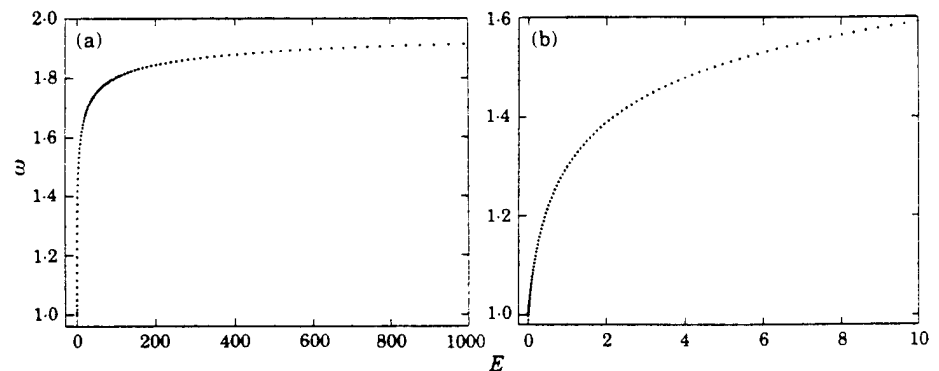

Figure 4. The dependence of the frequency ω on energy E; $a = b = c = 1$, $A = B = 0$, $\mu = 0$. (a) $0 \leqslant E \leqslant 1000$; (b) $0 \leqslant E \leqslant 10$.
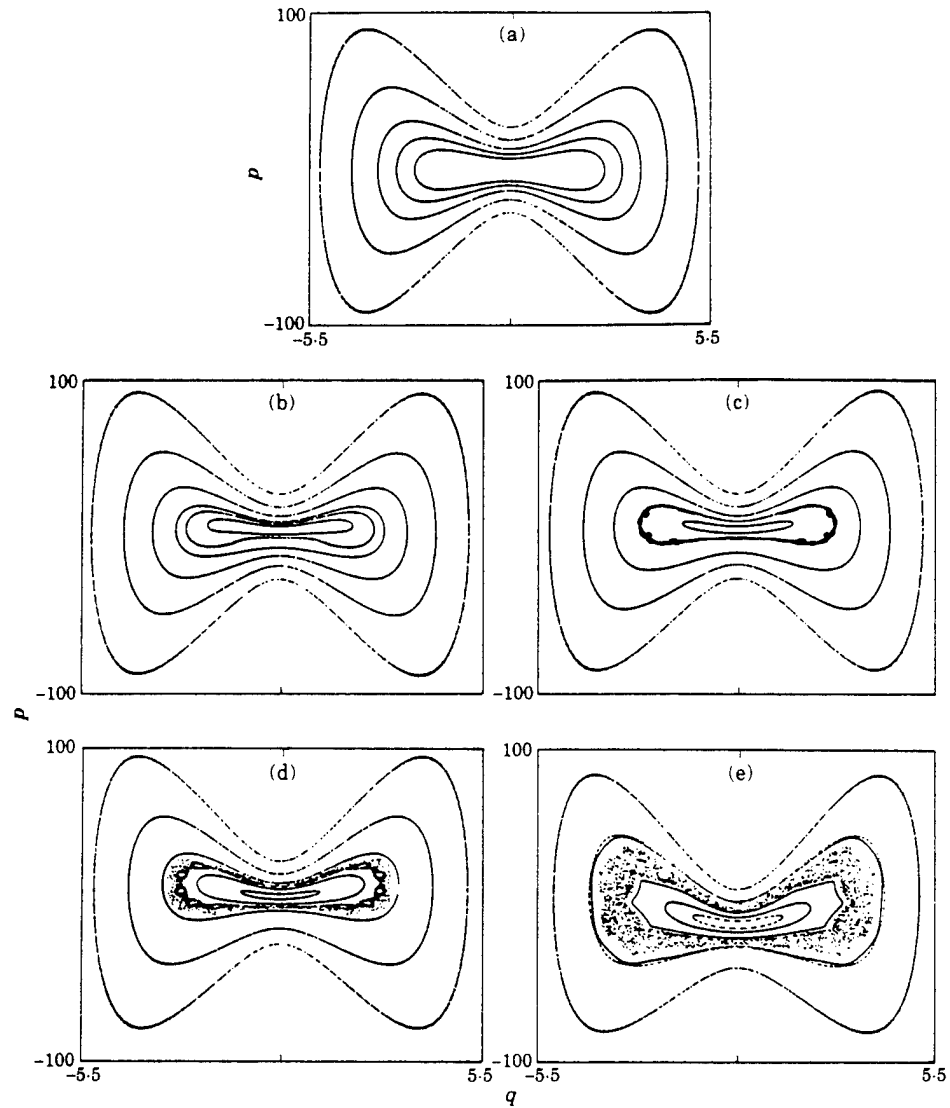
Figure 5. The onset of the chaotic region due to an increase in B: $a = b = c = 1$, $A = 0$, $\mu = 0$, $v = \pi/2$. (a) $B = 0$; (b) $B = 1$; (c) $B = 2$; (d) $B = 4$; (e) $B = 10$.

If the dissipation μ is non-zero, every trajectory falls on to limit cycles or strange attractors, as we expect. Typical limit cycles and strange attractors are shown in Figures 6 and 7. The evolution of the phase portrait in the course of the increase of damping for some fixed values of A and B is presented in Figures 6(a)–(c). For zero damping and $A = 1$, $B = 10$, the Poincaré map is shown in Figure 6(a). There are some characteristic regions numbered 1, 4, 13 and 4a. Region 1 corresponds to conditionally periodic motions with the two most pronounced frequencies, the frequency of the exciting force (which is equal to 1) and the frequency of free vibrations. Region 4 corresponds to a subharmonic resonance with period 4. The centers of four islands are the tracks of the periodic trajectory with period 4. Analogously, 13 islands marked by number 13 correspond to the subharmonic resonance with period 13, while 4 other islands, numbered 4a, are another subharmonic resonance of period 4. We show in this figure only the most *visible*
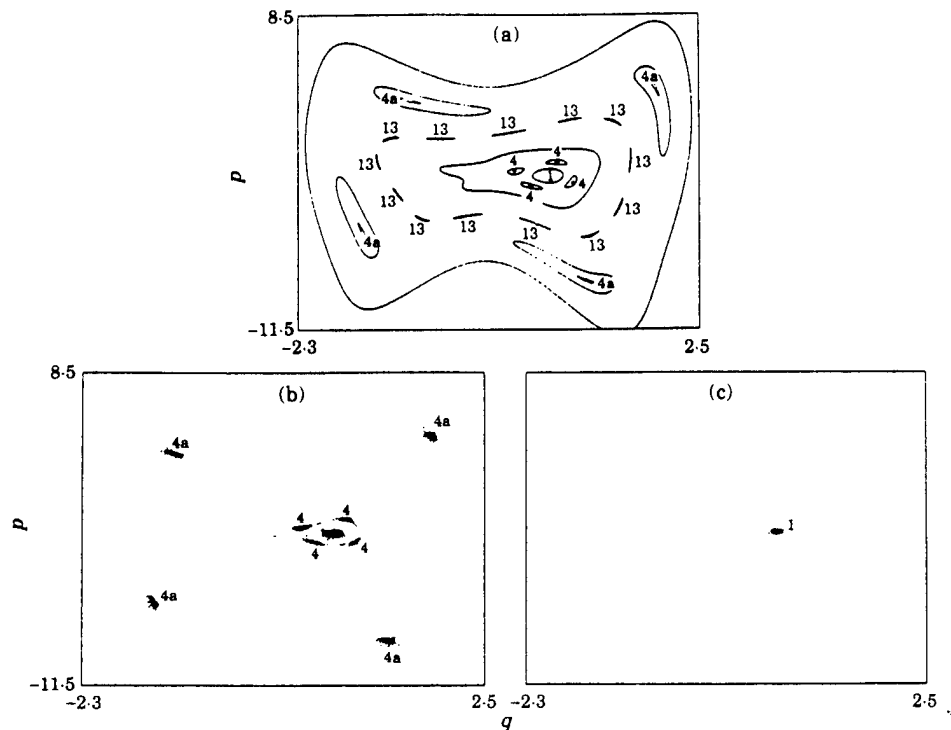
Figure 6. The influence of dissipation on the vibrations of a cantilever beam: $a = b = c = 1$, $A = 1$, $B = 10$, $v = 2\pi$. (a) $\mu = 0$, (b) $\mu = 0.01$; (c) $\mu = 0.1$.

resonances: there are many other resonances which occupy a small part of the phase space. In Figure 6(b) are shown the successive positions of a number of trajectories if one switches on a small dissipation, $\mu = 0.01$. It is seen that three limit cycles appear, one of which was period 1 which the others have period 4. The subharmonic resonance of period 13 is killed off by the dissipation. This is a general rule: only resonances with small periods survive after the addition of dissipation. If the dissipation is large enough ($\mu = 0.1$ in Figure 6(c)) only one limit cycle survives.

For large A and B, a strange attractor might appear. It is natural to assume that a strange attractor would emerge at the place occupied previously by a chaotic sea of Hamiltonian systems. This assumption is supported by the Poincaré maps in Figure 7(a)–(c), which show the evolution of the phase portrait due to dissipation. For zero dissipation (Figure 7(a)), we have some chaotic sea. The addition of a small amount of dissipation ($\mu = 0.1$) transforms it into a strange attractor, shown on Figure 7(b). This attractor looks close enough to the chaotic sea from which it was born. For a large value of dissipation ($\mu = 1$), we obtain the usual worm-like form of attractor which has been observed in many studies.

4.3. CONSTITUTIVE EQUATIONS

We can write the Lagrangian of the non-linear beam vibration model subjected to a harmonic force in the form

$$L = L_0 + Aq + Bq \sin vt, \tag{42}$$

where

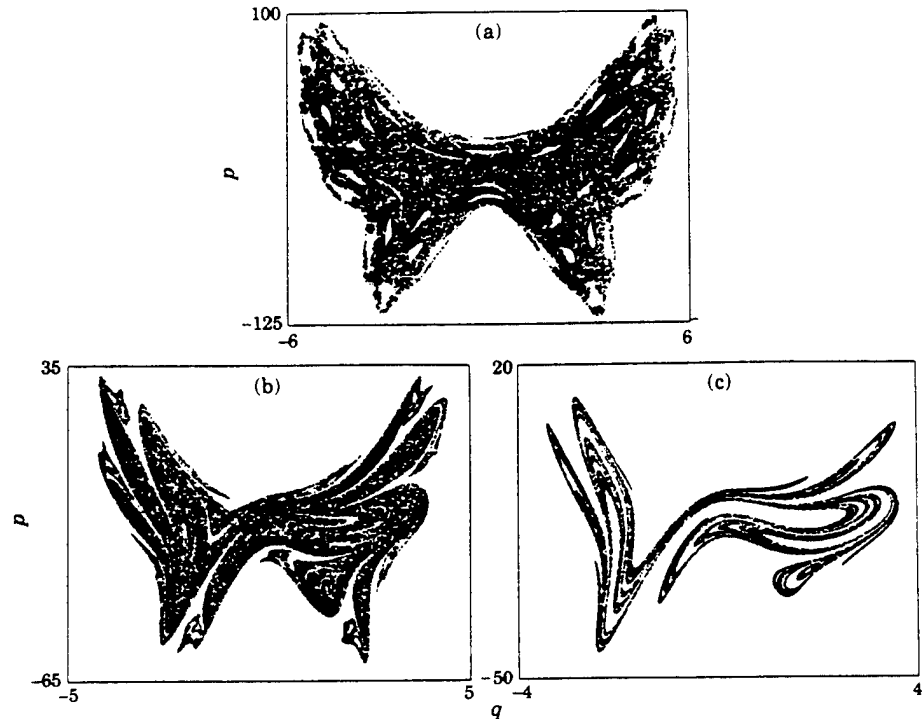$$L_0 = \tfrac{1}{2}\dot{q}^2(1 + cq^2) - \tfrac{1}{2}aq^2 - \tfrac{1}{2}bq^4. \tag{43}$$

Figure 7. The evolution of a chaotic sea into strange attractor; $a = b = c = 1$, $A = 1$, $B = 100$. $v = 2\pi$. (a) $\mu = 0$; (b) $\mu = 0\cdot1$; (c) $\mu = 1$.

To formulate constitutive equations for our model, we note that the time averaging operator $\langle\cdot\rangle$ is reduced for a periodic trajectory by taking the average along the period T:

$$\langle L \rangle \equiv \bar{L} = \frac{1}{T} \int_0^T L(p(t, A, B), q(t, A, B), A, B)\, dt.$$

Taking the time average, equation (42) becomes

$$\bar{L} = \bar{L}_0 + A\bar{q} + B\hat{q}. \tag{44}$$

The time averaged value of the Lagrangian $\bar{L}$ depends on A, B and the attractor (if there are a number of attractors):

$$\bar{L} = \bar{L}(A, B). \tag{45}$$

Now, we are going to check whether for the non-linear beam vibration, the dynamic potential $\mathcal{P}$ in equations (4) coincides with the averaged Lagrangian $\bar{L}(A, B)$:

$$\mathcal{P}(A, B) = \bar{L}(A, B). \tag{46}$$

The simplest way to check the existence of a dynamical potential is to test the validity of the reciprocal relation following from equations (4):

$$\partial\bar{q}/\partial B = \partial\hat{q}/\partial A. \tag{47}$$

The range of dissipation μ for which the reciprocal relation has acceptable accuracy can be observed in Tables 1–5. It can be seen that errors grow with an increase in the friction coefficient and reach about 2·6% for $\mu = 1$. For large values of A, for example $A = 10$,

TABLE 1

The accuracy of the reciprocal relation for $\mu = 0{\cdot}01$ $(a = b = c = 1, v = 2\pi)$

A	B	$\partial \bar{q}/\partial B$	$\partial \hat{q}/\partial A$	$\dfrac{|\partial \bar{q}/\partial B - \partial \hat{q}/\partial A|}{\max(\partial \bar{q}/\partial B)} \times 100$
1	1	0·00253801	0·00253800	0·000053
1	10	0·01881381	0·01881331	0·002658
10	1	0·00020625	0·00020628	0·000159
10	10	0·00199761	0·00199766	0·000266

TABLE 2

The accuracy of the reciprocal relation for $\mu = 0{\cdot}1$ $(a = b = c = 1, v = 2\pi)$

A	B	$\partial \bar{q}/\partial B$	$\partial \hat{q}/\partial A$	$\dfrac{|\partial \bar{q}/\partial B - \partial \hat{q}/\partial A|}{\max(\partial \bar{q}/\partial B)} \times 100$
1	1	0·00253761	0·00253682	0·004199
1	10	0·01881242	0·01880703	0·028651
10	1	0·00020624	0·00020624	0·000029
10	10	0·00199758	0·00199748	0·000532

TABLE 3

The accuracy of the reciprocal relation for $\mu = 1{\cdot}0$ $(a = b = c = 1, v = 2\pi)$

A	B	$\partial \bar{q}/\partial B$	$\partial \hat{q}/\partial A$	$\dfrac{|\partial \bar{q}/\partial B - \partial \hat{q}/\partial A|}{\max(\partial \bar{q}/\partial B)} \times 100$
1	1	0·00249902	0·00242185	0·413248
1	10	0·01867401	0·01818796	2·602815
10	1	0·00020573	0·00020471	0·005462
10	10	0·00199293	0·00198311	0·052586

TABLE 4

The accuracy of the reciprocal relation for $\mu = 2{\cdot}0$ $(a = b = c = 1, v = 2\pi)$

A	B	$\partial \bar{q}/\partial B$	$\partial \hat{q}/\partial A$	$\dfrac{|\partial \bar{q}/\partial B - \partial \hat{q}/\partial A|}{\max(\partial \bar{q}/\partial B)} \times 100$
1	1	0·00238890	0·00210686	1·544751
1	10	0·01825796	0·01642023	10·065363
10	1	0·00020420	0·00020016	0·022127
10	10	0·00197897	0·00194023	0·212181

TABLE 5

The accuracy of the reciprocal relation for $\mu = 5{\cdot}0$ $(a = b = c = 1, v = 2\pi)$

A	B	$\partial \bar{q}/\partial B$	$\partial \hat{q}/\partial A$	$\dfrac{|\partial \bar{q}/\partial B - \partial \hat{q}/\partial A|}{\max(\partial \bar{q}/\partial B)} \times 100$
1	1	0·00182529	0·00079677	6·604588
1	10	0·01557281	0·00764480	50·909309
10	1	0·00019410	0·00017123	0·146859
10	10	0·00188634	0·00166667	1·410600

TABLE 6

The error in the constitutive equations for $\mu = 0.01$, $a = b = c = 1$, $v = 2\pi$

A	B	$\partial \bar{L}/\partial A$	$\bar{q}$	$\dfrac{\|\partial \bar{L}/\partial A - \bar{q}\|}{\max \bar{q}} \times 100$
1	1	0.643936	0.591026	3.2605
2	2	0.829226	0.837931	0.5364
3	3	0.993152	1.004127	0.6763
5	5	1.256914	1.241057	0.9772
10	10	1.542458	1.622770	4.9491

TABLE 7

The error in the constitutive equations for $\mu = 0.01$, $a = b = c = 1$, $v = 2\pi$

A	B	$\partial \bar{L}/\partial B$	$\hat{q}$	$\dfrac{\|\partial \bar{L}/\partial B - \hat{q}\|}{\max \|\hat{q}\|} \times 100$
1	1	−0.01293267	−0.00996493	7.5124
2	2	−0.01605406	−0.01613266	0.1990
3	3	−0.01911899	−0.02076706	4.1718
5	5	−0.02507945	−0.02777094	6.8131
10	10	−0.03899240	−0.03950468	1.2968

reciprocal relations remain valid until $\mu = 5$, with errors less than 1.5%. The relations are virtually exact (with errors less than 0.03%) if $\mu \leq 0.1$. Note that we checked reciprocal relations for the limit cycle of period 1.

Numerical data allow us to express an approximate formula for $\bar{L}$ by means of a three-dimensional curve fitting algorithm. For the case $a = b = c = 1$ and $\mu = 0.01$, we obtain

$$\bar{L}(A, B) = c_9 A^3 + c_8 B^3 + c_7 A^2 B + c_6 A B^2 + c_5 A^2 + c_4 B^2 + c_3 AB + c_2 A + c_1 B + c_0, \quad (48)$$

where $c_0 = -0.184079$, $c_1 = -0.0097548$, $c_2 = 0.437283$, $c_3 = 0.005255$, $c_4 = -0.00423055$, $c_5 = 0.10604$, $c_6 = 0.00028865$, $c_7 = -0.00047238$, $c_8 = -0.0000255619$ and $c_9 = -0.00334188$. This means that the response can be found from the equations

$$\bar{q} = \partial \bar{L}/\partial A = 3c_9 A^2 + 2c_7 AB + c_6 B^2 + 2c_5 A + c_3 B + c_2,$$

$$\hat{q} = \partial \bar{L}/\partial B = 3c_8 B^2 + c_7 A^2 + 2c_6 AB + 2c_4 B + c_3 A + c_1. \quad (49)$$

The error in the constitutive equations (49) can be found in Tables 6 and 7. The approximate formula for $\bar{L}$, equation (48), satisfies the constitutive equations (49) with errors of less than about 7.5%.

5. CONCLUSIONS

We have proved that the dynamical response of cantilever beams to periodic excitation can be described in terms of a dynamical potential. We have found this potential for the limit cycle of the same period as the exciting force, and established the corresponding constitutive relations. To conclude, we would like to note that in the course of our study we encountered many lovely "creatures", one of which is shown in Figure 8. This is the Poincaré plot for a cantilever beam with parameter values of $a = 10$, $b = 0$, $c = 1$, $A = 0$, $B = 10$, $\mu = 0$ and $v = 2\pi$.
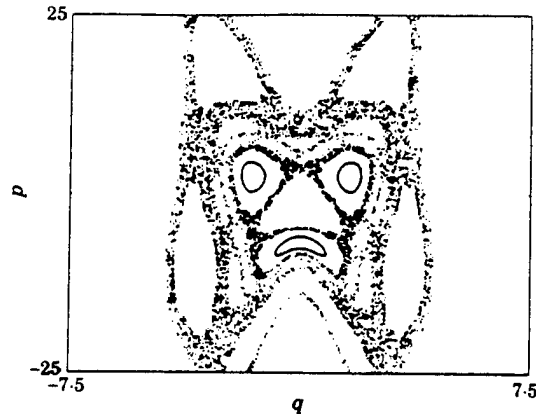
Figure 8. A Poincaré map for a cantilever beam; $a = 10$, $b = 0$, $c = 1$, $A = 0$, $B = 10$, $\mu = 0$, $\nu = 2\pi$.

ACKNOWLEDGMENTS

REFERENCES

1. V. I. ARNOLD 1989 *Mathematical Methods of Classical Mechanics*. New York: Springer-Verlag.
2. V. I. ARNOLD 1989 *Dynamical Systems*, volume 3. New York: Springer-Verlag.
3. J. J. STOKER 1950 *Nonlinear Vibrations*. New York: Interscience Publishers.
4. A. H. NAYFEH and D. T. MOOK 1979 *Nonlinear Oscillations*. New York: Wiley-Interscience.
5. F. C. MOON 1987 *Chaotic Vibrations: An Introduction to Chaotic Dynamics for Scientists and Engineers*. New York: Wiley Interscience.
6. S. P. TIMOSHENKO, D. H. YOUNG and W. WEAVER, JR. 1974 *Vibration Problems in Engineering*. New York: John Wiley; fourth edition.
7. L. MEIROVITCH 1967 *Analytical Method in Vibrations*. New York: Macmillan.
8. V. BERDICHEVSKY 1993 *International Journal of Engineering Science* **31**,   –   Reciprocal relations in nonlinear vibrations.
9. V. BERDICHEVSKY 1983 *Variational Principles of Continuum Mechanics*. Moscow: Nauka.

Thermodynamics and Parametric Response of Slightly Dissipative Systems

V. Berdichevsky

Mechanical Engineering, Wayne State University,

Detroit, MI 48202

Abstract. A point of view on thermodynamics is presented which raises some natural questions on parametric response of various engineering devices. In this regard parametric response of a "black box" device is considered. The major information about the black box is that its inside is governed by Hamiltonian equations complicated by a small dissipation. It is established that such systems inherit a "thermodynamical property": parametric response is always potential. Nonlinear oscillator is considered as an illustrative example. Parametric response of slightly dissipative open systems has also some special structure. It is discussed for the case of internal flows, a representative example of which is a gas flow in compressors.

1. Introduction. Thermodynamical description of a body assumes that its dynamics has two different time scales. Classical thermodynamics describes macromotion which is slow compared to fast micromotion of particles making up the body; micromotion is the subject of statistical mechanics. This point of view goes back to L. Boltzmann [7]. Why does macromotion obey to so specific laws as the first and the second laws of thermodynamics? The remarkable point is that the laws of thermodynamics take place, at least in equilibrium case, if microdynamics posesses two properties: it is Hamiltonian and ergodic [8]. It is not essential that the number of degrees of freedom is large [3, 4]. The laws of equilibrium thermodynamics are true even for one-degree-of-freedom systems, although they do not contain much information in this degenerated case. (Perhaps, the number of degrees of freedom should be large for validity of the laws of nonequilibrium thermodynamics). In this regard the question arises: Which "thermodynamics" do we get if fast motion is not Hamiltonian or ergodic? It seems that nothing like the first or the second law of thermodynamics is valid in general. However, it is very likely that the systems inherit some "thermodynamical properties" if they are "slightly non-Hamiltonian." An important case of "slightly non-Hamiltonian" systems is the case of Hamiltonian systems damped by small dissipation. There are many engineering situations of this type. It is enough to mention

that all high Reynolds number turbulent flows fall in this category. Among other examples are piezoelectric transducers, compressors, electromotors, etc. This paper aims to outline the statement of the problem and present some results of its study.

Generally speaking, any engineering device can be considered as a black box which is controlled by some inputs $x_1, x_2 ..., x_n$ and have some outputs $y_1, y_2 ..., y_n$.
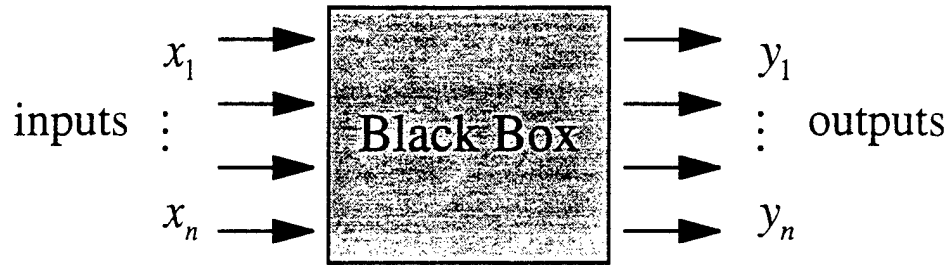

Fig. 1

Without loss of generality we may assume that the numbers of inputs and outputs coincide. The behavior of the device is characterized by the dependence of the outputs y_i on the inputs x_i:

$$y_1 = y_1(x_1,...,x_n) ,..., \quad y_n = y_n(x_1,...,x_n) \qquad (1.1)$$

Equations (1.1) form "the passport" of the device. They are analogous to constitutive equations of thermodynamics. Nothing specific can be said about these equations in general. However, "thermodynamical property" appears if we make additional assumptions: 1) internal dynamics is governed by classical mechanics, 2) dissipation is small, 3) parameters $x_1, x_2 ..., x_n$ are changed slowly compared to the internal dynamics of the black box, 4) attractor of the internal motion is ergodic, 5) system is closed, i.e., consists of the same material particles.

It is shown in this paper that the constitutive equations are potential in this case: there exists function $P(x_i,....,x_n)$ such that

$$y_1 = \frac{\partial P}{\partial x_1} ,..., \quad y_n = \frac{\partial P}{\partial x_n} \qquad (1.2)$$

The term "dynamical potential" introduced in [5] is used here for function P.

If the set of variables $x_1,...,x_n$ contains a parameter determining the time scale then an analog of entropy appears among the arguments of function P. (It is discussed later in Section 2).

Of course, as in classical thermodynamics, potentiality does not take place for an arbitrary choice of the output characteristics y_i, but y_i can be chosen in such a way that potentiality holds.

Potentiality reduces the number n of experimentally determined functions (1.2) to just one function, dynamical potential P. The larger the number of parameters the more benefits one gets from the fact of the existence of dynamical potential. In a sense, dynamical potential is analogous to energy in classical thermodynamics.

Potentiality of constitutive equations is an asymptotical property which appears if dissipation tends to zero, in the same way as potentiality of constitutive equations in classical thermodynamics.

The assumption that the system is closed is essential for validity of (1.2). To consider the corrections of (1.2) caused by openness of the system the case of open turbulent flow is discussed in Section 5. An additional term appears in (1.2):

$$y_i = \frac{\partial P}{\partial x_i} + I(x_i)\frac{\partial \Theta(x_i)}{\partial x_i} \qquad (1.3)$$

where Θ is the average time which particles spend inside the flow field, I is the product of averaged dynamical enthalpy, average velocity and cross-sectional area at the outlet. Constitutive equations (1.3) hold under some additional assumptions formulated in Section 5.

Relations (1.3) are based on a variational principle for open flows of ideal fluid which is formulated in Section 4. Formula (1.3) might be of interest in theory of compressors since it captures the influence of design on performance characteristics. It would be very interesting to check this formula experimentally. The specifics of fluid flow seem not to be important for validity of (1.3), and similar relations should be true for other open systems.

We start from the discussion of the simplest system: nonlinear oscillator. Thermodynamics of nonlinear oscillator has been considered in [5, 6]. Here the relations from [5] are extended by including the frequency of excitation in the set of control parameters; this is an important extension because the parameter reciprocal frequency turns out to be the temperature of vibrations.

Further contents of the paper is completely covered in Sections 4.6, 4.7, 4.8 of the Attachment 1 and is ommitted here.

Dynamical Potential of a Single-Degree-of-Freedom Nonlinear

Mechanical Oscillator

P. Matusov[1]

Mechanical Engineering, Wayne State University, Detroit MI 48202.

email: peter@peter.eng.wayne.edu

Total number of pages:	22
Number of figures:	8
Address for correspondence:	Peter Matusov
	UCSD/SIO/Marine Physical Laboratory
	Mail stop 0238
	La Jolla, CA 92093-0238
Email:	pmatusov@mpl.ucsd.edu,
phone:	(619) 534 1085
fax:	(619) 534 7132

[1] Now at: Marine Physical Lab, Scripps Inst. of Oceanography, University of California, San Diego, La

Jolla, CA 92093-0238.

Summary

It was shown recently that the averaged characteristics of nonlinear vibrations are potential functions of load parameters, if the dissipation is small. In this paper the existence of a dynamical potential is verified in experiment with a nonlinear oscillator with one degree of freedom. However, near the resonance the effect of dissipation cannot be neglected, and no dynamical potential exists. The limits of applicability of the description of vibrations in terms of dynamical potential are outlined.

Introduction

It is known that the dynamics of nonlinear structures can be extremely complex (see, e.g., [1-3]). For engineering purposes, however, some averaged characteristics and estimates can be more useful. In this sense, a tool for prediction the averaged characteristics as functions of the load parameters without modeling of the system's dynamics is extremely welcome.

For the systems without dissipation, the variational principle can be employed to describe the motion, and Lagrange's function (or elastic energy only for static problems) is a tool to examine the system's response under the action of external loads. Recently, it has been shown in [4-7] that in some cases the averaged characteristics of motion can be easily derived from a single function, a dynamical potential, which plays for a dynamical system the role similar to potential energy for static load-deflection problems. The existence of the dynamical potential was demonstrated theoretically for various non-linear oscillators without friction, including an important case of vibrations of cantilevered beams [6]. However, physical systems possess dissipation which may be significant; the variational principle for the dissipative system is yet to be strictly formulated, and the applicability of description in terms of the dynamical potential needs to be verified. Nevertheless, it seems reasonable that, small dissipation should not make substantial changes in average properties of motion, and some kind of variational consideration can still be employed. The estimates of the errors due to the small friction were made in [7] for the case of a

simplest one-degree-of-freedom non-linear oscillator. This validity of the concept of dynamical potential was also examined in numerical experiments [6] for vibrations of a cantilevered beam.

Let us consider the behavior of a single-degree-of-freedom nonlinear mechanical oscillator (Fig.1) under the action of periodic external force $F(t)=a\sin\nu t$:

$$m\ddot{q}^{2} + f(q,\dot{q}) + \frac{\partial U(q)}{\partial q} = F(t) \qquad (1)$$

The friction force $f(q,\dot{q})$ is assumed small. In such a system the friction causes the oscillator's motion to approach the attractor in phase space, so that the averaged characteristics of the motion will not depend on initial conditions.

The equation (1) can also be represented in the variational form

$$\frac{\partial L}{\partial q} - \frac{\partial}{\partial t}\left(\frac{\partial L}{\partial \dot{q}}\right) = f(q,\dot{q}), \qquad (2)$$

where the Lagrange's function is

$$L(q,\dot{q},t) = \frac{1}{2}\dot{q}^{2} - U(q) + F(t)q \ . \qquad (3)$$

The control parameters are the amplitude a and frequency ν of the external force.

It was shown [4] that, the average value of Lagrange's function $\overline{L} = \langle L \rangle^2$ over the attractor plays the role of the dynamic potential, P. Two important averaged characteristics of vibrations, the response

$$\overline{q} = \langle q \sin \nu \, t \rangle \tag{4a}$$

and temperature

$$T = \left\langle \overset{\bullet}{q}{}^2 \right\rangle \tag{4b}$$

are linked to the control parameters a and ν by the potential relations

$$\overline{q} = \frac{\partial P}{\partial a}, \qquad T = \frac{\partial P}{\partial \ln \dfrac{\nu}{\nu_0}}, \tag{5}$$

where ν_0 is the eigenfrequency of the linear vibrations. Note that the temperature and response are bound by the reciprocal relations

$$\frac{\partial \overline{q}}{\partial \ln \nu} = \frac{\partial^2 P}{\partial a \, \partial \ln \nu} = \frac{\partial T}{\partial a}. \tag{6}$$

---

[2] Here and below angular brackets denote the time averaging along the trajectory: for any function Φ, <Φ> indicates the quantity $\langle \Phi \rangle = \lim\limits_{\tau \to \infty} \dfrac{1}{\tau} \int\limits_0^\tau \Phi(t) \, dt$.

The validity of (4)-(6) was proven theoretically for the linear vibrations ($U(q) = \frac{1}{2}q^2$)

with small dissipation in [7], and an analytical expression for the dynamical potential has been derived. However, no experimental evidences of the existence of the dynamical potential for nonlinear vibrations is known yet. To fill this gap, the experiment with a single-degree-of-freedom oscillator was conducted.

Experiment

The experimental verification of the concept of the dynamical potential for the nonlinear vibrations of an oscillator with one degree of freedom is in general very simple. For this purpose, one needs to excite an oscillator with external force in a domain of the force amplitudes and frequencies, and to measure the response and temperature. If two latter quantities fulfilled the reciprocal relations (6) (which is also an indicator of consistency of measurements), the dynamical potential P could be reconstructed.

To conduct these measurements, one needs some tools for excitation and recording of the vibrations. In reality, most instrumentation from the vibrations measurements toolbox (e.g., vibro-exciters and accelerometers) are by the construction and principle of operation harmonic oscillators, and are tightly linked with a system under consideration. The vast majority of the experiments is conducted with the linear systems, and frequency ranges are chosen to usually far from the resonant frequencies of the instruments, and the

dynamical features of instrumentation do not interfere with measurements. In some more sophisticated systems a deep negative feedback is used to suppress the dynamical properties of the exciter of vibrations. However, it was found in the preliminary experiments, the feedback may even lead to the self-oscillations if quality factor of the studied oscillator is high enough. A different device and technique were thus explored.

Experimental set-up and sensors. A simple device was employed, providing the oscillator itself, an excitation engine, and measuring device in a single unit (see Fig.2). Two small low-frequency electro-dynamical speakers were attached to the heavy steel frame coaxially, and an aluminum cylinder glued between their voice coils. Such a suspension allows the cylinder to move in the axial direction within the limits ±6 mm from the equilibrium position; the speaker's cone suspension geometry ensures the absence of lateral vibrations, and provides restriction on the amplitude of the axial vibrations. A lateral elastic link was provided to enhance the non-linearity in the suspension: a 0.05 mm-thick, 4mm-wide, and 10 mm-long steel strip attached to the frame and the cylinder with a very small initial stress.

Two remarkable features of electromagnetic devices were employed: (a) a certain amount of current fed to the coil results in the force which is directly proportional to the current, and (b) if a coil is moved across the region with magnetic field with a certain velocity, the induction voltage produced at the coil terminals is directly proportional to the velocity. In both cases, the proportionality coefficient is equal to the product of the wire length in the coil and magnetic induction, which is the same for both excitation and measurement coils, since the identical speakers are used. It makes the calibration

7

essentially simple. Moreover, the speakers are designed in such a way that a certain portion of coils remains at all times within the region of strong magnetic field even at very large coil displacements, ensuring linearity of the coils as the force and velocity transducers.

The friction in the considered mechanical model is contributed mostly by visco-elastic losses in the speaker diaphragm's suspension, losses resulting from air flow around the moving body and diaphragms of the speakers, and electrical losses due to finite impedance of excitation and measurement devices. The losses due to sound radiation are negligible in the range of frequencies in which the experiments were carried out. Thus, all losses may be incorporated as viscous friction, and evaluated by a single parameter C:

$$f(q,\dot{q}) = C\dot{q} \ . \tag{7}$$

The non-dimensionalized form of dissipation coefficient, $\xi = C / v$, will be employed below, characterizing the relative energy loss during one period of oscillations.

A special power amplifier (current source) was designed to provide a certain current in the force-exerting coil independent on the motion of the coil and its impedance, controlled by the voltage applied to the amplifier's input. The force output of the coil was measured in Newtons/Volt by the method of counterbalance: a voltage applied to the input of current source resulted in some force exerted by the coil, displacing the aluminum cylinder (suspended mass) from the equilibrium position. The displacement was then compensated by the controlled counterforce and its value was measured. Such a

procedure was performed for various equilibrium positions within the limits of the expected vibration amplitudes, ensuring the linearity of the force transducer.

The receiver coil, as a velocity transducer, was also calibrated by means of an accelerometer. The acceleration magnitude of 10 m/s^2 has been maintained within the frequency range from 32 to 78 Hz, and the dependence of the voltage output of the coil on actual velocity magnitude was measured (Fig.3). The velocity transducer showed acceptable accuracy of $\pm$ 1.5% .

Spring. Fig.4 illustrates the static load-deflection dependence of the spring used. The measurements were made within the acceptable range of current through the force-exerting coil. It can be seen that the spring is quite linear within the displacement range 0.4 cm, and it takes much higher force to displace the system out of these limits. Such a behavior can be expected from the geometry of used suspension. At the linear interval of load characteristics, the spring has a compliance of 0.28 cm/N with accuracy 3%. The solid curve at the figure illustrates the polynomial fit of experimental data, expressed by the formula

$$\Phi \equiv \frac{\partial U}{\partial q} = 3.8756\,q \; + \; 0.37827\,q^2 \; - \; 7.122\,q^3 \; + \; 0.83379\,q^4 \; + \; 35.44\,q^5 \; ,$$

where force is measured in Newtons and displacement in centimeters.

Data acquisition and processing. The input signal for the force transducer was provided and the velocity sensor output measured by a PC-based Data Translation data acquisition system. A DT-Vee code was derived to provide measurements within a certain force

amplitude - frequency domain, and calculate the response and temperature of the vibrations according to the expressions (4a) and (4b). The raw response and temperature data were later processed to calculate the reciprocal relations and reconstruct the dynamical potential.

Temperature and response. Figures 5 and 6 represent the temperature and response of the oscillator in the same force amplitude - frequency domain: $0<F<0.5N$, $20<v/2\pi<40Hz$. The analysis of data belonging in the low-force region of the parameters domain (quasi-linear motion) allow to estimate the dissipation coefficient $\xi \approx 0.02$. The frequency shift of the maximum of temperature up by 2 Hz from the linear resonance frequency of 26 Hz indicates the strongly nonlinear regime of oscillations at higher force magnitudes. The further increasing of force amplitude could result in the physical damage of suspension near the resonance and thus was not exercised. It can also be seen that the typical large values of the response are of an order of 0.5 cm. Note that the absolute value of displacement can be significantly larger than the response value, because of the presence of cosinusoidal component of amplitude $\hat{q} = \langle q \cos v \, t \rangle$, which reaches its maximum value close to the resonance. Our measurements indicate thus that the vibrations in our system substantially exceed the limits of linear displacements (Fig.4).

Another observation can be made: within the chosen domain of parameters the shift of the resonant frequency due to the non-linearity is of the same order as the breadth of linear frequency response curve (of an order of 1 Hz), and thus non-linearity and dissipation play comparable roles in governing the oscillator's motion near the resonance.

Reciprocal relations. For the dynamical potential to exist, the reciprocal relations (6) are to be satisfied (with some acceptable accuracy). The cross-derivatives of the response and temperature have been calculated, and the ratio

$$\frac{\partial \bar{q}}{\partial \ln v} \bigg/ \frac{\partial T}{\partial a} \tag{8}$$

has been examined. The exact equality (6) corresponds to the unity value of the ratio (8). The ratio (8) is plotted in Fig.7 as a function of the force amplitude and frequency in a topographic way, where the white area corresponds to the value of (8) being within the limits [0.9...1.1]. It can be seen that the reciprocal relations are fulfilled fairly well far from the resonance, and are inconsistent within an approximately 4 Hz-wide region near

it for all force amplitudes. It means that, in the very vicinity of the resonance the dissipation plays a key role in the system's dynamics and cannot be neglected, and no dynamical potential exists. Nevertheless, the consistency of reciprocal relations in the most part of force-frequency domain ensures the possibility of reconstruction of the dynamical potential.

Reconstruction of the dynamical potential. To build the dynamical potential, a force-frequency domain left of 28Hz was selected. The reconstruction was conducted by means of numerical integration of response and temperature data within this domain. Since the dynamical potential is determined up to an additive constant, the procedure of integration has been conducted in the following way. First, for each frequency in the range 28...40 Hz the response $\bar{q}$ was integrated with respect to force amplitude a, resulting in some function of both force amplitude and frequency:

$$P_1(a,v) = \int\limits_{a=0}^{a=a_{max}=0.5N} \overline{q}(a,v)\,da\,.$$

Another function of these parameters, $P_2(a,v)$, was obtained by the integration of the response $\overline{q}$ with respect to logarithm of frequency up to $v_{max} = 80\pi\ s^{-1}$, with the function $P_1(a,v = v_{min} = 56\pi\ s^{-1})$ used as a starting curve for integration:

$$P_2(a,v) = P_1(a,v_{min}) + \int\limits_{v_{min}}^{v_{max}} T(a,v)\,d\ln\frac{v}{v_0}\,.$$

Should the reciprocal relations be fulfilled exactly, these two functions would be the same - the dynamical potential. In our computations, however, the inaccuracies in the experimental data resulted in discrepancy of these two functions, with relative error averaging near 7% and reaching the maximum at v_{max} of approximately 20%. Figure 8 represents the mean value of these two functions $P(a,v)=(P_1+P_2)/2$, which may be considered as the dynamical potential. The dynamical potential is measured in Joules.

The experimentally derived dynamical potential can be approximated by some simple analytical function of the force amplitude and frequency, allowing rapid estimates of the averaged characteristics of motion under given load parameters.

Concluding remarks.

1. It is shown in a laboratory vibration experiment with a single degree of freedom nonlinear oscillator that the concept of dynamical potential can be employed for description of averaged characteristics of motion under given load parameters. As an example, the dynamical potential is reconstructed for the considered oscillator.

2. In the same time, it was found that even relatively small dissipation (of order 0.01) can qualitatively change the system's dynamics near the resonance, and apparently no dynamical potential can be constructed. This situation occurs when the response of the system is approximately equally governed by both non-linearity and dissipation, which in terms of measurable quantities mean that the nonlinear frequency shift of the resonance is of the same order as the breadth of the resonant curve (in given domain of loads and deformations). Some systems, however, may exhibit the resonance at the frequencies far from the linear eigenfrequency ("strong" non-linearity), and the estimates of the response and temperature can be successfully derived from the dynamical potential.

3. Should the dynamical potential be deemed useful in the research in non-linear vibrations, the data of multiple experiments with various mechanical or electrical systems can be used to create a library of such functions, greatly reducing the need in numerical simulations or experiments with physical systems.

References.

1. V.I. Arnol'd 1989 Dynamical Systems, volume 3. New York: Springer-Verlag.

2. A.H. Nayfeh and D.T. Mook 1979 Nonlinear Oscillations. New York: Wiley-Interscience.

3. F.C. Moon 1987 Chaotic Vibrations: An Introduction to Chaotic Dynamics for Scientists and Engineers. New York: Wiley-Interscience.

4. V. Berdichevsky 1983 Variational Principles of Continuum Mechanics. Moscow: Nauka Publishers.

5. V. Berdichevsky 1993 International Journal of Engineering Science 31, 1215-1218. Reciprocal relations in nonlinear vibrations

6. V.L. Berdichevsky, W.W.Kim, and A.Ozbek 1995 Journal of Sound and Vibration 179, 151-164. Dynamical Potential for non-linear vibrations of cantilevered beams.

7. V. Berdichevsky 1996 Thermodynamics and parametric response of slightly dissipative systems.

Figure Captions

Figure 1. Mechanical Model.

Figure 1. Experimental setup. 1-steel baseplate, 2-excitation speaker, 3-voice coil, 4-diaphragm suspension, 5-aluminum cylinder, 6-lateral link, 7-steel frame stud, 8-receiver speaker.

Figure 3. Velocity calibration: the receiver coil output as function of the velocity magnitude.

Figure 4. Static load-deflection curve for the spring used in the experiment.

Figure 5. Temperature of the oscillator as function of the force amplitude and frequency.

Figure 6. Response of the oscillator as function of the force amplitude and frequency.

Figure 7. Checking the validity of reciprocal relations.

Figure 2. Dynamical potential as function of force amplitude and frequency.

Figure 1.

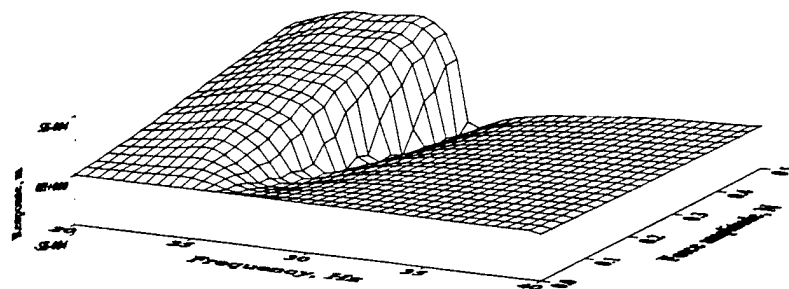Figure 2.

16
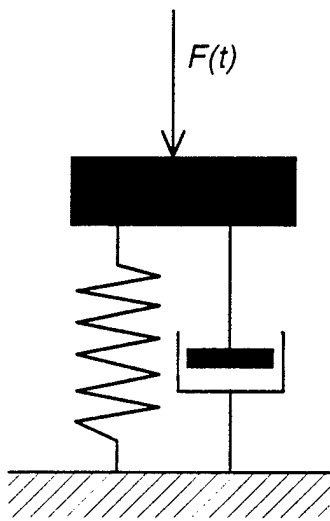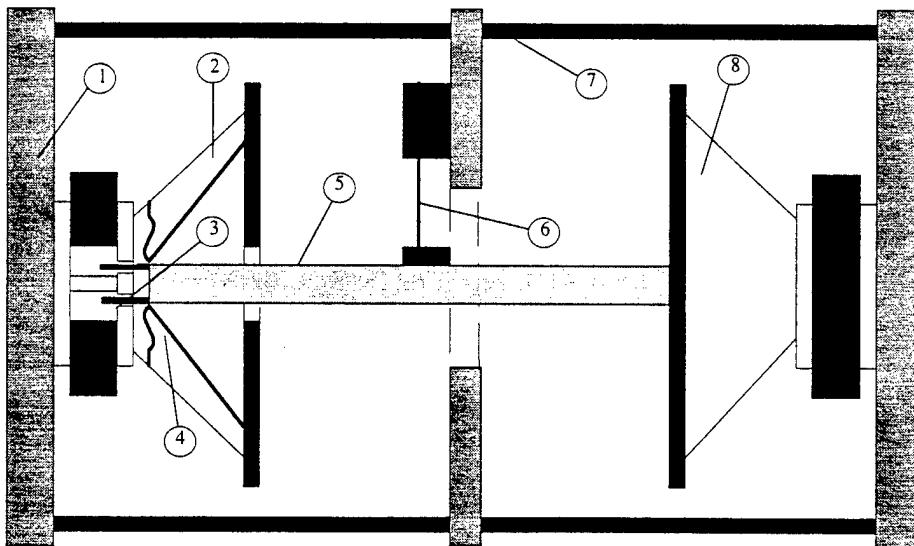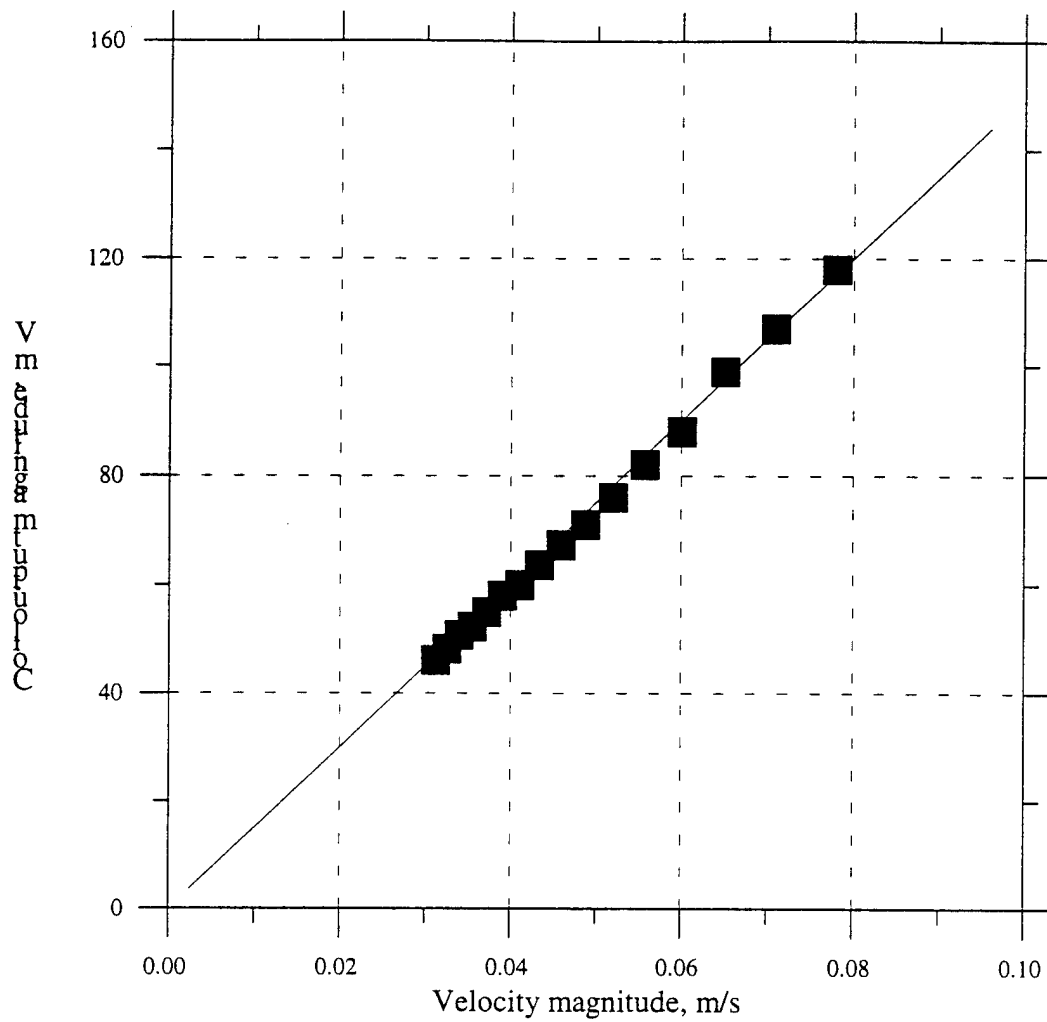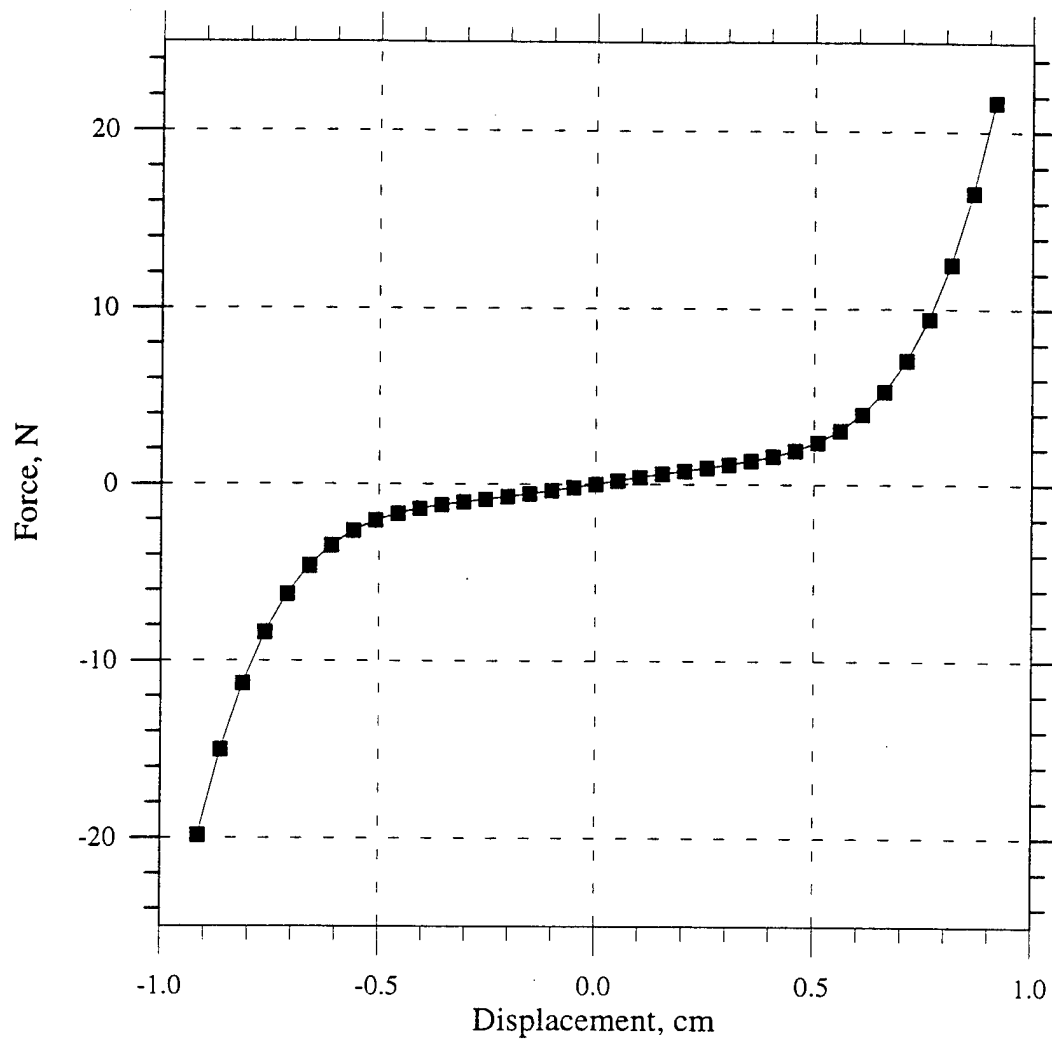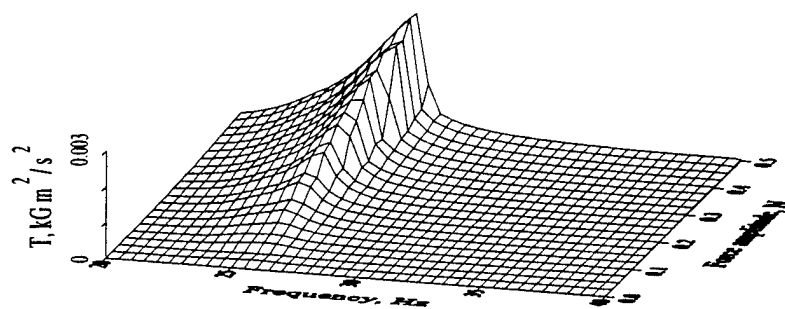
Figure 3.

Figure 4.

Figure 5.

Figure 6.
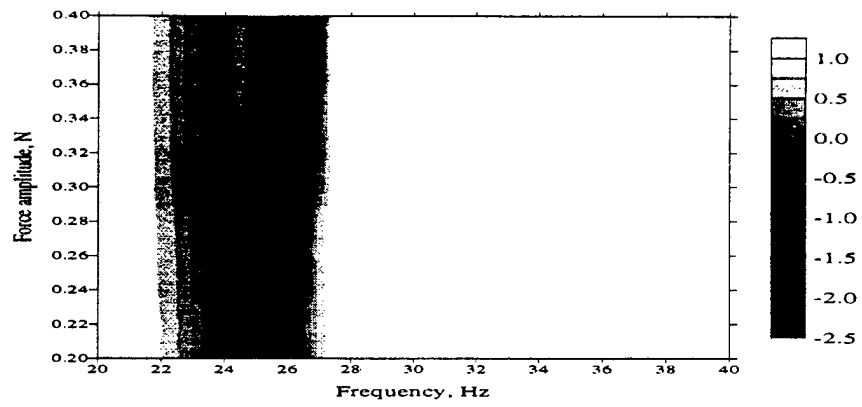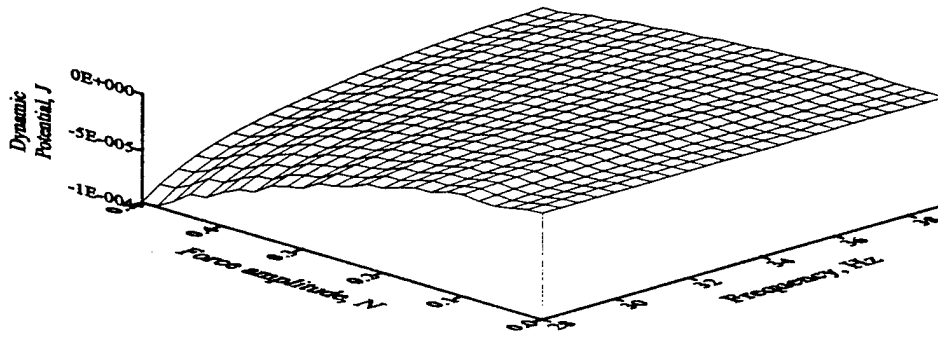
Figure 7.

Figure 8.

Proceedings of the Eighth International Symposium on

CONTINUUM MODELS AND DISCRETE SYSTEMS

Varna, Bulgaria

11 – 16 June 1995

Editor

Konstantin Z Markov

Faculty of Mathematics and Informatics
University of Sofia
Bulgaria

HOMOGENIZATION PROBLEM FOR BULK DIFFUSIONAL CREEP

V. BERDICHEVSKY

Mechanical Engineering, Wayne State University,
Detroit, MI 48202, USA

and

B. SHOYKHET

Reliance Electric, Cleveland, OH 44117, USA

Abstract. The problem of homogenization for bulk diffusional creep in polycrystals with periodic microstructure is considered. The cell problem is derived in linear and nonlinear cases. Constitutive equations of macroscopic theory are obtained in an explicit form for the linear case. The stationary cell problem is posed for secondary creep. The stationary cell problem has a variational form, and the corresponding variational principle is formulated. Some results of numerical simulations for honeycomb structure are presented.

1. Introduction

We have been studying the problem of homogenization for creep in polycrystals where the leading mechanism of creep is the bulk diffusion of vacancies. The foundation of the theory of diffusional creep was laid down by Nabarro [1], Herring [2], Coble [3] and Lifshitz [4]. We have been following a nonlinear version of the theory presented in [5]. The statement of the homogenization problem is the following. Consider a polycrystalline body V consisting of a very large number of grains. The characteristic grain size ϵ is much smaller then the characteristic size L of region V. The body is loaded by some surface forces. Mechanical deformations inside the grains are governed by the equations of diffusional creep which are presented below. If $\epsilon \ll L$, it is natural to expect that deformation of the body can be described by some displacement fields which are practically constant on the distances of order ϵ, i.e. by "averaged" displacements. The problem of homogenization concerns the derivation of the equations for averaged (or macro) displacements and the study of microdeformations of the grains. The problem of homogenization is an asymptotical problem with a small parameter ϵ/L. We are going to consider homogenization problem for polycrystals with periodic microstructure. The experience gained in various homogenization problems shows that macroequations for bodies with periodic and random structures are similar (see, for example, [6]).

The system of equations of bulk diffusional creep is as follows. The "elastic part" of the system of equations consists of equilibrium equations for the stress tensor σ^{ij}

$$\frac{\partial \sigma^{ij}}{\partial x^j} = 0, \quad (1.1)$$

and the constitutive equations

$$\sigma^{ij} = \frac{\partial F}{\partial \epsilon_{ij}^{(e)}}, \quad (1.2)$$

where free energy F is a given function of elastic strains $\epsilon_{ij}^{(e)}$, vacancy concentration c and temperature T. Elastic strains are defined as the difference of the total strains, determined by the displacement vector w_i and the plastic strains ϵ_{ij}^{p}. We consider "geometrically linear" theory, therefore

$$\epsilon_{ij}^{(e)} = \frac{1}{2}\left(\frac{\partial w_i}{\partial x_j} + \frac{\partial w_j}{\partial x_i}\right) - \epsilon_{ij}^{(p)}. \quad (1.3)$$

Small Latin indices run values 1, 2, 3 and correspond to the projections on the axes of a Cartesian frame. Temperature T is assumed to be maintained constant. In "geometrically linear" creep the deformation of the grain boundaries can be neglected in the calculation of stresses and strains and the nonlinearity is kept in the constitutive equations only.

To close the system of equations one has to formulate the evolution law for plastic strains $\epsilon_{ij}^{(p)}$. The major feature of bulk diffusional creep is the consistency of plastic deformations: there exists a vector of plastic displacements $w_i^{(p)}$ such that plastic deformations $\epsilon_{ij}^{(p)}$ are

$$\epsilon_{ij}^{(p)} = \frac{1}{2}\left(\frac{\partial w_i^{(p)}}{\partial x_j} + \frac{\partial w_j^{(p)}}{\partial x_i}\right). \quad (1.4)$$

Therefore, the usual equations of elasticity should be complimented by three equations for plastic displacements $w_i^{(p)}$. These are the equations which relate the flux of vacancies and the corresponding "irreversible" flux of material

$$w_i^{(p)} = D_i^j \frac{\partial}{\partial x^j}\frac{\partial F}{\partial c}, \quad (1.5)$$

where D_i^j is the diffusivity tensor.

System of equations (1.1)-(1.5) is closed by the diffusion equation for vacancy concentration

$$\frac{\partial c}{\partial t} = \frac{\partial}{\partial x^i}D^{ij}\frac{\partial}{\partial x^j}\frac{\partial F}{\partial c}, \quad (1.6)$$

The boundary conditions on the grain boundaries have the form ($\sigma_{nn} = \sigma^{ij}n_in_j$, where n_i are the components of unit normal vector at the boundary, σ_a

are the tangent projections of the vector $\sigma_i^j n_j$, vectors are denoted by bold letters, Greek indices run values 1, 2; $[A]$ stands for the difference of values of A on two sides of the grain boundary Σ)

$$[u_n] = 0, \qquad (1.7)$$

$$\sigma_\alpha = 0 \quad \text{on each side of } \Sigma, \qquad (1.8)$$

$$[\sigma_{nn}] = 0, \qquad (1.9)$$

$$\sigma_{nn} = \frac{\partial F}{\partial c} \quad \text{on each side of } \Sigma. \qquad (1.10)$$

Eq. (1.7) expresses the continuity of the normal component of the total displacement at the grain boundary. The tangent component of the displacements can be discontinuous: we assume that the process of stress relaxation at the boundary occurs much faster than the bulk diffusion. Therefore, Eq. (1.8) is accepted. The condition (1.9) of continuity of the normal stresses is reciprocal to (1.7). Eq. (1.10) controls the creation of vacancies at grain boundaries.

We do not formulate the boundary conditions on the polycrystal boundary ∂V because they do not affect the averaged equations and the cell equations.

In the linear case, free energy density is a quadratic function of $\epsilon_{ij}^{(e)}$ and c

$$F = \frac{1}{2} A^{ijkl} \epsilon_{ij}^{(e)} \epsilon_{kl}^{(e)} + \frac{1}{2} A(c - c_0)^2, \qquad (1.11)$$

where A^{ijkl} are the elastic moduli, c_0 is an equilibrium value of vacancy concentration. The material constant A can be found from elementary statistical consideration: $A = \rho_0 kT/mc_0$, m is the mass of one atom, ρ_0 is the mass density and k is the Boltzman constant.

In the following sections we formulate the results of the study of the homogenization problem for the system (1.1)–(1.10) under the natural assumption on the convexity and the smoothness of F. Before presenting the results, some description of a periodic structure is to be done.

We assume that the grains coincide with the cells of a periodic structure. Let ϵ be a characteristic size of the grain. We introduce dimensionless coordinates

$$y_i = x_i/\epsilon \qquad (1.12)$$

and define the periodic structure in the space of dimensionless coordinates y by the unit cell ω and the translation symmetry group G. The characteristic size of the unit cell is equal to unity. For $l \in G$ we denote by $\omega(l)$ the image of the unit cell ω under the translation l. It is assumed that different cells $\omega(l)$ may have in common the boundary points only, and that the union of the cells covers the whole y-space. It can be shown that the boundary $\partial \omega$ of the unit cell is comprised of the set of pairs of surfaces (or lines in 2D case) $S_1, S_1', S_2, S_2', \ldots, S_r, S_r'$, such that for every surface S_α there exists a translation $l_\alpha \in G$, mapping S_α onto S_α'. For hexagonal structure this notation is explained on Fig. 1. Obviously, the translation $-l_\alpha$ maps S_α' onto S_α. Thus the periodic structure induces the certain mapping of the cell boundary $\partial \omega \Longleftrightarrow \partial \omega$, which will be used for the formulation of the boundary conditions. For every point $y \in \partial \omega$ we denote by $l(y)$ the corresponding translation vector. The points y and $y' = y + l(y)$ will be referred to as the corresponding points. Note that $l(y)$ is constant within each surfaces S_α, S_α'.
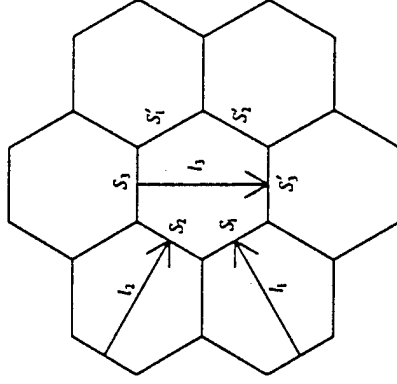

Fig. 1. Hexagonal structure. The translation vectors shown by arrows map the corresponding parts of the cell boundaries.

The unit normal n to the cell boundary is assumed to be directed outward the cell, therefore at the corresponding points y and y' we have

$$n(y) + n(y') = 0. \qquad (1.13)$$

Let $f(y)$ be an arbitrary function, which is continuous within each grain, but may be discontinuous at the grain boundaries. Function $f(y)$ is called periodic if

$$f(y + l) = f(y) \quad \text{for any } y \in \partial \omega \text{ and for any } l \in G. \qquad (1.14)$$

If function $f(y)$ is known within the unit cell, it can be extended to the whole space by the formula (1.14).

2. Asymptotic Expansions

For $\epsilon \to 0$ the first two terms of asymptotical expansion of the displacement field has the form

$$w_i(x, t) = \bar{w}_i(x, t) + \epsilon \psi_i(x, y, t), \qquad (2.1)$$

where the "averaged" displacements do not depend on ϵ, $y_i = x_i/\epsilon$ and ψ_i are some periodic functions of y.

Asymptotical expansion of diffusion vacancy concentration starts with a periodic function of the fast variables

$$c = c(x, y, t). \quad (2.2)$$

Functions $\psi_i(x, y, t)$ and $c_i(x, y, t)$ determine microfields while functions $\bar u_i$ are the required functions in macroequations. Functions ψ_i and c can be found from the following cell problem.

3. Cell Problem

The system of equations of the cell problem consists of equilibrium equations

$$\frac{\partial \sigma^{ij}}{\partial x^j} = 0, \quad (3.1)$$

constitutive equations

$$\sigma^{ij} = \frac{\partial F}{\partial \varepsilon_{ij}^{(e)}}, \quad (3.2)$$

strain-displacement equations

$$\varepsilon_{ij}^{(e)} = \bar\varepsilon_{ij} + \frac{1}{2}\left(\frac{\partial \psi_i}{\partial y_j} + \frac{\partial \psi_j}{\partial y_i}\right) - \varepsilon_{ij}^{(p)}, \quad (3.3)$$

the law of evolution of plastic strains

$$\frac{\partial \varepsilon_{ij}^{(p)}}{\partial t} = \frac{1}{2\varepsilon^2}\left(\frac{\partial}{\partial y^i}D_{,j}^k \frac{\partial}{\partial y^k}\frac{\partial F}{\partial c} + \frac{\partial}{\partial y^j}D_{,i}^k\frac{\partial}{\partial y^k}\frac{\partial F}{\partial c}\right), \quad (3.4)$$

and the diffusion equation

$$\frac{\partial c}{\partial t} = \frac{1}{\varepsilon^2}\frac{\partial}{\partial y^i}D^{ij}\frac{\partial}{\partial y^j}\frac{\partial F}{\partial c} \quad (3.5)$$

Here $\bar\varepsilon_{ij}$ are the macrostrains which are considered as some parameters in the cell problem, $\bar\varepsilon_{ij}$ do not depend on y-coordinates but might be some functions of time.

Note that the factor ε^2 in Eqs. (3.4) and (3.5) can be deleted by scaling of time, and the Eqs. (3.1)–(3.5) do not contain ε after scaling.

We search for the solution ψ_i, c of Eqs. (3.1)–(3.5) which is periodic in y-variables and obey the following boundary conditions

$$\sigma_{nn} = \frac{\partial F}{\partial c}, \quad y \in \partial\omega, \quad (3.6)$$

$$\sigma_\alpha = 0, \quad y \in \partial\omega, \quad (3.7)$$

$$\psi_n\big|_y + \psi_n\big|_{y+l(y)} = 0, \quad c\big|_y = c\big|_{y+l(y)}, \quad y \in \partial\omega. \quad (3.8)$$

If parameters $\bar\varepsilon_{ij}$ are given functions of time t, the system has, probably, a unique solution. Uniqueness can be proved in the linear case.

4. Macroequations

Let us define macrostresses as averaged values of stresses

$$\bar\sigma^{ij} = \frac{1}{|\omega|}\int_\omega \sigma^{ij} d^3x, \quad (4.1)$$

where $|\omega|$ is the cell volume. Then $\bar\sigma^{ij}$ is a functional of $\bar\varepsilon^{ij}$ which can be found from the cell problem:

$$\bar\sigma_{ij} = \text{Functional}(\bar\varepsilon_{ij}). \quad (4.2)$$

It can be shown that macrostresses obey the equilibrium equation

$$\frac{\partial \bar\sigma^{ij}}{\partial x^j} = 0, \quad (4.3)$$

and macrostrains relate to macrodisplacements by the usual formula

$$\bar\varepsilon_{ij} = \frac{1}{2}\left(\frac{\partial \bar u_i}{\partial x_j} + \frac{\partial \bar u_j}{\partial x_i}\right). \quad (4.4)$$

Eqs. (4.3), (4.4), (4.2) and (3.6) form a closed system of equations for macrodisplacements.

5. Macroequations in Linear Case

From now on we consider the linear case when free energy is given by (1.11). It can be shown, that the system (3.1)–(3.8) satisfies the Boltzman superposition principle, and, hence, the stress-strain relation (4.2) has the form

$$\bar\sigma^{ij} = \int_0^t Q^{ijkl}(t-\xi)\dot{\bar\varepsilon}_{kl}(\xi)\,d\xi$$

$$= Q^{ijkl}(0)\bar\varepsilon_{kl} + \int_0^t \frac{\partial Q^{ijkl}(t-\xi)}{\partial t}\bar\varepsilon_{kl}(\xi)\,d\xi. \quad (5.1)$$

Here the function $Q^{ijkl}(t)$ is the macrostress component $\bar\sigma^{ij}(t)$ caused by the application of the strain $\bar\varepsilon_{kl}(t) = 1$ for $t > 0$, $\bar\varepsilon_{kl}(t) = 0$ for $t \le 0$, while all the other strain components are equal to zero. Tensor $Q^{ijkl}(0)$ is the elastic moduli tensor of polycrystal. The inversion of the relation (5.1) renders

$$\bar\varepsilon^{ij} = \int_0^t R_{ijkl}(t-\xi)\dot{\bar\sigma}^{kl}\,d\xi$$

$$= R_{ijkl}(0)\sigma^{kl} + \int_0^t \frac{\partial R_{ijkl}(t-\xi)}{\partial t}\sigma^{kl}(\xi)\,d\xi. \quad (5.2)$$

The function $R_{ijkl}(t)$ has the sense of the macrostrain component $\bar\varepsilon_{ij}(t)$ caused by the constant macrostress $\bar\sigma^{kl}(t) = 1$ for $t > 0$, $\bar\sigma^{kl}(t) = 0$ for $t \le 0$, while all the other stress components are zeros. The values $R_{ijkl}(t)$ are the components of the tensor of the elastic compliance of the polycrystal. Due to that it is convenient to decompose $R_{ijkl}(t)$ into the sum

$$R_{ijkl}(t) = R_{ijkl}(0) + K_{ijkl}(t), \quad K_{ijkl}(0) = 0, \qquad (5.3)$$

where the functions $K_{ijkl}(t)$ are the creep macrostrains. The creep curves $K_{ijkl}(t)$ have a square root asymptotics for small values of t:

$$K_{ijkl}(t) \sim t^{1/2}, \quad \frac{\partial K_{ijkl}(t)}{\partial t} \sim t^{-1/2}.$$

Hence, at the initial moment, the creep rate tends to the infinity as $t^{-1/2}$.

An important feature of the constitutive equations (5.1), (5.2) is that these equations are not local: there is a memory of the prehistory of the process. This means that local theories of primary creep are not adequate at least in the case of bulk diffusional creep.

6. Secondary Creep

Generally speaking, the macroscopic constitutive equations are given by the integral operators (5.1) or (5.2). However, for "slow" loading processes and developed creep it is possible to use as an approximation the creep law

$$\dot{\bar\varepsilon}_{ij} = E_{ijkl}\bar\sigma^{kl}, \quad \bar\sigma^{kl} = \bar\sigma^{kl} - \delta^{kl}\bar\sigma^{ss}/3, \qquad (6.1)$$

or

$$\bar\sigma^{ij} = c^{ijkl}\dot{\bar\varepsilon}_{kl}, \qquad (6.2)$$

$$\dot{\bar\varepsilon}_{kk} = 0. \qquad (6.3)$$

The macrocharacteristics of the secondary creep E_{ijkl} are the limits of the creep rates $K_{ijkl}(t)$ when $t \to \infty$. The fact that the creep rates tend to some constants when $t \to \infty$ constitutes the basis of the approximation (6.1)–(6.3). Tensor e^{ijkl} is the inverse tensor to E_{ijkl}.

It turns out that for the secondary creep the creep macrocharacteristics and the microfields may be found from the following variational principle.

Let $\dot{\bar\varepsilon}_{ij}$ be an arbitrary constant creep rates, satisfying the incompressibility condition (6.3). Denote by $J(C)$ the following functional of function $C(y)$

$$J(C) = \frac{1}{2}\int_\omega d^{ij}\frac{\partial C}{\partial y^i}\frac{\partial C}{\partial y^j}d^2y + \frac{1}{2}\int_{\partial\omega}\dot{\bar\varepsilon}_{ij}n^i l^j C_i d^2y. \qquad (6.4)$$

Here $d^{ij} = AD^{ij}/\epsilon^2$.

Consider the minimization problem

$$J(C) \to \min_C. \qquad (6.5)$$

Minimum is sought on the set of all functions C obeying the constraints

$$C(y) = C(y + l(y)), \quad y \in \partial\omega, \qquad (6.6)$$

$$\int_{\partial\omega} C \cdot l \times n\, d^2 y = 0. \qquad (6.7)$$

After the solution of the variational problem (6.4)–(6.7) is found, the deviator of macrostresses is defined by the formula

$$\bar\sigma^{ij} = \frac{A}{2|\omega|}\left(\int_{\partial\omega} C n^i l^j d^2 y - \delta^{ij}\int_{\partial\omega} C n^s l^s d^2y/3\right). \qquad (6.8)$$

The solution C of the problem (6.4)–(6.7) depends linearly on the parameters $\dot{\bar\varepsilon}_{ij}$. Hence plugging this solution in (6.8) one obtains macrostresses in terms of creep velocities $\dot{\bar\varepsilon}_{ij}$, i.e. the relation (6.2), and the macrocharacteristics e^{ijkl}.

So, the solution of the variational problem (6.4)–(6.8) gives us macroequations of creep and the microfield of vacancy concentration. We have to also determine microstresses. To this end we note that the solution $C(y)$ of the variational problem is determined up to an arbitrary constant C_0. We fix this constant by the condition

$$\int_{\partial\omega}(C(y) - C_0)n^s l^s d^2y = 0. \qquad (6.9)$$

Then the microstresses at the cell boundary are determined by formulas (3.6) and (3.7) which for the linear case takes the form

$$\sigma_{nn}(y) = A(C(y) - C_0), \quad \sigma_\alpha = 0, \quad y \in \partial\omega. \qquad (6.10)$$

Now we may consider the elasticity problem for the cell with the boundary conditions (6.10). The necessary condition for solubility of this problem (total external force and moment are zeros) is satisfied due to the choice of the additive constant C_0 made through Eq. (6.9).

Denote by $\sigma^{ij}(y)$ the solution of the elasticity problem. The microstresses of the nonstationary problem (3.1)–(3.8) tends to the sum $\sigma^{ij}(y) + \delta^{ij}\bar\sigma^{ss}/3$.

Remark 1. For some cell shapes, the relations (6.7) may be automatically satisfied. In particular, it is true if for any $y \in \partial\omega$ the normal vector $n(y)$ to the cell boundary is parallel to the translation vector $l(y)$. The regular 2D hexagonal structure used in the next Section for numerical examples, possesses this property. It can be shown, that in this case the solution of the cell problem (3.1)–(3.8) is determined up to a rotation of the cell as a rigid body. It does not influence the computation of constants in the constitutive equations (6.1) and (6.2).

the other pair of sides. The remaining two sides consist of two pieces: material leaves
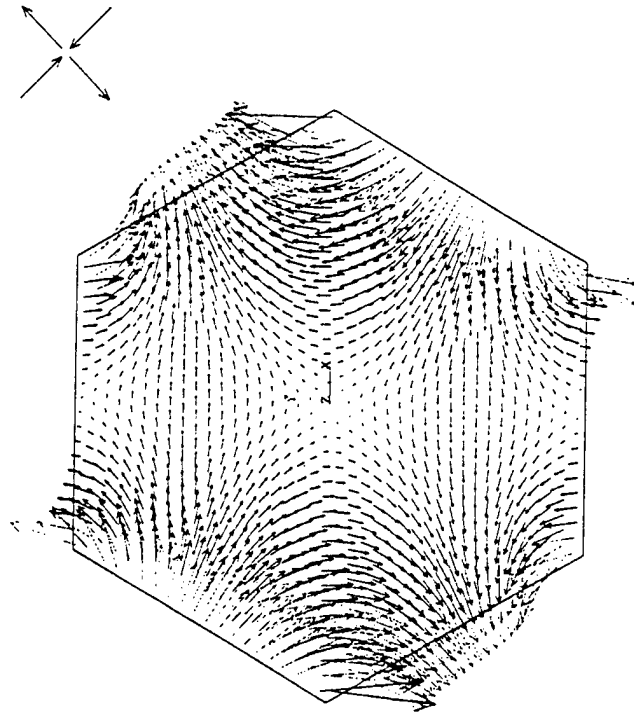one piece and arrives at the other one.

Fig. 2. Creep velocity distribution during the secondary creep.

Conclusions

Three interesting outcomes of this study seem worthy noting.

First, the constitutive macroequations of diffusional creep turn out to be non-
local. It is not seen how to eliminate the non-locality by introducing additional
internal variables. Probably, the elimination of the non-locality on the macroscale is
impossible in principle. Since this seems to be the case, a search for the adequate
local constitutive equations for the diffusional creep is unlikely to be successful.

Second, there is an intrinsic material time $\theta = tDA/\epsilon^2$. Strain-time depen-
dence (for constant stresses) is universal for intrinsic time in the sense that it does not
depend on the material and on the temperature (temperature dependence penetrate
through the material constants D and A).

Remark 2. Let us normalize the diffusivity tensor in (3.5):

$$D^{ij} = D\bar{D}^{ij}, \tag{6.10}$$

where D is some characteristic value of tensor D^{ij}. Analysis of physical dimensions
shows that creep rate constants can be represented as follows:

$$E_{ijkl} = \bar{E}_{ijkl}\frac{D}{\epsilon^2}, \tag{6.11}$$

where the dimensionless constants $\bar{E}_{ijkl}$ depend on the constants $\bar{D}^{ij}$ and the unit cell
shape only. An important consequence is that the creep rates in secondary creep do
not depend on the elastic properties.

Remark 3. The characteristic time of approaching the steady creep under the
constant load is ϵ^2/DA.

7. Numerical Results

The numerical modeling were done for the two-dimensional regular hexagonal
structure, shown in Fig. 1. For definiteness, it was assumed that grains are isotropic,
and hence only four physical constants are needed: Young modulus E, Poisson ratio
ν, the constant A in (1.11), diffusivity constant D in (6.11) (with $\bar{D}^{ij} = \delta^{ij}$), and the
grain size ϵ.

Secondary Creep Rates. In creep, the periodic hexagonal structure behaves
isotropically. Thus, the creep law (6.1) contains just one macrocharacteristic, viscosity
μ:

$$\bar{\sigma}^{ij} = \mu\dot{\epsilon}^{ij}. \tag{7.1}$$

The dimension analysis of the cell problem shows that μ depends on the grain size ϵ
and the diffusivity coefficient D only

$$\mu = a\frac{\epsilon^2}{D}, \tag{7.2}$$

where a is some constant. Numerical simulations give the following value of the con-
stant a for hexagonal structure

$$a = 0.344. \tag{7.3}$$

The formulae (7.2) and (7.3) inspire an assumption that the similar relation
between macro- and micro-characteristics takes place for the random structure as well,
where ϵ is the averaged grain size and D is the characteristic diffusion coefficient for
monocrystals, while the coefficient a is of the order of unity.

Microdeformation. Distribution of creep velocity over the cell in the regime of
secondary creep is shown in Fig. 2. The orientation of shear stress applied is given
at the right top of Fig. 2. It can be seen that there are three pairs of opposite cell
sides with different properties. Material departs from one pair of sides and arrives at

Third, as the variational principle shows, the creep rates do not depend on the elastic properties in secondary creep: only diffusion constants, the grain size and the grain geometry are important. Formula (7.2) is an example of such a dependency. The discussion of these issues in full detail will be presented in another paper.

References

1. F. R. N. Nabarro, *Deformation of Crystals by the Motion of Single Ions*, Report of a Conference on Strength of Solids, The Physical Soc., 1948, p. 75.

2. C. Herring, *J. Appl. Phys.* **21** (1950) 437.

3. R. J. Coble, *J. Appl. Phys.* **34** (1963) 1679.

4. I. M. Lifshitz, *Soviet Physics JETP* **17** (1963) 909.

5. V. Berdichevsky, P. Hazzledine and B. Shoykhet, *Micromechanics of Diffusional Creep*, Preprint, 1994.

6. V. Berdichevsky, *Variational Principles of Continuum Mechanics*, Nauka, Moscow, 1983. (in Russian.)

NONLINEAR BEHAVIOR IN A COMPOSITE MEDIUM: THE IMPORTANCE OF RESONANCES AND PERCOLATION

D. J. BERGMAN
School of Physics and Astronomy
Raymond and Beverly Sackler Faculty of Exact Sciences,
Tel Aviv University, Tel Aviv 69978, Israel

Abstract. The nonlinear response of a composite medium to an external field can be greatly enhanced if the system is near a percolation threshold p_c or near a strong, isolated resonance. The latter situation, which can be achieved in the electric properties of metal-dielectric composites, can result in bistability of the dielectric response even at low field amplitudes. The former situation is realizable in electric properties of metal-insulator composites, as well as in elastic properties of an elastic solid with a random distribution either of voids or of rigid inclusions. The enhancement of nonlinear response near p_c can be described by a scaling theory which makes some non-trivial predictions regarding the critical behavior. Calculational methods are also described. For nonlinear behavior near p_c these include simple approximations as well as numerical simulations of random discrete network models. Calculational methods for nonlinear behavior near a sharp resonance include a "zero virtual work" principle along with an appropriate ansatz for the trial field.

1. Introduction

The phenomenon of weakly nonlinear response, like the following relation between the electric field E and the current density J in an electrical conductor

$$J = \sigma E + b|E|^2 E, \quad b|E|^2 \ll \sigma, \tag{1}$$

is quite common. However, in order to be observable and lead to interesting new modes of physical behavior, the nonlinear term should not be too small. Besides increasing the magnitude of the applied or volume averaged field ⟨E⟩, another way to increase the relative importance of that term is to mix together different materials so as to form a composite medium in such a way that the local electric field becomes extremely non-uniform. In order to analyze the properties of such a medium, where each component has a J vs. E relation like (1) but with different values of σ, b, it is natural to adopt a perturbation approach. In this way, Strond and Hui showed that the volume averaged fields ⟨J⟩, ⟨E⟩, are related as follows [1]

Attachment 8

MICROMECHANICS OF DIFFUSIONAL CREEP

V. BERDICHEVSKY

Mechanical Engineering, Wayne State University, Detroit, MI 48202, U.S.A.

P. HAZZLEDINE

UES Inc., 4401 Dayton-Xenia Road, Dayton, OH 45432, U.S.A.

B. SHOYKHET

Reliance Electric, Cleveland, OH 44117, U.S.A.

Abstract—In polycrystalline materials at high temperatures and low stresses, creep occurs mostly by the diffusion of vacancies through the grain bodies and over the grain boundaries. A continuum theory of vacancy motion is considered to analyze diffusional creep on a microscopical level. A linear version of such a theory was formulated by Nabarro, Herring, Coble and Lifshitz. We revise this theory from the perspectives of continuum mechanics and present it in a thermodynamically consistent nonlinear form. A certain difficulty, which one has to overcome in this endeavor, is the absence of Lagrangian coordinates in diffusional creep, the major building block of any theory in continuum mechanics. A linearized version of the theory is studied for the case of bulk diffusion. We consider the derivation of macro constitutive equations using the homogenization technique. It is shown that macroequations are nonlocal in time and nonlocality is essential in primary creep. For secondary creep polycrystals behave as a viscoelastic body. For secondary creep, a variational principle is found which determines microfields and macromoduli in stress–strain rate constitutive equations. A two-dimensional honeycomb microstructure and single crystal deformation are studied numerically by a finite element method. © Elsevier Science Ltd. All rights reserved. © 1997 Elsevier Science Ltd.

1. INTRODUCTION

Predictions of the mechanical behavior of solids can be roughly classified as short-term and long-term predictions. In short-term prediction, the behavior can be elastic or plastic, depending on the level of stress. For sufficiently low stresses, solids behave elastically. However, over long time periods, even under very low stresses, solids develop irreversible deformations. This phenomenon is called creep.

There are three points worth stressing in a discussion of creep. First, everything creeps. Actually, solids creep even at zero external load, due to the fact that practically no polycrystalline body is in thermodynamic equilibrium. Second, creep is an energy driven phenomenon. Materials creep in order to decrease their energy (or other thermodynamical potential, depending on the external conditions). The energy of a polycrystal, for example, can be decreased by moving grain boundaries. This occurs in reality, but very slowly, by means of thermodynamic fluctuations. The rate of change is magnified significantly by elevating the temperature and/or applying an external load. Third, the mechanisms of creep are stress and temperature dependent.

Two major creep mechanisms are movement of dislocations and diffusion of vacancies. A typical deformation mechanism map is shown in the stress–temperature plane in Fig. 1. Above the curve (high stresses) the dominating mechanism is dislocation motion. Below the curve (low stresses) deformations occur by the diffusion of vacancies. It is believed that at low temperatures, vacancies move mostly over the grain boundaries (Coble creep), while for high temperatures, motion of vacancies through the lattice dominates (Herring–Nabarro creep or bulk diffusional creep). Diffusional creep is the leading phenomenon in many technological processes at high temperatures. Superplasticity, sintering and void formation occur mostly by diffusional creep. In this paper we focus on a thermodynamically consistent theory of diffusional
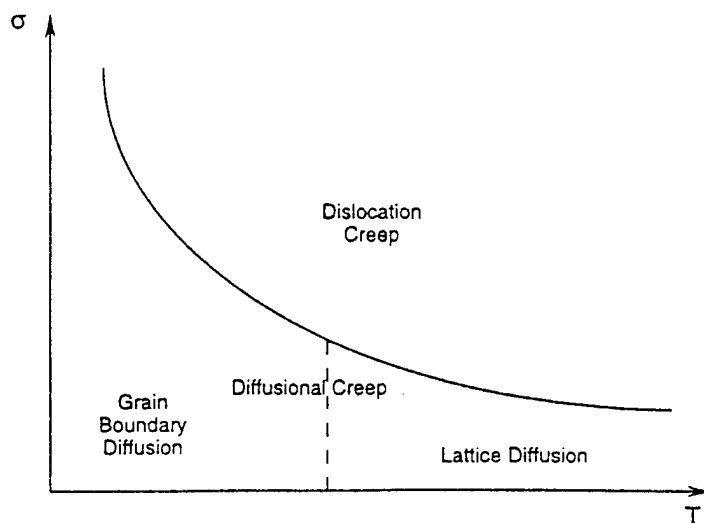
Fig. 1. Deformation mechanism map.

creep. The foundations of this theory were laid down by Nabarro [1], Herring [2], Coble [3] and Lifshitz [4]. Extensive reviews of various aspects of creep theory can be found in [5–24].

The mechanism of plastic deformation caused by bulk diffusional creep can be viewed as follows. Let a monocrystal be loaded by an external force (Fig. 2). Consider the right-hand side of the monocrystal. A surface external force might be thought of as a set of forces applied to each atom of the very right column of atoms (Fig. 2(a)). Because of thermal fluctuations some of the atoms of this column can jump to a new equilibrium position (Fig. 2(b)). Then the next atoms may jump into the vacant places and we see that vacancies enter the crystal body. Then vacancies can migrate inside the body and leave the body at the free surface (Fig. 2(d)).

The motion of vacancies is accompanied by the corresponding motion of material in the opposite direction. The moved material is shaded in Fig. 2(e). Since the motion of vacancies is dispersed over the material, one observes an effective elongation of the specimen (Fig. 2(f)).
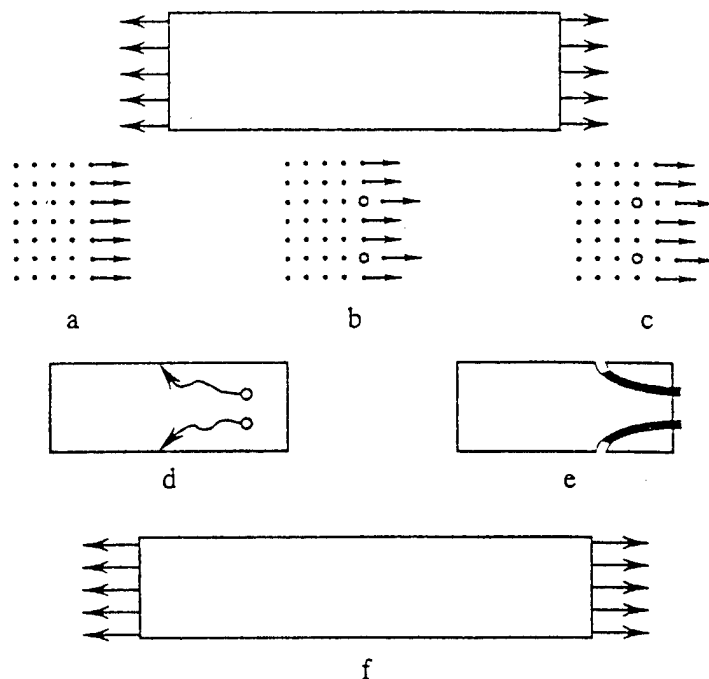

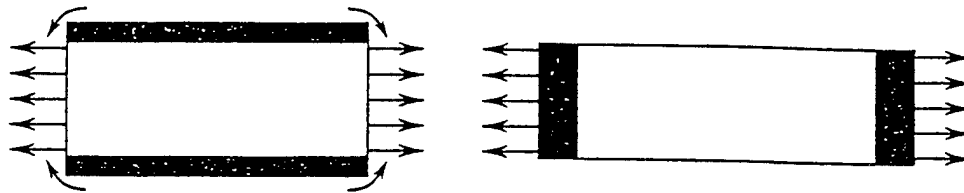Fig. 2. Mechanism of plastic deformation caused by bulk diffusional creep.

Fig. 3. Boundary diffusion.

In the case of boundary diffusion, material flows over the boundaries from unloaded to loaded pieces of the boundary and that yields some macroscopic plastic deformation. This process is shown schematically in Fig. 3, the moving material is shadowed.

A typical strain–time dependence for constant stresses is shown in Fig. 4. There are two different regimes of the plastic flow. Initially, strains grow fast, then the strain rate decays until it approaches some limiting value. These two regimes are referred to as primary and secondary creep.

The aim of this paper is to construct the microequations of diffusional creep in the framework of continuum mechanics and develop a homogenization procedure to derive macroequations of creep. There are a number of reasons for pursuing these goals. First, a phenomenological approach to the derivation of macroequations for creep provides too many options. Realization of our program may help to choose the right one.

Second, the problem seems challenging from the perspective of continuum mechanics. Looking at the sketch of boundary diffusional creep shown in Fig. 5, one may observe that the basic notion of continuum mechanic, Lagrangian coordinates, cannot be used in this case. Really, material points which were on the grain boundary moves into the grain body, which is in clear contradiction to the main postulate of continuum mechanics [25, 26] on the existence of a diffeomorphism between the deformed and undeformed states and, as a consequence, to the existence of Lagrangian coordinates. If a continuum deformation were a diffeomorphism, the material points, which are on the boundary, stay on the boundary forever. Lagrangian coordinates are used in continuum mechanics, for example, in the definition of velocity: one has to ask "velocity of what?". We suggest a way to overcome this difficulty.
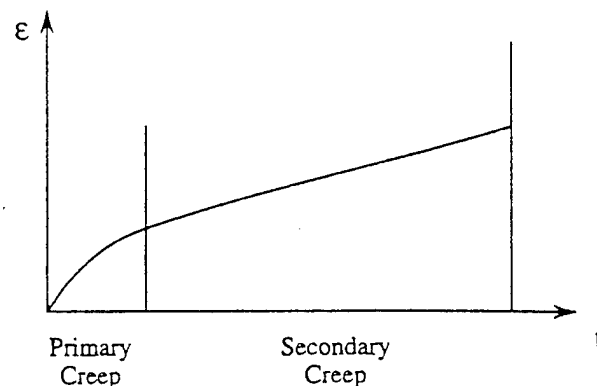

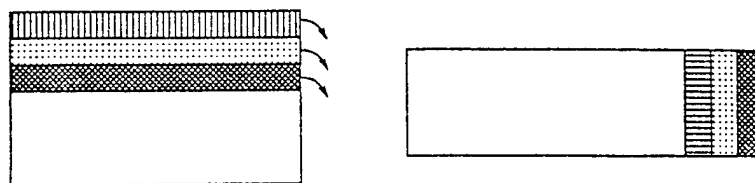Fig. 4. Typical creep strain–time dependence.

Fig. 5. Mixing by boundary diffusion.

Third, a theory of diffusional creep must be a building block for the theory of dislocational climb which is, at the moment, in a primitive stage.

The contents of the paper are as follows. Section 2 describes the main feature of the model for bulk diffusional creep, which is the existence of a plastic displacement field. This is an unusual situation in plasticity. The general kinematic relations for the bulk diffusion and surface diffusion are given in Section 3. In Section 4 the closed system of equations of diffusional creep is developed from thermodynamic considerations. The linear version of the general theory is presented in Section 5. In the rest of the paper a linear theory of bulk diffusional creep is studied, which aims to derive macroscopic laws for grain structure starting from a micromodel. This is referred to as a homogenization problem. In Section 6 the formulation of the homogenization problem is given for a particular case of periodic grain structure. The theorem of uniqueness of the solution is proved, which is evidence for the correctness of the basic equations. In Section 7 the general type of macroscopic constitutive relations is established. Secondary creep is considered in Section 8. It is proved that, under constant loads, the transient solution tends to a steady-state solution and the closed system of equations is found, which allows one to find the macrocharacteristics of the secondary creep without "tracing" the transient solution. A numerical example of the solution of this system is presented in Section 9. A dimensional analysis of the equations and numerical modeling of the transient process are discussed in Section 10.

2. MICROMECHANICS OF BULK DIFFUSIONAL CREEP: A LOGICAL SKELETON OF THE THEORY

The logical structure of the theory is especially simple in the case of bulk diffusional creep and before going into detailed discussion, we outline it briefly. The key point of the bulk diffusional creep is that plastic strains $\varepsilon_{ij}^{(p)}$ are compatible. There exists plastic displacement $w_i^{(p)}$ such that (in the linear case)

$$\varepsilon_{ij}^{(p)} = \frac{1}{2} \left(\frac{\partial w_i^{(p)}}{\partial x_j} + \frac{\partial w_j^{(p)}}{\partial x_i} \right). \tag{1}$$

Here, and in the following, small Latin indices run through values 1, 2 and 3, and correspond to projections on the Cartesian axis of the observer frame; x_i are the observer coordinates.

The compatibility of plastic deformation is a pure kinematical hypothesis. It aims to model the process of deformation shown schematically in Fig. 2(e). In contrast to a general creep theory where six additional equations are to be given for six unknown functions $\varepsilon_{ij}^{(p)}$, in bulk diffusional creep one has to give only three additional equations for $w_i^{(p)}$.

It is clear that the plastic rate $\dot{w}_i^{(p)}$ should be related to vacancy motion. Some kinematical and thermodynamical consideration shows that the corresponding relation (in its simplest version) is

$$\dot{w}_i^{(p)} = D \frac{\partial c}{\partial x_i} \tag{2}$$

where c is vacancy concentration, dot denotes time derivative and D is the diffusion coefficient.

Equation (2) reduces the number of closing equations to one: an equation for vacancy concentration c. This last equation is the diffusion equation for c

$$\frac{\partial c}{\partial t} = D \Delta c. \tag{3}$$

Equations (1)–(3) should be complemented by the usual equations of elasticity and provided with the boundary conditions. Now we proceed to detailed considerations.

3. CONTINUUM KINEMATICS

We are going to model, in terms of continuum mechanics, the following physical phenomenon. If an external load is applied to an atomic lattice containing a cloud of vacancies, vacancies migrate in some preferred direction. The motion of vacancies causes the motion of atoms in the opposite direction. The motion of atoms is perceived by an observer as an irreversible plastic deformation of the material. Our first step is to establish a kinematical relation which relates the motion of vacancies to the motion of the material.

We model the motion of vacancies and material by two continua with velocities u_i and v_i correspondingly. We assume that vacancies are not created inside the material and can only come from the boundary. Then, as we shall argue:

$$v_i^{(e)} = (1 - c)v_i + cu_i \tag{4}$$

where $v_i^{(e)}$ is an "elastic" velocity. If the elastic velocity $v_i^{(e)}$ is zero, the relation equation (4) expresses velocity of material (atoms) v_i in terms of velocity of vacancies u_i and vacancy concentration c.

Usually, vacancy concentration is negligible in comparison to unity. Nevertheless, we keep the factor $(1 - c)$ until the final calculations in order to underline the physical origin of various terms. Equation (4) is a postulate which is motivated by the following reasons.

Consider a piece of crystal lattice, a "representative volume of material," and think of v_i as the average velocity of all the atoms of this piece

$$v_i = \frac{1}{N_a} \sum_\alpha v_i^\alpha \tag{5}$$

where N_a is the number of atoms, v_i^α is the velocity of the αth atom and the sum is taken over all of atoms of the piece. Similarly, velocity of vacancies is the average value of the velocities of all vacancies:

$$u_i = \frac{1}{N_v} \sum_\alpha u_i^\alpha. \tag{6}$$

Here N_v is the number of vacancies and u_i^α is the velocity of the αth vacancy. The volume average velocity $\bar{v}_i$ is, by definition:

$$\bar{v}_i = \frac{1}{N} \left(\sum_\alpha v_i^\alpha + \sum_\alpha u_i^\alpha \right) \tag{7}$$

where N is the total number of lattice sites

$$N = N_a + N_v. \tag{8}$$

It follows from equations (5)–(8) that

$$\bar{v}_i = (1 - c)v_i + cu_i \tag{9}$$

where the volume fraction of vacancies c is, by definition,

$$c = \frac{N_v}{N}. \tag{10}$$

Relation equation (9) holds for a mixture of any two substances. Now we must express in some way the fact that we are dealing with diffusion of vacancies. We may assume that in the process of position exchange between an atom and a vacancy the velocities of the atom and the vacancy are equal in magnitude and opposite in sign. Therefore, in accordance with equation (7), $\bar{v}_i = 0$. Then equation (9) links the velocities of atoms and vacancies. It is clear that atoms and vacancies might have another common additional velocity. Then $\bar{v}_i$ is not zero, but equal to this

additional velocity. The additional velocity is not related to the process of vacancy diffusion or irreversible deformation. We identify this velocity with "elastic" velocity and denote it by $v_i^{(e)}$. Then equation (9) takes the form equation (4).

Note that the term "elastic" velocity is not quite exact. If one defines elasticity as, that part of deformation which disappears after unloading, then velocity $v_i^{(e)}$ might have a contribution form a plastic rigid motion, a motion of the monocrystal after unloading as a rigid body. However, we take some liberties in the terminology to simplify the notations and use the term elastic velocity for the sum of the "real" elastic velocity and plastic velocity of rigid motion.

The flux of vacancies relative to material J_i is given by

$$J_i = c(u_i - v_i^{(e)}). \tag{11}$$

In accordance with equations (4) and (11) material velocity v_i can be expressed in terms of elastic velocity and vacancy flux as

$$v_i = v_i^{(e)} - \frac{1}{1-c} J_i. \tag{12}$$

This is a key kinematical relation.

Since vacancies can be generated only on the boundary, vacancy concentration obeys the conservation law

$$\frac{\partial c}{\partial t} + \frac{\partial c u_i}{\partial x_i} = 0. \tag{13}$$

Equations (4), (11)–(13) form the basic kinematical relations of bulk diffusional creep. Now we are going to incorporate into this picture the surface diffusion.

Consider a grain in a polycrystal. It occupies a region V. Region V depends on time. Imagine that at an initial instance, t_0, we cut the grain out of the polycrystal and unload it. The grain occupies some region, V_0, in an unloaded state. We refer both regions to some Cartesian coordinates, x^i. Besides, we introduce in the region V_0 some coordinates curvilinear in general, ξ^a, which, in a "usual" situation, play the role of Lagrangian coordinates. Indices a, b and c run through values 1, 2 and 3, and correspond to projections on the axis ξ^a.

There is one-to-one correspondence between the observer's coordinates x_i and coordinates ξ^a

$$x^i = \hat{x}^i(\xi^a). \tag{14}$$

Without loss of generality mapping equation (14) may be identical, however, it is convenient to leave it without specifications because coordinates x^i and ξ^a obey to different groups of transformations [27]. This is why we use another group of Latin indices, a, b and c, in the notation for Lagrangian coordinates.

At each moment of time, t, there is mapping of the region, V_o, to region V

$$x^i = x^i(\xi^a, t). \tag{15}$$

If this mapping is a diffeomorphism, then ξ^a are Lagrangian coordinates. In this case, if a point, ξ^a, lies on the boundary, ∂V_o, of the region, V_o, its image is on the boundary, ∂V, of the region, V, for all instants, t. Velocity is defined as the velocity of the particle ξ^a: $v^i = \partial x^i(\xi^a, t)/\partial t$. This is a classical kinematical scheme of continuum mechanics (see, for example, [25–27]). As one sees from Fig. 5, this is not the case for boundary diffusion creep and we have to change the kinematical scheme. We introduce, as a "primary" kinematical object, the region V which is changed in time. In this region two velocity fields, material velocity v^i and vacancy velocity u^i are defined. If mapping equation (15) were a diffeomorphism and $v^i = \partial x^i(\xi^a, t)/\partial t$, then the normal velocity of the boundary surface ∂V is equal to $v_i n_i$. In the case of boundary diffusion these velocities are different. We denote the difference by u:

$$v_{\text{boundary}} = v^i n_i + u. \tag{16}$$

Velocity, u, is caused by the material flow over the boundary. It appears as an additional

independent kinematical characteristic. However, a "more fundamental" characteristic might be introduced as primary characteristics of boundary diffusion: boundary mass flux J^α. Boundary mass flux is defined in the following way. The mass of the material is conserved in the boundary flow, therefore, a law of conservation of mass should exist. Denote by J^α the vector of mass flow on the surface. Greek indices run through values 1 and 2, and correspond to projections on the boundary surface. If γ is a curve on the boundary and v_α is the unit normal vector to γ at a point P, then the scalar $J^\alpha v_\alpha \Delta s$ means the mass flow through the arc of γ of the length Δs at the point P. Let ρ be the mass density of material. Then the law of conservation of mass has the form

$$\rho u = \nabla_\alpha J^\alpha \tag{17}$$

where ∇_α is the covariant derivative on the surface ∂V.

Mass density obeys also the law of conservation of mass inside the region V

$$\frac{\partial \rho}{\partial t} + \frac{\partial \rho v^i}{\partial x^i} = 0. \tag{18}$$

Equations (16)–(18) provide the conservation of mass in volume V

$$\frac{\partial}{\partial t} \int_{V(t)} \rho \mathrm{d}^3 x = \int_V \frac{\partial \rho}{\partial t} \mathrm{d}^3 x + \int_{\partial V} \rho v_{\text{boundary}} \mathrm{d}^2 x = - \int_V \frac{\partial \rho v^i}{\partial x^i} \mathrm{d}^3 x + \int_{\partial V} \rho v_{\text{boundary}} \mathrm{d}^2 x$$

$$= \int_{\partial V} \rho (v_{\text{boundary}} - v^i n_i) \mathrm{d}^2 x = \int_{\partial V} \rho u \mathrm{d}^2 x = \int_{\partial V} \nabla_\alpha J^\alpha \mathrm{d}^2 x = 0.$$

It is natural to consider J^α as the primary characteristics of boundary diffusion, then velocity u is determined by equation (17).

Now we come to the point where we have to introduce displacements. It is natural to define a field of elastic displacements $w_i^{(e)}(t,x)$ which has the domain $V(t)$. Vector $w_i^{(e)}(t,x)$ means the displacement of a crystal from the imaginary unloaded state to the actual state $V(t)$. If there are no plastic strains, the displacement $w_i^{(e)}(t,x)$ relates to velocity by the formula

$$\frac{\partial w_i^{(e)}}{\partial t} + v_k^{(e)} \frac{\partial w_i^{(e)}}{\partial x_k} = v_i^{(e)}. \tag{19}$$

Equation (19) can be rewritten as

$$\left(\delta_i^k - \frac{\partial w_i^{(e)}}{\partial x_k} \right) v_k^{(e)} = \frac{\partial w_i^{(e)}}{\partial t}. \tag{20}$$

The latter relation can be considered as a system of linear equations with respect to velocity $v_k^{(e)}$, if the displacement field is known. We keep formulas equations (19) and (20) as the definition of the vector of elastic displacements if velocity $v_k^{(e)}$ is considered as a primary quantity. Remember that, by our convention, plastic (and, hence, elastic) deformations are consistent for diffusional creep and a vector of elastic displacements exists.

4. THERMODYNAMICS OF DIFFUSIONAL CREEP

We derive the basic equations of diffusional creep following the usual thermodynamical approach: we assume an expression for free energy of the material and construct the equations in a way to warrant the negativity of the time derivatives of free energy.

The free energy F of a polycrystal has, by our assumption, an energy density per unit volume F:

$$\mathfrak{F} = \int_{V(t)} F \mathrm{d}^3 x. \tag{21}$$

We accept that energy density F is a function of the gradient of elastic displacement $w_{i,j}^{(e)}(\equiv \partial w_i^{(e)}/\partial x^i)$, vacancy concentration c and temperature T:

$$F = F(w_{i,j}^{(e)}, c, T). \tag{22}$$

Temperature T is maintained constant.

Note that the assumption equation (22) taken together with the definition of elastic displacements equation (19) extracts a special class of models. For example, if elastic displacement is defined, instead of equation (19), by the formula

$$\frac{\partial w_i^{(e)}}{\partial t} + v_k \frac{\partial w_i^{(e)}}{\partial x_k} = v_i^{(e)}, \tag{23}$$

which may have some virtue, we would arrive at a class of models which differs from the one under consideration in the nonlinear case.

Let us find the time derivative of free energy. We assume first that region $V(t)$ is occupied by a crystal and all fields are smooth inside V. We have

$$\frac{d\tilde{\mathfrak{F}}}{dt} = \int_V \left(\frac{\partial F}{\partial w_{i,j}^{(e)}} \frac{\partial}{\partial x^j} w_{i,t}^{(e)} + \frac{\partial F}{\partial c} \frac{\partial c}{\partial t} \right) d^3x + \int_{\partial V} (v^i n_i + u) d^2x. \tag{24}$$

After substituting in equation (24) the expression for $(\partial c/\partial t)$ from equation (13) and integration by parts we obtain

$$\frac{d\tilde{\mathfrak{F}}}{dt} = \int_V \left[-\left(\frac{\partial}{\partial x_k} \frac{\partial F}{\partial w_{i,k}^{(e)}} \right)(\delta_{im} - w_{i,k}^{(e)})v^{(e)m} + (cv^{(e)i} + J^i) \frac{\partial}{\partial x^i} \frac{\partial F}{\partial c} \right] d^3x$$

$$+ \int_{\partial V} \left[\frac{\partial F}{\partial w_{i,j}^{(e)}} n_j (\delta_{ik} - w_{i,k}^{(e)})v^{(e)k} - \frac{\partial F}{\partial c}(cv^{(e)i} + J^i)n_i + F(v^i n_i + u) \right] d^2x. \tag{25}$$

Here we expressed also $\dfrac{\partial w_i^{(e)}}{\partial t}$ in terms of elastic velocity from equation (20).

For further transformations we need an identity [27]

$$\left(\frac{\partial}{\partial x_k} \frac{\partial F}{\partial w_{i,k}^{(e)}} \right)(\delta_{im} - w_{i,m}^{(e)}) = \frac{\partial}{\partial x_k} \left(\frac{\partial F}{\partial w_{i,m}^{(e)}}(\delta_{im} - w_{i,m}^{(e)}) + F\delta_m^k \right) - \frac{\partial F}{\partial c} \frac{\partial c}{\partial x^m}. \tag{26}$$

This identity can be checked by direct inspection. Using equations (26) and (12) we can rewrite equation (25) in the form

$$\frac{d\tilde{\mathfrak{F}}}{dt} = \int_V \left(-\frac{\partial \sigma^{km}}{\partial x^k} v_m^{(e)} + J^i \frac{\partial}{\partial x^i} \frac{\partial F}{\partial c} \right) d^3x + \int_{\partial V} \left(\sigma^{ij} n_j v_i^{(e)} - \left(\frac{\partial F}{\partial c} + \frac{F}{1-c} \right) J^i n_i + Fu \right) d^2x. \tag{27}$$

Here we introduced a notation

$$\sigma_i^j = \frac{\partial F}{\partial w_{m,j}^{(e)}}(\delta_{mi} - w_{m,i}^{(e)}) + \left(F - c\frac{\partial F}{\partial c} \right)\delta_i^j. \tag{28}$$

It is seen from this expression that σ_i^j have the sense of components of a stress tensor.

Assume that J^i do not depend on $v_m^{(e)}$. Since σ_i^j do not depend on $v_m^{(e)}$ as well and $v_m^{(e)}$ can be chosen arbitrarily, equation (27) can comply with negativity of dF/dt if, and only if, the equilibrium equations hold

$$\frac{\partial \sigma_i^j}{\partial x^j} = 0. \tag{29}$$

The simplest expression for the vacancy flux which does not contradict the negativity of dF/dt is

$$J^i = - D^{ij} \frac{\partial}{\partial x^j} \frac{\partial F}{\partial c} \tag{30}$$

where D^{ij} is a positive tensor.

Consider now the boundary terms. Let V be a polycrystal. Denote by Σ the grain boundary surface. Then the surface terms in dF/dt take the form

$$\int_{\Sigma} \left(\left[\sigma^{ij} v_i^{(e)} - \frac{\partial F}{\partial c} + \frac{F}{1-c} J^j \right] n_j + [Fu] \right) d^2x \tag{31}$$

where for any quantity A the symbol $[A]$ means the difference of A at two sides of the surface Σ.

Let us present the surface force $\sigma^{ij} n_j$ as a sum of normal force $\sigma_{nn} n^i (\sigma_{nn} \equiv \sigma^{ij} n_i n_j)$ and tangent traction. Similarly, $v_i^{(e)}$ is the sum of the normal velocity $v_n^{(e)} n_i (v_n^{(e)} \equiv v_i^{(e)} n^i)$ and the tangent velocity. Then

$$\sigma^{ij} v_i^{(e)} n_j = \sigma^{\alpha j} v_\alpha^{(e)} n_j + \sigma_{nn} v_n^{(e)}.$$

Greek indices α, β, γ run through values 1 and 2, and correspond to projection on the tangent plane to Σ. Using also equation (12) we rewrite equation (31) in the form

$$\int_{\Sigma} ([\sigma^{\alpha j} v_\alpha^{(e)}] n_j + [\sigma_{nn}(v_n + u)] + \left[\left(\frac{\sigma_{nn} - F}{1-c} - \frac{\partial F}{\partial c} \right) J^i \right] n_j - [(\sigma_{nn} - F)u] d^2x). \tag{32}$$

It is natural to require continuity of the total normal velocity of the adjacent grains

$$[v_n + u] = 0. \tag{33}$$

Since σ_{nn} (as well as other "generalized forces" in equation (32)) does not depend on velocity, it is necessary that σ_{nn} be continuous:

$$[\sigma_{nn}] = 0. \tag{34}$$

The normal vacancy flux $J^i n_i$ can be arbitrary and vacancies on two sides of the grain boundary seem to be produced at independent rates. Therefore, it is natural to accept that the corresponding coefficient at $J^i n_i$ in equation (32) are zeros: at both sides of the boundary surface

$$\frac{\sigma_{nn} - F}{1-c} - \frac{\partial F}{\partial c} = 0. \tag{35}$$

In accordance with equation (17), the last term in equation (32) can be written as

$$\int_{\Sigma} [(\sigma_{nn} - F)u] d^2x = \int_{\Sigma} \left[\frac{\sigma_{nn} - F}{\rho} \nabla_\alpha J^\alpha \right] d^2x = - \int_{\Sigma} \left[J^\alpha \nabla_\alpha \frac{\sigma_{nn} - F}{\rho} \right] d^2x. \tag{36}$$

Here we integrated by part and dropped the term on the polycrystal boundary. Finally,

$$\frac{dF}{dt} = \int_V J^i \frac{\partial}{\partial x^i} \frac{\partial F}{\partial c} d^3x + \int_{\partial V} \left([\sigma^{\alpha j} v_\alpha^{(e)}] n_j - \left[J^\alpha \nabla_\alpha \frac{\sigma_{nn} - F}{\rho} \right] \right) d^2x. \qquad (37)$$

There are different models which obey the negativity of equation (37). The most plausible version is based on the assumptions that $\sigma^{\alpha j} n_j$ are continuous and surface fluxes of material J^α are independent on both sides of Σ. Then, neglecting reciprocal effects, one can put

$$\sigma^{\alpha j} n_j = -\mu^{\alpha\beta} [v_\beta^{(e)}] \text{ on } \Sigma \qquad (38)$$

$$J^\alpha = d^{\alpha\beta} \nabla_\beta \left(\frac{\sigma_{nn} - F}{\rho} \right) \text{ on each side of } \Sigma. \qquad (39)$$

Note that, in contrast to σ_{nn}, the energy density is not continuous on Σ, therefore, material fluxes J^α are different on the two sides of Σ. However, this is a nonlinear effect. The equations derived in this section close the system of equations of diffusional creep.

5. LINEARIZED THEORY

In the linear case the system of equations is simplified greatly. First, in this case one can neglect the changes of region V in the process of deformation. Second, kinematical relations take a simple form

$$v_i^{(e)} = \frac{\partial w_i^{(e)}}{\partial t} = v_i + cu_i \qquad (40)$$

$$v_i = v_i^{(e)} - J_i \qquad (41)$$

$$\frac{\partial c}{\partial t} + \frac{\partial J_i}{\partial x_i} = 0 \qquad (42)$$

$$\rho u = \nabla_\alpha J^\alpha. \qquad (43)$$

Third, energy density is a quadratic function of elastic strains

$$\varepsilon_{ij}^{(e)} = 1/2 \left(\frac{\partial w_i^{(e)}}{\partial x^j} + \frac{\partial w_j^{(e)}}{\partial x^i} \right) \qquad (44)$$

and the deviation $s = c - c_o$ of vacancy concentration from its equilibrium value c_o (for brevity from now on the function s will be referred to as vacancy concentration)

$$F = \frac{1}{2} A^{ijk\ell} \varepsilon_{ij}^{(e)} \varepsilon_{k\ell}^{(e)} + \frac{1}{2} A s^2 + \text{function of } T. \qquad (45)$$

Here $A^{ijk\ell}$ are Young moduli, while A is an additional material constant. From some statistical reasoning [5]

$$A = \frac{\rho_0 T}{m c_0} \qquad (46)$$

where m is the mass of one atom, ρ_o is the mass density of an ideal lattice. In equation (45) we neglect an interaction term $A^{ij} \varepsilon_{ij}^{(e)} (c - c_0)$.

In accordance with equation (28), the stress tensor σ^{ij} in the linear theory has the form

$$\sigma^{ij} = A^{ijk\ell}\varepsilon^{(e)}_{k\ell}.$$ (47)

It obeys the equilibrium equations

$$\frac{\partial \sigma^{ij}}{\partial x^j} = 0.$$ (48)

Vacancy flux J^i is given by equation (30)

$$J^i = -AD^{ij}\frac{\partial s}{\partial x^j}.$$ (49)

Therefore, equation (42) transforms to the usual diffusion equation

$$\frac{\partial s}{\partial t} = \frac{\partial}{\partial x^i}\left(AD^{ij}\frac{\partial s}{\partial x^j}\right).$$ (50)

We assume that diffusion constants obey the positive definiteness condition

$$D^{ij}\xi_i\xi_j \geq D\,\xi_i\xi_i \text{ for } \forall \xi_i\xi_i > 0.$$ (51)

On the grain boundary we have from equations (33)–(35), (38) and (39)

$$[v_n] = 0$$ (52)

$$[\sigma_{nn}] = 0$$ (53)

$$\sigma_{nn} = As \text{ at each side of grain boundary}$$ (54)

$$\sigma^{\alpha j}n_j = -\mu^{\alpha\beta}\left[\frac{\partial w^{(e)}_\beta}{\partial t}\right]$$ (55)

$$J^\alpha = \frac{d^{\alpha\beta}}{\rho}\nabla_\beta\sigma_{nn} \text{ at each side of the grain boundary.}$$ (56)

It follows from equations (43) and (56) that the law of growth of grain boundaries due to boundary diffusion

$$\rho u = \nabla_\beta \frac{d^{\alpha\beta}}{\rho}\nabla_\alpha\sigma_{nn}.$$ (57)

Equations (40)–(57) form a closed system of equations of diffusional creep.

6. HOMOGENIZATION PROBLEM

From now on we shall consider a special case of the linearized theory, formulated in Section 5, when there is no boundary diffusion and, hence, the only irreversible deformation is due to the bulk vacancy diffusion. Formally this means that coefficients $d^{\alpha\beta}$ in equation (39) are supposed to be zero, which eliminates equations (56), (43) and (57) from the system equations (40)–(57).

Further we assume that constants $\mu^{\alpha\beta}$ in boundary conditions equation (55) are zero, which neglects the tangent stresses at the grain boundary:

$$\sigma^{\alpha j}n_j = 0 \text{ at each side of grain boundary.}$$ (58)

This is equivalent to an additional assumption that the process of shear stress relaxation at the grain boundaries is much faster than the bulk diffusion process and is completed immediately

after the load is applied, so that the adjacent grains can slide without resistance along their common boundary.

In the absence of the boundary diffusion the deformation of the region V is described by the displacement field w_i (x^i,t), defined in V and related to the velocity v_i by the formula

$$v_i(\mathbf{x},t) = \dot{w}_i(\mathbf{x},t)\mathbf{x} \in V. \tag{59}$$

We introduce also the plastic displacements, which are determined by the flux J_i by means of the relation

$$\dot{w}_i^{(p)}(\mathbf{x},t) = -J_i(\mathbf{x},t)\mathbf{x} \in V. \tag{60}$$

Then the displacements w_i are the sum of the elastic and plastic displacements

$$w_i = w_i^{(e)} + w_i^{(p)}. \tag{61}$$

Similarly for the strains:

$$\varepsilon_{ij} = 1/2\left(\frac{\partial w_i}{\partial x^j} + \frac{\partial w_j}{\partial x^i}\right), \varepsilon_{ij}^{(p)} = 1/2\left(\frac{\partial w_i^{(p)}}{\partial x^j} + \frac{\partial w_j^{(p)}}{\partial x^i}\right)\varepsilon_{ij} = \varepsilon_{ij}^{(e)} + \varepsilon_{ij}^{(p)}. \tag{62}$$

Instead of equation (52), the continuity condition of normal displacement will be employed:

$$[w_n] = 0. \tag{63}$$

Condition equation (52) follows from equation (63), but not vice versa. The difference is that equation (63) excludes the possibility that the normal displacements are discontinuous at the moment $t = 0$ when the load is applied.

It is also necessary to complement the equations above with initial conditions for vacancy concentration and plastic displacements:

$$s(\mathbf{x},t) = 0, \mathbf{x} \in V, t = 0 \tag{64}$$

$$\mathbf{w}^{(p)}(\mathbf{x},t) = 0, \mathbf{x} \in V, t = 0. \tag{65}$$

The closed system of equations in the case considered in the absence of boundary diffusion and with zero boundary shear stresses, consists of the equations (44), (47)–(50), (53), (54), (58) and (60)–(65).

Consider a polycrystalline body containing a huge number of grains. We are going to derive a theory for predicting the mechanical behavior of the body. The experience gained in the averaging of random structures shows that most results for bodies with random and periodic structures are qualitatively similar. (See, for example, [27].) Therefore, we consider a body with a periodic microstructure (Fig. 6) loaded with some constant or variable traction. The problem is to find microfields of elastic and plastic deformations and macroscopic constitutive equations.

For simplicity and consistency with the performed numerical modeling, only the 2-D plane strain case of regular hexagonal periodical microstructure (Fig. 6(b)) will be considered. The reason is that with boundary condition equation (58) not all microstructures can withstand the

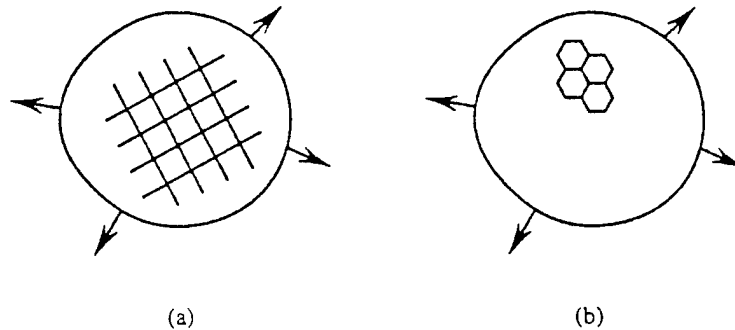(a)   (b)

Fig. 6. Microstructures.

instantaneous application of the external traction. For example, the rectangular microstructure (Fig. 6(a)) cannot be loaded by shear stresses, applied parallel to the grain boundaries. In other words, any macrodeformation of the structure should be the result of the application of macrostresses. Here we decided to use one structure which possesses the necessary properties rather than to formulate general restrictions on the grain geometry, which can be solved in 2-D, as well as in the 3-D case. An accurate formulation of that property will be done at the end of this section after the formulation of the homogenization problem.

We consider the asymptotical statement of the homogenization problem when the period of the microstructure L tends to zero and averaged equations are the corresponding limit equations (see, for example, [27]). Before presenting the results, some description of the periodic structure is to be done.

We assume that the grains coincide with the cells of the periodic structure. Let ω^+ be an arbitrary cell and ϵ be half the distance between the opposite hexagon edges, which will be taken for the characteristic size of the grain. The boundary $\partial\omega^+$ of the cell ω^+ is comprised of three pairs of lines S_1, S'_1, S_2, S'_2, S_3, S'_3 such that for every line S_α, there exists a translation $l_\alpha \in G$, mapping S_α onto S'_α. This notation is explained in Fig. 7.

The periodical regular hexagonal grain structure M is obtained by translation of that cell by all elements of translation symmetry group, generated by vectors l^1 and l^2:

$$G = \{ l^{mk} | l^{mk} = ml^1 + kl^2, m,k = 0, \pm 1, \pm 2,... \}. \tag{66}$$

For $l \in G$ we denote by $\omega(l)$ the image of the cell ω^+ under the translation l. Different cells $\omega(l)$ may have in common the boundary points only, and the union of the cells covers the whole plane. Obviously, the translation $-l_\alpha$ maps S'_α onto S_α. Thus, the periodic structure induces the certain mapping of the cell boundary $\partial\omega^+ \leftrightarrow \partial\omega^+$, which will be used for the formulation of the boundary conditions. For every point $x \in \partial\omega^+$ we denote by $l(x)$ the corresponding translation vector. The points x and $x' = x + l(x)$ will be referred to as the corresponding points. Note that $l(x)$ is constant within each line S_α, S'_α.

The unit normal n to the cell boundary is assumed to be directed outward from the cell, therefore at the corresponding points x and x' we have

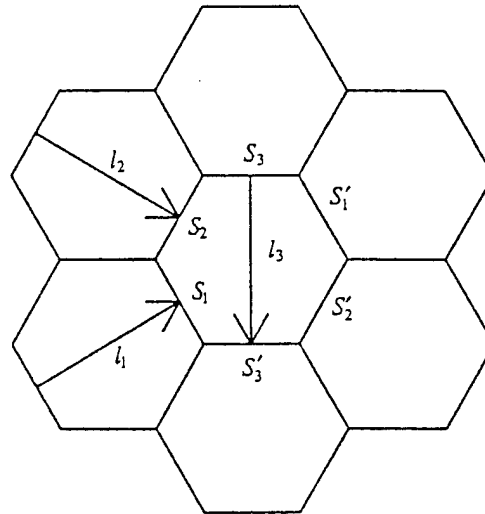$$n(x) + n(x') = 0, l(x) = -2\epsilon n(x). \tag{67}$$

Fig. 7. Hexagonal structure. The translation vectors mapping the corresponding parts of the cell boundaries, shown by arrows.

Let $f(x)$ be an arbitrary function, which is continuous within each grain, but may be discontinuous at the grain boundaries. Function $f(x)$ is called periodic if

$$f(\mathbf{x} + \mathbf{l}) = f(\mathbf{x}) \text{ for any } \mathbf{x} \in \dot{\omega}^+ \text{ and for any } \mathbf{l} \in G. \tag{68}$$

Here $\dot{\omega}^+$ is the interior of a cell ω^+.

If function $f(x)$ is known within any cell, it can be extended to the whole space by the formula equation (68). From now on the term "periodic function" will be used in the sense of the above definition, unless otherwise is explicitly indicated.

Denote by ω^- the cell, such that $S_i = \omega^+ \cap \omega^-$. It follows from equation (68) and the definition of the corresponding points that

$$[f] \equiv f^+ - f^- \equiv f(\mathbf{x}^+, t) - f(\mathbf{x}^-, t) = f(\mathbf{x}, t) - f(\mathbf{x}', t) \text{ for } \mathbf{x} \in S_i. \tag{69}$$

Thus, for periodic functions the discontinuity conditions can be expressed in terms of function values within one cell, which allows us to formulate the cell problem. Instead of applying the formal procedure of homogenization (see, for example, [27]) we use here an "intuitive" approach, which is easier to implement. Of course, it gives the some results as the general approach.

Averaged constitutive equations by their physical sense relate a macroscopically homogeneous deformation of a "large" (compared with grain size ϵ) specimen to averaged stresses. Instead of "large" specimen we consider the whole plane loaded by stress $\bar{\sigma}^{ij}(t)$ at infinity. One has to find microstresses in periodic structure and macrostrains $\bar{\epsilon}_{ij}(t)$. One may prescribe at infinity macrostrains $\bar{\epsilon}_{ij}(t)$ as functions of time; then macrostresses $\bar{\sigma}^{ij}(t)$ and microdeformations in periodic structure should be found. For definiteness, we consider the case of given macrostresses.

If there were no grain boundaries, the homogeneous plane deformation history would be generated by the displacement field

$$\bar{w}_i(\mathbf{x}, t) = \bar{\epsilon}_{ij}(t)x^j. \tag{70}$$

The grain structure results in additional periodic displacements $W_i(x,t)$, so that total displacements are given by the sum

$$w_i(\mathbf{x}, t) = \bar{\epsilon}_{ij}(t)x^j + W_i(\mathbf{x}, t). \tag{71}$$

Since the first term in equation (71) is obviously continuous over space coordinates, it follows from equations (63) and (69) that the field $W_i(x,t)$ satisfies the condition

$$W_n(\mathbf{x}, t) + W_n(\mathbf{x}', t) = 0 \text{ for } \mathbf{x} \in \partial\omega^+ \Rightarrow \dot{W}_n(\mathbf{x}, t) + \dot{W}_n(\mathbf{x}', t) = 0. \tag{72}$$

The vacancy concentration s is a periodic function. With equation (69) taken into account, equations (53) and (54) link the normal stress values and vacancy concentration at the corresponding points of the boundary:

$$\sigma_{nn}(\mathbf{x}, t) = \sigma_{nn}(\mathbf{x}', t) \text{ for } \mathbf{x} \in \partial\omega^+ \tag{73}$$

$$s(\mathbf{x}, t) = s(\mathbf{x}', t) \text{ for } \mathbf{x} \in \partial\omega^+. \tag{74}$$

The macrostresses, or averaged stresses, are defined by formula

$$\bar{\sigma}^{ij}(t) = \frac{1}{|\omega^+|} \int_{\omega^+} \sigma^{ij}(\mathbf{x}, t) \mathrm{d}^2 x. \tag{75}$$

The full set of equations is as follows: equations (44), (47)–(50), (53), (54), (58), (60)–(62), (71)–(75). For further references that system of equations is referred to system P. Initial conditions for the system P are equation (64) and (65). It is implied that all equations included in system P and initial conditions should be satisfied in the cell ω^+.

Now we are going to show, that the chosen microstructure cannot be subjected to instantaneous macrodeformation, if stresses are zero. With zero stresses and zero vacancy

concentration s, the elastic strain coincides with the total strain and is equal to zero, hence the displacement field w_i within cell ω^+ is rigid body motion:

$$w_i = \bar{\varepsilon}_{ij}x^j + W_i = \lambda e_{ij}x^j + a_i, \mathbf{x} \in \omega^+, \lambda, a_i = \text{const}, e_{11} = e_{22} = 0, e_{12} = -e_{21} = 1. \quad (76)$$

Relation equation (76) allows us to express the displacement W_i in terms of macrostrains and rigid body motion:

$$W_i = -\bar{\varepsilon}_{ij}x^j + \lambda e_{ij}x^j + a_i. \quad (77)$$

Inserting equation (77) into the continuity condition equation (72) yields

$$0 = W_n(\mathbf{x}) + W_n(\mathbf{x}') = (-\bar{\varepsilon}_{ij}x^j + \lambda e_{ij}x^j + a_i)n^i(\mathbf{x}) + (-\bar{\varepsilon}_{ij}x'^j + \lambda e_{ij}x'^j + a_i)n^i(\mathbf{x}')$$

$$= (-\bar{\varepsilon}_{ij}x^j + \lambda e_{ij}x^j + a_i)n^i(\mathbf{x}) - (-\bar{\varepsilon}_{ij}x'^j + \lambda e_{ij}x'^j + a_i)n^i(\mathbf{x})$$

$$= (-\bar{\varepsilon}_{ij} + \lambda e_{ij})(x^j - x'^j)n^i(\mathbf{x}) = -(-\bar{\varepsilon}_{ij} + \lambda e_{ij})l^j(\mathbf{x})n^i(\mathbf{x})$$

$$= \bar{\varepsilon}_{ij}l^j(\mathbf{x})n^i(\mathbf{x}) - e_{ij}l^j(\mathbf{x})n^i(\mathbf{x}) = \bar{\varepsilon}_{ij}l^j(\mathbf{x})n^i(\mathbf{x}) - \lambda n(\mathbf{x}) \otimes 1(\mathbf{x}) = \bar{\varepsilon}_{ij}l^j(\mathbf{x})n^i(\mathbf{x}), \mathbf{x} \in \partial\omega^+. \quad (78)$$

The vector product $\mathbf{n} \otimes \mathbf{l}$ in equation (78) vanishes because these vectors are collinear at each boundary point (see equation (67)). Since normal is constant along each edge of the hexagon, equation (78) provides three homogeneous linear equations with respect to three macrostrain components $\bar{\varepsilon}_{ij}$. A direct check shows that its determinant is not zero, which implies that all macrostrains have to be zero.

Let R be the set of periodic displacement fields V_i, defined at the cell ω^+ by formula for rigid body motion

$$V_i = \lambda e_{ij}x^j + a_i, \lambda, a_i = \text{const} \quad (79)$$

and extended to the whole plane by the periodicity condition equation (68). Under the displacement V_i each cell shifts by the constant vector a_i and rotates around its center by the angle λ. It follows from equations (76)–(78) that any such a field satisfies the continuity condition equation (72) and does not produce macrodeformation. Figure 9 illustrates the movement of the cells. The holes that one can see at the corners of the hexagons, are a second-order effect and are ignored by the small deflection theory used here.

THEOREM 1. Consider the solution of the system P with initial conditions equations (64) and (65). Macrostresses $\bar{\sigma}^{ij}(t)$ are given functions of time. The total and elastic displacements of this solution are defined with the accuracy of the arbitrary displacement field from set R. All the other components of the solution, such as vacancy concentration, plastic displacements and strains, elastic strains, macrostrains and stresses are uniquely defined.

PROOF. Introduce the notations

$$I(t) = \frac{1}{2}\int_{\omega^*} As^2 d^2x + \frac{1}{2}[\varepsilon^{(e)}, \varepsilon^{(e)}], [\varepsilon^{(e)}, \varepsilon^{(e)}]$$

$$\equiv \int_{\omega^*} A^{ijkt}\varepsilon_{ij}^{(e)}\varepsilon_{kt}^{(e)} d^2x, [\nabla s, \nabla s] \equiv \int_{\omega^-} AD^{ij}\frac{\partial s}{\partial x^i}\frac{\partial s}{\partial x^j}d^2x. \quad (80)$$

Since the system P is linear, it is sufficient to prove, that if macrostresses are zero, then the system P with initial conditions equation (64) and (65) has only zero solution for all components with the exception of displacements, which belong to the set R. At the initial moment $t = 0$ the plastic displacement is zero because of equation (65), the displacements coincide with the elastic displacements and since the macrostresses are zero, the macrostrains are also zero at the moment $t = 0$. Hence

$$I(0) = 0. \quad (81)$$

Using inequality equation (C.6) for $t^* = 0$ from Appendix C, we know that functional $I(t)$ is zero for $t \geq 0$. Hence

$$s(t) = 0, \varepsilon_{ij}^{(e)} = 0, t \geq 0 \Rightarrow \sigma_{ij} = 0, \varepsilon_{ij}^{(p)} = 0. \tag{82}$$

Hence, the displacement of the cell is rigid body motion, given by the formula equation (76). It was proved above, that in order to satisfy the continuity condition equation (72), the macrostrains have to be zero. The uniqueness theorem is proved.

REMARK 1. Let us consider the loading case when the non-zero macrostresses are applied only at some time interval $[0, t^*]$, and were removed afterwards. Then from inequality equation (C.6) we conclude that vacancy concentration s and elastic strains $\varepsilon_{ij}^{(e)}$ exponentially tend to zero, hence the stresses also tend to zero. In other words, after unloading the residual stresses are relaxing to zero exponentially with respect to time.

We conclude this section with the presentation of averaged stresses in terms of values of normal microstresses at the grain boundary (see Appendix B):

$$\bar{\sigma}^{ij} = \frac{\epsilon}{|\omega^+|} \int_{\partial \omega^-} \sigma_{nn} n^i n^j \mathrm{d}x. \tag{83}$$

Relation equation (83) is valid for an arbitrary stress field satisfying equilibrium equation (48) and boundary conditions equations (58) and (73). With equation (54) taken into account, the averaged stresses can be expressed in terms of the values of vacancy concentration at the grain boundary:

$$\bar{\sigma}^{ij} = \frac{A\epsilon}{|\omega^+|} \int_{\partial \omega^-} s n^i n^j \mathrm{d}x. \tag{84}$$

It can be checked (see Appendix B) that for arbitrary constant C, the following identity holds:

$$C\delta^{ij} = \frac{\epsilon}{|\omega^+|} \int_{\partial \omega^-} C n^i n^j \mathrm{d}x. \tag{85}$$

It follows from equations (84) and (85), that if vacancy concentration is constant over the grain boundary then the corresponding macrostress tensor is spherical and the plane is under hydrostatic compression or tension.

7. BOLTZMAN SUPERPOSITION PRINCIPLE AND MACROEQUATIONS.

As has already been stated above, the macromodel should provide the relations between macrostresses and macrostrains $\bar{\sigma}^{ij}(t)$ and $\bar{\varepsilon}_{ij}(t)$. It seems almost obvious, that any parabolic type linear system such as P satisfies the Boltzman superposition principle and, hence, the stress–strain relation would involve an integral operator.

Let us first assume that at $t = 0$ the unit tension along axis x^1 is instantaneously applied to the polycrystal and remains unchanged for $t > 0$. Then the only non-zero stress component is $\bar{\sigma}^{11}(t) = 1$. Denote by $\aleph(t)$, the solution of system P with initial conditions equations (64) and (65), corresponding to load case under consideration:

$$\aleph(t) = \{\bar{\varepsilon}_{ij}(t), \sigma^{ij}(\cdot, t), \varepsilon_{ij}(\cdot, t), \varepsilon_{ij}^{(e)}(\cdot, t), \varepsilon_{ij}^{(p)}(\cdot, t), s(\cdot, t), W_i(\cdot, t), w_i(\cdot, t), w_i^{(e)}(\cdot, t) w_i^{(p)}(\cdot, t)\}. \tag{86}$$

Solution $\aleph(t)$ is defined only for $t \geq 0$. Let us formally define it for $t < 0$:

$$\aleph(t) = 0 \text{ for } t < 0. \tag{87}$$

If the same tension $\bar{\sigma}^{11}(t) = 1$ is applied at some time $t_1 > 0$, then the solution is obviously equal to $\aleph(t - t_1)$ for $t \geq 0$. Let us stress that $\aleph(t - t_1) = 0$ for $t < t_1$ because of the definition equation (87).

The next step is to consider the load history, when at discrete moments $t_i = i\Delta$, $i = 1,2,...,$ k tension increments $d\bar{\sigma}^{11}(t_1), d\bar{\sigma}^{11}(t_2),...,d\bar{\sigma}^{11}t_k$ are applied. Then at any particular time t, $t_m < t < t_{m+1}$, the total tension $\bar{\sigma}^{11}(t_i)$ is given by the formula

$$\bar{\sigma}^{11}(t) = \sum_{i=1}^{m} d\bar{\sigma}^{11}(t_i) \tag{88}$$

and the solution is given by the sum

$$\sum_{i=1}^{m} d\bar{\sigma}^{11}(t_i)\aleph(t - t_i). \tag{89}$$

Extension of the formula equation (89) to a continuous loading process provides the following formula for the solution:

$$\int_0^t \dot{\sigma}^{11}(\xi)\aleph(t - \xi)d\xi. \tag{90}$$

Let us denote by $R_{ij,kl}(t)$ the macrostrain $\bar{\varepsilon}_{ij}(t)$ corresponding to the application of the macrostress $\bar{\sigma}^{kl}(t) = 1, t > 0$. The values $R_{ij,kl}(t)$ at $t = 0$ are components of the tensor of elastic compliances of a polycrystal. Because of that it is convenient to decompose $R_{ij,kl}(t)$ into the sum

$$R_{ij,kl}(t) = R_{ij,kl}(0) + K_{ij,kl}(t), \quad K_{ij,kl}(0) = 0. \tag{91}$$

By its mechanical sense the function $K_{ij,kl}(t)$ is the $\bar{\varepsilon}_{ij}$ creep strain component caused by constant load $\bar{\sigma}^{kl}(t) = 1$, while the other macrostress components are equal to zero. Then for an arbitrary loading process the following holds:

$$\bar{\varepsilon}_{ij}(t) = \int_0^t R_{ij,kl}(t - \xi)\dot{\sigma}^{kl}(\xi)d\xi = R_{ij,kl}(0)\bar{\sigma}^{kl}(t) + \int_0^t \frac{\partial K_{ij,kl}(t - \xi)}{\partial t}\bar{\sigma}^{kl}(\xi)d\xi. \tag{92}$$

Equations of the type equation (92) are widely used for creep modeling of polymers and concrete.

So we arrive at the conclusion. In order to find macrostrains, caused by an arbitrary loading process, it is necessary and sufficient to know instantaneous elastic moduli tensor $R_{ij,kl}(0)$ and creep tensor $K_{ij,kl}(t)$, which components are creep strains caused by the corresponding constant macrostresses. Thus, in numerical modeling or experiment one may consider only loading cases when constant load is instantaneously applied to the body and remains unchanged. This is nothing else, but the classical experiment to find the creep property of a material.

Inversion of equation (92) renders

$$\bar{\sigma}^{ij}(t) = \int_0^t Q^{ij,kl}(t - \xi)\dot{\varepsilon}_{kl}(\xi)d\xi = Q^{ij,kl}(0)\bar{\varepsilon}_{kl}(t) + \int_0^t \frac{\partial Z^{ij,kl}(t - \xi)}{\partial t}\bar{\varepsilon}_{kl}(\xi)d\xi \tag{93}$$

$$Q^{ij,kl}(t) = Q^{ij,kl}(0) + Z^{ij,kl}(t), \quad Z^{ij,kl}(0) = 0. \tag{94}$$

Here $Q^{ij,kl}(t)$ is the macrostress component $\sigma_0^{ij}(t)$ caused by the instantaneous application of a macrostrain $\bar{\varepsilon}_{kl}(t) = 1$, while all the other macrostrain components are equal to zero. The tensor $Q^{ij,kl}(0)$ is the elastic moduli tensor of the polycrystal.

It is worth mentioning that creep curves $K_{ij,kr}(t)$ for small values of t have an asymptotic behavior

$$K_{ij,kr}(t) \sim t^{1/2}, \quad \frac{\partial K_{ij,kr}(t)}{\partial t} \sim t^{-1/2} \tag{95}$$

and, hence, the creep rate tends to infinity as $t^{-1/2}$ when t tends to zero:

$$\hat{\varepsilon}_{ij}(t) \sim t^{-1/2}, t \to 0. \tag{96}$$

An important feature of the constitutive equations (92) and (93) is that these relations are not local: there is a memory of the history of the process. This means that local theories of primary creep are not adequate at least in the case of bulk diffusional creep.

8. SECONDARY CREEP

Generally speaking, the macroscopic constitutive equations are given by the integral operators equations (92) and (93). However, for "slow" loading processes and a developed creep it is possible to use as an approximation the creep law

$$\hat{\varepsilon}_{ij} = E_{ijkl} \bar{\sigma}'^{kl}, \bar{\sigma}'^{kl} = \bar{\sigma}^{kl} - \delta^{kl} \bar{\sigma}^{ss}/2 \tag{97}$$

or

$$\bar{\sigma}'^{ij} = e^{ijkl} \hat{\varepsilon}_{kl}. \tag{98}$$

Also the incompressibility condition is imposed:

$$\hat{\varepsilon}_{kk} = 0 \tag{99}$$

which reflects the physically obvious fact that there is no volume change from bulk vacancy diffusion. A tensor e^{ijkl} is the inverse tensor to E_{ijkl}.

The macrocharacteristics of the secondary creep E_{ijkl} are the limits of the creep rates $\dot{K}_{ijkl}(t)$ when $t \to \infty$. The fact that under constant applied macrostresses the creep rates tend to some constants when $t \to \infty$ will be formulated and justified below and constitutes the basis of the approximation equations (98) and (99).

We start from formal description of how to compute the constants involved in the secondary creep law equation (98). It turns out that they may be found from the following variational principle. Let $\hat{\varepsilon}_{ij}$ be an arbitrary constant macroscopic creep rates, satisfying the incompressibility condition equation (99). Denote by $J(s)$ the following functional of function $s(\mathbf{x})$.

$$J(s) = \frac{1}{2} [\nabla s, \nabla s] - \epsilon \int_{\partial \omega^-} \hat{\varepsilon}_{ij} n^i n^j s \, dx. \tag{100}$$

Here the notation equation (80) is used. Consider the minimization problem

$$J(s) \to \min_s. \tag{101}$$

Minimum is sought on the set of all functions s obeying the constraints equation (74). It follows from equations (85) and (99) that the term linear with respect to s in equation (100) is zero for $s = \text{const}$, hence the solution s^* of the problem is determined up to an arbitrary constant. We fix this constant by the condition

$$\int_{\partial \omega^-} s^*(\mathbf{x}) n^k n^k \, dx = 0. \tag{102}$$

The necessary and sufficient condition of the minimum is the following identity, which should hold for every function satisfying the condition equation (74)

$$[\nabla s^*, \nabla s] = \epsilon \int_{\partial\omega^+} \hat{\epsilon}_{ij} n^i n^j s \, dx \text{ for } \forall s : s(\mathbf{x}) = s(\mathbf{x}'), \mathbf{x} \in \partial\omega^+. \tag{103}$$

The differential form of the problem equation (101) is derived from equation (103):

$$\frac{\partial}{\partial x^i} A D^{ij} \frac{\partial s}{\partial x^j} = 0, \mathbf{x} \in \omega^+ \tag{104}$$

$$[J_n](\mathbf{x}) = -2\epsilon\hat{\epsilon}_{ij} n^i(\mathbf{x}) n^j(\mathbf{x}), \mathbf{x} \in \partial\omega^+, [J_n](\mathbf{x}) \equiv J_n(\mathbf{x}) + J_n(\mathbf{x}'), \mathbf{x} \in \partial\omega^+ \, J_n(\mathbf{x})$$

$$\equiv -A D^{ij} \frac{\partial s(\mathbf{x})}{\partial x^j} n_i(\mathbf{x}), \mathbf{x} \in \partial\omega^+. \tag{105}$$

After the solution s^* of the variational problem equations (100), (74), (101) and (102) are found, the deviator of macrostresses is defined by the formula equation (84) which takes the form

$$\bar{\sigma}'^{ij} = \frac{A\epsilon}{|\omega^+|} \int_{\partial\omega^-} s^* n^i n^j dx. \tag{106}$$

Macrostresses $\bar{\sigma}'^{ij}$ are deviatoric because of condition equation (102) since

$$\bar{\sigma}'^{kk} = \frac{A\epsilon}{|\omega^+|} \int_{\partial\omega^-} s^* n^k n^k dx = 0. \tag{107}$$

The solution s^* depends linearly on the parameters $\hat{\epsilon}_{ij}$. Hence, by putting this solution into equation (106) one obtains macrostresses in terms of creep velocities $\hat{\epsilon}_{ij}$, i.e. the relation equation (98). In more detail, consider two solutions, corresponding to two linear independent loading cases:

$$s^{12} = s^{21} \text{ corresponds to } \hat{\epsilon}_{12} = \hat{\epsilon}_{21} = 1/2, \hat{\epsilon}_{11} = 0, \hat{\epsilon}_{22} = 0,$$

$$s^{11} = -s^{22} \text{ corresponds to } \hat{\epsilon}_{12} = \hat{\epsilon}_{21} = 0, \hat{\epsilon}_{11} = -\hat{\epsilon}_{22} = 1/2. \tag{108}$$

Then the solution s^* is the linear combination

$$s^* = \hat{\epsilon}_{ij} s^{ij}. \tag{109}$$

Substitution of equation (109) into equation (106) provides the formulas for the macrocharacteristics e^{ijkl}:

$$e^{ijkl} = \frac{A\epsilon}{|\omega^+|} \int_{\partial\omega^-} (s^{kl}) n^i n^j dx. \tag{110}$$

It is obvious that only two constants among e^{ijkl} are independent.

So far it was shown how to find the deviator of macrostresses if macroscopic constant incompressible creep rates are given. Let us prove that the secondary creep law is reversible. Multiplying equation (106) by $\hat{\epsilon}_{ij}$ we obtain after summation over repeated indices and using equation (103):

$$\bar{\sigma}'^{ij}\hat{\epsilon}_{ij} = \frac{A\epsilon}{|\omega^+|} \int_{\partial\omega^-} s^*\hat{\epsilon}_{ij} n^i n^j dx = \frac{A}{|\omega^+|} [\nabla s^*, \nabla s^*]. \tag{111}$$

The left-hand side of the relation equation (111) is zero if and only if all creep rates $\hat{\epsilon}_{ij} = 0$, which means that the matrix of the quadric form $\hat{\epsilon}_{ij} = e^{ijkl}\hat{\epsilon}_{ij}\hat{\epsilon}_{kl}$ is positive definite, hence the law equation (98) may be inverted.

Now we can describe how to find creep rates and vacancy concentration for secondary creep. Let macrostresses $\bar{\sigma}^{0ij}$ be given constants. First the deviator of tensor $\bar{\sigma}^{0ij}$ should be calculated

$$\bar{\sigma}^{0\,'ij} = \bar{\sigma}^{0ij} - \delta^{ij}p, p = \bar{\sigma}^{0kk}/2. \tag{112}$$

Then the creep rates $\dot{\varepsilon}_{0ij}$ are found satisfying the creep law equations (97)–(99). The vacancy concentration s^0 is the sum of the constant p and the solution of the variational problem equation (101), corresponding to creep rates $\dot{\varepsilon}_{ij}^0$:

$$s^0(\mathbf{x}) = p + \dot{\varepsilon}_{ij}^0 s^{ij}(\mathbf{x}). \tag{113}$$

The last step to define the microcharacteristics of the secondary creep is to determine the elastic strains and stresses within the cell ω^+. The normal stresses at the cell boundary are determined from equation (51), since the vacancy concentration s^0 is found:

$$\sigma_{nn}(\mathbf{x}) = As^0(\mathbf{x}), \mathbf{x} \in \partial\omega^+. \tag{114}$$

Formulas equations (58) and (114) define surface tractions at the grain boundary. Thus, the elastic displacements, elastic strains and stresses inside the cell may be found from the solution of the elasticity problem equations (44), (47), (48), (58) and (114), if the principal vector and moment produced by surface tractions are zero, which they are as is shown in Appendix B. Denote this solution as $w_i^{0(e)}, \varepsilon_{ij}^{0(e)}, \sigma^{0ij}$. At this point all the characteristics of secondary creep are determined.

THEOREM 2. Under constant applied macrostresses $\bar{\sigma}^{0ij}$ the solution of the system P with initial conditions equations (64) and (65) reveals the following asymptotic behavior:

$$s(\mathbf{x},t) \to s^0(\mathbf{x}), \dot{\varepsilon}_{ij}(t) \to \dot{\varepsilon}_{ij}^0, \varepsilon_{ij}^{(e)}(\mathbf{x},t) \to \varepsilon_{ij}^{0(e)}(\mathbf{x}), \sigma^{ij}(\mathbf{x},t) \to \sigma^{0ij}(\mathbf{x}). \tag{115}$$

PROOF. It is shown in Lemma 2, <appr id = "C", that the difference between two arbitrary solutions of the system P, corresponding to the same loading process $\bar{\sigma}^{ij}(t)$, tends to zero in the following sense:

$$s^1(\mathbf{x},t) - s^2(\mathbf{x},t) \to 0, \dot{\varepsilon}_{ij}^1(t) - \dot{\varepsilon}_{ij}^2(t) \to 0, \varepsilon_{ij}^{1(e)}(\mathbf{x},t) - \varepsilon_{ij}^{2(e)}(\mathbf{x},t) \to 0, \sigma^{1ij}(\mathbf{x},t) - \sigma^{2ij}(\mathbf{x},t) \to 0. \tag{116}$$

Let us stress that solutions need not satisfy initial conditions equations (64) and (65) and need not have the same initial conditions. This means that if some particular solution of the system P is found, then any other solution tends to it, regardless of the initial conditions. Thus, to find the asymptotics of the solution of the problem it is sufficient to find some particular solution of the system P. We shall use upper case index "0" for all quantities related to this solution. This implies that the functions introduced above with the same index are part of this particular solution.

Let us first define macrostrains as a constant strain rate process:

$$\bar{\varepsilon}_{ij}^0(t) = \dot{\varepsilon}_{ij}^0 t. \tag{117}$$

Second, define the plastic displacement. Since the plastic displacement velocity is expressed in terms of the vacancy concentration from equations (60) and (49), the only freedom left is to define the plastic displacements at $t = 0$. We pose

$$w_i^{0(p)}(\mathbf{x},0) = - w_i^{0(e)}(\mathbf{x})\mathbf{x} \in \omega^+. \tag{118}$$

Then

$$w_i^{0(p)}(\mathbf{x},t) = - w_i^{0(e)}(\mathbf{x}) - tJ_i^0(\mathbf{x}), J_i^0 \equiv - AD^{ij}\frac{\partial s^0}{\partial x^j}, \mathbf{x} \in \omega^+ \mathbf{x} \in \omega^+. \tag{119}$$

Third, since the elastic and plastic displacements are defined over the cell, the additional displacement in the equation (71) ought to be as follows:

$$W_i^0(\mathbf{x},t) = - t\dot{\varepsilon}_{ij}^0 x^j - tJ_i^0(\mathbf{x}), \mathbf{x} \in \omega^+. \tag{120}$$

To conclude the construction of the particular solution, it is necessary to check the continuity

condition equation (72). It obviously holds at $t = 0$ and, hence, it is enough to check a second condition in equation (72) for $t > 0$. It follows from equations (105) and (119) that

$$[\dot{W}_n^0] = -\dot{\varepsilon}_{ij}^0 n^i n^j - [\dot{J}_n^0] = 0. \tag{121}$$

The theorem is proved.

REMARK 2. let us normalize the diffusivity tensor:

$$D^{ij} = D\bar{D}^{ij} \tag{122}$$

where D is some characteristic value of tensor D^{ij} and introduce dimensionless coordinates

$$y^i = \frac{x^i}{\epsilon} \tag{123}$$

which maps the cell ω^* onto unit cell Ω. The functional equation (100) is transformed to

$$J(s) = \frac{1}{2} \int_\Omega \bar{D}^{ij} \frac{\partial s}{\partial y^i} \frac{\partial s}{\partial y^j} d^2 y - \frac{\epsilon^2}{AD} \int_{\partial\Omega} \dot{\varepsilon}_{ij} n^i n^j s \, d^y. \tag{124}$$

Then secondary creep macrocharacteristics can be represented as follows:

$$e^{ijkl} = \bar{e}^{ijkl} \frac{\epsilon^2}{D}, E_{ijkl} = \bar{E}_{ijkl} \frac{D}{\epsilon^2} \tag{125}$$

where dimensionless constants $\bar{e}^{ijkl}$ and $\bar{E}_{ijkl}$ depend on the constants $\bar{D}^{ij}$ and the unit cell shape only. An important consequence is that secondary creep rates do not depend on the elastic properties and even on the value of the constant A. Elastic properties influence only stress microfields.

14. NUMERICAL RESULTS FOR SECONDARY CREEP

For definiteness, it was assumed that grains are isotropic, and hence only four physical constants are needed: Young modulus E, Poison ratio v, the constant A in equation (54), diffusivity constant D in equation (122) (with $\bar{D}^{ij} = \delta^{ij}$) and the grain size ϵ.

14.1 Secondary creep rates

In creep, the periodic hexagonal structure behaves isotropically. Thus, the creep law equation (97) contains just one macrocharacteristic—the viscosity μ:

$$\bar{\sigma}'^{ij} = \mu \dot{\varepsilon}^{ij} \tag{126}$$

The dimensional analysis of the cell problem shows that μ depends on the grain size ϵ and the diffusivity coefficient D only

$$\mu = a \frac{\epsilon^2}{D} \tag{127}$$

where a is some constant. Numerical simulations give the following value of the constant a for the hexagonal structure

$$a = 0.26. \tag{128}$$

Formulas equations (127) and (128) inspire an assumption that a similar relation between

macro- and micro-characteristics exists for the random structure as well, where ϵ is the averaged grain size and D is the characteristic diffusion coefficient of monocrystals, while the coefficient a is of the order of unity.

14.2 Microdeformation.

The distribution of creep velocity over the cell in the regime of secondary creep is shown in Fig. 8. The orientation of shear stress applied is given at the right top of Fig. 8. It is seen that there are three pairs of opposite cell sides with different properties. Material departs from one pair of sides and arrives at the other pair of sides. The remaining two sides consist of two pieces: material leaves one piece and arrives at the other one.

15. DIMENSIONAL ANALYSIS AND TRANSITION TIME TO SECONDARY CREEP

Let E be some characteristic value of tensor A^{ijkt}. Similar to equation (122), normalize the tensor A^{ijkt} using the value E:

$$\tilde{A}^{ijkt} \equiv \frac{A^{ijkt}}{E}. \tag{129}$$

Let us assume that dimensionless parameters $\tilde{A}^{ijkt}$ and $\tilde{D}^{ijkt}$ remain unchanged in our analysis. Then a solution of the system P depends on four constants: E, D, A (see equation (54)) and ϵ-characteristic grain size.
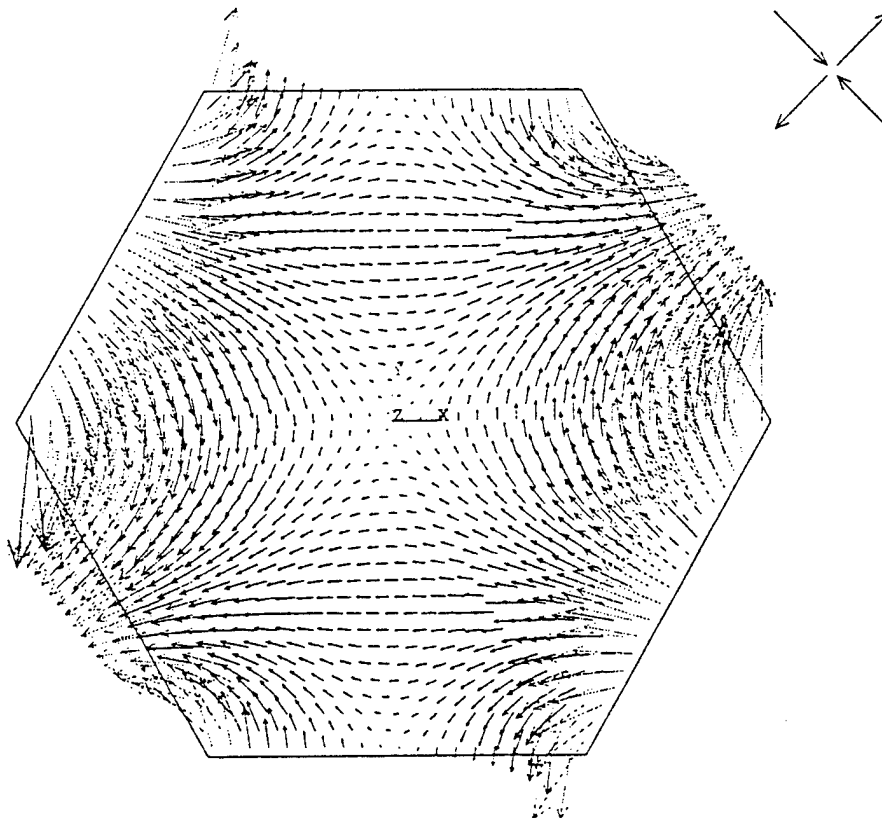

Fig. 8. Creep velocity distribution during the secondary creep.

Our intent is to transform the system P to dimensionless form. In addition to dimensionless space coordinates y^i (see equation (122)) introduce intrinsic time τ and normalized displacements and flux:

$$\tau = t\,\frac{AD}{\epsilon^2}\,;\,\dot{f} \equiv \frac{\partial f}{\partial \tau}\,,\tilde{w} = \frac{1}{\epsilon}\,\mathbf{W},\,\tilde{w} = \frac{1}{\epsilon}\,\mathbf{W},$$

$$\tilde{w}^{(e)} = \frac{1}{\epsilon}\,\mathbf{w}^{(e)},\,\tilde{w}^{(p)} = \frac{1}{\epsilon}\,\mathbf{W}^{(p)},\,\tilde{J}_i = \frac{1}{\epsilon}\,\frac{\epsilon^2}{AD}\,J_i,\,\tilde{\sigma}^{ij} = \frac{1}{A}\,\sigma^{ij}. \tag{130}$$

Vacancy concentration and strains need not to be normalized. Then system P is reduced to the system $\tilde{P}$:

$$\varepsilon_{ij}^{(e)} = 1/2\left(\frac{\partial \tilde{w}_i^{(e)}}{\partial y^j} + \frac{\partial \tilde{w}_j^{(e)}}{\partial y^i}\right) \tag{131}$$

$$\tilde{\sigma}^{ij} = e\tilde{A}^{ijke}\varepsilon_{ke}^{(e)} \tag{132}$$

$$\frac{\partial \tilde{\sigma}^{ij}}{\partial y^j} = 0 \tag{133}$$

$$\tilde{J}^i = -\tilde{D}^{ij}\frac{\partial s}{\partial y^j} \tag{134}$$

$$\frac{\partial s}{\partial \tau} = \frac{\partial}{\partial y^i}\left(\tilde{D}^{ij}\frac{\partial s}{\partial y^j}\right) \tag{135}$$

$$\tilde{\sigma}_{nn} = s,\mathbf{y} \in \partial\Omega \tag{136}$$

$$\tilde{\sigma}^{\alpha j}n_j = 0,\mathbf{y} \in \partial\Omega \tag{137}$$

$$\tilde{w}_i'^{(p)}(\mathbf{y},\tau) = -\tilde{J}_i(\mathbf{y},\tau)\,\mathbf{y} \in \Omega \tag{138}$$

$$\tilde{w}_i = \tilde{w}_i^{(e)} + \tilde{w}_i^{(p)} \tag{139}$$

$$\varepsilon_{ij} = 1/2\left(\frac{\partial \tilde{w}_i}{\partial y^j} + \frac{\partial \tilde{w}_j}{\partial y^i}\right),\varepsilon_{ij}^{(p)} = 1/2\left(\frac{\partial \tilde{w}_i^{(p)}}{\partial y^j} + \frac{\partial \tilde{w}_j^{(p)}}{\partial y^i}\right)\varepsilon_{ij} = \varepsilon_{ij}^{(e)} + \varepsilon_{ij}^{(p)} \tag{140}$$

$$\tilde{w}_i(\mathbf{y},\tau) = \bar{\varepsilon}_{ij}(\tau)y^j + \tilde{W}_i(\mathbf{y},\tau) \tag{141}$$

$$\tilde{W}_n(\mathbf{y},\tau) + \tilde{W}_n(\mathbf{y}',\tau) = 0 \text{ for } \mathbf{y} \in \partial\Omega \Rightarrow \tilde{W}'n(\mathbf{y},\tau) + \tilde{W}'n(\mathbf{y}',\tau) = 0 \tag{142}$$

$$\tilde{\sigma}_{nn}(\mathbf{y},\tau) = \tilde{\sigma}_{nn}(\mathbf{y}',\tau) \text{ for } \mathbf{y} \in \partial\Omega \tag{143}$$

$$s(\mathbf{y},\tau) = s(\mathbf{y}',\tau) \text{ for } \mathbf{y} \in \partial\Omega \tag{144}$$

$$\bar{\tilde{\sigma}}^{ij}(\tau) = \frac{1}{|\Omega|}\int_\Omega \tilde{\sigma}^{ij}(\mathbf{y},\tau)\mathrm{d}^2y. \tag{145}$$

Initial conditions:

$$s(\mathbf{y},\tau) = 0,\tilde{w}^{(p)}(\mathbf{y},\tau) = 0,\mathbf{y} \in \Omega,\tau = 0. \tag{146}$$

We see that the only dimensionless parameter, $e = E/A$, remains in the equations. To get a feeling what may be the actual value of parameter e, let us consider copper at 1000 K temperature. It is known that equilibrium value of vacancy concentration varies in broad range is $C_0 \sim 10^{-8}\text{--}10^{-4}$. Then it follows from equation (46) that $e \sim 0.01\text{--}100$.

Let us study numerically how the solution depends on parameter e. For simplicity computations were done for the problem of compression of a single crystal by absolutely rigid
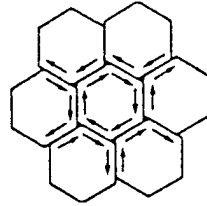
Fig. 9.

frictionless pistons (see [4]). Region Ω is a square, the characteristic size is the distance from its center to the edges (see Fig. 10). Vertical crystal edges are free. For simplicity let us assume that the crystal is isotropic. Under this assumption the compression of the crystal will not result in piston rotation and from symmetry considerations we may assume that the displacement of the cell center is zero. Let $\bar{\varepsilon}(\tau)$ be the vertical displacement of the upper piston, which is the unknown function and which is analogous to the macrostrain in system P. The normal average stress $\bar{\sigma}$ at the contact between the pistons and the crystal surfaces serve as an analog to the macrostresses. The piston is loaded by a constant force, such that the average stress is equal to -1.

$$\bar{\sigma} \equiv \frac{1}{2} \int_{-1}^{1} \bar{\sigma}_n(y^1,1,\tau)\mathrm{d}y^1 = \frac{1}{2} \int_{-1}^{1} \bar{\sigma}_n(y^1, -1,\tau)\mathrm{d}y^1 = -1. \tag{147}$$

The system of equations of the problem of compression of a single crystal is the set equations (131)–(139) and (147), initial conditions equation (146) plus boundary conditions:

$$\bar{\sigma}_{nn}(\pm 1, y^2, \tau) = 0, \ -1 \le y^2 \le 1 \tag{148}$$

$$\bar{w}_n(y^1, \pm 1, \tau) = \pm \bar{\varepsilon}(\tau), \ -1 \le y^1 \le 1. \tag{149}$$

The Theorems 1 and 2 can be proven for this problem as well.

The steady-state solution for secondary creep can be obtained in closed form and the value of the steady-state creep rate is $\dot{\bar{\varepsilon}} = 1.7$. Hence, the analog of the formulas equations (126) and (127) in this case is

$$\bar{\sigma} = 0.588 \, \dot{\bar{\varepsilon}} \, \frac{\epsilon^2}{D}. \tag{150}$$

One may notice that the numerical coefficients in equations (126) and (128) and in equation (150) are of the same order of magnitude.
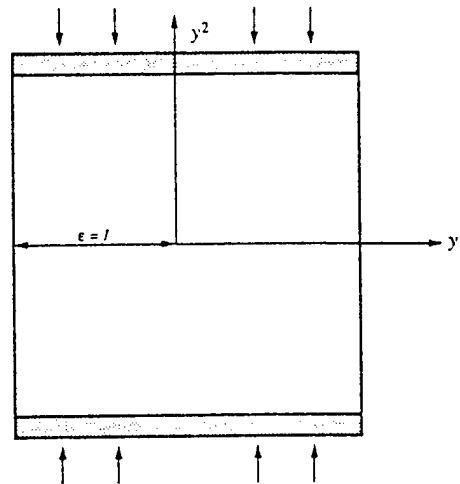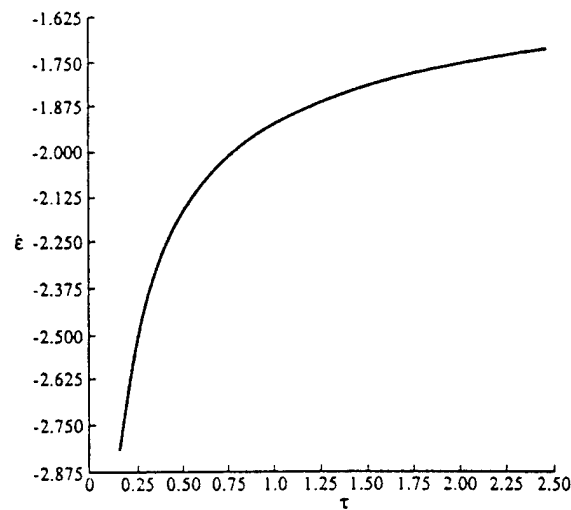

Fig. 10.

Fig. 11.

Let us discuss numerical results for the transient solution. Parameter e values were chosen to be 0.1, 1, 10, which is in the middle of the expected range.

1. As was expected, for small values of dimensionless time τ creep rates fit very well the asymptotic $\sim \tau^{-1/2}$ (See Fig. 11–13).

2. When τ is large, a steady-state creep rate of 1.7 is achieved (see Table 1). A practically steady-state is reached at $\tau \sim 1$ (see Table 1).

3. Parameter e somewhat affects the transition time necessary to reach the steady-state creep rate. The smaller the e the larger the transition time. However, the modeling results do not allow us to conclude what kind of dependency is it. As one can see from Table 1, the transition time for $e = 0.1$ is much larger, than for $e = 1$, but there is no noticeable difference between cases with $e = 1$ and 10.

4. At the first moment of load application, the only non-zero stress component is $\bar{\sigma}^{22}$ and it is equal to -1 over Ω. With creep developed, stresses tend to limit, which do not depend on the parameter e, which is as it should be because of Theorem 2. Figure 14 shows the stress distribution at the piston–crystal contact for $e = 10$, $\tau = 0.5$. Stars mark
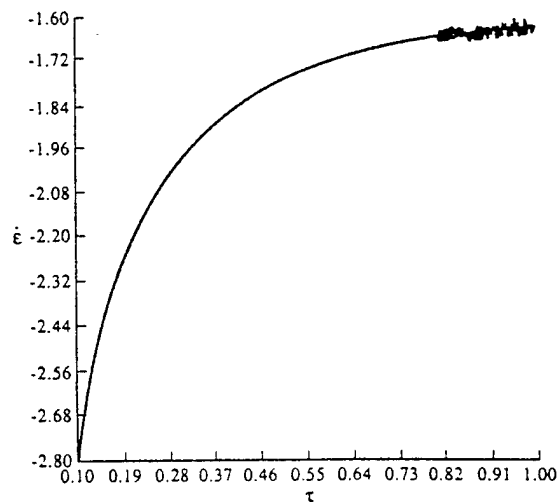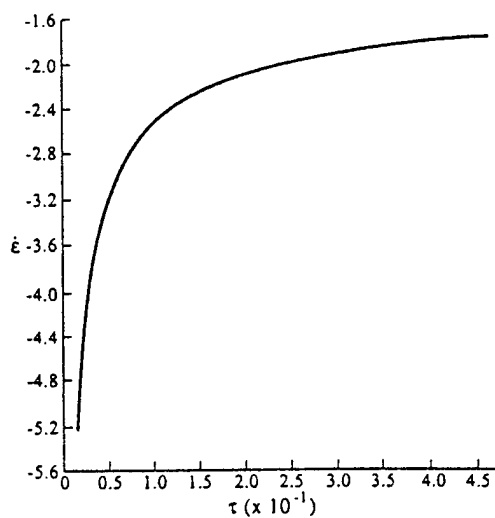

Fig. 12.

Fig. 13.

asymptotical the steady-state stress distribution. The transition time to steady-state stresses is of the same magnitude, as the transition time needed for the creep rate to become constant.

Table 1. Stabilization of the creep rate for various values of parameter e

e	0.1		1		10	
τ	2.5	0.8	0.65	0.3	0.5	0.25
$\dot{\bar{\varepsilon}}$	1.74	2	1.72	2	1.73	2

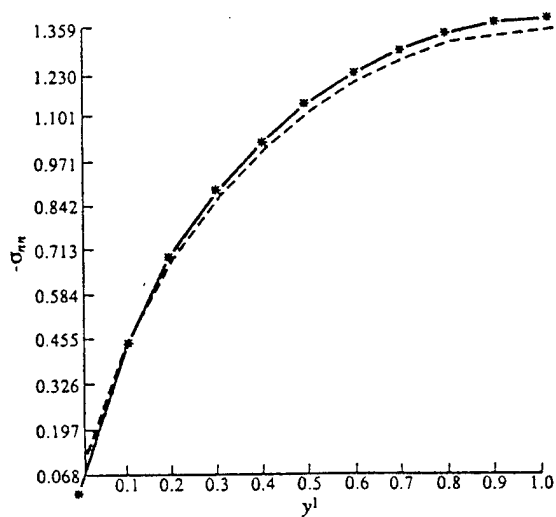Asymptotic value of $\dot{\bar{\varepsilon}}$

Fig. 14.

16. CONCLUSIONS.

Three interesting results of this study seem worth noting. First, the constitutive macroequations of diffusional creep turn out to be nonlocal. It is not obvious how to eliminate the nonlocality by introducing additional internal variables. Probably, the elimination of the nonlocality on the macroscale is impossible in principle. Since this seems to be the case, a search for adequate local constitutive equations for creep is doomed to failure. Second, there is an intrinsic material time $\tau = tDA/\epsilon^2$. Strain–time dependence (for constant stresses) is universal for intrinsic time in the sense that it does not depend on the material and on the temperature (the temperature dependence comes from the material constants D and A). Third, as the variational principle shows, creep rates do not depend on the elastic properties in secondary creep: only diffusion constants, the grain size and the grain geometry are important. Formula equation (87) is an example of such a dependency.

APPENDIX

A. THE EFFECT OF GRAIN BOUNDARY STRESS RELAXATION ON APPARENT ELASTIC MODULUS

The assumption equation (58) that shear stresses at the grain boundaries can be neglected in creep problem is believed to be correct by many authors. It would be interesting to find an experimental evidence that such an effect is real. It may not be an easy task, because the numerical modeling revealed surprisingly low influence of grain shear stress relaxation on apparent elastic modulus. In more detail, the averaged elastic properties were computed for the periodic structure described in Section 6. Boundary conditions equation (58), (72) and (73) were applied and averaged elastic moduli were calculated from the solution of the periodic elasticity problem. For definiteness it was assumed that grains are isotropic and, hence, only two elastic constants need to be calculated. In addition, it is obvious that if the hydrostatic pressure tensor is applied to the plane, the structure does not "feel" the cuts made and, hence, the bulk modulus of the polycrystal is the same as the bulk modulus of the grain itself:

$$\frac{E^*}{2(1 - v^*)} = \frac{E}{2(1 - v)} \tag{A.1}$$

where E, v and E^*, v^* are Young's modulus and Poisson's ratio of the grain and the polycrystal correspondingly. Because of that the ratios E^*/E and G^*/G depend only on Poisson's ratio. Results are listed in Table 2 and as one can conclude the Young and shear moduli drop no more than 20% as a result of shear stress relaxation.

B. PROPERTIES OF PERIODIC STRESS FIELDS, SATISFYING THE EQUILIBRIUM CONDITIONS

Let us prove formulas equations (83) and (85), which hold for an arbitrary stress field satisfying equilibrium equation (48) and boundary conditions equations (73) and (58). Multiplying equation (48) by x^k and integrating over cell ω^- we

Table 2. Apparent elastic moduli of polycrystal with fully relaxed shear grain boundary stresses

v	0.3	0.34	0.45
E^*/E	0.830	0.829	0.828
G^*/G	0.806	0.811	0.823
v^*	0.339	0.370	0.459

get

$$0 = \int_{\omega^-} \frac{\partial \sigma^{ij}}{\partial x^l} x^k d^2 x = - \int_{\omega^-} \sigma^{ij} \delta^k_j d^2 x + \int_{\partial\omega^-} \sigma^{ij} n_j x^k dx \Rightarrow \int_{\omega^-} \sigma^{ik} d^2 x = \int_{\partial\omega^-} \sigma^{ij} n_j x^k dx$$

$$= \int_{\partial\omega^-} \sigma_{nn} n^i x^k dx = \sum_{r=1}^{3} \left(\int_{S_r} \sigma_{nn}(x,t) n^i(x,t) x^k dx + \int_{S_r} \sigma_{nn}(x',t) n^i(x',t) x'^k dx' \right)$$

$$= \sum_{r=1}^{3} \left(\int_{S_r} \sigma_{nn}(x,t) n^i(x) x^k dx - \int_{S_r} \sigma_{nn}(x,t) n^i(x)(x^k + l^k(x)) dx \right)$$

$$= - \sum_{r=1}^{3} \int_{S_r} \sigma_{nn}(x,t) n^i(x) l^k(x) dx = - \frac{1}{2} \int_{\partial\omega^-} \sigma_{nn} n^i l^k dx = \frac{\epsilon}{2} \int_{\partial\omega^-} \sigma_{nn} n^i n^k dx \tag{B.1}$$

Formula equation (83) follows from equation (B.1) and definition equation (75). In order to prove equation (85) let us note that spherical tensor $\sigma^{ij} = C\delta^{ij}$ may be substituted in equation (83), which is reduced in this case to equation (85). Let s be an arbitrary function, satisfying periodicity condition equation (74). Let us define surface tractions on the cell boundary $\partial\omega^-$ by formulas equations (58) and (54). Then the principal vector **F** and principal moment M applied to the grain from these tractions, are zeros.

$$F = \int_{\partial\omega^-} \sigma_{nn}(x) n(x) dx = 0 \tag{B.2}$$

$$M = \int_{\partial\omega^-} \sigma_{nn}(x) n \otimes x dx = \sum_{r=1}^{3} \left(\int_{S_r} \sigma_{nn}(x)(n(x) \otimes x + n(x') \otimes x') dx \right)$$

$$= \sum_{r=1}^{3} \left(\int_{S_r} \sigma_{nn}(x) n(x) \otimes (x - x') dx \right) = - \sum_{r=1}^{3} \left(\int_{S_r} \sigma_{nn}(x) n(x) \otimes l(x) dx \right) = 0 \tag{B.3}$$

The last term in equation (B.3) is zero because of equation (67).

C. ASYMPTOTIC BEHAVIOR OF THE SOLUTION AT LARGE TIME.

LEMMA 1. For every solution of the system P the following identity holds:

$$\frac{dI}{dt} + A[\nabla s, \nabla s] = |\omega^-| \bar{\sigma}^{ij} \hat{\epsilon}_{ij}. \tag{C.1}$$

PROOF. It follows from equations (50) and (54) that

$$Q \equiv \frac{dI}{dt} + A[\nabla s, \nabla s] = A[\nabla s, \nabla s] + \int_{\omega^-} As \frac{\partial s}{\partial t} d^2 x + \int_{\omega^-} a^{ijkl} \epsilon^{(e)}_{ij} \dot{\epsilon}^{(e)}_{kl} d^2 x$$

$$= A[\nabla s, \nabla s] + \int_{\omega^-} A \frac{\partial}{\partial x^i} \left(D^{ij} \frac{\partial s}{\partial x^j} \right) d^2 x + \int_{\omega^-} \sigma^{kl} \dot{\epsilon}^{(e)}_{kl} d^2 x$$

$$= A[\nabla s, \nabla s] - A[\nabla s, \nabla s] + \int_{\partial\omega^-} \sigma_{nn} A D^{ij} \frac{\partial s}{\partial x^j} n_i dx + \int_{\omega^-} \sigma^{kl} \dot{\epsilon}^{(e)}_{kl} d^2 x = \int_{\partial\omega^-} \sigma_{nn} \dot{w}^{(p)}_n dx + \int_{\omega^-} \sigma^{kl} \dot{\epsilon}^{(e)}_{kl} d^2 x. \tag{C.2}$$

With equations (62) and (71) the elastic strains are expressed in terms of averaged strains, plastic strains and strains $\epsilon_{ij}(W)$ generated by field W:

$$\epsilon^{(e)}_{ij} = \bar{\epsilon}_{ij} + \epsilon_{ij}(W) - \epsilon^{(p)}_{ij}, \epsilon_{ij}(w) \equiv \frac{1}{2} \left(\frac{\partial w_i}{\partial x^j} + \frac{\partial w_j}{\partial x^i} \right), \dot{\epsilon}^{(e)}_{ij} = \dot{\bar{\epsilon}}_{ij} + \epsilon_{ij}(\dot{W}) - \dot{\epsilon}^{(p)}_{ij}. \tag{C.3}$$

Substitution of equation (C.3) into equation (C.2) yields

$$Q = \int_{\partial\omega^-} \sigma_{nn} \dot{w}^{(p)}_n dx + \int_{\omega^-} \sigma^{ij} (\dot{\bar{\epsilon}}_{ij} + \epsilon_{ij}(\dot{W}) - \dot{\epsilon}^{(p)}_{ij}) d^2 x$$

$$= \int_{\partial\omega^-} \sigma_{nn} \dot{w}^{(p)}_n dx + \int_{\omega^-} \sigma^{ij} \dot{\bar{\epsilon}}_{ij} d^2 x + \int_{\partial\omega^-} \sigma_{nn} (\dot{W}_n - \dot{w}^{(p)}_n) dx = |\omega^-| \bar{\sigma}^{ij} \dot{\bar{\epsilon}}_{ij} + \frac{1}{2} \int_{\partial\omega^-} \sigma_{nn} [\dot{W}_n] dx = |\omega^-| \bar{\sigma}^{ij} \dot{\bar{\epsilon}}_{ij}. \tag{C.4}$$

Boundary conditions equations (73) and (72) were used in the derivation equation (C.4). Lemma 1 is proved.

LEMMA 2. Let us assume that for $t \geq t^0$ macrostresses are equal to zero:

$$\bar{\sigma}^{ij}(t) = 0, t \geq t^*.$$ (C.5)

Then for an arbitrary solution of the system P the following estimations hold:

$$I(t) \leq e^{-\beta(t-t^*)}I(t^*), t \geq t^*. \beta = \text{const} > 0$$ (C.6)

and the following components of the solution tend to zero:

$$s \to 0, \varepsilon_{ij}^{(e)} \to 0, \sigma^{ij} \to 0, \hat{\varepsilon}_{ij} \to 0, t \to 0.$$ (C.7)

PROOF. For $t \geq t^*$ the identity equation (C.1) is reduced to the following:

$$\frac{dI(t)}{dt} + A[\nabla s, \nabla s] = 0.$$ (C.8)

It follows from equations (C.5) and (84) that

$$\int_{\partial \omega^-} sn^k n^k dx = \int_{\partial \omega^-} s dx = 0, t \geq t^*.$$ (C.9)

Then the following inequalities hold [28]:

$$\int_{\omega^-} As^2 d^2x \leq C_2[\nabla s, \nabla s]$$ (C.10)

$$\int_{\partial \omega^-} A^2 s^2 dx \leq C_3[\nabla s, \nabla s].$$ (C.11)

Adding, if necessary, to the solution some field $V \epsilon R$ we may modify the elastic solution so that at each moment t averaged over the cell ω^- elastic displacements and rotation are zero:

$$\int_{\omega^-} w_i^{(e)} d^2x = 0$$ (C.12)

$$\int_{\omega^-} \left(\frac{\partial w_1^{(e)}}{\partial x^2} - \frac{\partial w_2^{(e)}}{\partial x^1} \right) d^2x = 0.$$ (C.13)

Then [29]

$$\int_{\partial \omega^-} (w_n^{(e)})^2 dx \leq C_4[\epsilon^{(e)}, \epsilon^{(e)}], C_4 = \text{const}.$$ (C.14)

Let us prove that

$$[\epsilon^{(e)}, \epsilon^{(e)}] \leq C_5[\nabla s, \nabla s].$$ (C.15)

With equations (48), (58) and (54) taken into account, the left-hand side of equation (C.15) is reduced to

$$[\epsilon^{(e)}, \epsilon^{(e)}] = \int_{\omega^-} \sigma^{ij} \varepsilon_{ij}^{(e)} d^2x = \int_{\partial \omega^-} \sigma^{ij} n_j w_i^{(e)} dx = \int_{\partial \omega^-} \sigma_{nn} n_j w_n^{(e)} dx$$

$$= \int_{\partial \omega^-} Asn_j w_n^{(e)} dx \leq \sqrt{\int_{\partial \omega^-} A^2 s^2 dx} \sqrt{\int_{\partial \omega^-} (w_n^{(e)})^2} \leq C_6 \sqrt{[\epsilon^{(e)}, \epsilon^{(e)}]} \sqrt{[\nabla s, \nabla s]}.$$ (C.16)

The inequalities in equation (C.16) follow from equations (C.14) and (C.11). Estimation equation (C.15) follows from equation (C.16).

Combining equations (C.15) and (C.10) we obtain

$$A[\nabla s, \nabla s] \geq \beta I(t), \beta = \text{const}.$$ (C.17)

It follows from equations (C.8) and (C.17) that

$$0 = \frac{dI(t)}{dt} + A[\nabla s, \nabla s] \geq \frac{dI(t)}{dt} + \beta I(t)$$ (C.18)

which results in the basic relation

$$I(t) \leq e^{-\beta(t-t^*)}I(t^*) \Rightarrow I(t) \to 0, t \to \infty.$$ (C.19)

The first three statements in equation (C.7) follow immediately from equation (C.18). Since elastic strains and vacancy concentration tend to zero, the same is true for elastic and plastic strain rates, if the solution of the system P is sufficiently smooth. Hence

$$\Delta_{ij} \equiv \hat{\varepsilon}_{ij} + \varepsilon_{ij}(\dot{W}) = \hat{\varepsilon}_{ij}^{(e)} + \hat{\varepsilon}_{ij}^{(p)} \to , t \to \infty.$$ (C.20)

Using Levi–Civita formulas, we obtain the following equalities:

$$\dot{W}_i = -\hat{\varepsilon}_{ij} x^j + \lambda e_{ij} x^j + a_i + T(\Delta_{ij}), \lambda, a_i = \text{const}, T(\Delta_{ij}) \to 0.$$ (C.21)

The second and third terms in equation (C.21) represent the rigid body displacement, the last term stands for Levi–

Civita integrals. Substitution of equation (C.21) into continuity condition equation (72) is made similarly to evaluation equation (78) and yields

$$\hat{\varepsilon}_{ij}{}^{l}{}^{l}(x) n^{l}(x) + T_{n}(\Delta_{ij}). T_{n}(\Delta_{ij}) \rightarrow 0, t \rightarrow \infty. \tag{C.22}$$

Since the normal vector is constant over $S_{r}, r = 1,2,3$, the relation equation (C.22) provides three different conditions, which may be considered as a system of linear equations with respect to three components $\hat{\varepsilon}_{ij}$. The determinant of this system is not zero, and then it follows from equation (C.22) that $\hat{\varepsilon} \rightarrow 0, t \rightarrow \infty$. Lemma 2 is proved.

REFERENCES

1. Nabarro, F. R. N., Deformation of crystals by the motion of single ions. In *Report of a Conference on Strength of Solids*. The Physical Soc., 1948, pp. 75–90.
2. Herring, C. Diffusional viscosity of a polycrystalline solid. *Journal of Applied Physics* 1950, **21**, 437–445.
3. Coble, R. L. A model for boundary-diffusion controlled creep in polycrystalline materials. *Journal of Applied Physics* 1963, **34**, 1679–1682.
4. Lifshitz, I. M. On the theory of diffusion-viscous flow of polycrystalline bodies. *Soviet Physics JETP* 1963, **17**, 909–920.
5. Poirier, J. P., *Creep of Crystals*. Cambridge University Press, Cambridge, 1985.
6. Rabotnov, Yu., *Creep Problems in Structural Members*. Wiley, New York, 1969.
7. Flynn, C. P., *Point Defects and Diffusion*. Clarendon Press, Oxford, 1972.
8. Agulo-Lopez, F., Catlow, C. R. A. and Townsend, P. D., *Point Defects in Materials*. Academic Press, New York, 1988.
9. Shesterikov, S. and Lokotshendo, A. Creep and longterm strength of materials. *Itogi Nauki* 1980, **13**, 0
10. Crawford, J. H. and Slifkin, L. M., *Points Defects in Solids*. Plenum Press, New York, 1975.
11. Gruber, B. (ed.), Theory of crystal defects. *Proceedings of the Summer School in Hrarany, 1964*. Academic Press, New York, 1966.
12. Ashby, M. F. and Verral, R. A. Diffusion accommodated flow and super plasticity. *Acta Metallica* 1973, **21**, 149–163.
13. Murch, G. E. and Nowick, A. S. (eds), *Diffusion in Crystalline Solids*. Academic Press, New York, 1984.
14. Christian, J. W., *The Theory of Transformations in Metals and Alloys*. Pergamon Press, Oxford, 1975.
15. Varotsos, P. A. and Alexopoulos, K. D., *Thermodynamics of Point Defects and Their Relation with Bulk Properties*. North-Holland, Amsterdam, 1986.
16. Friedel, J., *Dislocations*. Pergamon Press, Oxford, 1964.
17. Cottrell, A. H., *Dislocations and Plastic Flow in Crystals*. Oxford, 1958.
18. Girifalco, L. A., *Statistical Physics of Materials*. Wiley, Newv York, 1973.
19. Kittel, C., *Introduction to Solid State Physics*. Wiley, New York, 1976.
20. Evans, H. E., *Mechanisms of Creep Fracture*. Elsevier Applied Sciences, Oxford, 1984.
21. Martin, J. W. and Doherty, R. D., *Stability of Microstructure in Metallic Systems*. Cambridge University Press, Cambridge, 1976.
22. Gomer, R. and Smith, C. S. (eds), *Structure and Properties of Solid Surfaces*. University of Chicago Press, 1953.
23. Rabotnov, Yu., *Mechanics of Deformable Solids*, 1965.
24. Gittus, J., *Creep, Viscoelasticity and Creep Fracture in Solids*. Wiley, New York, 1975.
25. Sedov, L. I., *A Course in Continuum Mechanics*. Vols 1–4. Wolters-Noordhoff, Groningen, 1971/1972.
26. Truesdell, C., *A First Course in Rational Continuum Mechanics*, 2nd edn. Academic Press, Boston, 1991.
27. Berdichevsky, V. L., *Variational Principles of Continuum Mechanics*. Nauka, Moscow, 1983.
28. Sobolev, S. L., *Applications of Functional Analysis in Mathematical Physics R.I., 1963*, Vol. 7. American Mathematics Society, Providence, R.I., 1963 (translation from Russian).
29. Friedrichs, K.O. On the boundary value problem of theory of elasticity and Korn's inequality. *Ann. Math.* 1947, **48**, 20